

Technische Universität München  
Ingenieurfacultät Bau Geo Umwelt  
Fachgebiet Satellitengeodäsie  
Univ.-Prof. Dr.phil.nat. Urs Hugentobler

# Comparing analysis of processing- and error models used in the Trimble Baseline Processor and the Bernese GNSS software

Andreas Schütz

Master's Thesis

**Bearbeitung:** 07.11.2016 – 07.05.2017

**Studiengang:** Geodäsie und Geoinformation (Master)

**Betreuer:** Univ.-Prof. Dr.phil.nat. Urs Hugentobler  
Joachim Tappe (Trimble)

**Kooperation:**  Trimble TerraSat  
Höhenkirchen-Siegersbrunn

## Declaration of Authorship

---

### Declaration of authorship

I hereby declare that the thesis submitted is my own unaided work. All direct or indirect sources used are acknowledged as references.

I am aware that the thesis in digital form can be examined for the use of unauthorized aid and in order to determine whether the thesis as a whole or parts incorporated in it may be deemed as plagiarism. For the comparison of my work with existing sources I agree that it shall be entered in a database where it shall also remain after examination, to enable comparison with future theses submitted. Further rights of reproduction and usage, however, are not granted here.

This paper was not previously presented to another examination board and has not been published.

---

first and last name

---

city, date and signature

---

## Short summary

In this thesis the new baseline postprocessing module inside the “Trimble Business Center”, the spatial data postprocessing office software from Trimble, is examined. It is completely built from scratch and introduces additional so called “Scientific settings”. To put the performance of this Trimble Baseline Processor (TBP) into contrast with a scientific software solution its results are compared to the Bernese GNSS Software, the product from the Astronomical Institute of the University of Bern. In total 866 baselines ranging from about one meter to approximately 9000 kilometers from different continents were processed using computation scenarios such as different tropospheric correction models, GPS only computation, reduced occupation timespans, usage of broadcast orbits and the evaluation of reproducibility of coordinates within one software. For the most the TBP shows slightly better performance in short and medium baselines in general as well as with broadcast orbits than Bernese, however regarding daily repeatability of coordinates and the processing of long baselines in general Bernese outperforms the TBP. The usage of different troposphere models shows a similar impact on the results of both processors. The results of the TBP are more stable when reducing the observation timespan compared to Bernese but a decrease in quality is also examinable. Overall both processors show high accuracy and quality in their results throughout most of the tests.

## Abstract

Diese Arbeit beschäftigt sich mit dem neuen Baseline Postprocessing Modul des "Trimble Business Center", der Office Software der Firma Trimble zur Verarbeitung raumbezogener Daten. Dieses Modul ist von Grund auf neu erstellt worden und beinhaltet zum ersten Mal die sogenannten „Scientific settings“. Um die Performance des Trimble Baseline Processor (TBP) einer wissenschaftlichen Software gegenüber zu stellen werden dessen Ergebnisse mit der der Bernese GNSS Software verglichen, dem Produkt des Astronomischen Instituts der Universität Bern. Insgesamt wurden 866 Basislinien mit einer Spanne von einem Meter bis circa 9000 Kilometer von unterschiedlichen Kontinenten unter der Verwendung mehrerer Szenarien wie unterschiedlicher Troposphärenmodelle, ausschließlich GPS Beobachtungen, verringerte Beobachtungszeiträume, Verwendung von Broadcast Orbits und unter dem Aspekt der Wiederholbarkeit von berechneten Koordinaten innerhalb einer Software prozessiert. Der TBP zeigt generell leicht bessere Ergebnisse als Bernese im Bereich kurzer und mittellanger Basislinien ebenso wenn Broadcast Orbits zur Berechnung verwendet werden. Bei langen Basislinien im Allgemeinen und in der Wiederholbarkeit der Koordinaten im Bezug auf Tageslösungen jedoch zeigt Bernese bessere Ergebnisse als der TBP. Der Übergang auf andere Troposphärenmodelle zeigt ähnliche Auswirkungen in den Ergebnissen beider Prozessoren. Der TBP liefert stabilere Ergebnisse als Bernese bei verkürzten Beobachtungszeiträumen, allerdings ist auch beim TBP ein signifikanter Rückgang in der Qualität ersichtlich. Summa summarum weisen jedoch beide Prozessoren eine hohe Genauigkeit und Güte in fast allen Tests auf.

---

### Acknowledgements

I want to thank Joachim Tappe, my supervisor at Trimble TerraSat, for thoroughly and consistently supporting me, ensuring my progress and always taking time from his day when I needed advice or had any requests.

I thank Professor Hugentobler from the TU Munich, for being my supervisor at the university, for enabling me to do this thesis outside the university, for working at the IAPG as Tutor and research assistant and in general his relentless support over the years of my study and his open door policy, for being a friend and supporter.

My next thank goes to Inga Selmke, Professor Hugentoblers' assistant, who helped me with any request I had regarding Bernese and could always be counted on.

Great thank also goes to Dr. Herbert Landau from Trimble TerraSat for enabling this cooperation between the TUM and Trimble.

And final thanks go to Igor Artushkin at Trimble and the Trimble QA for their support, help and time they took for me.

---

## Table of contents

1	Introduction .....	1
1.1	Motivation.....	1
1.2	Bernese setting standards: State of the art.....	1
1.3	Comparison of both processors.....	1
1.4	Overview .....	1
2	Fundamentals .....	2
2.1	Differencing Levels.....	3
2.1.1	Single Differences .....	3
2.1.2	Double Differences.....	4
2.1.3	Triple Differences .....	4
2.2	Modeling of atmospheric delays .....	5
2.2.1	Tropospheric modelling .....	5
2.2.1.1	Niell Mapping Function.....	6
2.2.1.2	Vienna Mapping Function 1.....	7
2.2.1.3	Global Mapping Function .....	8
2.2.1.4	Troposphere gradients .....	9
2.2.2	Ionospheric modelling .....	10
2.3	Linear combinations .....	12
2.3.1	Ionosphere - free linear combination .....	12
2.3.2	Wide - lane linear combination .....	13
2.3.3	Narrow - lane linear combination.....	13
2.3.4	Melbourne - Wübbena linear combination .....	14
2.4	Ambiguity Resolution.....	14
2.4.1	Sigma – Algorithm.....	15
2.4.2	LAMBDA - Algorithm .....	16
3	Test data, software packages and comparison.....	19
3.1	Software packages.....	19
3.1.1	Bernese GNSS Software v. 5.2.....	19
3.1.1.1	Introduction .....	19
3.1.1.2	Processing chain.....	21
3.1.2	Trimble Baseline Processor.....	24
3.1.2.1	Introduction .....	24
3.1.2.2	Processing chain.....	26
3.1.3	Baseline length dependent settings.....	28
3.2	Comparison.....	33

---

---

## Table of contents

---

3.2.1	Principle .....	33
3.2.2	Requirements for comparable results .....	34
3.2.3	Comparison tasks .....	39
3.2.3.1	Standard processing procedure .....	39
3.2.3.2	Influence of the tropospheric correction model .....	41
3.2.3.3	GPS only .....	41
3.2.3.4	Daily Repeatability .....	42
3.2.3.5	Broadcast ephemeris .....	42
3.2.3.6	Reduced occupation timespans .....	43
3.2.3.7	Ambiguity Resolution .....	43
3.2.4	Matlab evaluation toolbox.....	44
3.3	Choice of Test data .....	46
3.3.1	Short baseline network.....	46
3.3.2	Medium baseline network.....	47
3.3.3	Long baseline networks.....	48
3.3.4	Additional data and information .....	49
4	Results and discussion.....	50
4.1	Standard processing .....	51
4.1.1	Short baselines .....	51
4.1.2	Medium baselines .....	53
4.1.3	Long baselines .....	56
4.2	Influence of the tropospheric correction model .....	61
4.2.1	Niell Mapping Function.....	61
4.2.1.1	Short baselines .....	61
4.2.1.2	Medium baselines .....	63
4.2.1.3	Long baselines .....	66
4.2.2	VMF .....	68
4.2.2.1	Short baselines .....	68
4.2.2.2	Medium baselines .....	70
4.2.2.3	Long baselines .....	73
4.3	GPS only.....	75
4.3.1	Short baselines .....	75
4.3.2	Medium baselines .....	78
4.3.3	Long baselines .....	81
4.4	Daily Repeatability .....	84
4.4.1	Short Baselines .....	84
4.4.2	Medium Baselines .....	87

---

## Table of contents

---

4.4.3	Long Baselines.....	90
4.5	Broadcast Ephemeris .....	93
4.5.1	Short Baselines .....	93
4.5.2	Medium Baselines .....	96
4.6	Reduced occupation timespans .....	99
4.6.1	Short baselines .....	99
4.6.2	Medium baselines .....	109
4.7	Processing conclusion.....	120
4.8	Soft factors.....	122
4.8.1	Processing possibilities .....	122
4.8.2	Graphical User Interface .....	122
4.8.3	User friendliness .....	124
5	Outlook.....	125
	References.....	126
	Attachements .....	128

---

# 1 Introduction

As in every project of any kind, the application determines the functionalities and the user defines the complexity. It may therefore be of no surprise how two software applications built for the same purpose can differ when developed and implemented by a team at a university or a team inside a corporate firm, yet neither from a personnel nor financial resource point of view, but regarding design, performance and features.

## 1.1 Motivation

The name Trimble is a well-known brand in the field of positioning solutions, especially high precision GNSS data acquisition and processing. The company name is associated with high performance and high accuracy positioning for both hardware and software. Its office software suite, the “Trimble Business Center” (TBC) provides a wide variety of applications for every surveyor and construction company. For GNSS, its heart and soul is the baseline post processor. With a new version of TBC coming 2017, a completely built-from-scratch baseline postprocessor (TBP) is included. Featuring the so called “Scientific settings” the user is for the very first time enabled to choose between an adaptive processing or to adjust crucial inner processing settings by own means. This implies the usage for possible scientific applications and examinations. It is therefore necessary to closely examine these adjustable parameters and the overall performance in order to confirm its applicability for such use cases.

## 1.2 Bernese setting standards: State of the art

When thinking of scientific GNSS data evaluation two names come to mind: GIPSY, developed at the Jet Propulsion Laboratory in the USA, and the Bernese GNSS Software, developed at the Astronomical Institute of the University of Bern. The latter one, especially in Europe, has risen to the standard in precise GNSS data processing and is used in over 700 agencies and institutions over the globe. With its numerous functionalities and high accuracy as well as flexibility and modifiable programs, it is a powerful tool in geophysics, GNSS positioning and satellite orbit determination tasks as well as the determination of atmospheric properties such as ionospheric activity. The Bernese GNSS software serves as reference giving for many of these applications, and in the scope of this thesis its performance will be the benchmark for the TBP

### 1.3 Comparison of both processors

This thesis will reflect on the performance of the baseline postprocessing of the TBP with respect to the Bernese GNSS software. The necessary core procedures shall be identified and brought in contrast. Specific processing scenarios and test data need to be selected in order to determine quality statements. The final criterion for the comparison shall be the difference to a reference coordinate from higher accuracy as well as additional processing aspects regarding e.g. ambiguity resolution. The results will be conferred by a Matlab script and statistically evaluated.

### 1.4 Overview

At first some basic physical and mathematical models and techniques regarding GNSS baseline postprocessing are stated, treating measurement computation and error mitigation. Afterwards both software suites are introduced with technical and procedural aspects, the Matlab evaluation toolbox is explained and comparison scenarios are established and their motivation is explained. The corresponding choice of test data is stated based on the requirements of the processing tasks and finally the results are brought into contrast for discussion.

## 2 Fundamentals

The two very basic observation equations in GNSS positioning [Dach et al., 2015] [Leick, 1995] are the code measurement:

$$P_{F,k}^i = \rho_k^i + \kappa_F I_k^i + T_k^i + c\delta_k - c\delta^i \quad (2.1)$$

and carrier phase measurement:

$$L_{F,k}^i = \rho_k^i - \kappa_F I_k^i + T_k^i + c\delta_k - c\delta^i + \lambda_F n_{F,k}^i \quad (2.2)$$

With  $P_{F,k}^i$  as code measurement on carrier frequency  $F$  between receiver  $k$  and satellite  $i$ ,  $L_{F,k}^i$  as carrier phase measurement of carrier frequency  $F$  between receiver  $k$  and satellite  $i$ ,  $\rho_k^i$  as geometric distance between receiver  $k$  (at signal reception time) and satellite  $i$  (at signal transmission time) also containing hardware related biases such as e.g. differential code biases,  $\kappa_F$  as frequency dependent cofactor for the ionospheric correction (discussed in detail in section 2.2.2),  $I_{F,k}^i$  as the ionospheric refraction,  $T_k^i$  as the tropospheric refraction,  $c\delta_k$  as receiver clock error and other hardware delays w.r.t. GNSS time for receiver  $k$ ,  $c\delta^i$  as satellite clock error and other hardware delays w.r.t. GNSS time for satellite  $i$ ,  $\lambda_F$  as wavelength of carrier w.r.t. carrier frequency  $F$  and  $n_{F,k}^i$  as unknown integer number of full wavelengths (initial phase ambiguity). Note that for reasons of simplicity and display multipath, measurement noise and relativistic effects are not shown here (without limitation of the generality).

As both basic observation equations (2.1) and (2.2) show, there is a considerable amount of physical dependencies that affect the GNSS signal from the moment of its generation on board of the satellite until after its reception at the receiver on the ground. It is therefore the main task of any GNSS post processing application to account for all these perturbations in order to reveal the pure geometrical distance between satellite and receiver respective yield the true position of the antenna point on ground. There are several proven techniques of error mitigation and modelling for high precision post processing solutions on which some light shall be shed upon in the following chapters.

## 2.1 Differencing Levels

Equations (2.1) and (2.2) show the modelling of the measurement from a single satellite to a single receiver at a specific epoch. Given the fact that there is not just one but several satellites observed at the same time, there is more than one receiver on the ground tracking the same satellites at a given epoch and the observation time span is longer than one epoch, one can combine the overall observations to gain a more convenient access to the defect sizes respective the true geometric distance between satellite and receiver. The following is taken from [Dach et al., 2015] and [Leick, 1995]

### 2.1.1 Single Differences

At first the so called between-receiver single differences are formed. Therefore a satellite must be observed by at least two receivers at the same time. The single differences are:

$$P_{F,kl}^i = P_{F,k}^i - P_{F,l}^i \quad (2.3a)$$

$$L_{F,kl}^i = L_{F,k}^i - L_{F,l}^i \quad (2.3b)$$

with  $l$  denominating the second receiver observing. Resubstituting (2.1) and (2.2) into (2.3a) resp. (2.3b) yields:

$$P_{F,kl}^i = \rho_k^i - \rho_l^i + \kappa_F I_k^i - \kappa_F I_{F,l}^i + T_k^i - T_l^i + c\delta_k - c\delta_l \quad (2.3c)$$

$$L_{F,kl}^i = \rho_k^i - \rho_l^i - \kappa_F I_k^i + \kappa_F I_{F,l}^i + T_k^i - T_l^i + c\delta_k - c\delta_l + \lambda_F n_{F,k}^i - \lambda_F n_{F,l}^i \quad (2.3d)$$

and (2.3c) and (2.3d) in short notation:

$$P_{F,kl}^i = \rho_{kl}^i + \kappa_F I_{kl}^i + T_{kl}^i + c\delta_k - c\delta_l \quad (2.4)$$

$$L_{F,kl}^i = \rho_{kl}^i - \kappa_F I_{kl}^i + T_{kl}^i + c\delta_k - c\delta_l + \lambda_F n_{F,kl}^i \quad (2.5)$$

Note that (2.4) and (2.5) do not contain any satellite clock corrections or satellite related hardware delays anymore since they canceled out. This is the main reason to form between-receiver single differences.

### 2.1.2 Double Differences

If now at least two satellites are observed by two receivers at the same time, the so called double differences may be formed:

$$P_{F,kl}^{ij} = P_{F,kl}^i - P_{F,kl}^j \quad (2.6a)$$

$$L_{F,kl}^{ij} = L_{F,kl}^i - L_{F,kl}^j \quad (2.6b)$$

with  $j$  denominating the additional satellite observed. Resubstituting (2.4) and (2.5) into (2.6a) and (2.6b) using short notation yields:

$$P_{F,kl}^{ij} = \rho_{kl}^{ij} + \kappa_F I_{kl}^{ij} + T_{kl}^{ij} \quad (2.7)$$

$$L_{F,kl}^{ij} = \rho_{kl}^{ij} - \kappa_F I_{kl}^{ij} + T_{kl}^{ij} + \lambda_F n_{F,kl}^{ij} \quad (2.8)$$

Now also receiver clock errors and receiver related hardware delays cancel out due to the nature of the combination of observations (given that receiver clock corrections are known accurately enough for the calculation of the geometric distances  $\rho$ ). This is not entirely true since so called differential code biases remain, depending on the receiver tracking type (not shown here for reasons of simplicity). In the case of different receiver tracking types within one baseline, the observations at both sites are biased individually which leads to non-resolvable double difference ambiguities. The usage of correction files or estimation of these biases is therefore necessary.

### 2.1.3 Triple Differences

Given double differences of two successive epochs  $t_1$  and  $t_2$ , triple differences may be formed. The triple difference for phase observations is shown in (2.9):

$$L_{F,kl}^{ij}(t_2) - L_{F,kl}^{ij}(t_1) = \rho_{kl}^{ij}(t_2) - \rho_{kl}^{ij}(t_1) - \kappa_F (I_{kl}^{ij}(t_2) - I_{kl}^{ij}(t_1)) \quad (2.9)$$

The most common use case for triple differences is the so-called cycle slip detection. The receiver generates a reference signal which is shifted by an integer number of cycles to the received signal from the satellite (initial phase ambiguity  $n_{F,k}^i$ ).  $n_{F,k}^i$  remains the same (for each frequency of a satellite – receiver combination) as long as no cycle slip or loss of lock occurs, which means  $n_{F,k}^i$  cancels out of the triple difference observation. The change of the initial phase ambiguity however results in an offset for only one or two successive triple difference observations which then can be

detected. This is the main advantage of the triple differences and also the reason they usually are formed only for phase observables. Note that since the tropospheric refraction usually does not change quickly over time, so it is often neglected in this case. This is not the case for the ionospheric refraction which can change very rapidly with respect to both time and absolute value of Magnitude.

## 2.2 Modeling of atmospheric delays

An electromagnetic wave is in constant mutual reaction with its propagation medium through which it travels. In the case of GNSS radio signals the propagation medium is the earth's atmosphere with its different layers. The different parts of the atmosphere affect the signal depending on, for example, their composition or ionization. The atmospheric effect usually leads to a delay of the arriving signal at the receiver on ground since the velocity of the signal differs from its supposed velocity in vacuum. For modeling of delays, the atmosphere is usually split up in a dispersive and non-dispersive part, i.e. frequency-dependent and non-frequency-dependent. The dispersive part is also referred to as the ionosphere and the non-dispersive part the troposphere. The following shall give an overview over the commonly used models to account for atmospheric delays on GNSS signals.

### 2.2.1 Tropospheric modelling

The troposphere is the non-dispersive part of the atmosphere (within the frequency bands used in GNSS). The delay can be computed by the integral of the tropospheric refractivity over the line of sight from the receiver to the satellite. The common approach is to evaluate the tropospheric refraction in zenith direction and then translate the delay according to the elevation angle of the space vehicle using mapping functions. Later on, also an azimuthal dependence will be given with the introduction of so called troposphere gradients.

Yet the tropospheric delay is split up in the delay caused by the hydrostatic or dry zenith path delay (caused by dry gases present) and the wet zenith path delay (caused by e.g. water vapor). The common technique in modern procedures as shown in the following is to model the hydrostatic part a priori and to estimate the wet part which is, due to its quick and seemingly random changing, very unpredictable and thus very difficult to model. The general formula for the separated wet and dry modeling of the tropospheric delay depending on the satellite elevation can be written as [Davis et al., 1985]:

$$\Delta L(E) = \Delta L_h^z * mf_h(E) + \Delta L_w^z * mf_w(E) \quad (2.10)$$

with  $\Delta L$  as the total tropospheric delay at elevation  $E$ ,  $\Delta L_h^z$  and  $\Delta L_w^z$  as the hydrostatic and wet zenith path delay respectively and  $mf_h$  and  $mf_w$  as the respective hydrostatic and wet mapping functions. Since the wet zenith path delay is estimated usually and the hydrostatic zenith path delay can be determined quite accurately from the total pressure at a site and the sites' coordinates [Saastamoinen, 1973], the following shall focus on the mapping functions used in GNSS post-processing. Note that if not accounted for, the tropospheric delay can cause a pseudorange error from about 2 to 10 meters.

### 2.2.1.1 Niell Mapping Function

The mapping function introduced by Niell [1996] (NMF) does not require any surface meteorology measurements, the only input parameters (in addition to the satellite elevation) are the geographic latitude  $\Phi$  and height above sea level  $H$  of the receiver and the measurement time  $t$ .

The hydrostatic mapping function is introduced as:

$$M_{dry}(E, H) = mf(E, a_d, b_d, c_d) + \Delta mf(E, H) \quad (2.11)$$

with

$$\Delta mf(E, H) = \left[ \frac{1}{\sin E} - mf(E, a_{ht}, b_{ht}, c_{ht}) \right] * H \quad (2.12)$$

and the wet mapping function:

$$M_{wet}(E) = mf(E, a_w, b_w, c_w) \quad (2.13)$$

with  $mf(E, a, b, c)$  being the mapping normalized to unity at zenith [Marini, 1972]:

$$mf(E, a, b, c) = \frac{1 + \frac{a}{b}}{\sin E + \frac{1 + \frac{a}{b}}{\sin E + \frac{b}{c}}} \quad (2.14)$$

The indices of the coefficients  $a, b, c$  refer to dry for  $d$ , wet for  $w$  and coefficient used for height correction  $ht$ . There are empirical values for coefficients  $a_{ht}, b_{ht}, c_{ht}$  (one value per parameter) and for the coefficients of the wet mapping function  $a_w, b_w, c_w$ . For the latter coefficients the empirical values are stated at specific geographical latitudes which can be interpolated to the actual latitude of the receiver position (Note that the coefficient are stated for latitudes from 0 to 75 degrees and are assumed to be symmetrical for both hemispheres).

The hydrostatic coefficients  $a_d, b_d, c_d$  however are computed as a function of time and geographical latitude:

$$\xi(\Phi, t) = \xi_{avg}(\Phi) - \xi_{amp}(\Phi) \cos\left(2\pi \frac{t-T_0}{365.25}\right) \quad (2.15)$$

where  $\xi$  denotes the respective coefficient  $a_d, b_d, c_d$ ,  $\xi_{avg}$  and  $\xi_{amp}$  are the empirically determined average and amplitude value for the respective coefficient which can be interpolated w.r.t. the geographical latitude  $\Phi$ ,  $t$  as the time of measurement in form of day of year (DOY) and  $T_0 = 28$  as day of year 28.

The remarkable fact about this mapping function is that there is no meteorological data necessary to compute the mapping factor, yet it provides similar precision and accuracy as models which base on such data.

### 2.2.1.2 Vienna Mapping Function 1

The Vienna Mapping Function 1, or VMF1, uses the same series expansion by [Marini, 1972] as the NMF. Yet the approach and determination of the coefficients  $a, b, c$  is fundamentally different. The basic principle to solve for the coefficients is to determine the total tropospheric delay for a certain latitude and time and then fit the coefficients of the mapping function to the delay by a least squares adjustment. In the case of the NMF, the total tropospheric delay was computed using radiosonde data. The VMF1 however [Boehm et al., 2006a] uses data from numerical weather models, such as for example the models from the European Centre for Medium-Range Weather Forecasts (ECMWF) and computes the hydrostatic and total tropospheric delay using ray-tracing techniques. From the ECMWF monthly mean gridded atmospheric profiles (30° longitude by 15° latitude, consisting of 10 layers) comprising height, total pressure, temperature and water vapor pressure at 4 times a day were taken as well as different initial elevation angles of the incoming signal to determine the mapping functions. Also an additional delay caused by the geometric ray bending effect in the atmosphere is introduced to the hydrostatic and total mapping function yielding, when using eq. (2.10) as origin

$$mf_h(E) = \frac{\Delta L_h(E) + \Delta L_{bend}(E)}{\Delta L_h^Z} \quad (2.16)$$

For the hydrostatic mapping function and

$$mf_t(E) = \frac{\Delta L_h(E) + \Delta L_w(E) + \Delta L_{bend}(E)}{\Delta L_h^z + \Delta L_w^z} \quad (2.17)$$

for the total mapping function with  $\Delta L_{bend}(E)$  as delay caused by the geometric ray bending effect. Then the three coefficients  $a, b, c$  of both of the mapping functions are fitted to the 10 discrete mapping function values of each profile layer (per epoch and grid point). The mean value of coefficient  $b$  is equal for the hydrostatic and total mapping function [Boehm et al., 2006a]. In the next step, coefficient  $b$  is fixed to its mean value and the least squares adjustment is repeated, only estimating the coefficients  $a$  and  $c$ . The coefficient  $c$  then shows a variability depending on season and latitude which is modeled as:

$$c = c_0 + \left[ \left( \cos \left( \frac{doy-28}{365} * 2\pi + \Psi \right) + 1 \right) + \frac{c_{11}}{2} + c_{10} \right] + (1 - \cos\varphi) \quad (2.18)$$

where  $doy$  is the day of the year,  $\Psi$  identifies the hemisphere ( $\Psi = 0$  for northern and  $\Psi = \pi$  for southern) and  $\varphi$  is the latitude.  $c_0, c_{10}$  and  $c_{11}$  for the hydrostatic and total mapping functions are empirical parameters given in [Boehm et al., 2006a]. The reference epoch day 28 was adopted from the NMF. The biggest difference w.r.t. the NMF in eq. (2.18) is that coefficient  $c$  is no longer symmetrical for both hemispheres. The coefficients  $b$  and  $c$  of the wet mapping function are fixed to those of NMF at latitude  $45^\circ$  and coefficient  $a$  is estimated for each profile. The advantage of VMF1 is increased accuracy of tropospheric corrections and increased baseline repeatability when used for processing, but a continuous access to a provider of VMF1 coefficients, as for example the TU Vienna, has to exist (access to up-to-date files via internet download).

### 2.2.1.3 Global Mapping Function

As a compromise between accuracy and independency of regularly updated correction files the so-called Global Mapping Function GMF was established by [Boehm et al., 2006b]. It allows the advantages of the high accuracy results of the VMF1 (with slight deficits) while using only the station coordinates and day of year as input parameters (as in the NMF). Therefore the empirical determinations for the coefficients  $b$  and  $c$  of the VMF1 are used, together with an empirical representation of the coefficient  $a$ . Values for the hydrostatic and wet coefficient  $a$  were determined from September 1999 to August 2002 using the same strategy as in VMF1 (but with a  $15^\circ$  by  $15^\circ$  grid and only a single ray trace at  $3.3^\circ$  initial elevation).

This results in 36 monthly mean values at each grid point for both the hydrostatic and the wet coefficient  $a$ . Then mean values  $a_0$  and annual amplitudes  $A$  of a sinusoidal function were fitted to the time series of the  $a$  coefficient at each grid point [Boehm et al., 2006b]:

$$a = a_0 + A * \cos\left(\frac{doy-28}{365} * 2\pi\right) \quad (2.19)$$

where afterwards  $a_0$  and  $A$  for both the hydrostatic and wet component of the continued fraction form were expanded into spatial spherical harmonic coefficients up to a degree and order 9 in a least squares adjustment [Boehm et al., 2006b]:

$$a_0 = \sum_{n=0}^9 \sum_{m=0}^n P_{nm}(\sin\varphi) * [A_{nm} * \cos(m * \lambda) + B_{nm} * \sin(m * \lambda)] \quad (2.20)$$

The GMF therefore combines the accuracy (with a slight deficit) of the VMF1 mapping function with the convenience of using only easy accessible input parameters such as station coordinates and day of year as the NMF with a global validity [Boehm et al., 2006b].

#### 2.2.1.4 Troposphere gradients

The three mapping functions introduced previously share the common assumption that the troposphere is radially symmetric around the actual zenith direction of the station, hence the corrections only depend on the satellite elevation but not on the azimuth of the incoming signal. There are several established approaches to tropospheric gradient modeling, yet this thesis will only introduce the model of Chen and Herring [1997], since it was used in all computations discussed later on. As all gradient models this approach begins with an introduction of an azimuthal (with  $\alpha$  as azimuth) dependent component  $\Delta L_{az}(E, \alpha)$  to the overall tropospheric delay (equation (2.10)) with a dedicated mapping function  $mf_{az}$ :

$$\Delta L_{az}(E, \alpha) = \Delta L_{ns} * mf_{az}(E) \cos \alpha + \Delta L_{ew} * mf_{az}(E) \sin \alpha \quad (2.21)$$

For both the hydrostatic and wet component.  $\Delta L_{ns}$  refers to the delay in north-south direction and  $\Delta L_{ew}$  to the east west direction. The mapping function used in (2.21) is defined as:

$$mf_{az}(E) = \frac{1}{\sin E \tan E + C} \quad (2.22)$$

$C$  depends on the gradient of refractivity (for both the hydrostatic and the wet case) and the path of the signal ray through the atmosphere. It is, among other methods, acquired by fitting equation (2.22) to the elevation dependent results of the ray tracing solutions for the asymmetric part of the tropospheric delay. Applying horizontal tropospheric gradient corrections increases the repeatability of station coordinates and decreases the residual station height variations significantly [Chen and Herring, 1997].

### 2.2.2 Ionospheric modelling

The most common model for the ionosphere is a single layer model as shown in figure 1.

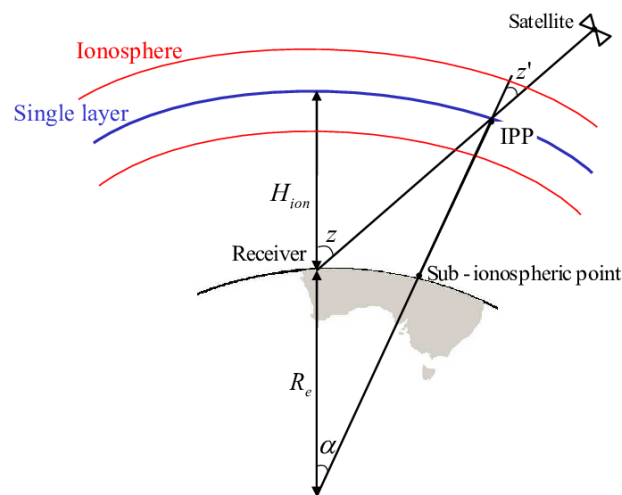


Figure 1: Ionospheric single layer model [Arora et al., 2015]

The ionosphere is treated as one infinitesimal layer containing all free electrons in the atmosphere at a certain height above the earth's surface (usually between 350 and 450 km, coinciding with the part of the highest electron density) [Hofmann-Wellenhof et al., 2001]. The amount of electrons interacting with the radio signal from the satellite defines the difference between geometrical range and measured range caused by the ionosphere (apart from the frequency of the signal). This is addressed by the Total Electron Content  $TEC$ , which is the Integral of the electron density over the path travelled by the signal. Usually the  $TVEC$ , the Total Vertical Electron Content, is modelled or estimated which can be imagined as a column from ground to the top of the ionosphere in zenith direction with 1 square meter ground area above the receiver position containing all free electrons. If this is the case the  $TEC$  has to be represented also by the satellite elevation, since the ionospheric pierce point (IPP) is not in the zenith of the receiver (see figure 1).

The absolute value for the ionospheric refraction  $I$  computes as:

$$I_k^i = \frac{1}{\cos z'} * \frac{40.3}{f^2} * TVEC \quad (2.23)$$

where

$$\sin z' = \frac{R_e}{R_e + H_{ion}} * \sin z \quad (2.24)$$

With (according to figure 1)  $z$  as the zenith angle between receiver and satellite at the receiver location,  $z'$  as the zenith angle at the ionospheric pierce point,  $R_e$  as the mean earth radius,  $H_{ion}$  as the mean value for the height of the ionosphere and  $f$  as the frequency observed [Hofmann-Wellenhof et al., 2001]. The value 40.3 is an approximate for the constant  $c^2 r_e / (2\pi)$ , with  $c$  as the speed of light in vacuum and  $r_e$  being the electron radius. Note that this formula is derived from the series expansion of the phase/group refractive index and does therefore not account for higher order terms.

The ionosphere is the dispersive part of the atmosphere, its interaction with a signal travelling through depends on the signals' frequency. In a first approximation the ionospheric refraction is proportional to  $\frac{1}{f^2}$  with  $f$  as frequency. It is therefore possible (as used in the observation equations) to state the ionospheric delay for one carrier frequency and express the delay on the other frequencies as a multiple. For example if  $I_k^i$  refers to the ionospheric delay for the L1 frequency (in eq. 2.1 and 2.2),  $\kappa_1 = 1$  (since  $\kappa_1 I_k^i = I_k^i$ ) and  $\kappa_2 = \frac{f_1^2}{f_2^2}$ . The ionosphere is the cause for the so called "phase advance" and "group delay". The phase and code measurements are advanced respective delayed by the same absolute value. This means the impact of the ionospheric refraction for both code and phase measurements within the same carrier is equal but with opposite signs [Hofmann-Wellenhof et al., 2001]. Note that if not accounted for the ionospheric delay can cause a pseudorange error from 10 to 30 meters on (during the measurement fast ionospheric changes can even cause loss of lock at the receiver).

## 2.3 Linear combinations

Linear combinations (LCs) are used for the same reason as the differencing approaches in section 2.1, which is to simplify the computation and reduce the impact of defect sizes. The principle of linear combinations however lies not in the combination of observations between different satellites, receivers or epochs, but in the varying combination of different signals within the observations of one satellite (given the fact that a multi frequency receiver was used to obtain the observations). In common processing tasks linear combinations are mainly formed to solve for the unknown integer ambiguities and, in the case of the ionosphere free linear combination, to compute absolute position solutions. The geometry – free linear combination is not mentioned here since it is used e.g. to derive ionospheric models but in the case of provided ionosphere models It has no practical use for classic GNSS post processing. The following is taken from Dach et al. [2015] an only the linear combinations w.r.t. the phase observables are stated (except for the Melbourne-Wübbena which requires phase and code). Note that the phase representation in its basic form is also valid for the code observables, but of course without the ambiguity terms.

### 2.3.1 Ionosphere - free linear combination

This particular pairing of signals eliminates, as the name indicates, the ionospheric path delay from the observations (the 99.9% of the first order ionospheric path delay to be precise). The basic form for zero differences  $L_3$  is given by:

$$L_3 = \frac{1}{f_1^2 - f_2^2} (f_1^2 L_1 - f_2^2 L_2) \quad (2.25)$$

with  $L_1$  and  $L_2$  being the phase observables on the respective frequency  $f_1$  and  $f_2$ . Resubstituting the Double Difference equation (2.8) into (2.25) and neglecting the tropospheric delay the ionosphere-free linear combination results in:

$$L_{3,kl}^{ij} = \rho_{kl}^{ij} + B_{3,kl}^{ij} \quad (2.26)$$

where the bias term in (2.26) is given by

$$B_{3,kl}^{ij} = \frac{1}{f_1^2 - f_2^2} (f_1^2 \lambda_1 n_{1,kl}^{ij} - f_2^2 \lambda_2 n_{2,kl}^{ij}) \quad (2.27)$$

With  $B_{3,kl}^{ij}$  being the ionosphere-free bias term. Note that this bias term can be reformulated using the wide-lane ambiguity  $n_{5,kl}^{ij}$  (discussed in section 2.3.2) and the narrow-lane ambiguity  $n_{N,kl}^{ij}$  (LC introduced in section 2.3.3):

$$B_{3,kl}^{ij} = c \frac{f_2}{f_1^2 - f_2^2} n_{5,kl}^{ij} + \frac{c}{f_1 + f_2} n_{N,kl}^{ij} \quad (2.28)$$

where the relationship  $n_{5,kl}^{ij} = n_{1,kl}^{ij} - n_{2,kl}^{ij}$  is used to derive (2.28) from (2.27), if the wide-lane ambiguity is known.

### 2.3.2 Wide - lane linear combination

The wide-lane LC

$$L_5 = \frac{1}{f_1 - f_2} (f_1 L_1 - f_2 L_2) \quad (2.29)$$

Can be used in its Double differenced form (neglecting ionospheric and tropospheric refraction in this display)

$$L_{5,kl}^{ij} = \rho_{kl}^{ij} + \frac{c}{f_1 - f_2} (n_{1,kl}^{ij} - n_{2,kl}^{ij}) \quad (2.30)$$

with its formal wavelength  $\lambda_5 = \frac{c}{f_1 - f_2} \approx 86 \text{ cm}$  to fix cycle slips and resolve the wide-wide lane ambiguities to their integer values. This becomes easier due to the increased wavelength w.r.t.  $\lambda_1$  and  $\lambda_2$ . Note that equation (2.29) and (2.30) increase the measurement noise significantly and precise corrections for the atmospheric delay, especially the ionosphere, are crucial.

### 2.3.3 Narrow - lane linear combination

The narrow-lane LC

$$L_N = \frac{1}{f_1 + f_2} (f_1 L_1 + f_2 L_2) \quad (2.31)$$

with its characteristic narrow-lane wavelength  $\lambda_N = \frac{c}{f_1 + f_2} \approx 11 \text{ cm}$  is usually not used as stand-alone combination of measurements like e.g. the wide-lane linear combination, but rather appears within other LCs in parts (e.g. the ionosphere-free linear combination, where the second term on

the right hand side of eq. (2.28) contains the narrow-lane wavelength). Also the code narrow-lane linear combination is used in the following Melbourne-Wübbena LC.

### 2.3.4 Melbourne - Wübbena linear combination

The Melbourne-Wübbena LC

$$L_6 = \frac{1}{f_1 - f_2} (f_1 L_1 - f_2 L_2) - \frac{1}{f_1 + f_2} (f_1 P_1 + f_2 P_2) \quad (2.32)$$

consists of the phase wide-lane LC (eq. 2.29) and the code narrow-lane LC (eq. (2.31) with code observations). It eliminates the effect of the atmosphere (iono- and troposphere), the geometry  $\rho$  (implicitly contained in the geometry). It is used to solve for the wide-lane ambiguities for nearly arbitrary long baseline lengths since (2.32) in its double differenced form yields  $L_{6,kl}^{ij} = \lambda_5 n_{5,kl}^{ij}$ . The determining factor for the success of ambiguity resolution however is the quality of the code measurements (approx. with an RMS of maximum 1m, due to the formal wide-lane wavelength) and the usage of precise differential code biases.

## 2.4 Ambiguity Resolution

Due to its nature as an electromagnetic wave the carrier phase observable is ambiguous by an integer number of cycles respective wavelengths. Since phase observations are used for precise position processing applications getting access to these integer valued ambiguities is of very significant importance not only for position accuracy but also for processing performance (since ambiguity parameters usually cover a high percentage of the unknown variables to be solved in the normal equation system of the procedure). Unfortunately in the zero difference case of the observation equations the integer ambiguity cannot be separated clearly from other terms such as receiver and satellite clock corrections, their corresponding hardware delays and the initial phase shift between the satellite and the receiver. The common approach therefore is to use double differenced ambiguities where these biases have either canceled out or may be neglected. At first the ambiguities are estimated together with all other parameters to retrieve real values for the  $n_{F,kl}^i$  terms in the so called "Float solution" (float since the ambiguity parameters are estimated as float instead of integer numbers). Then one (between receiver) single difference ambiguity is selected as reference (per session, baseline and satellite) and all others are estimated as difference. Note that if there is a loss of lock or any other occurrence where all phase measurements are re-initialized within one session, the session is divided up and an additional reference ambiguity must

be selected for the observation time after the re-initialization [Dach et al., 2015]. However what may differ for various software solutions are the decision criteria for the respective reference ambiguity and, in case of partial ambiguity fixing, the choice of the corresponding subset of ambiguities.

The steps described in the above provide the initial float ambiguity parameters together with the dependencies between each other. The task now is to obtain the integer values of the ambiguities. There is a variety of algorithms from which one can choose, yet for this thesis only two are of significant interest since the TBP uses the Lambda algorithm and Bernese uses the Sigma algorithm. Note that in the following the two algorithms shall not be derived or proven but merely explained in their general approach. The initial system of observation equations (after linearization) is given as following:

$$y = Aa + Bb + e \quad \text{or} \quad (B, A) * \begin{pmatrix} b \\ a \end{pmatrix} - y = v \quad (2.33)$$

where  $y$  is the vector of observed minus computed double differenced carrier phases,  $a$  is the vector containing all ambiguity parameters (hence the unknown integer ambiguities),  $b$  is the vector containing all real valued non-ambiguity parameters (station coordinates, tropospheric refraction etc.),  $A$  and  $B$  are the corresponding design matrices and  $e$  and  $v$  are measurement noise vector respectively residual vector.

#### 2.4.1 Sigma – Algorithm

The Sigma dependent algorithm is described by Dach et al. [2015] and is used by the Bernese GNSS Software. Note that in this description a slightly different nomenclature is used.

Now let  $a_i$  and  $a_j$  be two double differenced ambiguity parameters relative to the same reference ambiguity. Using the corresponding element of the cofactor matrix  $Q_{ii}$  and the square root of the a posteriori variance factor  $\sigma_0$  the a posteriori RMS error  $m_i$  in the initial least-squares adjustment (2.33) is computed for each parameter by:

$$m_i = \sigma_0 \sqrt{Q_{ii}} \quad (2.34)$$

and for the difference  $a_i - a_j$  by:

$$m_{ij} = \sigma_0 \sqrt{Q_{ii} - 2 * Q_{ij} + Q_{jj}} \quad (2.35)$$

The RMS errors of every possible double difference ambiguity  $m_i$  (2.34) and  $m_{ij}$  (2,35) are then sorted in ascending order and within one iteration step the  $N_{max}$  ambiguities with the lowest RMS error are rounded to the nearest integer given the fact that  $m_i < \sigma_{max}$  respectively  $m_{ij} < \sigma_{max}$  and that within the confidence interval  $(a_i - \xi m_i, a_i + \xi m_i)$  respectively  $(a_{ij} - \xi m_{ij}, a_{ij} + \xi m_{ij})$  lies exactly one integer number. The fixed integer values are then introduced in the next iteration step and the procedure restarts for the remaining unresolved ambiguities and their differences. The process is terminated after all ambiguities have been resolved or in one iteration step no additional ambiguity parameter fulfills the statistical criteria stated above. Within the Bernese GNSS Software the parameters  $N_{max}$ ,  $\sigma_{max}$  and  $\xi$  can be set by the user. Note that after the ambiguities are resolved there is no validation procedure (as it is usual after e.g. the Lambda algorithm). In general this procedure can be considered as “cautious” since, if unsure, an ambiguity parameter is rather left as float value than risking fixing it to a wrong integer value.

#### 2.4.2 LAMBDA - Algorithm

LAMBDA stands for Least-squares AMBiguity Decorrelation Adjustment. It is derived and explained in detail in Teunissen [1995] and it has risen to the most common approach for precise and efficient ambiguity estimation within the GNSS community. The overall algorithm can be divided into two main segments: First, the decorrelation and re-ordering of the float ambiguity estimates, second, the actual integer ambiguity search. Note that this section shall only give a brief description of the working principle of the algorithm, for a more detailed description and derivation the reader is referred to Teunissen [1995]. The following procedure is taken from de Jonge and Tiberius [1996], who give a low level description of the implementation of the LAMBDA method. It is shown [Teunissen, 1995] that with a full decorrelation of the ambiguities the integer minimization (or search for integer ambiguities) becomes a simple rounding of the real valued ambiguities to their nearest integer value. Therefore a  $Z$ -transformation yielding  $Q_{\hat{z}} = Z^* Q_{\hat{a}} Z$  is formed by diagonalizing  $Q_{\hat{a}}$ . The initial float ambiguities  $\hat{a}$  are transformed accordingly:  $\hat{z} = Z^* \hat{a}$ . The requirements regarding the  $Z$ -transformation are volume preservation and that the transformation matrix  $Z$  is an integer matrix.  $Z$  can be found, for example, by decomposing  $Q_{\hat{a}}$  using the inverse  $LDL^*$ -decomposition and approximating  $L$  with an integer matrix. The elements of  $D^{-1}$  however can be interpreted as the conditional variances  $d_i^{-1} = \sigma_{\hat{a}_{i+1, \dots, n}}^2$  of the double difference ambiguities. The actual transformation/de-correlation is then performed in sub steps using sequential integer Gauss transformations (which are later on combined to the  $Z$  matrix).

Matrices  $L$  and  $D$  are partitioned as following and a single integer Gauss transformation  $T$  shall be given as:

$$L = \begin{bmatrix} L_{11} & 0 & 0 \\ L_{21} & L_{22} & 0 \\ L_{31} & L_{32} & L_{33} \end{bmatrix}, \quad D = \begin{bmatrix} D_{11} & 0 & 0 \\ 0 & D_{22} & 0 \\ 0 & 0 & D_{33} \end{bmatrix} \text{ and } T = \begin{bmatrix} 1 & 0 \\ \alpha & 1 \end{bmatrix} \quad (2.36)$$

where  $\alpha$  realizes the coefficient for the integer approximation. Since  $T$  is a 2x2 matrix used for de-correlating two consecutive ambiguities ( $i$  and  $i + 1$ ) contained in  $L_{22}$  it is of order 2,  $L_{11}$  is of order  $i - 1$  and  $L_{33}$  is of order  $n - i - 1$  (where  $n$  is the number of ambiguities). The transformation matrix  $Z$  for a single de-correlation step is then given as:

$$Z = \begin{bmatrix} I_{i-1} & 0 & 0 \\ 0 & T & 0 \\ 0 & 0 & I_{n-i-1} \end{bmatrix}; \quad \overline{L}_{32} = \begin{bmatrix} l_{i+2,i} + \alpha l_{i+2,i+1} & l_{i+2,i+1} \\ l_{i+3,i} + \alpha l_{i+3,i+1} & l_{i+3,i+1} \\ \vdots & \vdots \\ l_{n,i} + \alpha l_{n,i+1} & l_{n,i+1} \end{bmatrix}; \quad \overline{L}_{22} = \begin{bmatrix} 1 & 0 \\ l_{i+1,i} + \alpha & 1 \end{bmatrix} \quad (2.37)$$

where  $\overline{L}_{32}$  and  $\overline{L}_{22}$  in (2.37) are the transformed partitions of the corresponding submatrices from (2.36). In an ideal case the choice of  $\alpha = -l_{i+1,i}$  yields full de-correlation but due to the integer constraint  $\alpha = -[l_{i+1,i}]$  (the nearest integer) is used. This results in an absolute value equal to or smaller than 0.5 for every non-diagonal element of  $L$ . Note that any element of (2.36) that is not stated in (2.37) is not affected by the transformation. It can therefore be seen as a column-wise transformation.

Since the actual integer ambiguity search is basically the determination of the estimated integer ambiguity set with the highest likelihood (practically speaking: the valid set of ambiguities with the lowest conditional variances) and the transformation did not flatten the conditional variance spectrum (for a detailed explanation of the latter the reader is referred to [Teunissen, 1995]) the conditional variances within  $D$  are reordered so that the most precise ambiguity is at position  $n$ , meaning that  $d_n \leq \dots \leq d_1$ . With  $d'_{i+1} = d_i + l_{i+1,i}^2 d_{i+1}$ , two conditional variances are interchanged if  $d'_{i+1} < d_{i+1}$ . Alternatingly a de-correlation step and a reordering step are performed, starting from the very last ambiguity the algorithm tries to reach the first one. At each step the interchange criterion is evaluated and if an interchange is executed the process starts again at the very last ambiguity. The algorithm is completed successfully if during one sweep from position  $n$  to position 1 no further interchanges can be performed (yielding the desired sorting of the ambiguity conditional variances and implicitly also the transformation of every element). The final transformation matrix  $Z$  can now be seen as a sequence of partial transformations and permutations combined to one matrix. The actual integer ambiguity search is now performed on

the transformed ambiguities  $\hat{z} = Z^* \hat{a}$ . The innovation in this procedure lies in the efficiency of the search when using the transformed ambiguities (due to the modified conditional variance spectrum). The resulting ambiguity search space is an ellipsoidal region in the  $R^n$ , and for the search within this region there is no standard technique associated with the LAMBDA method, therefore in this context this shall not be discussed in further detail. The search could be performed for example by a sequential conditional least-squares estimation. Within the sought multiple candidates for the integer ambiguity vector are stored and in the end one is chosen by a validation criterion (e.g. maximum likelihood). The definitive vector of estimated integer ambiguities then needs to be retransformed into the initial ambiguity space using the inverse of the computed  $Z$ -transformation.

## 3 Test data, software packages and comparison

The comparison between two data post processing tools is not trivial, especially in the case of GNSS where due to its large community and tens of years of research various approaches exist. One can therefore not simply “click the run button” and expect to get coinciding results up to the millimeter level. The differences can range from the high level aspect, such as processing algorithms, physical corrections and stochastic estimation models on to low level aspects such as data handling routines, programming language, OS, etc. The focus of this thesis however lies on the comparison of the mathematical and scientific approaches between two tools rather than on an implementation aspect.

### 3.1 Software packages

The part of both software packages treated in this thesis is the baseline post processing, the very heart of every GNSS evaluation tool. It includes all important generic features such as atmospheric correction and ambiguity resolution. It is the step between the preprocessor performing the data selection (observation data screening and outlier detection) and preparation (e.g. cycle slip detection) and the network adjustment. The latter one is not performed in this context, yet the preprocessing is necessary. Note that further processing capabilities and an overview over the full spectrum of data processing applications will be given in section 4.8.1 Processing possibilities.

#### 3.1.1 Bernese GNSS Software v. 5.2

##### 3.1.1.1 Introduction

This particular GNSS software of the University of Bern was developed by a purely scientific driven approach. The modules are written in Fortran 90 and it is platform independent due to its usage of PERL as cross-platform scripting language and a C++ GUI from the Qt4 library. Figure 2 shows the Bernese GUI. In the empty middle the different settings pages appear where file names, parameter values and general processing options have to be entered. This interface binds together all underlying scripts and transfers the input parameters to them. Every program module (script) can be run directly from the console without the need of the interface. This also means every Fortran script can be altered by the user. If there is for example a large network processed at once and certain thresholds are exceeded (e.g. Maximum number of simultaneously processed ambiguities)

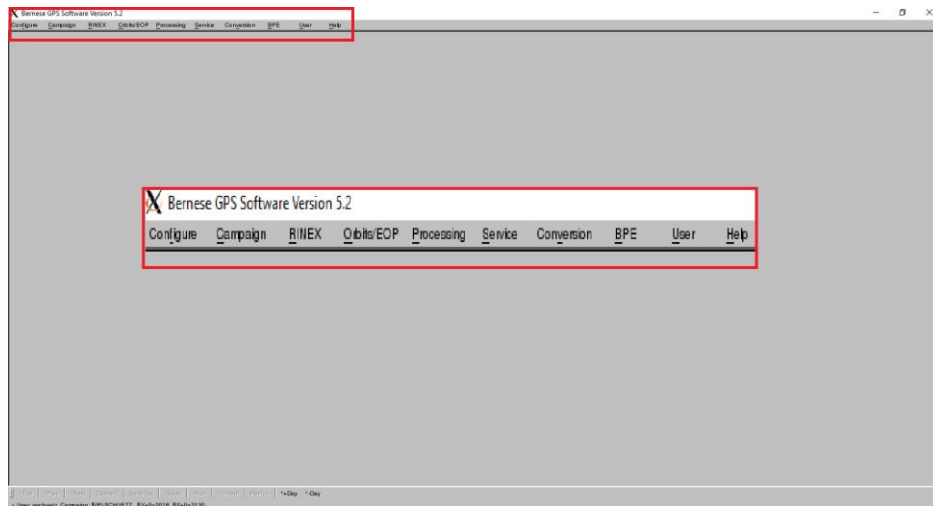


**Figure 2: Bernese default window**

an error message is produced advising the user either to reduce the amount of stations or observations processed at once or to increase the threshold in the respective script. It is even possible to embed self-written scripts. This reason and the fact that nearly every parameter for the actual data processing can be set by the user makes this software so appealing for the scientific community. The impact of single tiny changes on the results can be tested and also problematic data can be investigated from every aspect. Data processing can be tailored to the exact needs of the user, whether it is performance, accuracy or stability of the result over time.

Within Bernese every processing step (read data, clock synchronization, forming baselines, etc) has to be initiated manually in sequence and the corresponding settings have to be specified. This also means implicitly that the success/failure of a specific module holds information about the data properties and problematic data or inadequate processing settings can be pointed out immediately. For large networks however it is possible to automatize this process by a so called PCF (Process Control File), where first a BPE (Bernese Processing Engine) is set up and then the tasks specified in the PCF are worked off sequentially. The settings needed for every program module can be passed to the engine via a dedicated settings page stored in its dedicated directory or through declaring them in a Perl script wrapped around the actual program call (i.e. the BPE is hosting the PCF, the PCF calls the Perl script which contains the input/settings for the Bernese program(s) and the Perl script can call multiple Bernese programs sequentially). Every desired processing chain can therefore be implemented by the user with own preferred settings. Also every program produces a specific output file with general information about input and output parameters, settings summary and final results. The degree of output can be specified so far that also intermediate results e.g. from every iteration step of a certain process are shown in the report file.

## 3.1.1.2 Processing chain

The general processing chain for the Bernese GNSS Software used within this thesis is shown in figure 3. Note that for some procedures several possible processing chains exist, the one(s) chosen are the approaches recommended by the user manual and tutorial.

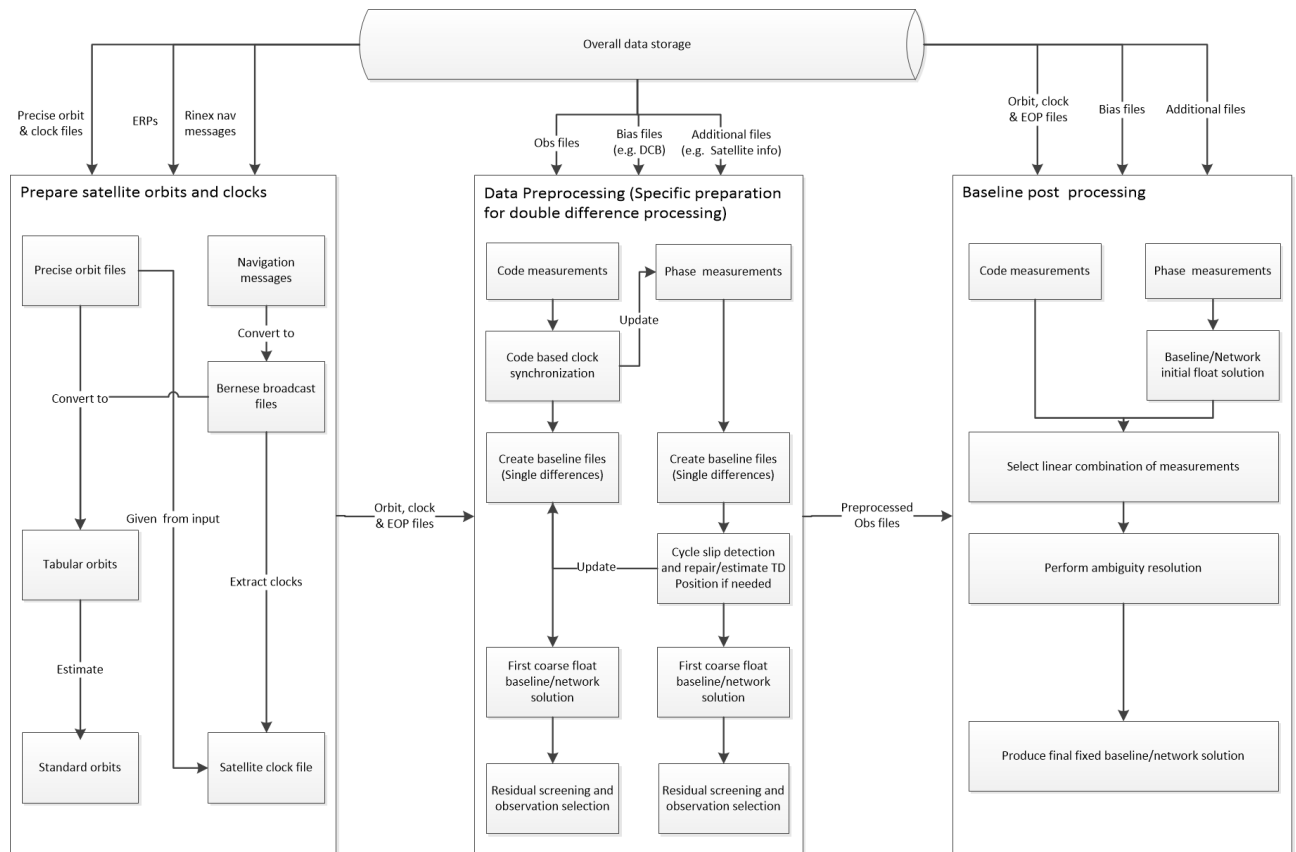


Figure 3: Bernese Processing Chain

Note that for reasons of simplicity the ERP processing part for the orbit determination is not mentioned here.

At first it is necessary to produce valid orbits which can be acquired from either precise orbits (e.g. from the IGS) or directly from the broadcast navigation message of the satellites. Within the conversion (transformation from earth-fixed to inertial frame) to “Tabular orbits” (program PRETAB for precise and BRDTAB for broadcast orbits) the satellite clock information needs to be extracted from the files. Within the experiments of this thesis in the case of precise orbits also precise clock files from the IGS were used. The final step is the generation of standard orbits (program ORBGEN). This step includes the actual estimation of the orbits used for processing later on. It allows the user to set specifics about the interpolation, arc numbers, parameters regarding single satellites etc. The actual settings used for the experiments will be stated in chapter 3.2.2.

After generating the orbits the data preprocessing may begin. While reading the RINEX data files into Bernese (reading and converting the RINEX files into Bernese format, one observation for

code and one for phase measurement data; program RXOBV3), if not existing, a “Station Coordinate File” is produced. Prior to this a “Station Information File” and an “Abbreviation table” has to be generated based on the RINEX observation files (program RNX2STA). The first file stores the station coordinates with a flag indicating the source, respective the assumed quality of the coordinate. The second one stores all additional information about the station such as antenna eccentricities, antenna type, receiver type, etc. The abbreviation table merely stores the link between the full station name and its given abbreviation within further processing.

The first step of the actual processing then is the “Code based Clock Synchronization” (program CODSPP). This has to be done in order to synchronize the receivers of all stations to GPS (or whatever satellite system is desired) time to provide a consistent basis for all further processing and to account for millisecond jumps of the receiver. Also for PPP or in general to coarsely confirm the station position the coordinates can be estimated during this process. Note that only code measurements are used within this procedure so the resulting coordinates are very inaccurate. The resulting clock corrections are then stored in both the phase and the code measurement files in case later on only phase measurements are used. Note that the quality of the orbit files, satellite clocks and differential code bias input files have a drastic impact on the result. First ionospheric and tropospheric corrections can be applied to the measurements, where the user can set his preferred correction model. Also within this program, observations for which no receiver clock correction could be estimated are flagged in both file types and on demand code outliers can be flagged in both file types, too. Flagged observations in general are not used in any analysis program.

Creating the baseline files afterwards (program SNGDIF) is then simply forming single (between receiver) differences between a pair of stations and storing them in a new “Single difference Observation File”, again of these files for code and one for phase measurements.

The next step is the phase preprocessing (program MAUPRP). The main task here is to flag observations at low elevations (below the elevation cutoff angle), small pieces of observations (significantly fractioned observations) and most important observations where a cycle slip occurred. Again it is possible to introduce a priori atmospheric corrections for which the user can set his preferred model. Also initial ambiguities are set up in this procedure. The cycle slip detection is based on the principle of triple differencing as explained in section 2.1.3. The initial single difference observation files are then updated with the modifications done by the phase preprocessing. Using the resulting difference files a first baseline/network solution is now produced (program GPSEST). Usually for this very first estimation only phase data is processed with the ionosphere linear combination in a rudimentary estimation with no higher order ionosphere correction or ambiguity estimation. Tropospheric corrections should be applied a priori and also estimated within the process. The biggest interest of this estimation lies in generating the residuals

of the observations which are then screened to detect large outliers (program RESRMS). The screening process then again flags the observations (program SATMRK) identified as outliers in the single difference files. The initial estimation (GPSEST) and the residual screening (RESRMS + SATMRK) are repeated until only clean observations remain. Dismissing a large number of observations in this process is usually a sign for unaccounted problems in the data or severely false input parameters. Therefore this procedure is mainly used to determine problematic stations (or satellites despite being not mentioned in the satellite problem file).

After finishing the preprocessing at first a float solution of the baselines/network is produced. Therefore the same estimation as before the residual screening is performed but this time with only clean observations (GPSEST). The ambiguities are specified by a real valued number and initial tropospheric corrections and coordinates are estimated as starting point for the ambiguity resolution. The following selection of the linear combination then depends on the baseline length primarily, (program BASLST), the available correction data (ionospheric corrections for Wide Lane, DCBs for Melbourne-Wübbena) and the availability of high quality code measurements (the latter selections have to be made by the user). The ambiguity resolution strategy has to be chosen accordingly, though for most applications the sigma dependent algorithm is used since it is the most reliable (exclusively used in the experiments). The actual ambiguity resolution is then performed by running the estimation program (GPSEST) once for each baseline and linear combination/ambiguity type. The actual settings will be discussed in detail in section 3.2.2. The final pass of GPSEST for each baseline then provides the estimated rover coordinates with fixed ambiguities, i.e. the fixed baseline with atmospheric corrections estimated for both stations. The actual pure baseline post-processing is finished after this step. A final network solution can be produced by running GPSEST again with all stations/observations at once instead of only one baseline at a time. Note that within the scope of this thesis this last step is not done anymore since it is not part of the actual baseline processing.

## 3.1.2 Trimble Baseline Processor

### 3.1.2.1 Introduction

This particular software is embedded into the office suite of Trimble, the “Trimble Business Center”. The implementation of the processing modules is done object oriented in C++. The GUI is provided by C# using a C++ interface to access the C++ processing libraries to enable a high level design with also high performance capabilities. The processing modules are highly optimized for performance, i.e. in the case of baseline post-processing every available CPU receives one baseline to process at a time. Figure 4 shows the basic GUI of the software after loading a small network. The office suite was developed for commercial purposes and originated in the USA.

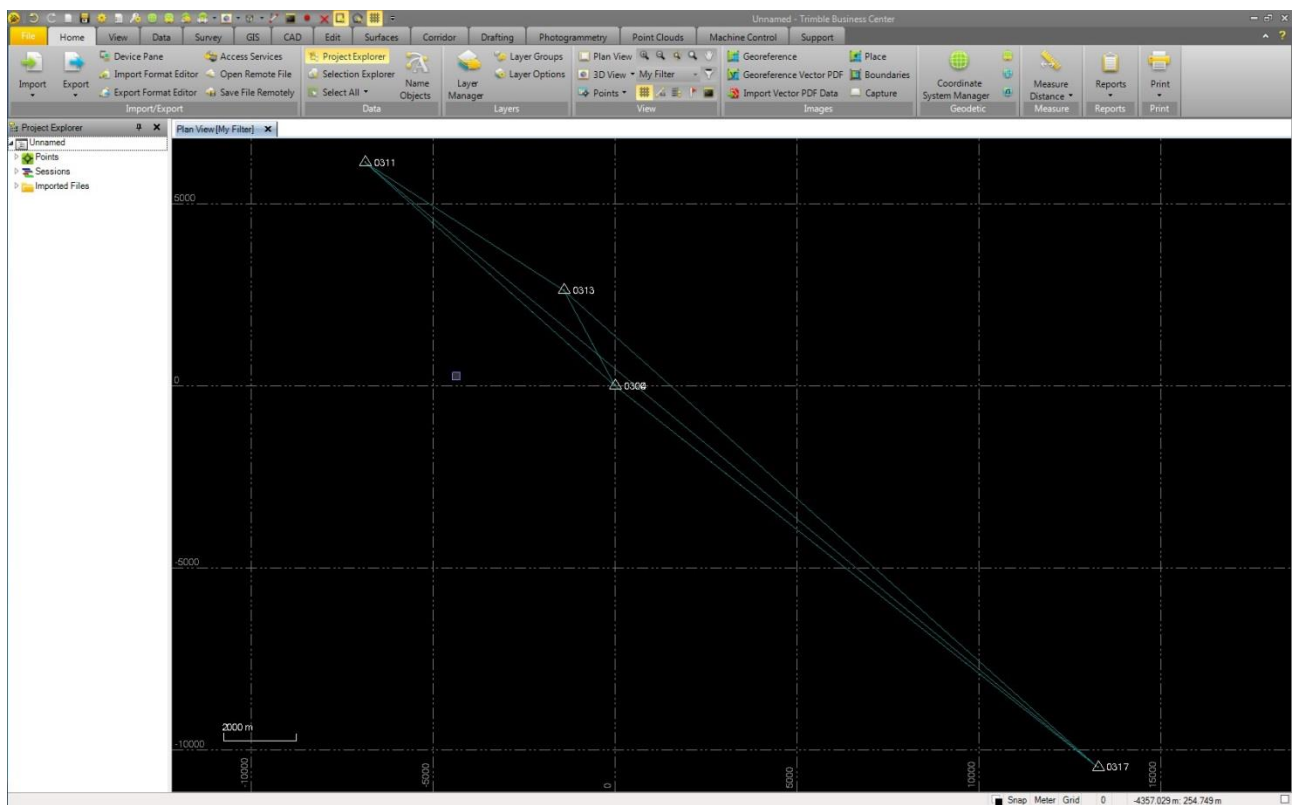


**Figure 4: Default view for current project**

The GUI gives a graphic representation of the current measurement project and its design and usage is similar to classic CAD applications. Supported file types may be imported by drag and drop or the explorer. Information about specific objects inside the project (in this case: points and baselines) can be accessed by right-clicking on the element in the grid view. Figure 5 shows the property window for one selected baseline. If not at hand, precise ephemeris files from the IGS can be added to the project by an embedded download application. The actual processing can now be

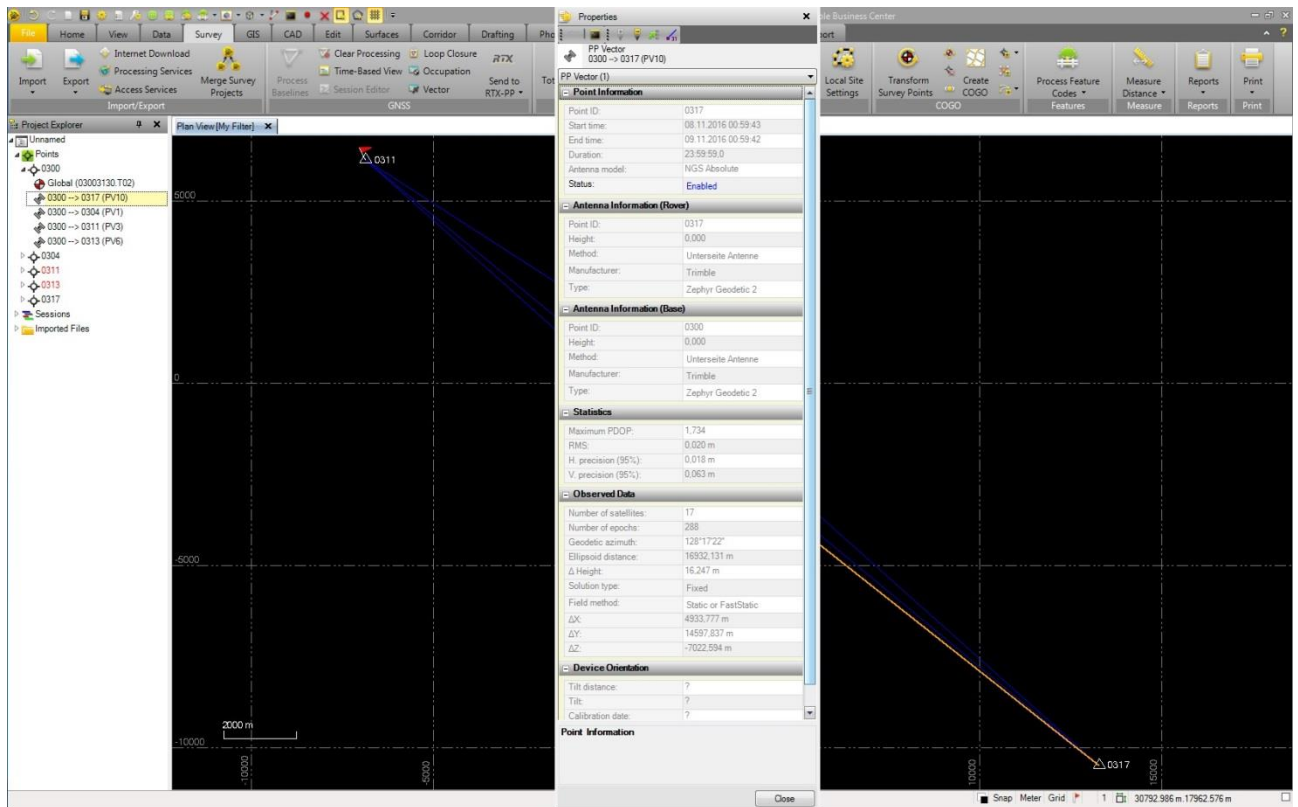


**Figure 5: Baseline/Vector property window**

done by one click on a button, if set to adaptive processing mode. In this mode only very general settings regarding the processing were possible, such as ephemeris type selection, satellite system selection (actually single satellite selection) etc. By default all baselines within the project are selected (every possible connection between two sites), yet the user can also select a subset of BL manually. Every processing step (receiver clock synchronization, phase preprocessing, etc) is done automatically as black box when starting the application. Every processing related setting is adjusted to the data set internally (e.g. thresholds for outlier detection) and processing procedures (e.g. linear combination of measurements) are predefined with respect to certain criteria. The basic idea behind this design is to keep the processing as effortless as possible and at the same time enable unexperienced or unprofessional users to have access to high quality processing results. These are (amongst others) the reasons this software is so popular among commercial users. When using the scientific mode however additional settings become accessible which allow the user a much more sophisticated impact on the processing. Options regarding linear combinations, troposphere model and statistical boundaries for ambiguity resolution can be set (the settings will be discussed in detail in section 3). The complete processing however is still done at once and initiated by one click on a button and intermediate results are not accessible. Nevertheless a very detailed high level report can be generated at the end containing information for example about processing results baseline by baseline, a satellite tracking plot, residual plots for each included satellite, etc.

## 3.1.2.2 Processing chain

Figure 6 shows the basic processing chain of the TBP. In its basic features it is very similar to the Bernese GNSS Software, the architecture of the process structures however is quite different.

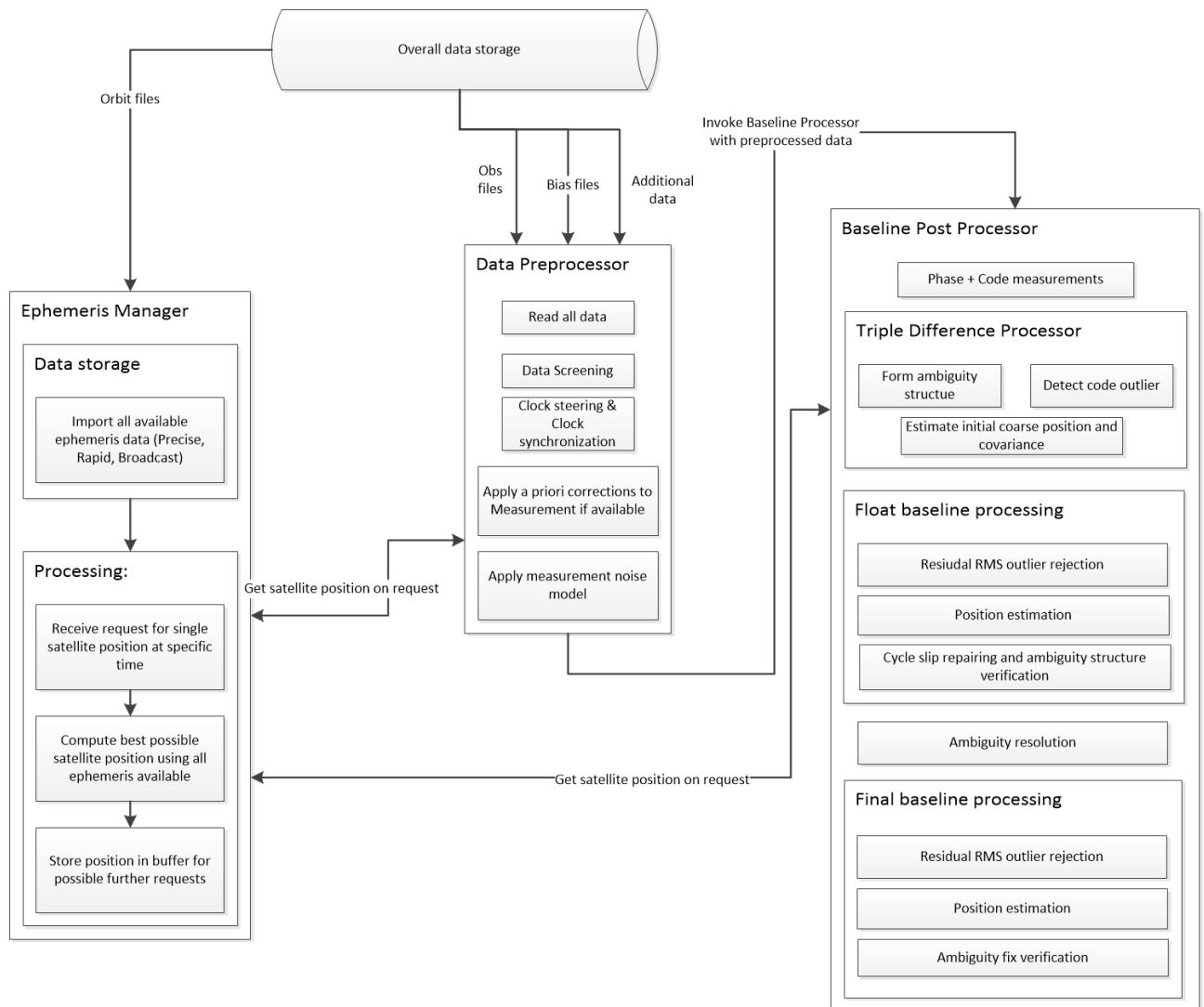


Figure 6: TBP Processing Chain

The processing starts with invoking a data preprocessor, if observation data is available. This module handles every data preparation task. The preprocessor first reads all observation files and checks specific installed data folders for bias files (e.g. Differential code biases, Ocean tide loading or Earth orientation parameter). If existing, the bias file is imported and used in further processing. A data screening for outliers is performed at the zero difference level. Next up the clock synchronization is performed to synchronize the receiver time with GPS time and if millisecond jumps are detected a software clock steering is applied to the observation data. Therefore satellite positions are needed. For every epoch where observation data is available a SV position is requested from the Ephemeris Manager. At the very beginning of the processing this module reads

in all available ephemeris data (even when precise orbits are available broadcast ephemeris are read and evaluated). On request, the module then computes the best available position and velocity vector for every SV on the fly and returns it to the preprocessor. The results are stored in a buffer to increase performance for further requests. During the clock synchronization and the clock steering also the SV state (position and velocity) assigned to the epoch is refined. This means, in the case of a clock jump for example, an initial SV state is received from the Ephemeris Manager. The receiver clock is then synchronized to GPS time and the clock steering is performed. If a clock jump is detected now the receiver time of reception (in GPS time) gets updated and another set of SV states are requested for the corrected timestamp. The preprocessor then continues by applying a priori corrections to the measurement (including atmospheric corrections, antenna corrections, observation noise model and corrections from bias files).

Using the prepared data a Baseline Postprocessor module is invoked. Both phase and code measurements are used and given to the Triple Difference Processor, which for the phase observation performs the cycle slip detection where also the initial ambiguities are set and for the code observations executes an outlier detection. Within Bernese the cycle slip detection is performed in the same style but still considered as part of the preprocessing (though the preceding tasks performed before the cycle slip detection more or less coincide). An initial coarse position and covariance at triple difference level is estimated and given to the float baseline post processing.

Initially outliers are removed. The RMS of the triple difference residuals is computed and used as a threshold to detect large residuals (though not particularly used for triple differences in the Bernese software standard processing, the outlier detection based on residuals follows the same principle but the thresholds may be set by the user). Afterwards the initial position and float ambiguities are estimated, upon which the ambiguity structure is verified and cycle slips are repaired (e.g. success probability tests to detect actual cycle slips within outliers) and the ambiguity resolution can be executed.

The final fixed baseline processing then starts with another residual screening respective RMS outlier detection (this is not done in Bernese since the residuals are considered "clean" when computing the float solution). The fixed rover coordinates are then estimated and as a last step the ambiguity fix is verified (this is again done by stochastic hypothesis tests).

The overall procedure and data flow in both software tools is quite similar however one has to remember that this is the commonly established approach for baseline post-processing.

### 3.1.3 Baseline length dependent settings

For processing and ambiguity resolution the baseline length is the most important aspect regarding the settings. Since for example for small baselines up to 20 kilometers the impact of the troposphere (given no large height difference between base and rover station or significant local climate or weather differences) on the measurements can be seen as nearly equal for both stations. This is also true for the ionosphere, since the signal paths from one satellite to both receivers are very close the ionospheric pierce point for both signals becomes nearly identical. This means regarding between-receiver differences (single or double) the correction terms nearly cancel out since for each separate signal the delay has approximately the same value and sign. Note that the atmospheric corrections still have to be modeled or accounted for in order to estimate a proper value for the signal delay. Yet an a priori model can be sufficient. Given no specific local obstacles in line of sight for both antennas this also means that both stations observe every satellite nearly the same amount of time within a session (given equal technical and tracking capabilities). In this very advantageous case it is therefore possible (though not necessary) to determine the L1 and L2 integer ambiguities directly without the usage of special linear combinations of measurements and also perform the final processing/coordinate estimation directly from the original frequencies.

With an increasing length of baselines this approach is not valid anymore. Starting somewhere from 20 to 40 kilometers length up to about 200 kilometers the influence of atmospheric delays and biases becomes significantly different for both observation sites. Also with an increasing distance between two stations the timespans and amount of simultaneously observed satellites decreases. The atmospheric delays have to be modeled and estimated separately for each site. This means, plainly speaking, that the number of parameters to be determined increases while the number of measurements decreases. Within this range of baseline lengths it is common practice to use the Wide-Lane linear combination to estimate the Wide-Lane ambiguities first, and then determine the Narrow-Lane ambiguities and furthermore the fixed baseline coordinates by applying the Ionosphere-free linear combination, yet this approach is not exclusively limited to this baseline length interval. Shorter baselines can be processed this way without any problem. For longer baselines it is rather difficult. Every combination of measurements respective pairing of satellite signals brings changes with it regarding measurement noise vulnerability and, due to the frequency dependency, the ionospheric refraction. As an example table 1 shows the coarse initial signal noise of the different GPS signals of L1 and table 2 shows the wavelength of the different linear combinations, their initial signal noise and the impact of the ionospheric refraction with respect to the original GPS L1 carrier where both basic carriers L1 and L2 are considered equally accurate

and uncorrelated. Note that the noise factor of  $L_6$ , the Melbourne-Wübbena linear combination refers to the noise of the P code on  $L_1$  and not the phase noise.

**Table 1: Signal noise in range of GPS  $L_1$**

Range	Noise
Code range (C/A-code)	10–300 cm
Code range (P-code)	10–30 cm
Phase range	0.2–5 mm

**Table 2: Noise and ionosphere of LCs w.r.t. original  $L_1$ , GPS**

LC	Description	Wavelength in cm	Noise rel to $L_1$	Ionosphere rel to $L_1$
$L_1$	Basic carrier	19	1.0	1.0
$L_2$	Basic carrier	24	1.0	1.6
$L_3$	Ionosphere-free LC	0	3.0	0.0
$L_4$	Geometry-free LC	$\infty$	1.4	0.6
$L_5$	Wide-lane LC	86	5.7	1.3
$L_6$	Melbourne-Wübbena LC	86	0.7	0.0

Therefore when using the Wide-Lane LC proper ionospheric corrections become crucial (as stated in section 2.2.2 the ionospheric refraction causes a minimum range delay of about 10 meters) since the increased phase noise is still far smaller than the impact of the ionosphere. However, in theory there is no baseline length limit for using the Wide-Lane LC when a precise enough ionosphere model is available.

Due to the lack of such precise ionosphere models with global coverage, usually for baselines above the aforementioned 200 kilometers the Melbourne-Wübbena LC is used since it eliminates the ionosphere and geometry completely and also provides estimates for the Wide-Lane ambiguities. Unfortunately this LC suffers from a very high measurement noise due to the usage of code observations. When no or only bad quality code measurements are available this LC is not applicable. In theory however there is no upper baseline length limit, simply when two stations do not observe enough satellites simultaneously anymore.

The other aspect with regard to the baseline length is the occupation timespan and the observation sampling rate. When processing baselines smaller than 20 kilometers several minutes of observations with a sampling rate of 1 second can be enough to produce a fixed solution. An increase in the observation timespan always comes with an improvement of the result. For long baselines (several thousand kilometers) this is even more crucial since the amount of simultaneously observed satellites is in general very low. In extreme cases for very long baselines even timespans where no satellite was observed by both sites are possible. It is therefore necessary to set a long enough observation session. Yet when processing longer timespans (several hours up to several days) the sampling rate may be decreased in order to speed up

processing, even for very long baselines. Given for example a medium baseline of about 100 kilometers and an occupation timespan of 1 day, an observation data sampling of 30 seconds is sufficient.

Yet there are no exact rules when to use a certain LC or minimum observation timespan, therefore implementations and recommendations can differ between software solutions from different manufacturers. Figure 7 shows the selection criteria within the Trimble Baseline processor and table 3 the recommendations in the Bernese User Manual.

## Processing mode

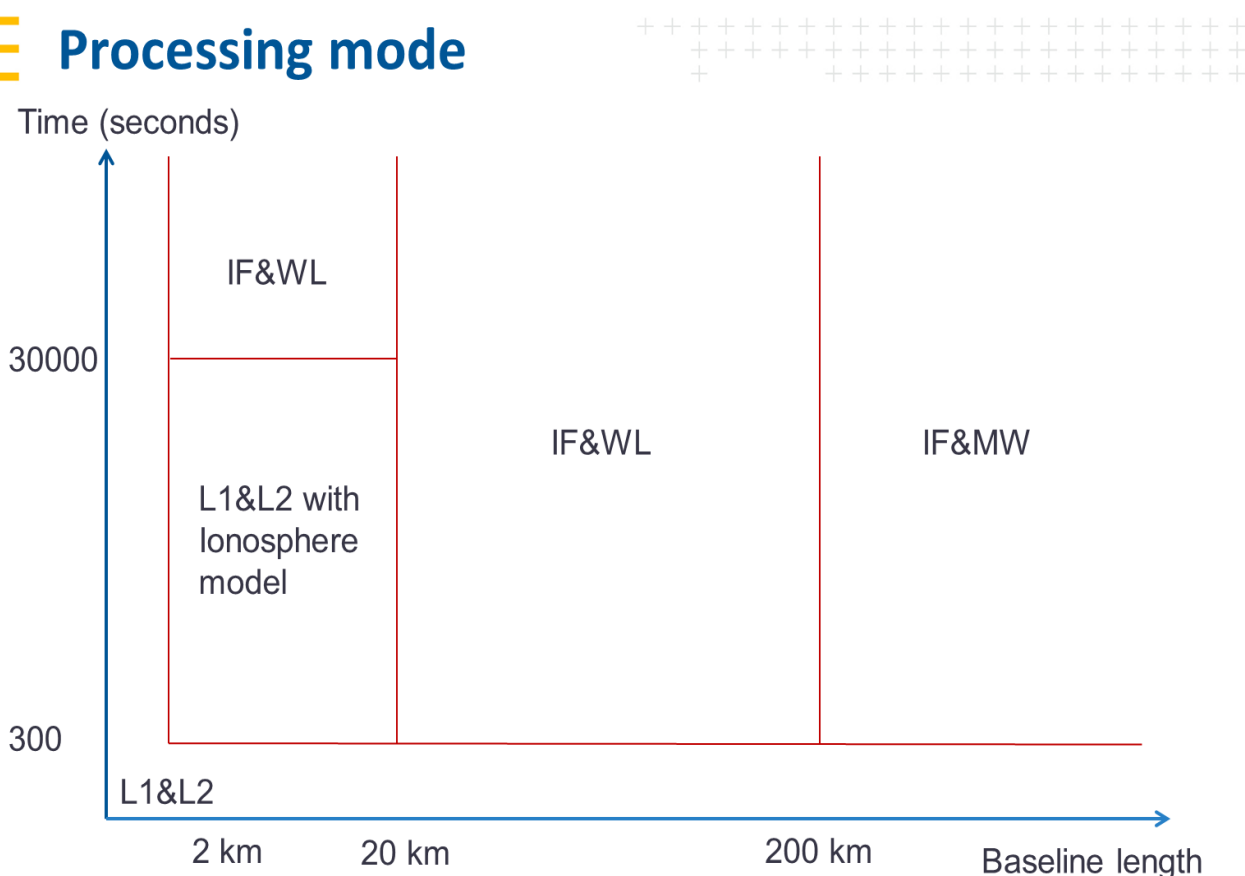


Figure 7: Linear combination selection TBP

Note that table 3 shows only an extract of the original table in the Bernese user manual since it also contains information about specific Bernese settings. Also note that the QIF, Quasi-Ionosphere-Free algorithm only needs to be used when processing long baselines without high quality P-code. The expected ambiguity resolution rate for this procedure lies at approximately 40% and it is not considered in this thesis since also the Trimble Baseline Processor has no equivalent strategy. Furthermore there is no ambiguity resolution algorithm assigned to the LCs in figure 7 since the TBP solely features the LAMBDA strategy. Also the area below and on the left of the red lines in figure 7 means ambiguities are resolved using L1&L2 original frequencies, however with increasing length the solutions will be forced to float and no ambiguity resolution will be

**Table 3: Linear combination selection Bernese**

Baseline length	Occupation time	P code obs. available	Ambi. Res. Strategy
20 - 40 km	> 1 Hour	No	L1&L2, L1, L2 (SIGMA)
< 10 km	> 1 Minute	No	L1&L2, L1 (SEARCH)
< 200 km	> 2 Hours	No	- L5 (SIGMA) - L3 (SIGMA)
< 6000 km	> 8 Hours	Yes	- L6 (SIGMA) - L3 (SIGMA)
< 2000 km	> 8 Hours	No	- L1&L2 (QIF)

performed. The abbreviations IF, WL and MW correspond to L3, L5 and L6 in the case of Bernese. The actual selection criteria from Bernese are very similar to those of the TBP regarding baseline length, for example the upper bound for the Wide-Lane LC and beyond the usage of Melbourne-Wübbena. The recommended threshold for L1&L2 processing for Bernese lies at 40 km where in the TBP it is set to 20 km by default. These thresholds (in the case of short to medium baselines) are not fix, so that even smaller baselines (down to 2 km) can also be processed e.g. the Wide-Lane LC. This is done for example in the TBP, where for short baselines (2-20 km) L1&L2 is replaced by IF&WL (respective L5L3) for occupation timespans longer than 8 hours and 20 minutes. The reason behind this is the ambiguity resolution becoming easier and the solution becoming more stable since for long observation timespans the data sampling rate is decreased (usually to 30 seconds as long as enough observations are available). In this scenario the IF&WL outperforms the direct L1&L2 approach.

Another aspect is the troposphere correction estimation. For the second strategy in table 3 (< 10 km) the Bernese manual recommends to not estimate troposphere at all, only to apply an a priori model. Within the TBP only for baselines up to 1 km no tropospheric correction is estimated (and for occupation timespans below 45 minutes despite the BL length) and solely the a priori model is applied. This is done since proximity of two stations and very short observation timespans render the troposphere estimation instable. For close stations (of course without significant height difference) the tropospheric refraction is close to equal for both as stated earlier. When introducing site specific troposphere parameters both stations are incorrectly treated as independent and due to local circumstances and observations used the result of the estimation will differ introducing an improper bias. For baselines longer than approximately 20 km or significant height differences an additional estimation to the a priori correction model is necessary. Within the Bernese GNSS Software one can choose between no a priori model, solely the a priori model and a priori model plus estimating site specific parameters. The TBP however per default sets the tropospheric correction with respect to the BL length where up to 1 km only the a priori model is used, from 2 to

50 km a relative tropospheric correction is estimated and from 50 km on site specific troposphere parameters are computed. This relative troposphere, as the name implies, states the difference of the tropospheric influence between the two sites rather than treating both stations independently. It is therefore a tradeoff resulting in the assumption that both stations do not underlie the same impact on the GNSS signals (where no estimation is needed since the effect cancels out) but at the same time are not completely independent with respect to said part of the atmosphere. This relative approach however is not available in Bernese.

Another aspect is the data sampling rate. For short baselines where the minimum occupation time is declared as several minutes, a data sampling of at least 1 second is necessary to produce reliable results, otherwise too few observations are available and the normal equation system becomes ill conditioned. For medium baselines according to the Bernese manual 2 hours for processing in with WL is needed. Depending on the quality of the observations a reduced sampling of 30 seconds already gives acceptable results. For observation timespans significantly longer a 30 second sampling is sufficient. A wider time interval than 30 seconds is in general not recommended since, the influence of bad observations (if not detected) increases and the overall redundancy of the estimation decreases. The solution again becomes ill conditioned. For very long baselines at least 8 hours of data are recommended, yet however such long baselines usually are processed using sessions with a length of at least one whole day. The sampling rate then again can be set to 30 seconds without compromising the result.

Figure 7 states that the TBP forms linear combinations of arbitrary baseline lengths when at least 5 minutes of data is available. This however does not mean that this is the required minimum occupation time for reliable results but simply the minimum threshold for the ambiguity resolution to be executed. For long baselines the processor will also for a longer timespan straightly go to a float solution if not enough observations are available.

### 3.2 Comparison

Given the processing chains of the two software suites and the various baseline length dependent processing modes a reasonable comparison shall now be elaborated. At first the basic idea of the comparison shall be declared. Next some criteria have to be established in order to verify the comparability of the results. Upon generating such results then several data processing scenarios shall be carried out in order to assess the performance, from which the results finally are evaluated by a Matlab toolbox.

#### 3.2.1 Principle

The very results used for comparison of course are the final coordinates estimated by both software suites. In theory, two software tools using the same methods to perform the same tasks, using the same data as input and corrections and are given the same settings should provide the same results. Since aspects regarding implementation (coding language, variable declaration, OS) cannot be examined properly there is however no sense in purely comparing the result from one GNSS tool with the other. For this reason the main aspect of the comparison is the difference of the estimated coordinates to reference coordinates. Surely, this again depends on from which source the reference is from and what software was used to generate it, but in general the long term average character of reference coordinates yields a stable form of comparison. The analysis is therefore done by establishing comparable results which are then evaluated regarding their difference from reference coordinates, their a posteriori sigmas and the success of the ambiguity resolution.

This is repeated for several specific processing scenarios/tasks which aim to cover the most frequently performed procedures and core functions of the two packages. This includes different processing settings and mainly different input data w.r.t. baseline length and occupation time. Due to its purpose, the Bernese GNSS software is optimal for processing medium to long baselines, using long observation time spans and even multisession processing w.r.t. the repeatability of the results. The TBP however, again due to its use cases, was initially optimized for short to medium baselines and also reduced occupation timespans but is now at full capability for both arbitrary baseline lengths and occupation timespans. This and the aforementioned baseline length dependent settings declare the necessity of a wide spread test data set in order to cover all possible scenarios of station networks, namely short BL from 0 to approximately 25 kilometers, 25 to 200 kilometers and longer 200 up to several thousands of kilometers. This however will be discussed in detail in section 3.2.3 and section 3.3.

### 3.2.2 Requirements for comparable results

In order to acquire inter software comparable results respective results generated on the same basis, the very first aspect is to provide input data from one hand. Therefore the test data taken from the Trimble archive (stored as t02 format) was converted into RINEX to guarantee the same data source. Also correction data such as for example antenna phase center corrections need to origin from the same source or have to be at the same level of precision (For example IGS and CODE orbit products). An overview over the used additional data is given in section 3.3.4.

Since the functionalities of the TBP shall be evaluated w.r.t. to the Bernese GNSS software, the approach for comparable results here is to adjust the Bernese settings in a way that they mirror the TBP as closely as possible. For the high level decisions such as for example LC selection this means that the thresholds from the TBP are also used in Bernese etc. On the low level this is rather difficult to fulfill. Since the settings as well as the results of the preprocessing are only vaguely accessible the focus within the Bernese GNSS software lies in preparing the data as precisely as possible.

The possible settings for the processing within the TBP are given in figure 8, 9, 10 and 11. Note that the following shall only review the relevant settings which can also be set in Bernese (The menu point “Quality” sets user defined thresholds for warnings regarding the coordinate accuracy).

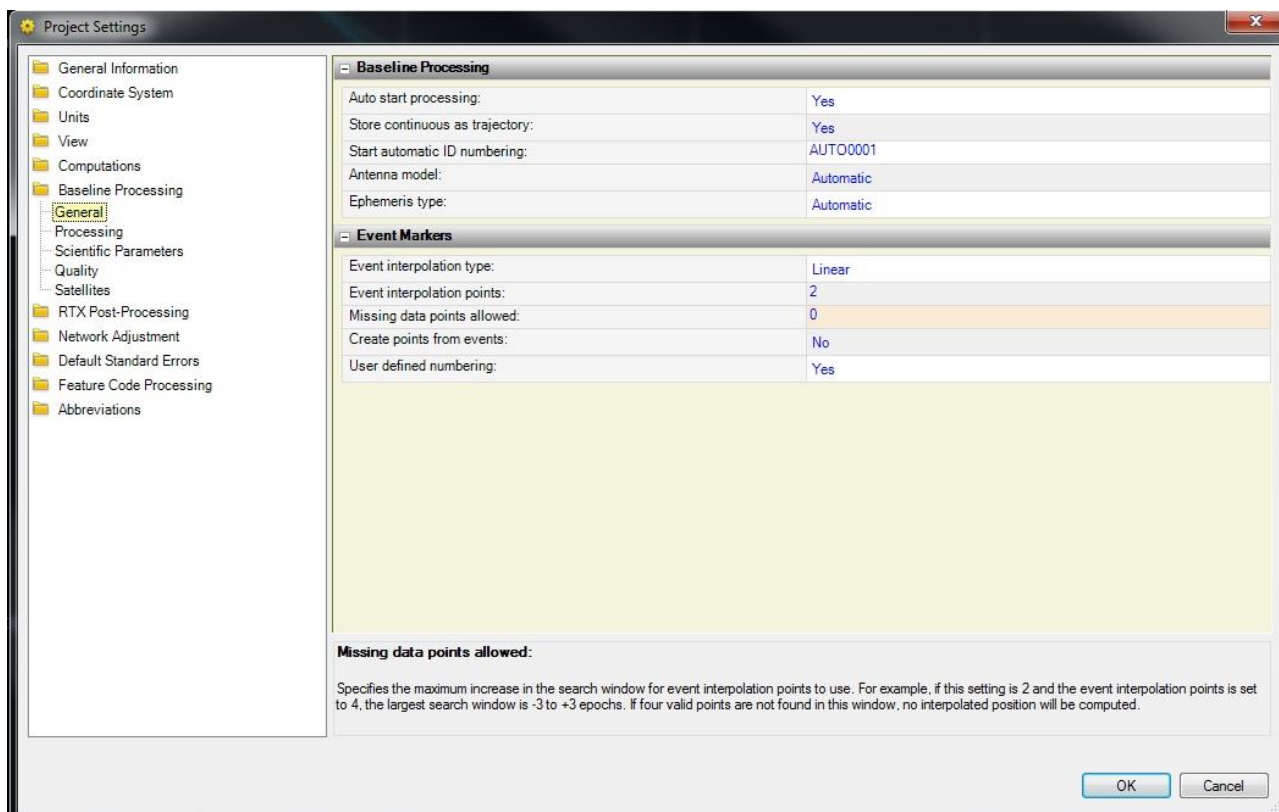


Figure 8: TBP general settings

The settings “Antenna Model” and “Ephemeris Type” in figure 8 can be set implicitly in the Bernese GNSS Software. “Antenna Model” refers to the usage of an IGS or NGS antenna model file (which are both included in the installation of TBC) which can also be selected in Bernese. “Automatic” sets the model to NGS. With “Ephemeris type” the user can choose between IGS precise Orbits (ultra-rapid, rapid and final) and broadcast ephemeris. This can be done in Bernese by generating standard orbits from either the navigation message for broadcast orbits or also IGS or CODE products for precise orbits. Note that there is no difference in the quality of the orbits of the IGS and CODE. The actual orbit file and antenna file has to be specified in Bernese in the programs CODSP, MAUPRP and GPSEST (in the scope of this thesis).

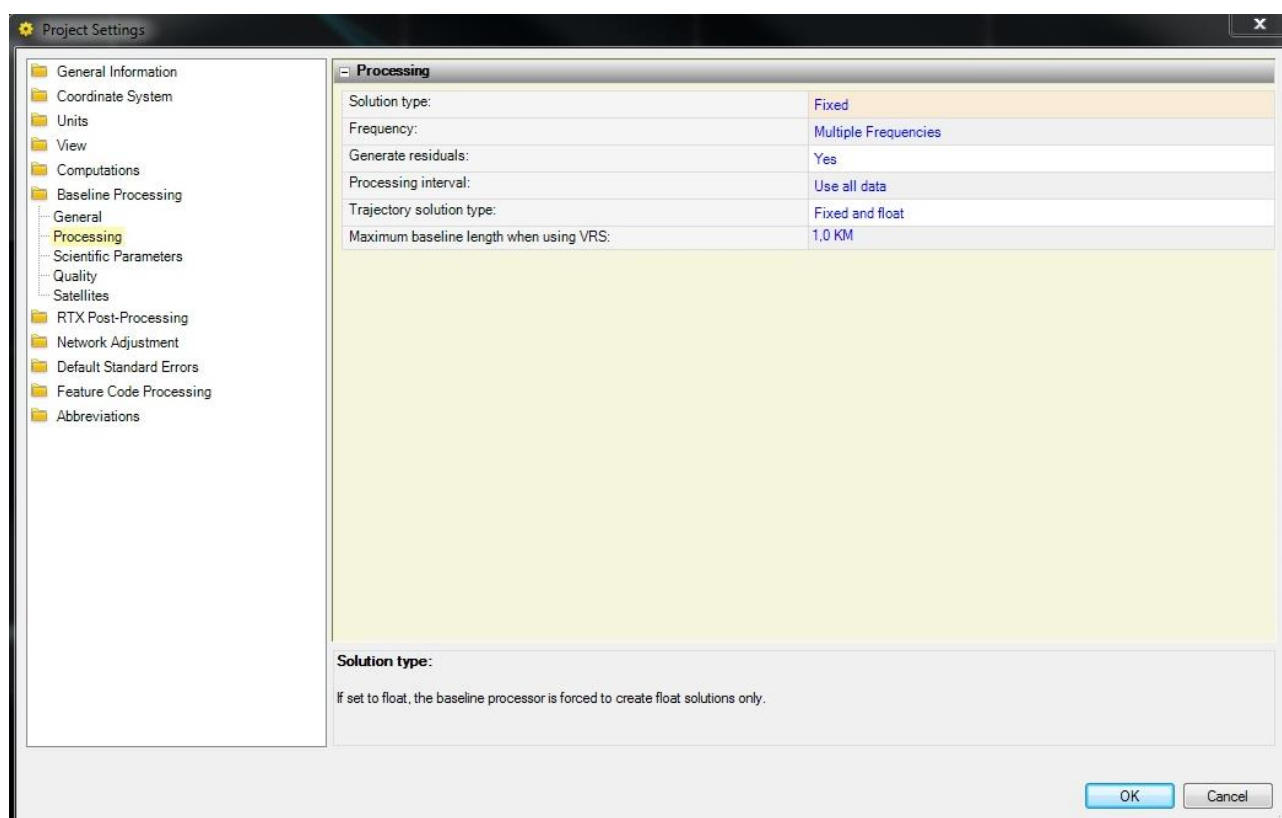


Figure 9: TBP processing settings

The settings from figure 9 are also transferrable to Bernese, however with again a little finesse. “Solution type Fixed” implies that an ambiguity resolution has to be performed w.r.t. the baseline length and observation data available (discussed in detail in section 3.2.3.1). Setting this point to “Float” would be equivalent to processing a baseline in Bernese using GPSEST and the setting “NONE” for “Resolution strategy” at panel 3.2. “Frequency” however does not translate directly into the Bernese scope since in TBC this point only allows you which original frequency(ies) to use, not however already LCs as the setting “Frequency” in panel 3.1 of GPSEST. “Generate residuals” is equivalent to specifying a “Residuals” file in panel 2.1 of GPSEST, meaning that residuals are written to files for further usage. “Processing Interval” corresponds to “Sampling interval” in panel 3.1 of GPSEST and specifies the data sampling used for processing (also affects the residuals).

The settings from figure 10 correspond to “Satellite system” and “Elevation cutoff angle” from panel 3.1 of GPSEST. Yet when importing observation data using RXOBV3 in Bernese also data sampling and satellite system have to be selected. Therefore when not importing all relevant data into Bernese these settings become futile. Note that also the special single satellite selection displayed in figure 10 can be realized in Bernese by adding “bad data” flags to a certain satellite in the satellite problem file (resulting in the exclusion of all observations regarding this SV).

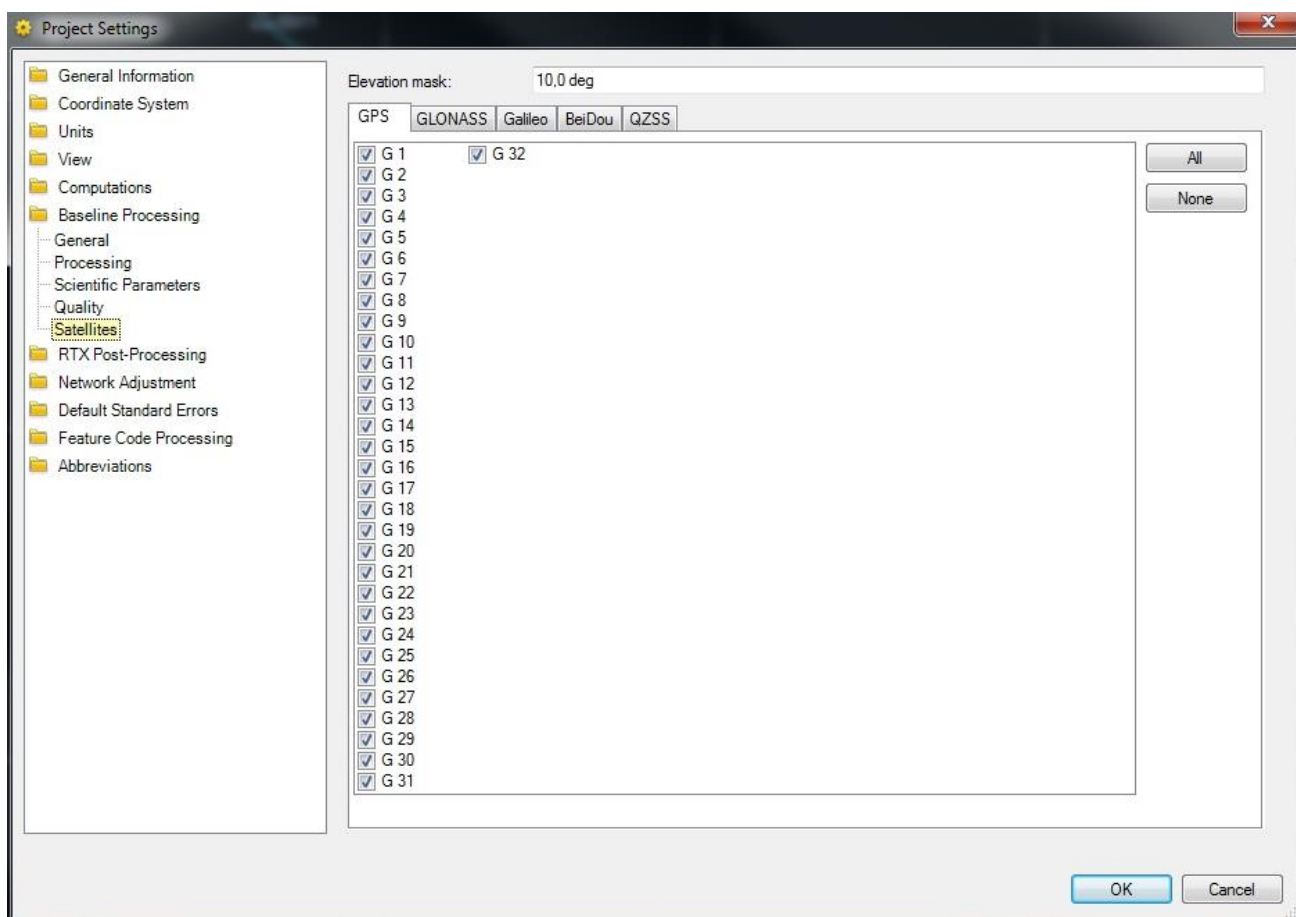


Figure 10: TBP satellite settings

The settings specified in figure 11 now establish the more relevant settings to this thesis. The “Linear combination control” corresponds to the setting “Frequency” in panel 3.1 of GPSEST (only TBC does not offer the Geometry free LC since it is not relevant in this scope), yet “Frequency” in figure 9 has to be set to multiple in order to enable all original frequencies. “Use code for position estimation” can be done in Bernese by specifying code files in GPSEST. “GLONASS carrier bias calibration” estimates the inter frequency bias of GLONASS phase observables regarding the receiver. An equivalent setting in Bernese is “Resolution between different frequency channels” in panel 3.2.2 in GPSEST. The settings regarding the ambiguity resolution however declare the thresholds for the hypothesis tests of the ambiguity sets. The “Partial contrast threshold” and “Contrast threshold” confer to the so called minimum success rate and relate to the ambiguity subset respective the overall ambiguities. This is very specific to the ambiguity resolution

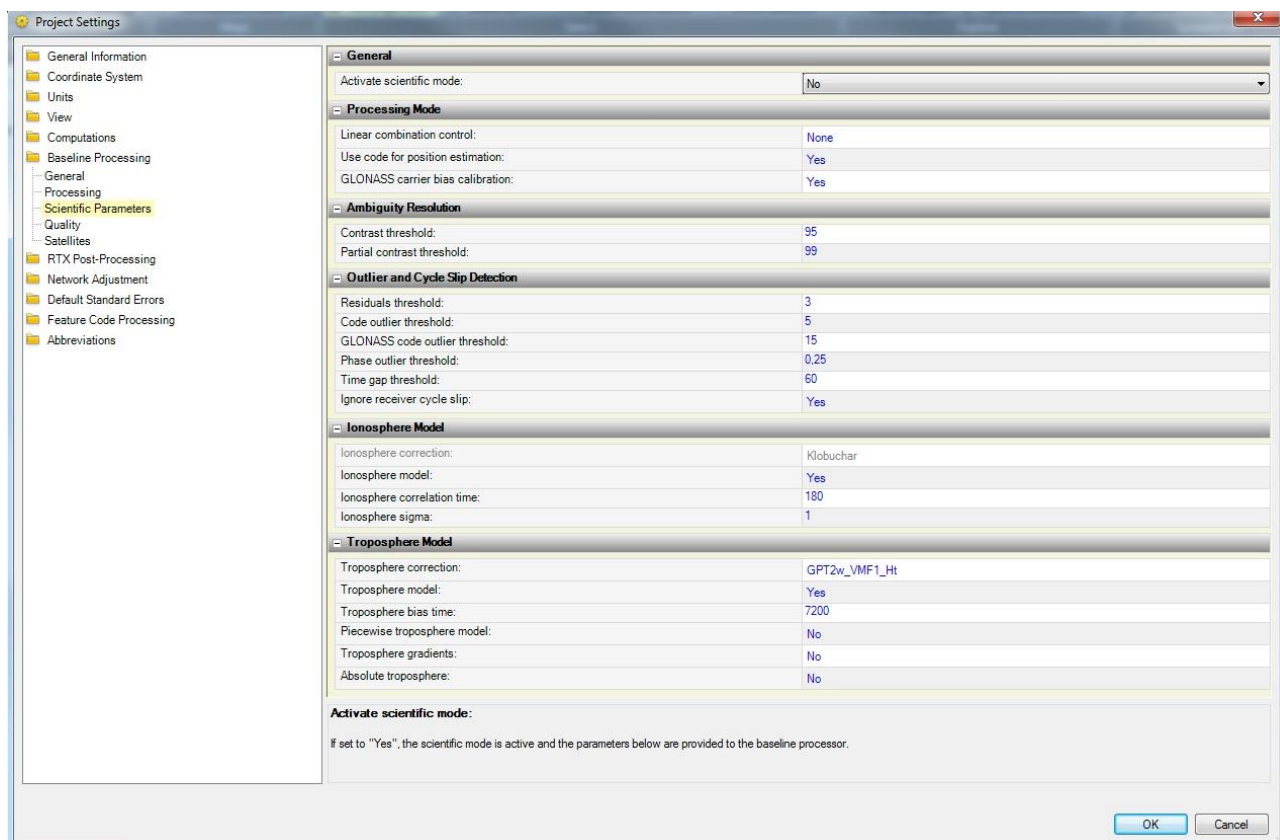


Figure 11: TBP scientific settings

algorithm and therefore has no counterpart in the GPSEST program. It is however comparable to “OPTIONS AND CRITERIA FOR TESTING” in panel 3.2.2 of GPSEST where statistical boundaries for the sigma algorithm can be set.

The “Outlier and Cycle Slip Detection” settings can be found in the Bernese programs MAUPRP and RESRMS. “Residuals threshold” corresponds to “DETECT LARGE RESIDUALS” of panel 2 in RESRMS, however the “Code outlier threshold”, “GLONASS code outlier threshold” and “Phase outlier threshold” refer to the observations and not the residuals. “Time gap threshold” can be transferred to “After an observation gap larger than” in panel 9 of MAUPRP where multiple ambiguities can be set up. “Ignore receiver cycle slip” can be done in Bernese when reading observation files with RXOBV3, where the checkbox “Ignore receiver cycle slip flag” can be selected. An ionospheric correction Klobuchar style is applied by default and cannot be deselected. This per se is not possible in the Bernese GNSS Software, however the usage of an ionosphere model e.g. provided by CODE enables the ionospheric correction. “Ionosphere model” refers to the estimation of the ionosphere (if set to yes) and the parameters correlation time and sigma have to be set. This setting is only possible if “Linear combination control” is set to “None” and is used for baselines between 2 and 20 km below an occupation timespan of 8.33 hours. There are several options within Bernese to estimate ionospheric parameters, however with the primary target to establish ionosphere maps. The setting in Bernese closest to the meaning of TBCs’ is arguably “Stochastic ionosphere parameters” in panel 5.1 of GPSEST where also time

dependent ionosphere parameters may be estimated as stochastic parameters. Finally the troposphere parameters again relate to Bernese, with the “Troposphere correction” being the “ZPD model and mapping function” in panel 3.2 of GPSEST, “Troposphere model” enabling the troposphere estimation, “Absolute troposphere” meaning the estimation of site specific troposphere parameters as in GPSEST panel 5.1, “Piecewise troposphere model” meaning multiple troposphere biases per session in combination with “Troposphere bias time”, this can be referred to GPSEST panel 6.4.1 where zenith path delay mapping function and parameter spacing can be set and also “Troposphere gradients” corresponding to “Gradient estimation model” in GPSEST panel 6.4.1 but without parameter spacing since it is fixed to 24 hours within the TBP.

These are the settings that have to be addressed to create comparable results between both the software packages. Another aspect which has to be kept in mind is that this evaluation only treats baseline postprocessing. This means that in contrast to a classic postprocessing of a GNSS station network there is no network adjustment performed in the end (both software suites offer a network adjustment, but since the pure baseline processing is examined an adjustment would smoothen the results to strong in order to identify baseline related effects) . The results which are compared are the estimated coordinates after the ambiguity fixing. Furthermore within the TBP only two stations are treated once. For every baseline a new instance of a baseline postprocessor is invoked, using only the data of the rover and base station. This has to be addressed in Bernese. The preprocessing steps in Bernese can be executed simultaneously for all stations within a network since CODSP only treats single stations at zero difference level and MAUPRP only treats triple differences of each baseline. GPSEST however has to be used with care when producing the float solution previous to ambiguity resolution. This program by default performs a network adjustment of all stations connected. By setting “Correlation strategy” to “BASELINE” in panel 3.1 of GPSEST however, every baseline is treated and processed individually, therefore allowing to set up several files in one run. Furthermore within TBC every baseline within the net is processed, meaning every possible connection is formed. Therefore, in order to steer the baseline generation procedure and enable an easy setup of desired networks the strategy STAR is used by program SNGDIF to create baselines ensuring one specific base station.

Finally, in the case of very bad a priori coordinates the TBP will compute initial coordinates on its own (or uses the Trimble online service RTX PPP). In Bernese a PPP would be necessary in order to ensure good quality a priori coordinates. To establish an equal basis and ensure that both processors use the a priori coordinates the reference coordinates are introduced as such to the processing. Note that for this thesis not the actual TBC was used to compute the results but a command line version established for development. This however is no different from the actual functionalities of TBC, only the GUI is removed and the settings are passed via a configuration file. The data import is handled via a dedicated folder structure.

### 3.2.3 Comparison tasks

The following scenarios were chosen in order to achieve a funded comparison between both GNSS post processing software packages. The motivation behind each aspect will be stated briefly and the necessary information for generating the results will be presented, including Bernese respective TBP related program settings. The information about the TBP is valid for both the TBC and the command line version mentioned previously.

#### 3.2.3.1 Standard processing procedure

At first a standard processing procedure has to be established against which the results from the other experiments are compared. It shall also reflect the most common and yet precise enough approach to GNSS postprocessing which is used in real data analysis. Therefore the processing shall consist of every baseline length interval (short medium long), 24 hours of observation data at a 30 second sampling rate featuring GPS and GLONASS (no other system), precise ephemeris data, standard ionosphere corrections for both software suites (CODE GIM for Bernese, internal Klobuchar for TBP) and GMF as troposphere mapping function. VMF1 however is the default correction within TBC, but it is based on GPT2 and not on the downloadable files from, e.g. the TU Vienna (this however does not affect the quality of the corrections, it simply means that it is like GMF an analytical backup of the VMF1). Since Bernese does only offer the VMF based on the up to date grid files, GMF was chosen as reference mapping function since both GNSS packages provide the same GPT based GMF corrections. The troposphere is estimated at a 2 hour window using the wet GMF as mapping function and for baselines longer than 20 km troposphere gradients according to Chen and Herring are estimated with a 24 hour parameter spacing. The baseline length dependent settings from the TBP (figure 7) are set up for the ambiguity resolution in Bernese.

Precise orbits are created using IGS final orbits for GPS and GLONASS using programs PRETAB and ORBGEN according to the Bernese GNSS Software Tutorial [Dach & Fridez, 2016], chapter 3 (with the only difference that IGS orbits were used and the C04\_2016 ERP file, and no atmospheric and ocean tide loading is applied). Observation files are imported using RXOBV3 again according to the Bernese GNSS software tutorial chapter 4 after creating station information files for each data set using RNX2STA. The a priori coordinates introduced are not from the Rinex observation files but are the reference coordinates written to a .CRD file. The observation data sampling for RXOBV3 is 30 seconds. Again program CODSPP is executed as proposed in the Bernese tutorial, chapter 4, but with the previously used pole file and, the standard orbit and clock

produced from the IGS file and the code bias input file called ALL.DCB (concatenation of all DCB types from the corresponding weekly mean values provided by CODE). Program SNGDIF executed in STAR strategy with respective base station (described in detail in section 3.3), no further changes to the default settings. Again, program MAUPRP executed as recommended in the software tutorial, chapter 4, with the respective coordinate files and satellite orbits and clocks. For a first float solution (only used for residual screening), GPSEST is executed with (only mentioning the settings different from default, default input also includes standard orbits, ERP files, CRD files) a specified output residual file, GPS/GLO as satellite systems an ionosphere free linear combination at a 30 second data sampling and an elevation cutoff angle of 10 degree with correlation strategy baseline. The coordinates of the base station used as base station in SNGDIF for the STAR strategy are fixed manually and site specific troposphere parameters are estimated with a spacing of 2 hours, no gradient however. The residuals are then screened using RESRMS (again according to the Bernese tutorial, chapter 5, but with 30 seconds as the corresponding sampling rate). The observation files are then cleaned by the program SATMRK using the edit file provided by RESRMS. This process (GPSEST, RESRMS, SATMRK) is repeated until only a negligible number of observations is discarded. Finally GPSEST is executed using nearly the same settings as above but with introducing an ionosphere model, estimating troposphere gradients for baselines longer than 20 kilometers and specifying coordinate and troposphere estimates to be written to output files. The ambiguity resolution is then performed by setting up a BPE using either the PCF L1L2WideLane.PCF for short and medium baselines or GNSAMBAP.PCF for long baselines where one baseline at a time is processed on its own. Both PCFs use the standard scripts GNSL12AP, GNSL12\_P (L1L2), GNSL53AP, GNSL53\_P (Wide-lane Narrow-lane), GNSAMBAP and GNSAMB\_P (Melbourne-Wübbena) from the RNX2SNX.PCF with an additional script called EXTRACT just to form the ambiguity resolution summary using GPSXTR. For additional information on the standard scripts within the PCF the reader is referred to the Bernese GNSS Software manual [Dach et al, 2015]. The scripts were slightly modified, in a sense that basic information such as fixed station or troposphere model can be set from within the script. Note that the troposphere model and every other bias or correction file needs to be set or used consistently throughout the whole processing, for example setting the troposphere model to GMF (dry and wet respective) in every program that applies troposphere corrections. The program BASLST in the scripts GNSL12AP and GNSL53AP realizes the length dependent selection of the ambiguity resolution strategy. The processing is now finished since no network adjustment needs to be performed. Note that in Bernese for the correction of the ionosphere GIMs from CODE were used. The TBP does not offer an import for such corrections, its ionosphere corrections are modelled after Klobuchar. This is also the reason no comparison of the ionospheric influence is performed in this thesis.

#### 3.2.3.2 Influence of the tropospheric correction model

The tropospheric correction model is a crucial part of the GNSS error modelling. It has been a large part of research and lots of models exist. With having GMF in the standard processing procedure one of the most prominent and accurate is already in use. To get a grip of the magnitude of the impact on the results the troposphere model has however, results are produced using VMF1 on the one hand as most precise troposphere modelling available, and the Niell mapping function on the other hand as origin of both the VMF and GMF. The computation is quite simple, it just consists of the standard processing procedure but one time executed with "NIELL" as ZPD mapping function (again dry and wet respective) and one time with VMF as ZPD mapping function (again, wet and dry part). Within Bernese the VMF1 grid files (available at the official homepage of the TU Vienna for download) have to be specified in the input, within TBC however the VMF is formed using GPT2 as weather input data. For the TBP the settings are met accordingly. Note that again in Bernese the troposphere model has to be specified in any program using the corrections, meaning in the case of VMF that also the input files need to be set accordingly.

#### 3.2.3.3 GPS only

Using GPS and GLONASS is declared as the standard processing procedure. The usage of GLONASS of course provides a better coverage, i.e. more observations, however it is not trivial to integrate GLONASS in specific processing tasks due to its FDMA technology. Additional biases and offsets have to be estimated amongst different satellites (frequency channels) and an overall system time offset for GLONASS w.r.t. GPS has to be acquired. The task affected mostly is, of course, the ambiguity resolution. A pure GPS based solution is therefore easier to process and more stable in its results. Therefore a pure GPS solution for all data sets is computed using the same settings as the standard processing procedure but with only GPS data. This was realized in Bernese by importing only GPS data from the original observation files, the other settings from the standard processing procedure stay untouched (if a satellite system is specified in the processing input to be used but no data is available it is simply skipped). Alternatively the satellite system selection in GPSEST can be set to GPS. The settings of the TBP are set accordingly (GLONASS is deactivated in the satellite settings respective all satellites are deselected).

#### 3.2.3.4 Daily Repeatability

In the case of processing different sessions the task is often to establish a possible time dependent change in the coordinates. In theory without any special circumstances the station coordinates should follow the continental drift, if every other effect is accounted for properly (of course in order to achieve such an accuracy a high precision network adjustment needs to be evaluated, which is of no interest here). Also, for classic survey, if an established network needs to be evaluated and points are observed e.g. in reoccupation the repeatability of the coordinate solutions at the same point is of high interest. If the fixed rover coordinates of two daily solutions differ by a larger margin for no obvious reason, chances are the processing did not work properly. Of course when only using short occupation timespans the results are not stable enough to represent a repeatable coordinate. Hence daily solutions of all data sets are computed using the standard procedure for the previous and the following day of the current evaluation session. Due to the proximity of the daily solutions the results should coincide in theory.

#### 3.2.3.5 Broadcast ephemeris

The IGS provides precise orbits (ultra-rapid) with a latency of about six hours. Final orbits take a little more time to compute and sometimes if for example no internet download is available or results need to be generated fast or if data is processed for a coarse overview broadcast ephemeris is used. These are obviously rather unprecise and are not recommended for high precision applications. It is however also of great interest since it shows the behavior and reliability of both packages for “bad” input data. Within TBC this is done by setting the “Ephemeris type” to “Broadcast”. In Bernese it requires the computation of standard orbits on basis of the Rinex navigation messages. This is done by at first concatenating all Rinex navigation files for each data set to one file for GLONASS and one for GPS using the programs CCRINEXC and CCRINEXN. Afterwards the concatenated navigation files are converted to the SP3c format using RXNPRE (with default settings). The final standard orbit file is then produced by the programs PRETAB and ORBGEN analogue to the standard processing procedure and also the further processing steps are executed accordingly.

Due to the rather limited quality of broadcast orbits there is no point in using them for long baselines. In TBC the usage of precise orbits is recommended from a baseline length of 50 kilometers on. For this experiment however short and medium baselines (up to a length of 200 km) are evaluated using broadcast ephemeris. This will also push both processors a little beyond their capabilities, showing their behavior apart from their comfort zone. Note that it was stated previously that the TBP Ephemeris manager uses all available ephemeris data to compute best possible satellite positions. For this very experiment the setting is still kept at automatic, but all

precise orbit files are removed from the data folder. Therefore only navigation files are available and the Ephemeris manager computes pure broadcast orbits.

#### 3.2.3.6 Reduced occupation timespans

Both software suites come with recommendations regarding minimum occupation times with respect to the baseline length processed. In order to assess their performance at the limit of these recommendations and below, and also for the case of classic survey where no entire day of observation data may be available short and medium baselines are reprocessed using various occupation timespans (since long baselines are only used for large networks and scientific applications a reduced occupation timespan is simply of no interest here). The tests therefore include small baselines with an occupation timespan of 1 hour and 10 minutes at two times of the same day, beginning at 1 am in the night and 1 pm after noon (UTC) and medium baselines with an occupation timespan of 2 hours respective 30 minutes (using the same day and start time as previously).

The settings are widely kept from the standard processing procedure, but the sampling interval is set to 1 second since 30 seconds would render the estimation ill conditioned. Also, due to the change of the linear combination selection in the TBP for baselines between 2 and 20 kilometers (L1&L2 instead of wide-lane for occupation timespans below 8.33 hours) the thresholds in program BASLST in L1L2WideLane.PCF are adapted accordingly.

#### 3.2.3.7 Ambiguity Resolution

The final task is to assess the performance of the ambiguity resolution. This is not trivial in a way of simply comparing the numbers of initial and resolved ambiguities, since both tools determine the related parameters independently (reference -, initial- and number of ambiguities). Therefore, serving as comparable variable, is the ratio of resolved w.r.t. to set up ambiguities (percentage of resolved ambiguities) since absolute values are not meaningful. The ratio is again brought into context with the corresponding baseline respective baseline length. The information is extracted from the .SUM files of GPSEXTR for Bernese and the log file of the TBP. Note that the TBP log file in this form is not available for the standard user since it is considered as debug output. In TBC the user has no access to direct ambiguity resolution information, only the status "FIXED" or "FLOAT" will be displayed.

### 3.2.4 Matlab evaluation toolbox

For the purpose of evaluating the results of both GNSS suites a Matlab toolbox was created to extract the relevant information from the dedicated output files. Figure 12 gives a general overview.

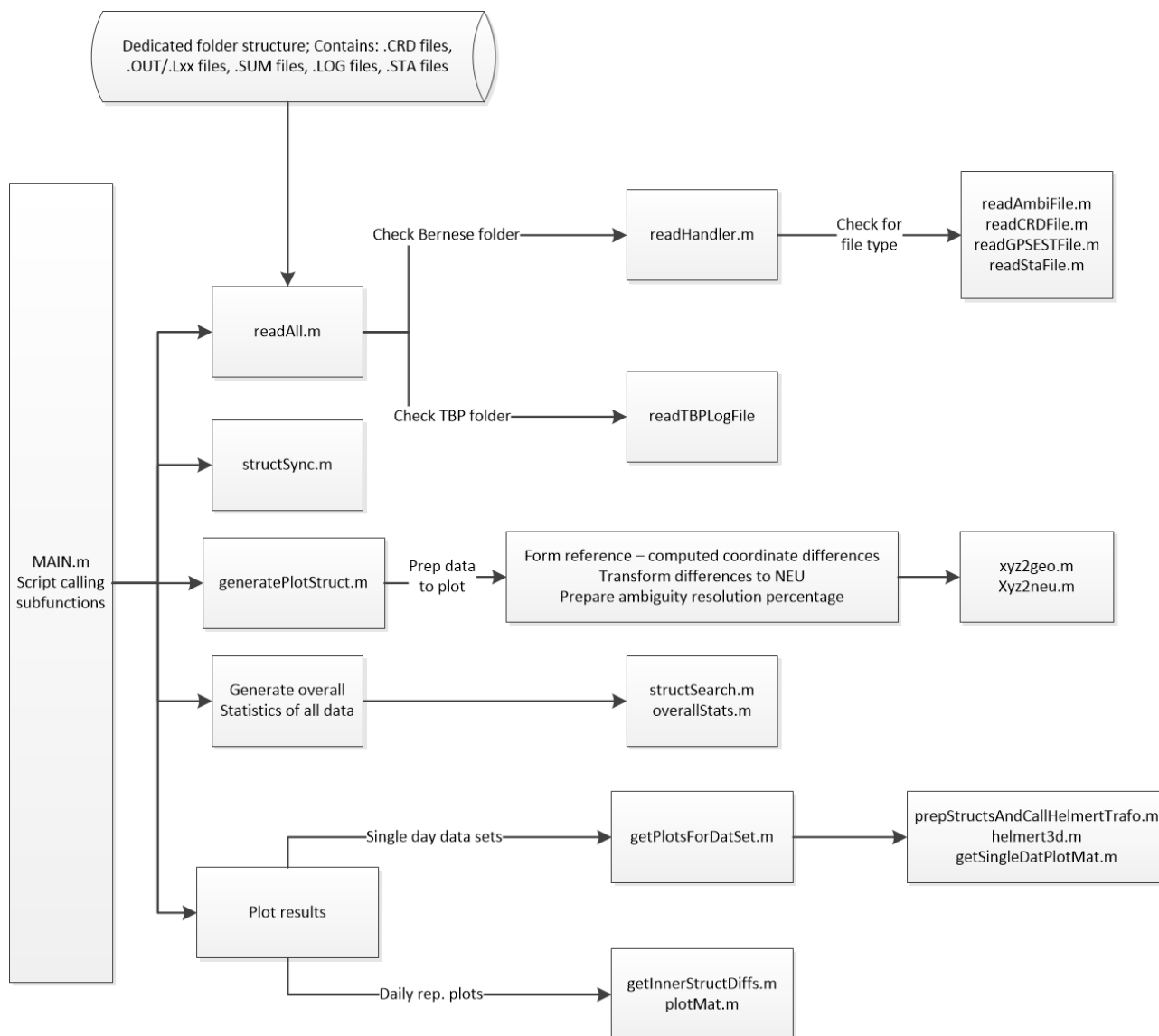


**Figure 12: Matlab evaluation toolbox flow chart**

The result files are stored in a dedicated folder structure, where the TBP log files are simply all in one folder named after the respective data set. Every file contains all relevant information such as ambiguities, coordinates, coordinate sigmas and station information. The Bernese output files are stored in nested folders which are named after the respective data set, session and fixed base station. One subdirectory consists of the GPSEST.OUT or .Lxx files from the ambiguity resolution runs (final coordinates and sigmas are extracted), the .SUM files from GPSEXTR containing the ambiguity resolution summaries (number of set up and resolved ambiguities are extracted and in the case of WL and MW the ambiguities from both the wide lane and the narrow lane run are used

to create a percentage value) and a .CRD file (to establish the fixed station of the baselines). The reference coordinates in form .CRD files and if necessary station information files are stored in a dedicated folder REFERENCE.

The script MAIN.m contains all calls to the sub scripts. With readAll.m the folder structure is searched for all available data and depending on the file type the function readHandler.m selects the appropriate reading function. Since there is only one type of log file for the TBP this is only necessary for Bernese. Furthermore the TBP log file reader was generated automatically using the Matlab internal script generation. This was not possible for the Bernese output files due to their irregular build. The results are then stored in structure arrays, one for Bernese and one for the TBP. These contain the single datasets (one dataset = one network at one session with a specific processing setting, e.g. NetworkxDoySettingxy). Each dataset has the fixed base station(s) as fields, and every base station field contains one field for each rover station with all respective results in addition to the base coordinates.

Since one run of the TBP console version for one dataset processes every possible baseline within (this is quite cumbersome to realize for large networks in Bernese, furthermore it produces a large overhead of data in the scope of this thesis) and the processing in Bernese was limited to only relevant network configurations the read in TBP data is reduced to match the Bernese result structure, which is done by structSync.m. The structure arrays now contain the results of the exact same datasets stored under the exact same fieldnames.

After that the script generatePlotStruct.m prepares the data to be plotted easily. The ambiguity percentage values are computed, the difference between computed rover coordinates and reference is formed and transformed to delta north east up (using functions xyz2geo.m and xyz2neu.m) and the structure array is simplified in a way that dataset fields contain only baseline specific fields stating reference and rover station which each hold the previously computed results in addition to base and rover coordinates and baseline length.

Then brief overall statistics are assembled using overallStats.m (uses subfunction structSearch.m), such as overall baselines processed etc.

Finally the results are processed, for the regular solutions (everything but daily repeatability) the function getPlotsForDatSet.m plots all results (delta north east up, sigma X Y Z, % of resolved ambiguities) separately and computes the 3D Helmert transformation (estimated coordinates into reference for each software solution independently) which are written to .txt files. For the daily repeatability corresponding results of two days (difference estimated minus reference coordinates) are subtracted from each other and plotted using the scripts getInnerStructDiffs.m and plotMat.m.

The function helmert3d.m is taken from the "Geodetic toolbox" (Peter Wasmeier, Chair of Geodesy, TUM) and the functions xyz2geo.m and xyz2neu.m are property of Trimble TerraSat.

### 3.3 Choice of Test data

As mentioned previously, the choice of test data is crucial for the experiments. In order to achieve a wide spread range of baselines several networks were chosen to represent small, medium and long baselines. The challenging task hereby is to find networks with consistent data supply and well known and reliable reference coordinates which fit the requirements. Using the Trimble QA archive, data from the following networks was acquired for the 7<sup>th</sup>, 8<sup>th</sup> and 9<sup>th</sup> of November 2016 (DOY 312, 313 and 314) in addition to the internally used reference coordinates. The following sections show the stations used and their locations. To augment the usability of the datasets some of the networks were processed repeatedly with varying base stations.

#### 3.3.1 Short baseline network

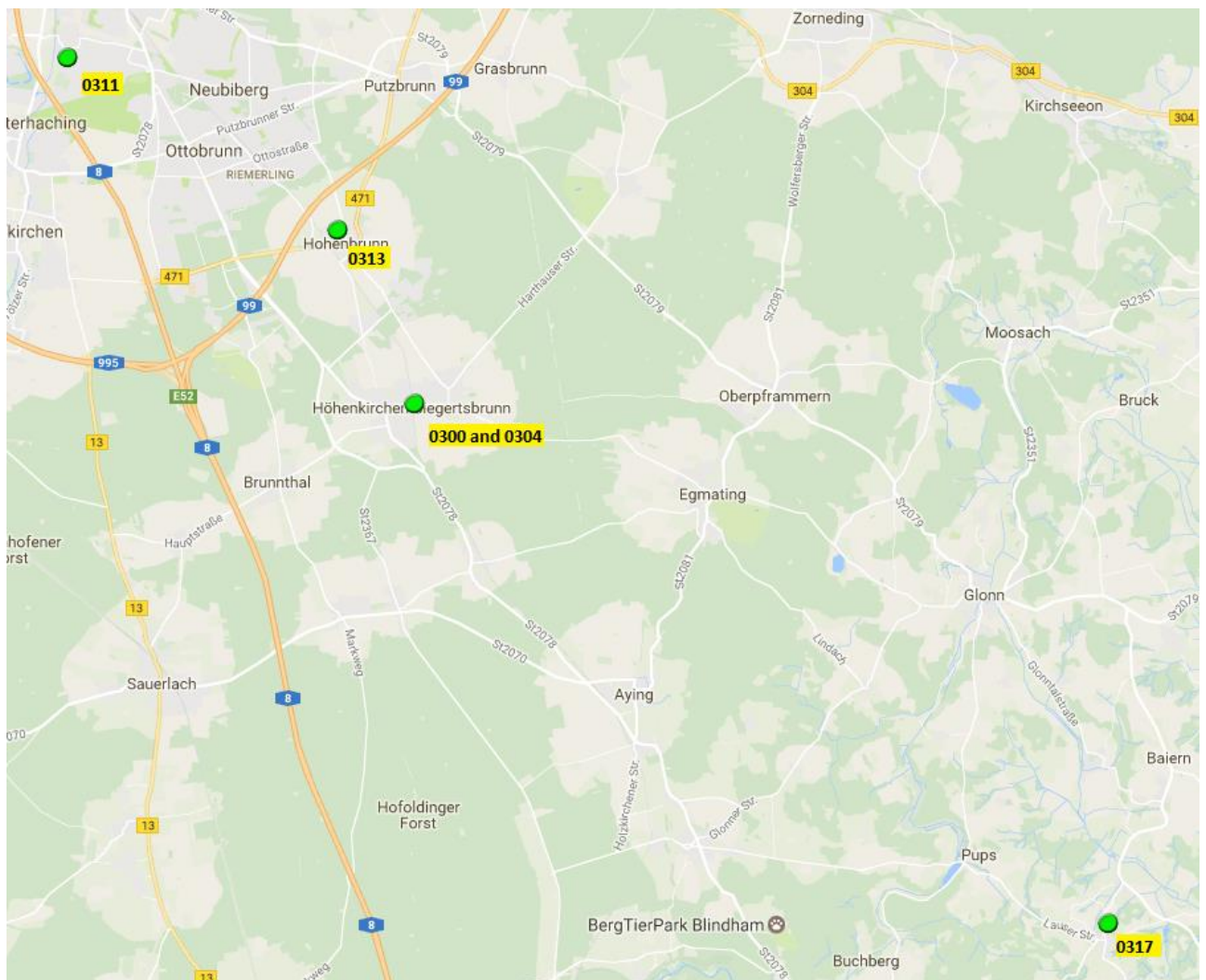


Figure 13: Short baseline network Hoehenkirchen

Figure 13 shows the short baseline network around Trimble TerraSat Hoehenkirchen. The network was processed using 0300 and 0304 (both located at the roof of the TerraSat building) and 0311 as reference stations. The baseline length ranges from about 1 meter to approximately 25 kilometers. The underlying maps from figures 13 to 16 are taken from Google Maps.

### 3.3.2 Medium baseline network

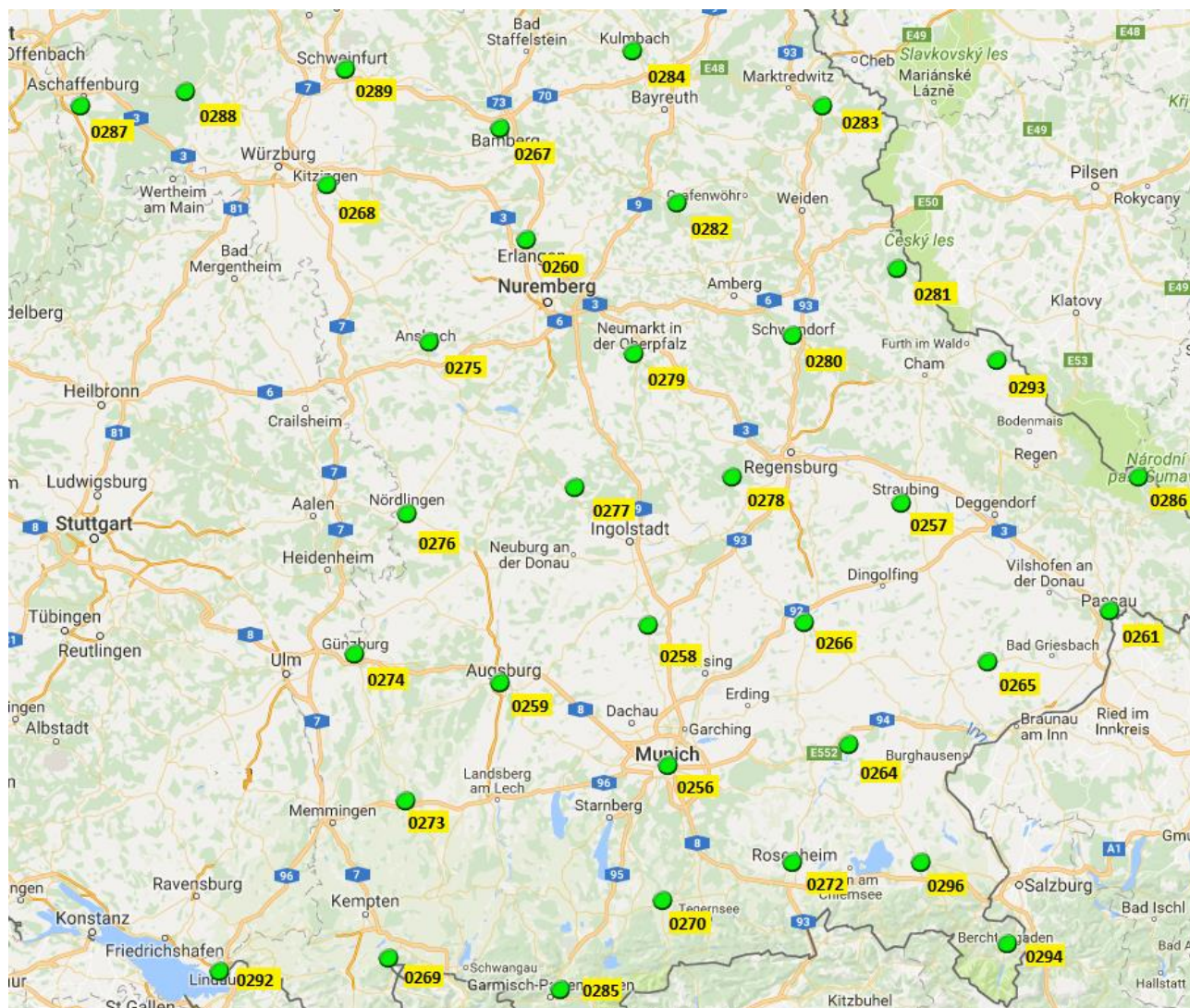


Figure 14: Medium baseline network SAPOS Bavaria

Figure 14 shows the medium baseline network, the official SAPOS network of Bavaria. Only one reference station per dataset was chosen here, station 0277, resulting in baseline lengths from approximately 40 to 200 kilometers. Since the reference coordinates were given in ETRS89 they were transformed to ITRF08 prior to the processing by using the Bernese program ETRS89. This is the main data set to assess the wide-lane linear combination performance.

### 3.3.3 Long baseline networks

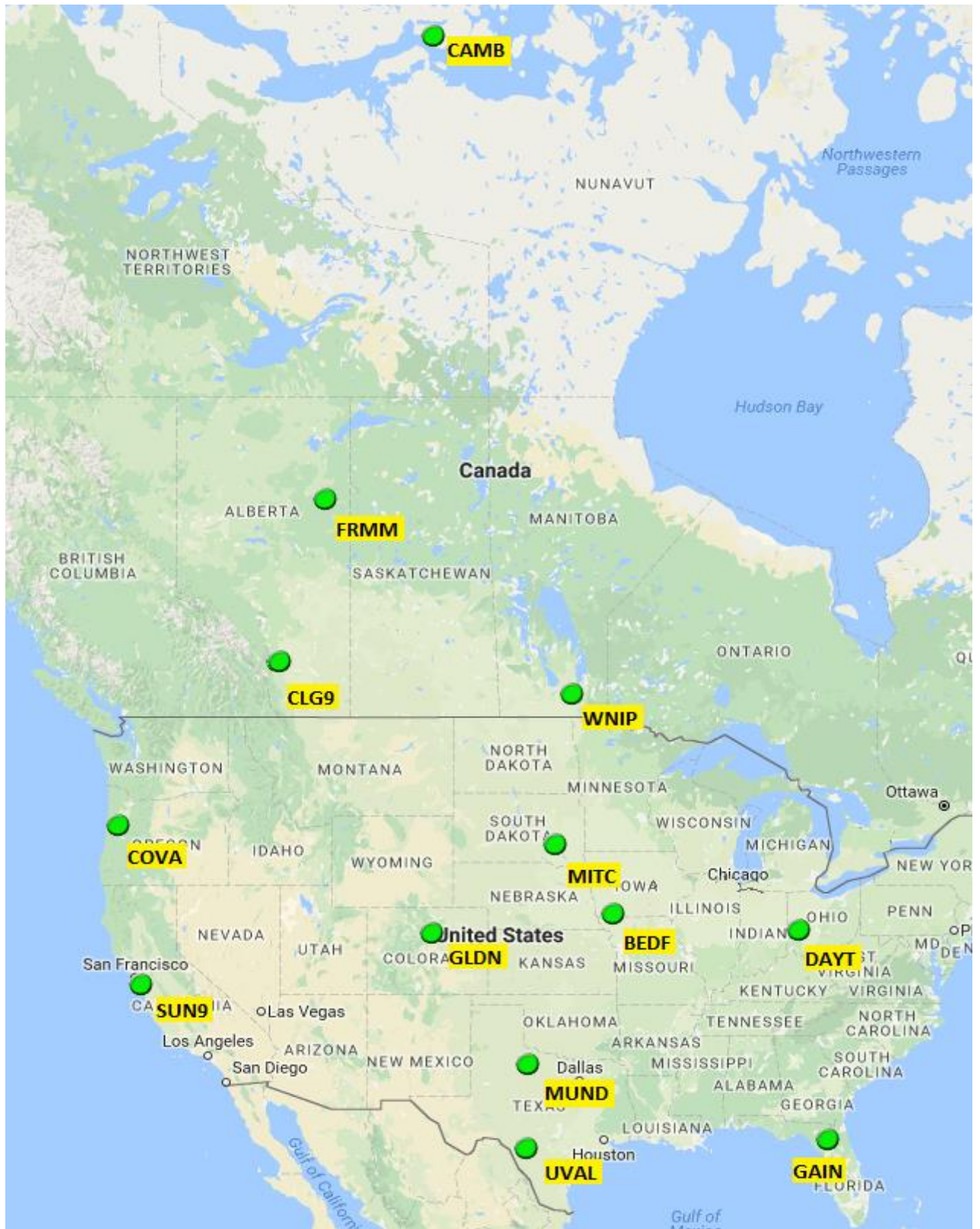


Figure 15: Long baseline network 1, USA - Canada



Figure 16: Long baseline network 2, Africa

Figure 15 and 16 show the long baseline networks chosen, USA-Canada and Africa respective. For USA-Canada the stations BEDF, CAMB and DAYT were fixed resulting in approximate baseline lengths of 400 to 6000 kilometers, and for Africa stations ACCR, AGAD, DUR9 and NAIK were fixed resulting in baseline lengths up to approximately 8500 kilometers.

### 3.3.4 Additional data and information

The observation data was taken from the QA archive of Trimble TerraSat which is stored in the t02 format and for Bernese converted to Rinex using the official Trimble Rinex converter ([http://www.trimble.com/support\\_trl.aspx?Nav=Collection-40773&pt=Trimble%20RINEX](http://www.trimble.com/support_trl.aspx?Nav=Collection-40773&pt=Trimble%20RINEX), available for free as public download). The antenna PCV file and precise final orbits for DOY 312 313 and 314 are official IGS products (official IGS ftp server), DCB, ionosphere and ERP files are official CODE products available at the CODE ftp server. The Bernese version is the official 5.2 running at a Linux server at IAPG, TUM and the TBP is the prerelease version from March 2017 as console application on a virtual test machine at Trimble TerraSat.

## 4 Results and discussion

The following chapter shall now display the processing results and put them into context between both software solutions. For a general overview, figure 17 shows the overall amount of baselines processed (866) with their respective lengths shown in 500 kilometer clusters.

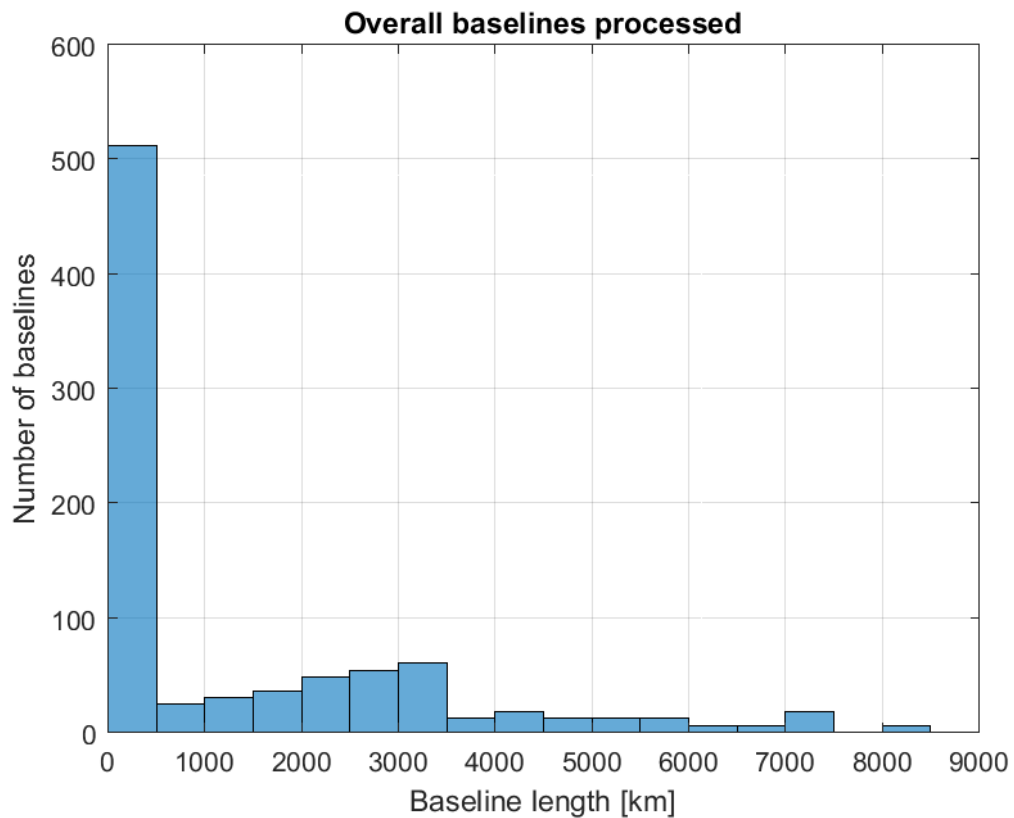


**Figure 17: Overview all baselines processed**

The extremely high number of the first interval relative to the other intervals stems from the experiments concerning only small and medium baselines such as the reduced occupation timespans and broadcast orbit evaluation.

## 4.1 Standard processing

### 4.1.1 Short baselines

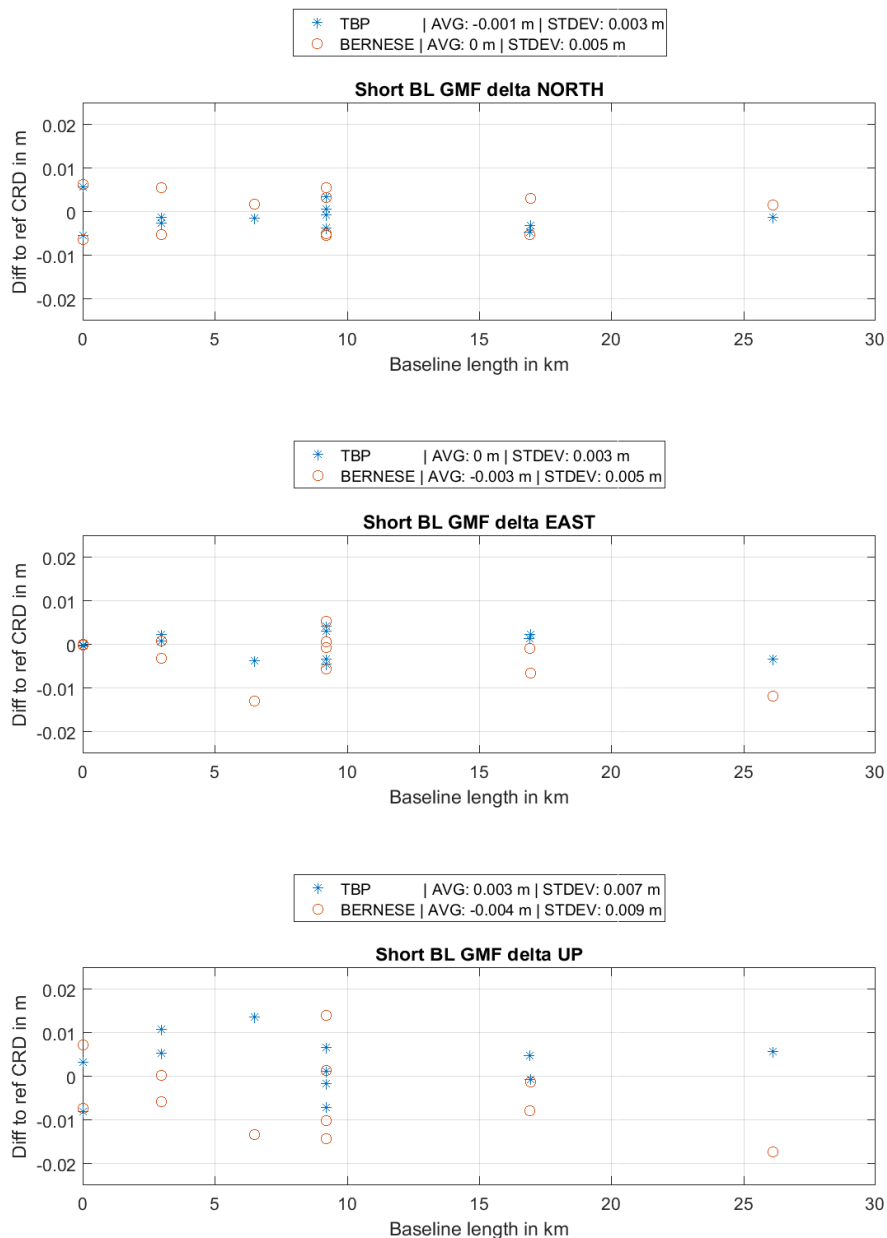


Figure 18: Delta NEU short baselines, standard processing

Figure 18 shows the difference computed minus reference rover coordinate in delta north east up for short baselines. In this setup all baselines except for the ones on the very left are computed using the wide-lane LC. The mirrored characteristic of the plot stems from the approach to fix different stations as base within one network successively and the average value and standard deviation are regarding all coordinate differences with respect to the reference coordinate. Regarding the horizontal component however, especially the east, the TBP results appear to be more consistent between different base stations regarding the final coordinate and the differences to the reference to not exceed 1 centimeter (above or below). For the very short baseline the results match perfectly. For the others though the Bernese solution appears to be more influenced by the base station than the TBP, also showing higher standard deviations and a -3mm average in the east component. The up component however shows an interesting property. Both processors are strongly influenced by the selection of the base station, however examining the baselines processed only once the TBP coordinates appear to be estimated smaller than the reference in general (reference – estimated = positive value => estimated < reference), whereas the Bernese results appear to be estimated slightly above the reference in general. This also shows in the average value of the up component, which shows different signs for both solutions. The TBP results however, judging by the average and standard deviation, appear to be more precise and accurate in this processing example. Also both processors differ from the reference in a similar manner (except for the sign), which indicates similar treatment of the observations. Table 4 shows the 3D Helmert transformation parameters for both processor solutions and confirm the overall slightly better fit of the TBP solution.

**Table 4 3D Helmert transformation parameters for TBP and Bernese, short baselines, Standard Processing**

	Bernese Parameters:	Bernese Accuracy:	TBP Parameters:	TBP Accuracy:
Translation X	-0.0024	0.0019	0.0027	0.0012
Translation Y	-0.0034	0.0019	0.0005	0.0012
Translation Z	-0.0033	0.0019	0.0014	0.0012
Rotation w.r.t. X	0.0000	0.0000	-0.0000	0.0000
Rotation w.r.t. Y	0.0000	0.0000	-0.0000	0.0000
Rotation w.r.t. Z	-0.0000	0.0000	0.0000	0.0000
Scale factor	1.000	0.0000	1.000	0.0000

Figure 19 on the right shows a histogram of all estimated coordinate sigmas (w.r.t. X Y Z), where three columns per mm sigma value are displayed regarding the respective amount of coordinates assigned with this sigma value. Both processors' sigma X values do not exceed 1 mm, this is also true for the TBPs' sigma Y and for most of the sigma Z. The Bernese sigma Y and Z values are more distributed between 1 and 2 mm, but again the overall accuracy is, as expected excellent. The actual distribution of the sigma values w.r.t. to the baseline length can be seen in figure A 1 in the appendix. Figure 19 on the left shows the average percentage of resolved ambiguities w.r.t. the baseline length. Both processors successfully solve nearly all ambiguities for all baselines, the TBP

however constantly shows 100 percent where Bernese varies between 90 and 100 percent. Again as in the coordinate sigma values no significant differences are established.

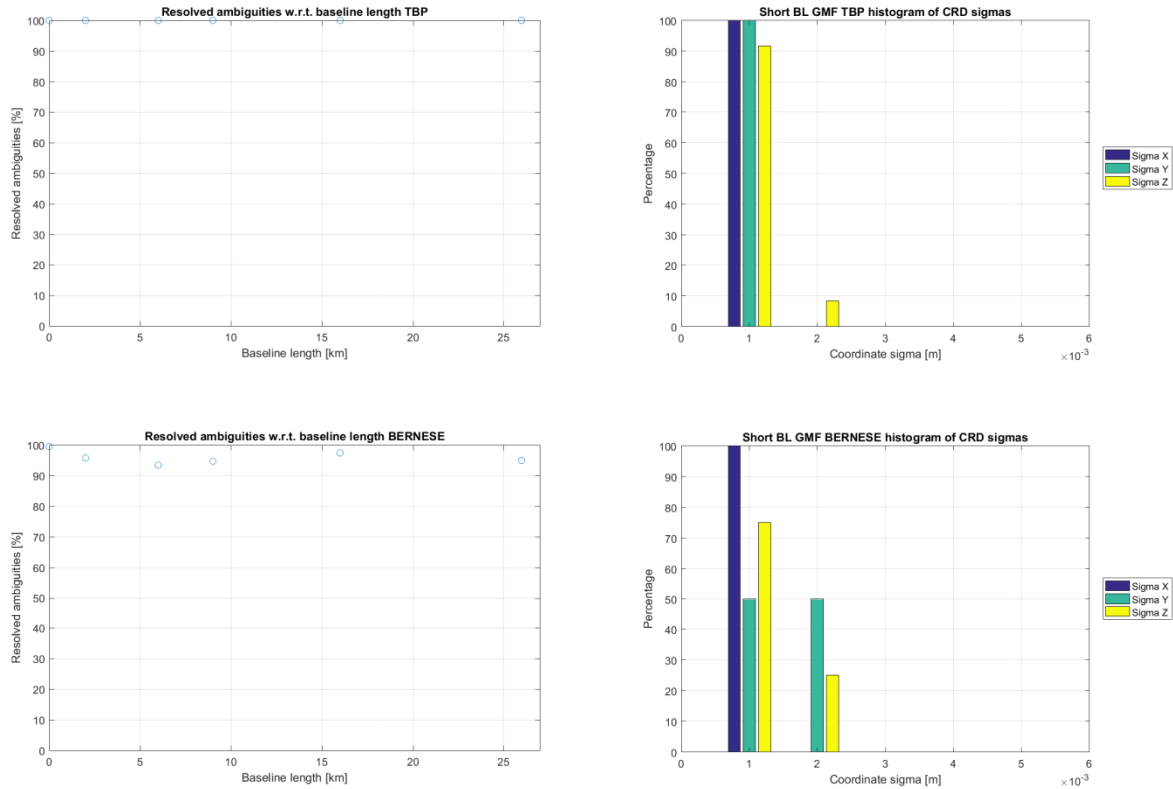


Figure 19: Left: Percentage of resolved ambiguities for short baselines, standard processing; Right: Histogram of coordinate sigmas for short baselines, standard processing;

#### 4.1.2 Medium baselines

Figure 20 shows, analogue to the previous section, the difference between the estimated coordinates and the reference. The ambiguity resolution hereby is computed using solely the wide-lane LC. Note that within this dataset only one station was fixed as base. Overall both solutions agree within a reasonable scope (sub 1.5 cm). Again however the TBP results fit slightly better in the north component, where Bernese again seems to estimate slightly too large values. The east component is fairly even, yet the TBP seems to have fewer discrepancies at the cm level. The up component however can be seen as equally well determined by both processors, since they show an average value and standard deviation of about the same magnitude. Both processors however estimate the up component slightly too high, implying a systematic offset with respect to the reference coordinates. Table 5 shows the 3D Helmert parameters for the solution. In contrast to the previous results of the short baselines, both solutions show similar characteristics with similar

## 4 Results and discussion

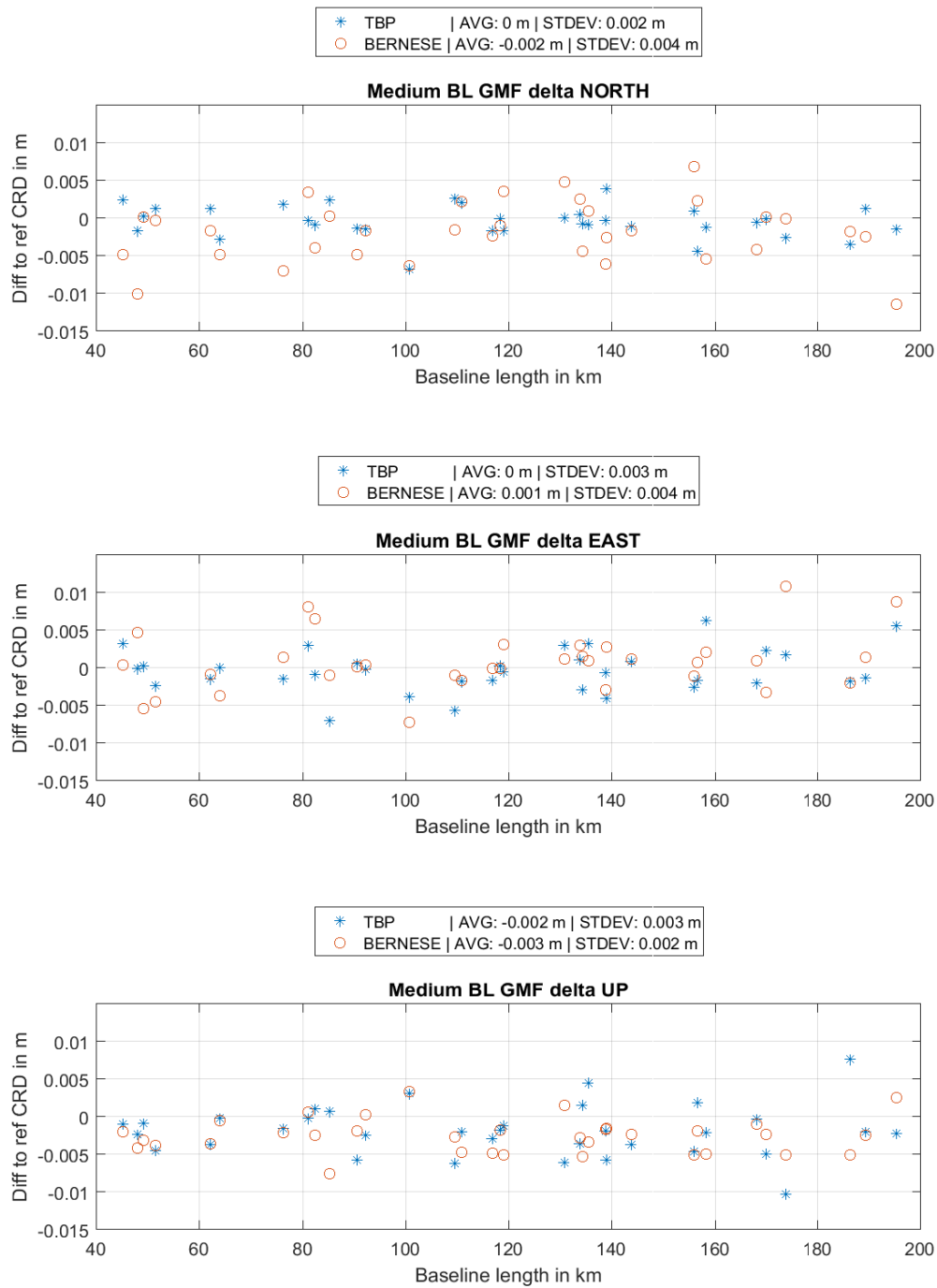
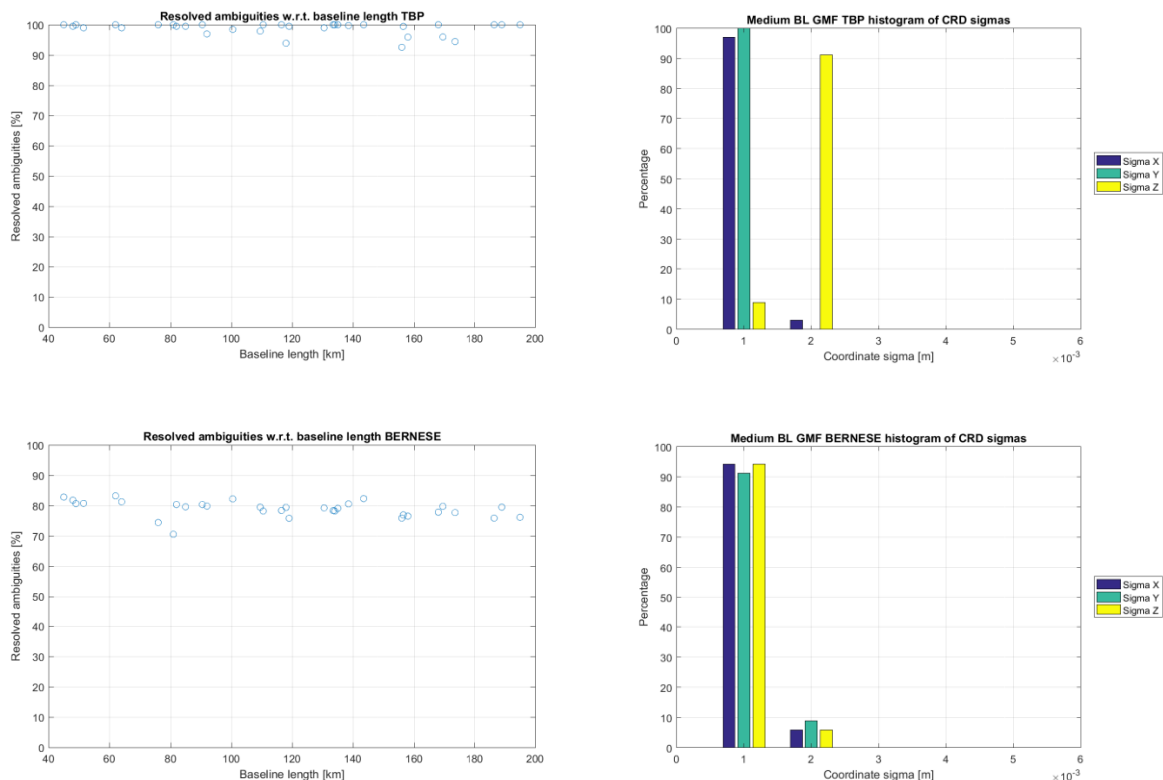


Figure 20: Delta NEU medium baselines, standard processing

and very high accuracies. This indicates that the reference coordinates have been produced using a slightly different assumption regarding error models (maybe a different troposphere model). It shows however that both processors perform nearly equally well, with a very slight advantage to the TBP in the horizontal component. The sigma values in figure 21 on the right confirm the successful solutions of both processors. The sigma values w.r.t. the baseline length are provided in figure A 2 in the appendix.

**Table 5: 3D Helmert transformation parameters for TBP and Bernese, medium baselines, Standard Processing**

	Bernese Parameters:	Bernese Accuracy:	TBP Parameters:	TBP Accuracy:
Translation X	-0.0005	0.0006	-0.0009	0.0005
Translation Y	0.0007	0.0006	-0.0005	0.0005
Translation Z	-0.0031	0.0006	-0.0017	0.0005
Rotation w.r.t. X	-0.0000	0.0000	0.0000	0.0000
Rotation w.r.t. Y	-0.0000	0.0000	0.0000	0.0000
Rotation w.r.t. Z	0.0000	0.0000	-0.0000	0.0000
Scale factor	1.000	0.0000	1.000	0.0000



**Figure 21: Left: Percentage of resolved ambiguities for medium baselines, standard processing; Right: Histogram of coordinate sigmas for medium baselines, standard processing;**

The ambiguity resolution shown in figure 21 on the left however differs quite a bit. Where the TBP resolves at least around 90 percent on average of the ambiguities of each baseline Bernese settles at around 80 percent. This reflects the intention behind the sigma dependent ambiguity resolution algorithm. Though the resulting coordinates are very good, not all ambiguities were fixed since the

preference is to rather leave an ambiguity value as float than compromise the resulting coordinate by fixing it to a wrong value. Therefore, even with a lower resolution percentage the estimated coordinates are of high quality.

### 4.1.3 Long baselines

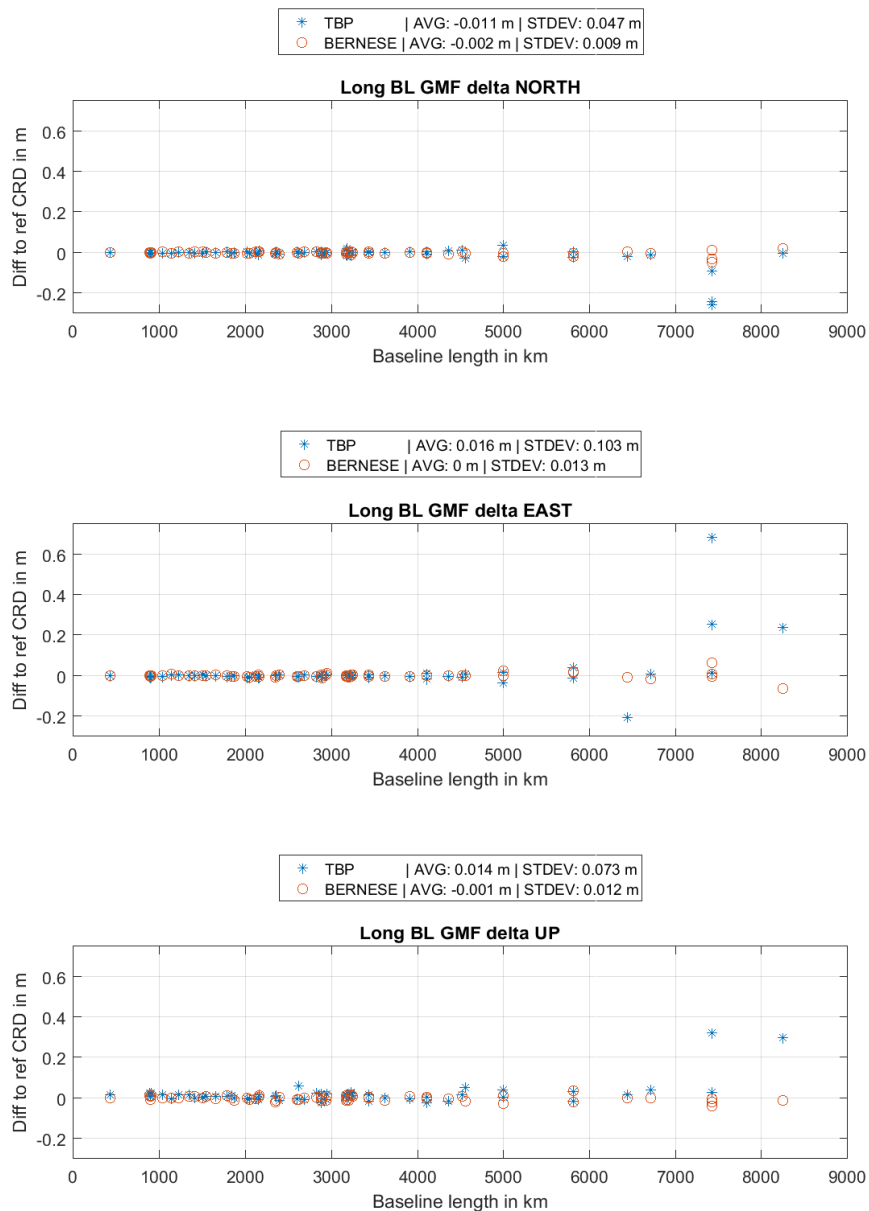


Figure 22: Delta NEU long baselines, standard processing

This dataset was processed using the Melbourne-Wübbena LC only. Figure 22 shows the difference between reference and estimated coordinates for long baselines. For baselines lengths beyond 7000 kilometers the TBP is not reliably able to establish a precise solution. The long baselines consist of two datasets, Africa and USA-Canada. The respective 3D Helmert transformation parameters are shown in table 6 and 7.

**Table 6: 3D Helmert transformation parameters for TBP and Bernese, Africa, Standard Processing**

	Bernese Parameters:	Bernese Accuracy:	TBP Parameters:	TBP Accuracy:
Translation X	0.0028	0.0032	0.0273	0.0242
Translation Y	0.0006	0.0032	0.0392	0.0242
Translation Z	-0.0026	0.0032	-0.0176	0.0242
Rotation w.r.t. X	0.0000	0.0000	0.0000	0.0000
Rotation w.r.t. Y	-0.0000	0.0000	-0.0000	0.0000
Rotation w.r.t. Z	-0.0000	0.0000	0.0000	0.0000
Scale factor	1.000	0.0000	1.000	0.0000

**Table 7: 3D Helmert transformation parameters for TBP and Bernese, USA-Canada, Standard Processing**

	Bernese Parameters:	Bernese Accuracy:	TBP Parameters:	TBP Accuracy:
Translation X	-0.0008	0.0009	-0.0018	0.0012
Translation Y	0.0000	0.0009	-0.0054	0.0012
Translation Z	-0.0001	0.0009	0.0051	0.0012
Rotation w.r.t. X	0.0000	0.0000	0.0000	0.0000
Rotation w.r.t. Y	0.0000	0.0000	0.0000	0.0000
Rotation w.r.t. Z	0.0000	0.0000	0.0000	0.0000
Scale factor	1.000	0.0000	1.000	0.0000

The transformation of the results from USA-Canada of Bernese shows remarkable accuracy. No systematic influence appears to bias the results. Also the parameters regarding the stations in Africa are promising, given that most of the baselines there exceed 5000 kilometers. The parameters for the TBP however show that for the dataset USA-Canada reasonable results were computed, whereas only the stations in Africa could not be handled properly (or some of the stations/baselines).

Figure 23 on the right shows the corresponding coordinate sigma values and on the left the percentage of resolved ambiguities. The ambiguity resolution percentage of Bernese drops below 20 percent for certain baselines, surprisingly not in total relation with the baseline length. This rather indicates the influence of a bad station used as base. The TBP however does not seem to have similar trouble resolving the ambiguities for these baselines. The coordinate sigma values merely surpass 1 cm for single stations, implying that the overall estimation process was considered successful within both processors. The coordinate sigma values w.r.t. baseline length are illustrated in figure A 3 in the appendix.

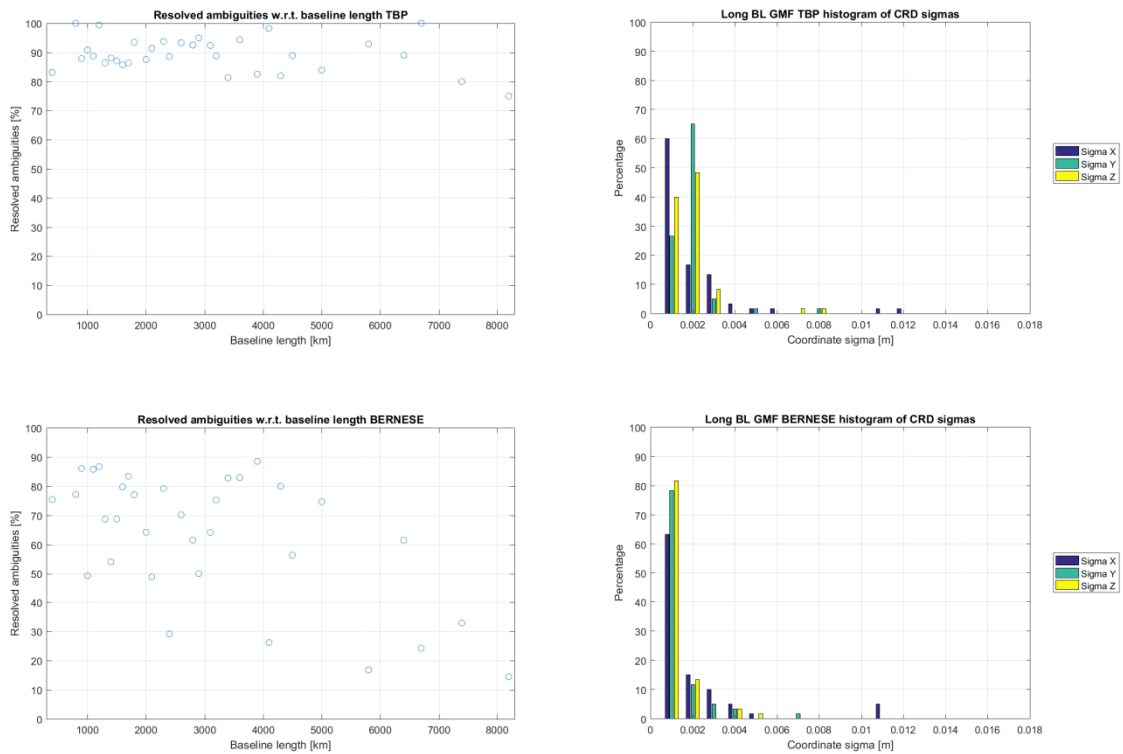


**Figure 23: Left: Percentage of resolved ambiguities for long baselines, standard processing; Right: Histogram of coordinate sigmas for long baselines, standard processing;**

In order to be able to compare reliable results, a baseline length cutoff at 6000 kilometers was established. The corresponding coordinate difference results are displayed in figure 24, yet unfortunately no transformation values are available. The Helmert parameters regarding USA-Canada are still valid though.

The results from Bernese show great consistence with the reference coordinate with a maximum discrepancy of 2 cm in the horizontal and maximum 4 cm in the up component. They are also fairly well distributed showing no sign of a systematic bias. The horizontal component of the TBP results can also be considered as quite accurate, yet it shows a slightly higher standard deviation than the Bernese results. The up component of the TBP results however appears to be estimated too low by an average value of 8 mm. Both processors however coincide at very long baselines within the cm level.

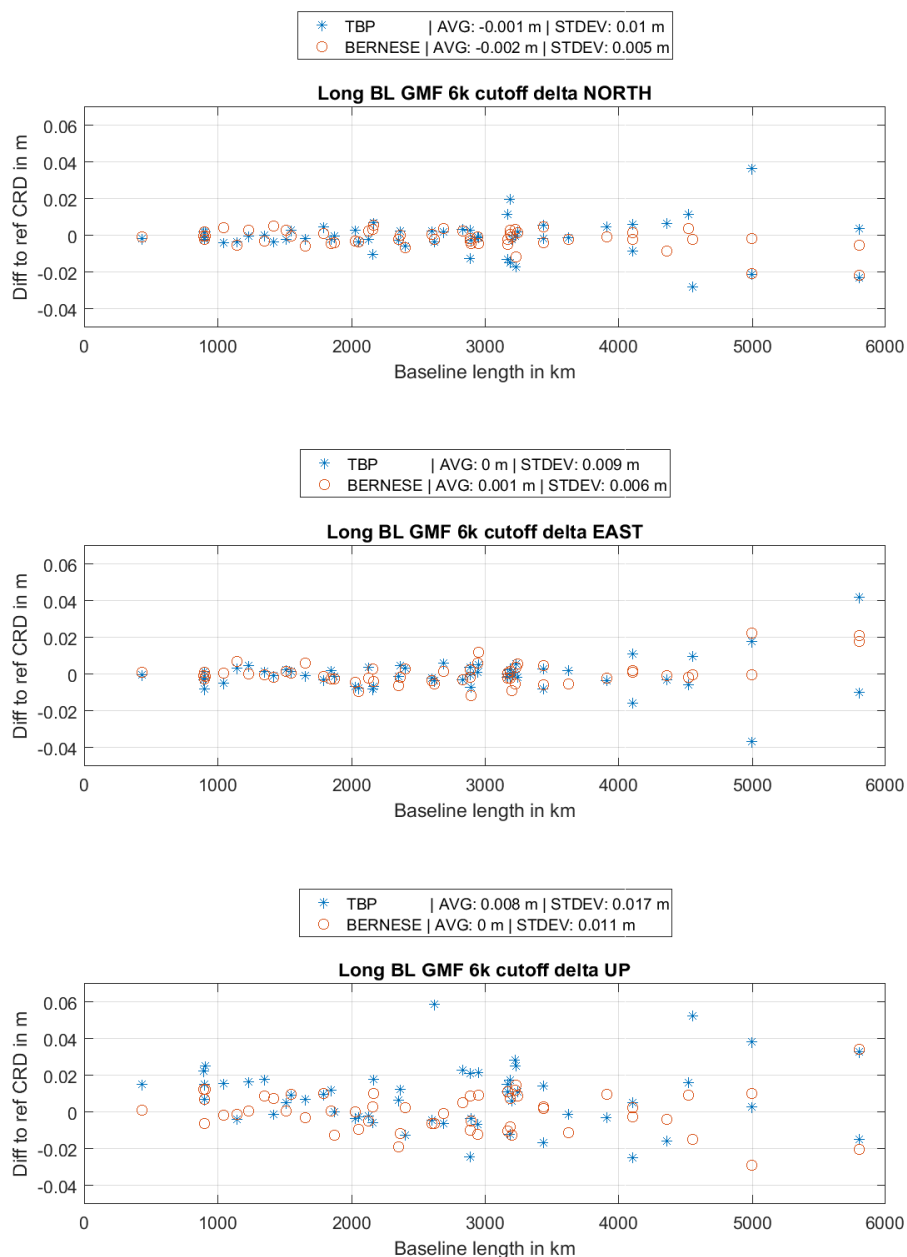


**Figure 24: Delta NEU long baselines, 6000 km cutoff, standard processing**

Figure 25 on the left shows the ambiguity resolution percentage and on the right the coordinate sigma values after the cutoff after 6000 km baseline length. The sigma values are again within the same magnitude and do not exceed 1 cm.

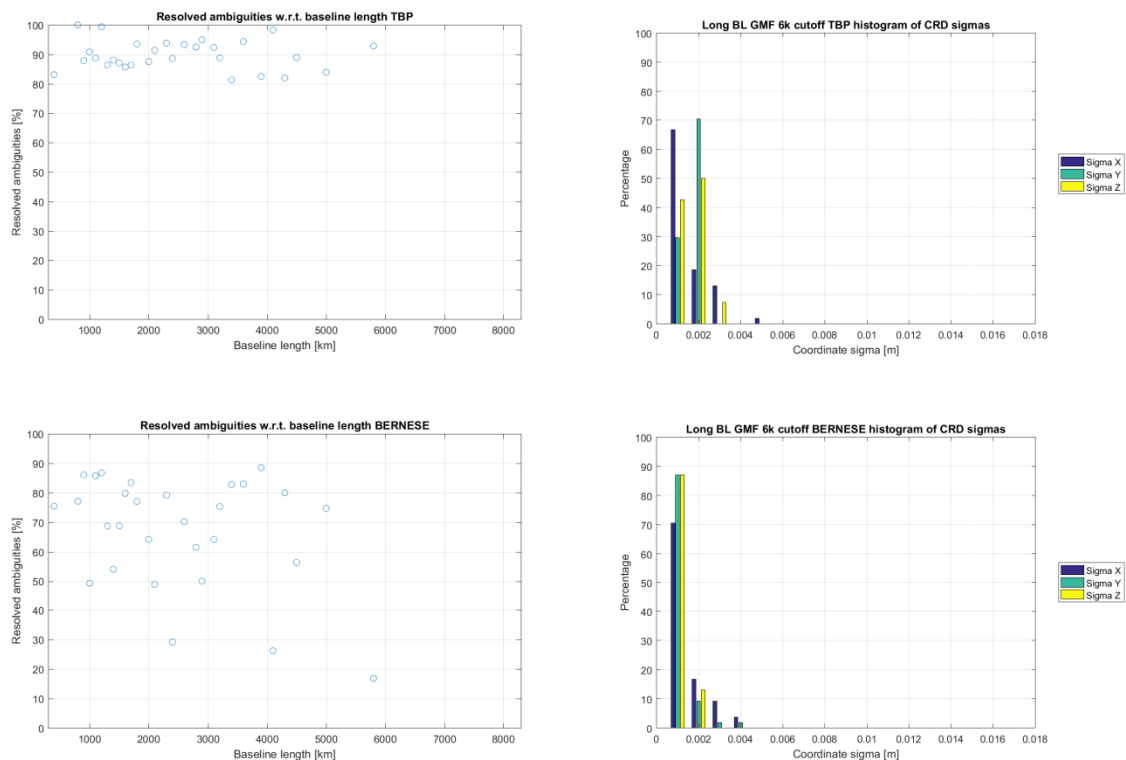


**Figure 25:** Left: Percentage of resolved ambiguities for long baselines, 6000 km cutoff, std processing; Right: Histogram of coordinate sigmas for long baselines, 6000 km cutoff, std processing;

The distribution of the coordinate sigma values w.r.t. baseline length for the 6000 km cutoff is shown in table A 4 in the appendix.

## 4.2 Influence of the tropospheric correction model

The following chapter displays the results regarding the usage of different troposphere models. It is expected that both processors show similar changes in the estimated coordinates with respect to the results of the standard processing procedure.

### 4.2.1 Niell Mapping Function

#### 4.2.1.1 Short baselines

Figure 26 shows the results for short baselines using the Niell mapping function. The coordinate differences as well as the coordinate sigma values (figure 27 right) and the percentage of resolved ambiguities (figure 27 left) do not show significant differences with respect to the standard processing solution. The translation of the Helmert transformation in table 8 is slightly smaller than before. The average values and standard deviations of the coordinate differences show, if at all, only a change of 1 mm (e.g. Bernese up STDEV 0.01 against the 0.009 from the standard processing example). The results meet the expectations fully since no significant changes are expected due to the very short baseline length and the similarity of the mapping functions. The coordinate sigma values w.r.t. to baseline length are displayed in figure A 5 in the appendix.

**Table 8: 3D Helmert transformation parameters for TBP and Bernese, short baselines, NMF**

	Bernese Parameters:	Bernese Accuracy:	TBP Parameters:	TBP Accuracy:
Translation X	-0.0022	0.0019	0.0025	0.0012
Translation Y	-0.0039	0.0019	0.0002	0.0012
Translation Z	-0.0025	0.0019	0.0010	0.0012
Rotation w.r.t. X	0.0000	0.0000	-0.0000	0.0000
Rotation w.r.t. Y	0.0000	0.0000	-0.0000	0.0000
Rotation w.r.t. Z	-0.0000	0.0000	0.0000	0.0000
Scale factor	1.000	0.0000	1.000	0.0000

## 4 Results and discussion

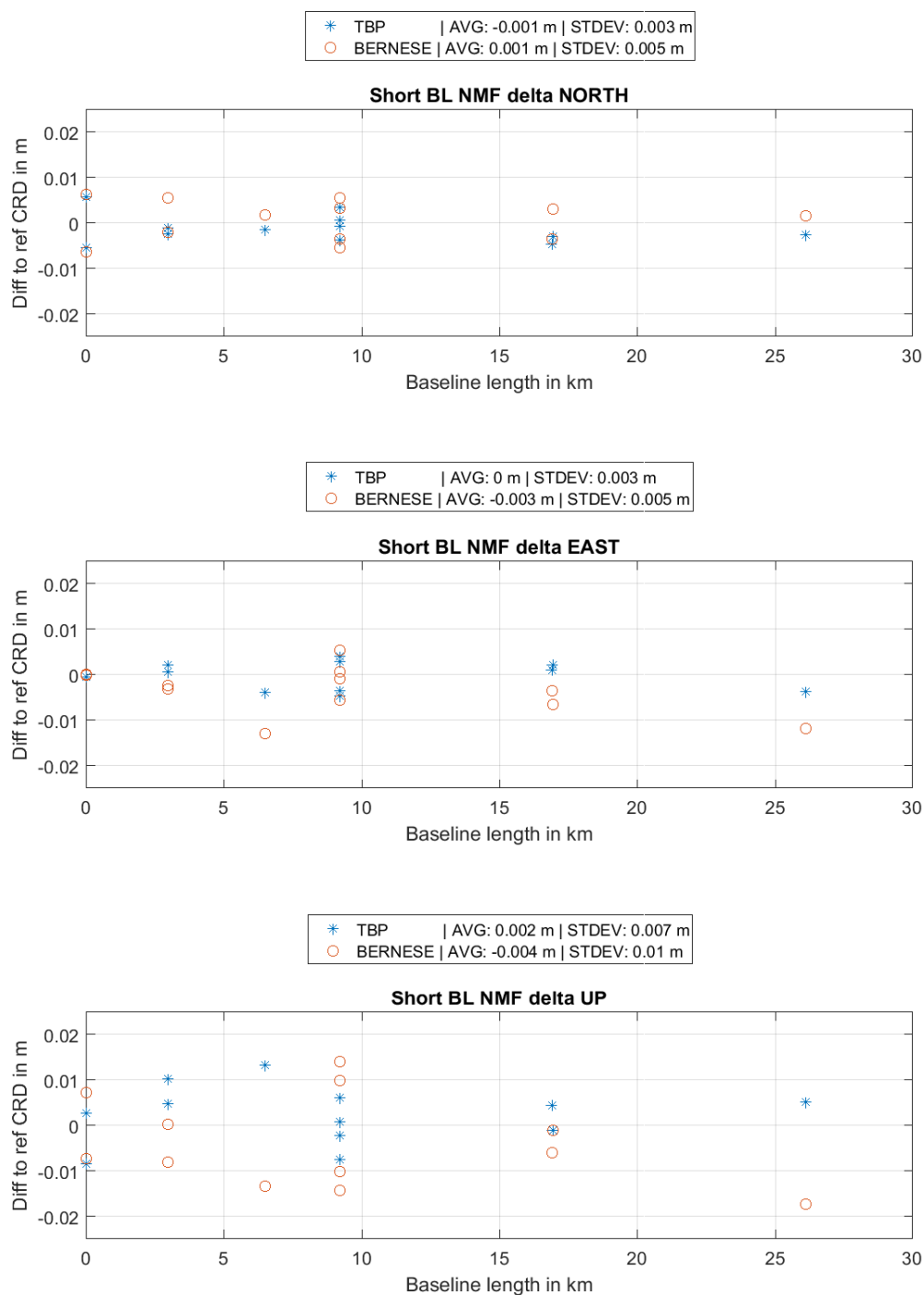


Figure 26: Delta NEU short baselines, NMF

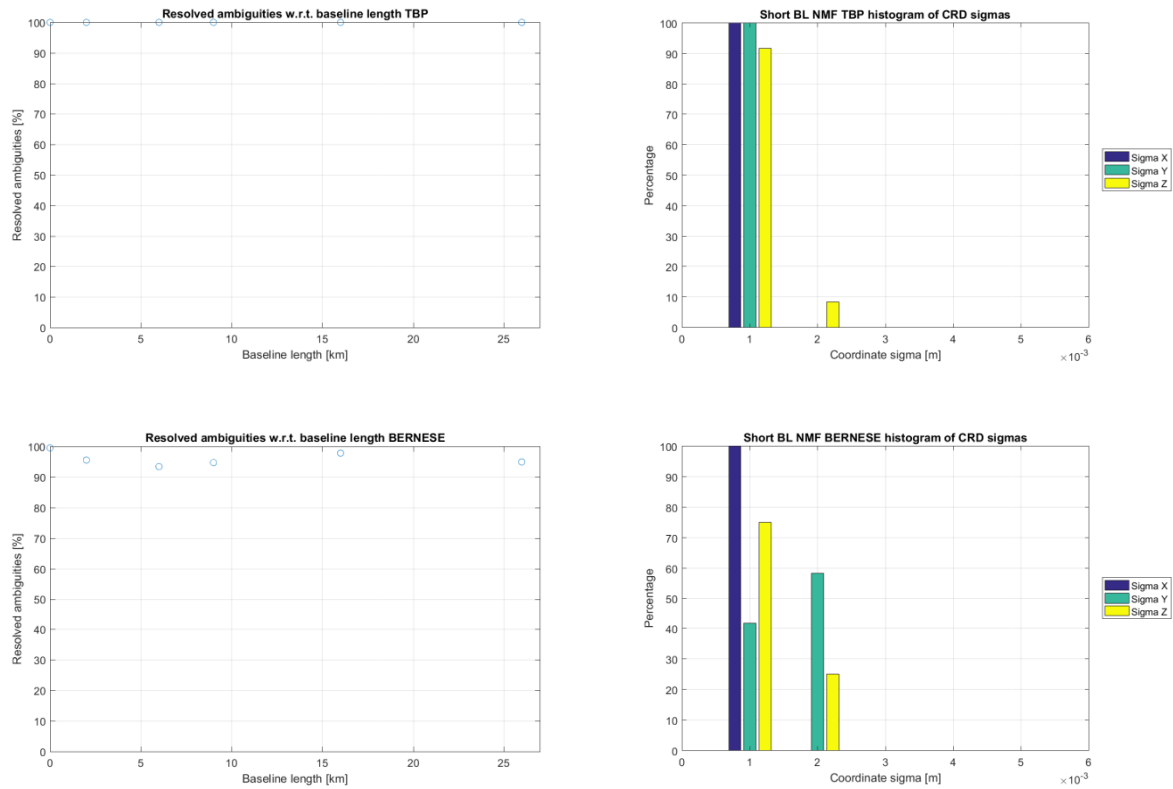


Figure 27: Left: Percentage of resolved ambiguities for short baselines, NMF; Right: Histogram of coordinate sigmas for short baselines, NMF;

#### 4.2.1.2 Medium baselines

The same expectations for medium baselines are valid as for short baselines. And again the results do not show significant changes in the coordinate difference plot (figure 28), as well as the ambiguity resolution percentage (figure 29 on the left) and the coordinate sigmas (figure 29 on the right). If anything the coordinate differences seem a little more spread than before, but again on the 1 mm level. Very subtle changes regarding the average values of the coordinate differences are visible in the horizontal component compared to the standard processing procedure. Again the coordinate sigma values w.r.t. the baseline length are illustrated in figure A 6 in the appendix. The translation of the Helmert transformation (table 9) of the TBP in the Z component decreases from -0.0017 (standard procedure) to -0.0026 when using the NMF and fits together nicely with the Bernese parameters.

## 4 Results and discussion

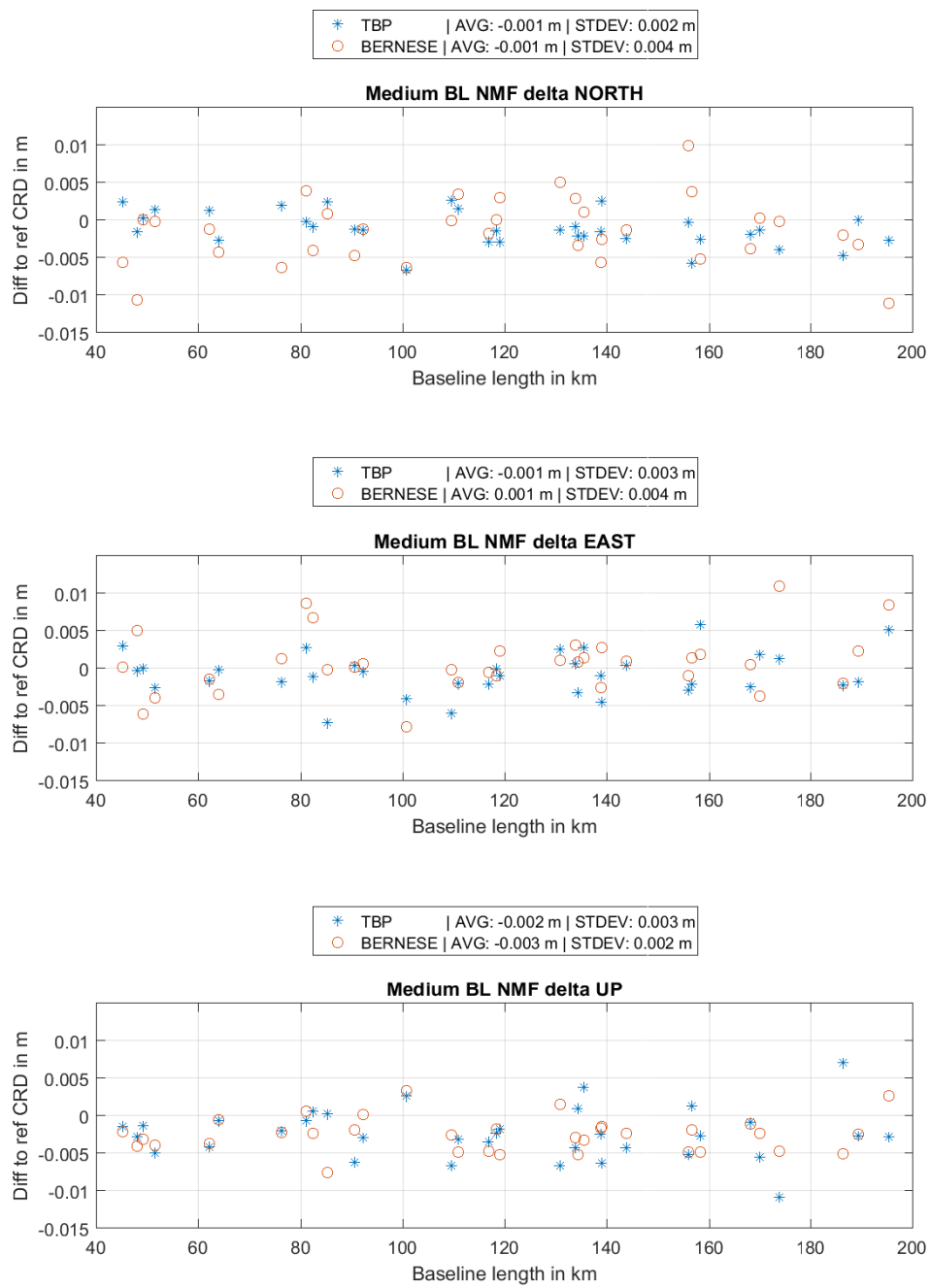
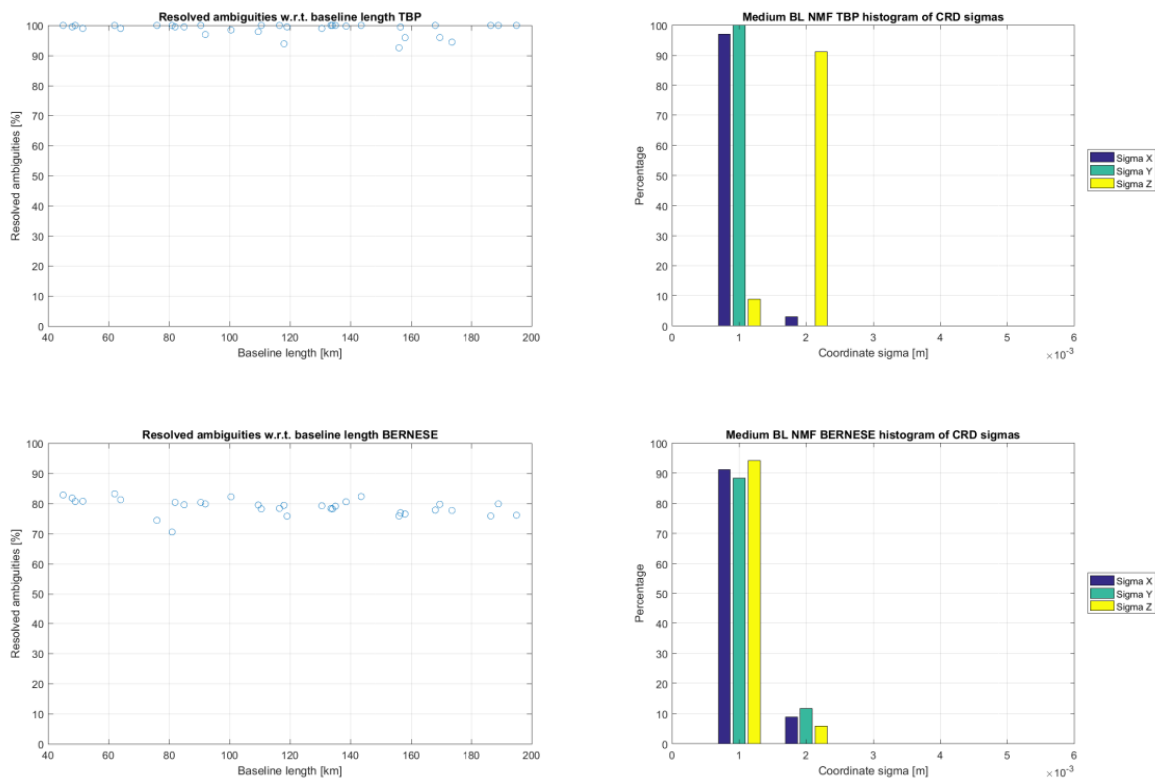


Figure 28: Delta NEU medium baselines, NMF

**Table 9: 3D Helmert transformation parameters for TBP and Bernese, medium baselines, NMF**

	Bernese Parameters:	Bernese Accuracy:	TBP Parameters:	TBP Accuracy:
Translation X	-0.0007	0.0006	-0.0006	0.0005
Translation Y	0.0006	0.0006	-0.0008	0.0005
Translation Z	-0.0029	0.0006	-0.0026	0.0005
Rotation w.r.t. X	-0.0000	0.0000	0.0000	0.0000
Rotation w.r.t. Y	-0.0000	0.0000	0.0000	0.0000
Rotation w.r.t. Z	0.0000	0.0000	-0.0000	0.0000
Scale factor	1.000	0.0000	1.000	0.0000



**Figure 29: Left: Percentage of resolved ambiguities for medium baselines, NMF; Right: Histogram of coordinate sigmas for medium baselines, NMF;**

## 4.2.1.3 Long baselines

Due to the processing failure of the TBP for several very long baselines the results for long baselines will be displayed up to a length of 6000 kilometers. Additionally only the transformation parameters for the USA-Canada data set are shown here since the transformation regarding Africa is biased too strongly by the float solutions. The results regarding the full baseline lengths as well as the transformation parameters for Africa processed with the NMF are stated in figures A8 to A 10 and table A 1 in the appendix as well as the coordinate sigma values w.r.t. the baseline length in figure A 7 for the cutoff as in the previous sections.

Again as expected the results do not show any significant differences w.r.t. the standard processing procedure regarding coordinate differences (figure 30), percentage of resolved ambiguities (figure 31, left) and coordinate sigmas (figure 31, right) apart from changes in the average and standard deviation of the coordinate differences at the mm level. The Helmert transformation parameters for USA-Canada NMF (table 10) change at the 0.1 mm level. The results, as expected, are a perfect match.

**Table 10: 3D Helmert transformation parameters for TBP and Bernese, USA-Canada, NMF**

	Bernese Parameters:	Bernese Accuracy:	TBP Parameters:	TBP Accuracy:
Translation X	-0.0008	0.0009	-0.0018	0.0012
Translation Y	0.0002	0.0009	-0.0054	0.0012
Translation Z	-0.0004	0.0009	0.0054	0.0012
Rotation w.r.t. X	0.0000	0.0000	0.0000	0.0000
Rotation w.r.t. Y	0.0000	0.0000	0.0000	0.0000
Rotation w.r.t. Z	0.0000	0.0000	0.0000	0.0000
Scale factor	1.000	0.0000	1.000	0.0000

## 4 Results and discussion

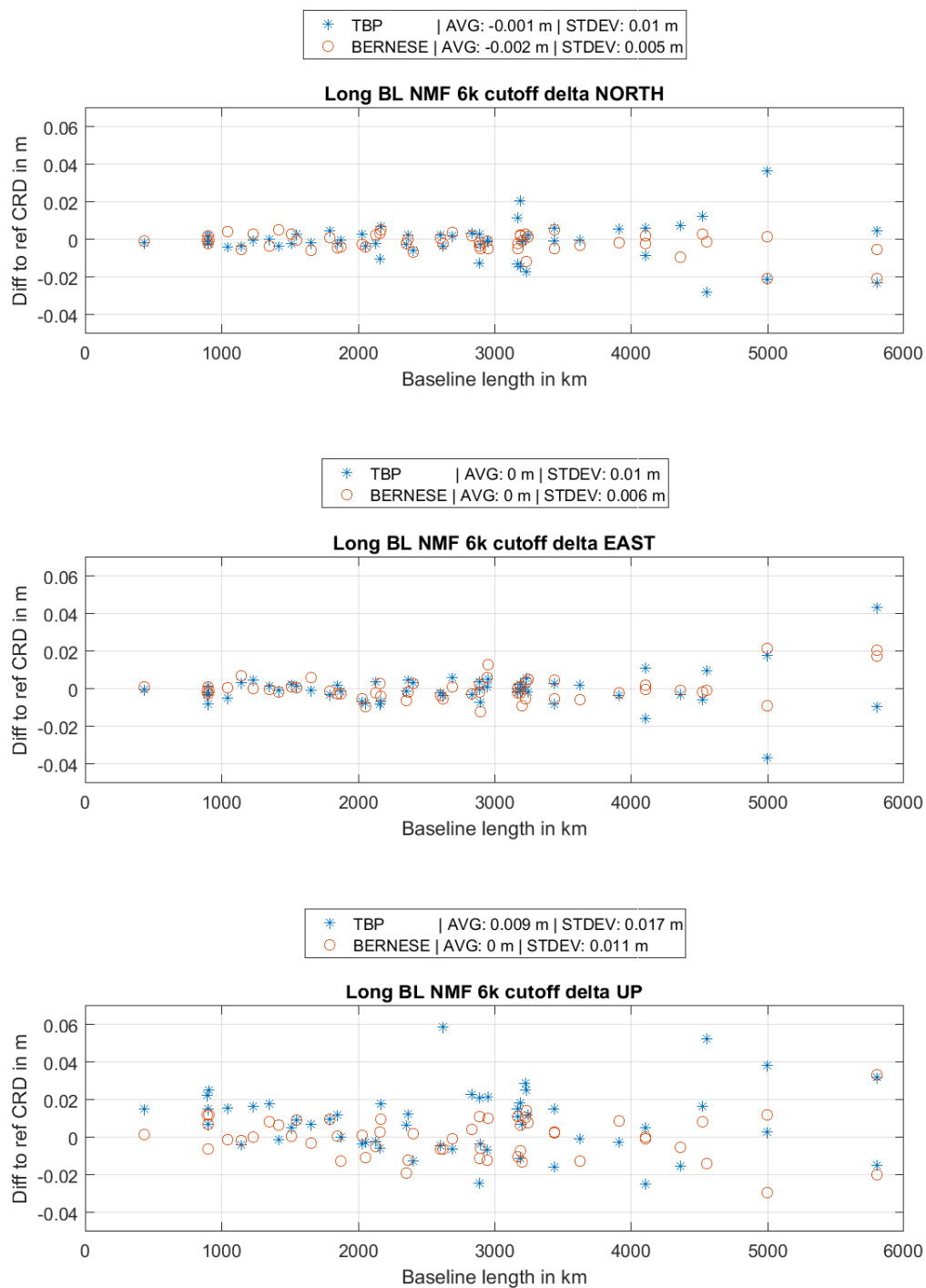


Figure 30: Delta NEU long baselines, 6000 km cutoff, NMF

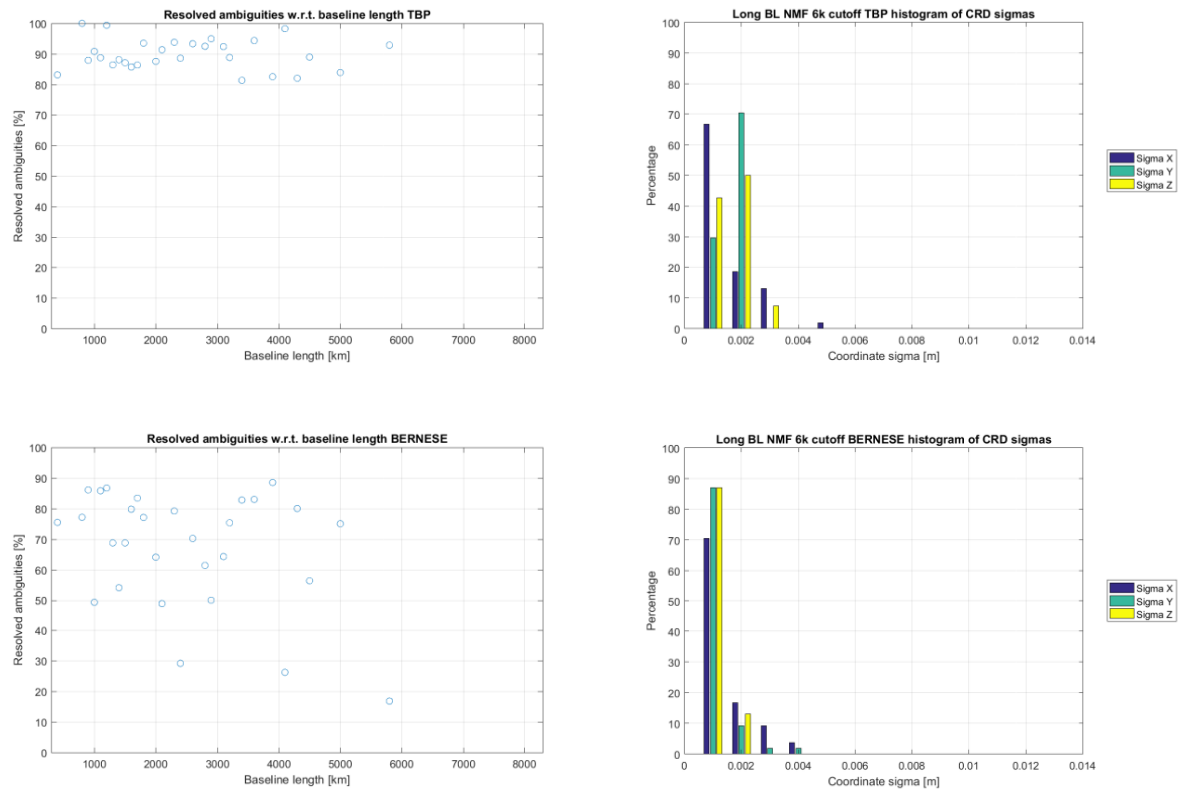


Figure 31: Left: Percentage of resolved ambiguities for long baselines, 6000 km cutoff, NMF; Right: Histogram of coordinate sigmas for long baselines, 6000 km cutoff, NMF;

## 4.2.2 VMF

### 4.2.2.1 Short baselines

Figure 32 shows the difference between reference coordinates and coordinates computed using the VMF mapping function. Due to the similarity between GMF and VMF and of course the very short baselines no significant differences w.r.t. the standard processing can be manifested except for again, changes at the 1 mm level for standard deviation and average value of the coordinate differences. Also the ambiguity resolution percentage (figure 33, left) and coordinate sigmas (figure 33, right) show great consistence. The 3D Helmert transformation parameters for the Bernese solution (table 11) also show great consistence. The results match the ones from the standard processing procedure, therefore no false bias is introduced by the change of the tropospheric correction model. The coordinate sigmas w.r.t. the baseline length is displayed in figure A 11 in the appendix.

## 4 Results and discussion

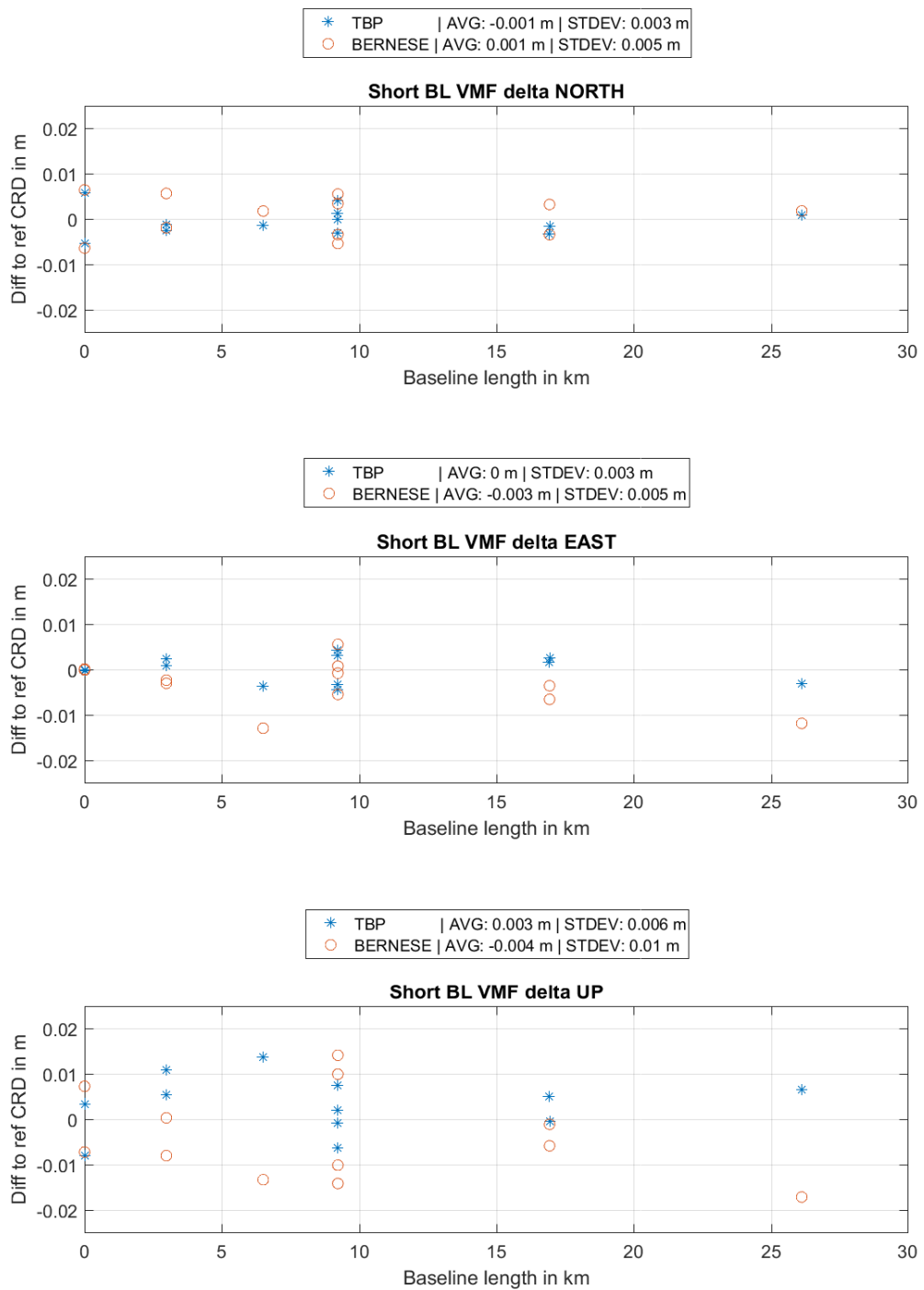
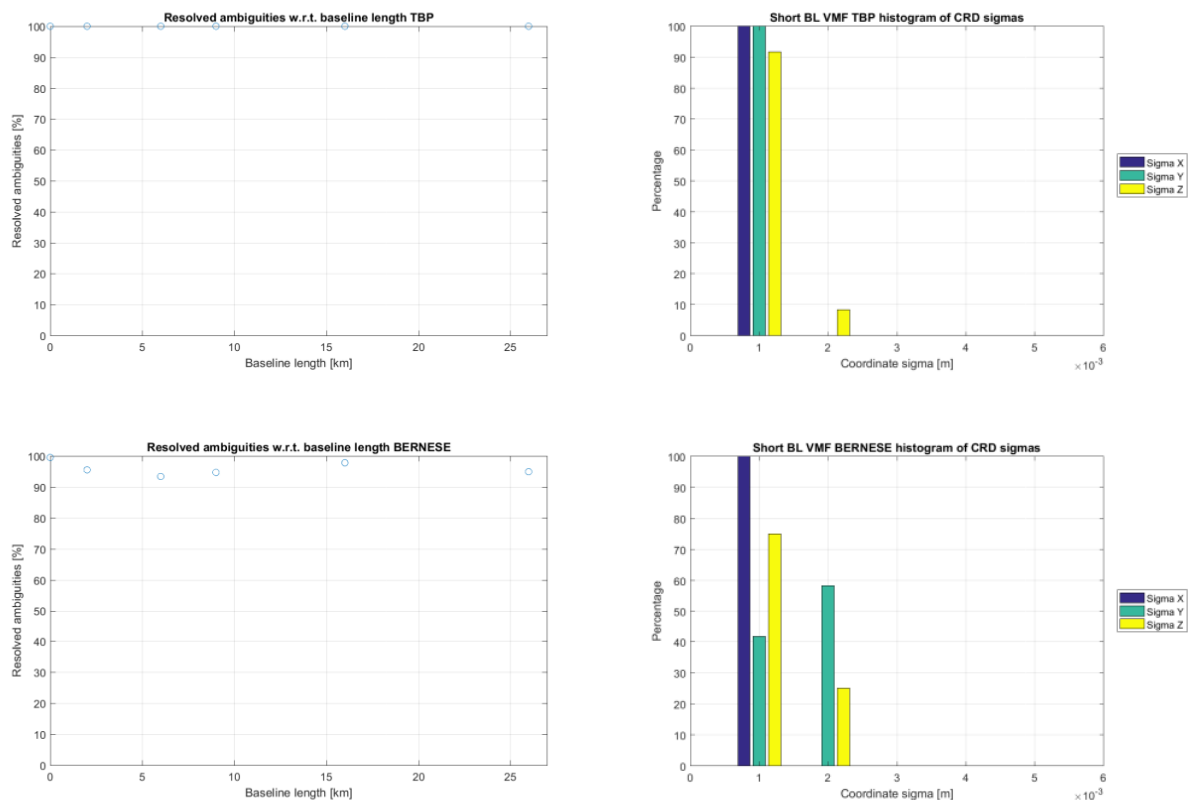


Figure 32: Delta NEU short baselines, VMF

**Table 11: 3D Helmert transformation parameters for TBP and Bernese, short baselines, VMF**

	Bernese Parameters:	Bernese Accuracy:	TBP Parameters:	TBP Accuracy:
Translation X	-0.0022	0.0019	0.0025	0.0012
Translation Y	-0.0039	0.0019	0.0005	0.0012
Translation Z	-0.0024	0.0019	0.0020	0.0012
Rotation w.r.t. X	0.0000	0.0000	-0.0000	0.0000
Rotation w.r.t. Y	0.0000	0.0000	-0.0000	0.0000
Rotation w.r.t. Z	-0.0000	0.0000	0.0000	0.0000
Scale factor	1.000	0.0000	1.000	0.0000



**Figure 33: Left: Percentage of resolved ambiguities for short baselines, VMF; Right: Histogram of coordinate sigmas for short baselines, VMF**

#### 4.2.2.2 Medium baselines

The distribution and magnitude of the coordinate sigmas (figure 34, right) and the percentage of resolved ambiguities (figure 34, left) are again not affected by the change of the mapping function for medium baselines. Figure 35 shows the differences between the estimated coordinates using the VMF mapping function w.r.t. the reference coordinates for medium baselines. Here in the north component the average value of the coordinate differences is reduced by 1 mm w.r.t. the standard processing for both the TBP and Bernese solutions and the standard deviation is decreased by one mm (only for Bernese). This is a subtle change, however the results from both tools show a

similar effect. The Helmert transformation parameters (table 12) regarding the translation in X and Y component decrease towards zero, however the Z component increases for both software solutions, which explains the change in delta north in figure 35. The coordinate sigma values w.r.t. to the baseline length are depicted in figure A 12 in the appendix.

**Table 12: 3D Helmert transformation parameters for TBP and Bernese, medium baselines, VMF**

	Bernese Parameters:	Bernese Accuracy:	TBP Parameters:	TBP Accuracy:
Translation X	0.0002	0.0005	-0.0002	0.0005
Translation Y	0.0007	0.0005	-0.0005	0.0005
Translation Z	-0.0039	0.0005	-0.0025	0.0005
Rotation w.r.t. X	-0.0000	0.0000	0.0000	0.0000
Rotation w.r.t. Y	-0.0000	0.0000	0.0000	0.0000
Rotation w.r.t. Z	0.0000	0.0000	-0.0000	0.0000
Scale factor	1.000	0.0000	1.000	0.0000

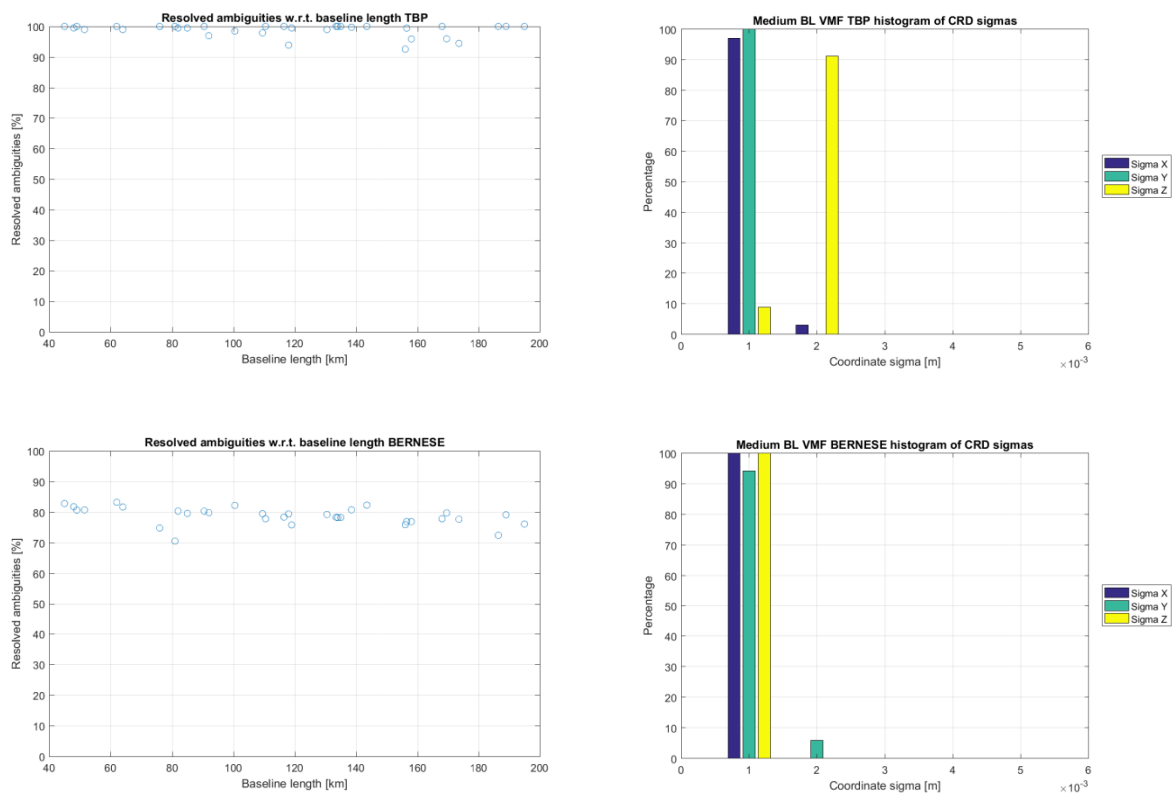


**Figure 34: Left: Percentage of resolved ambiguities for medium baselines, VMF; Right: Histogram of coordinate sigmas for medium baselines, VMF**

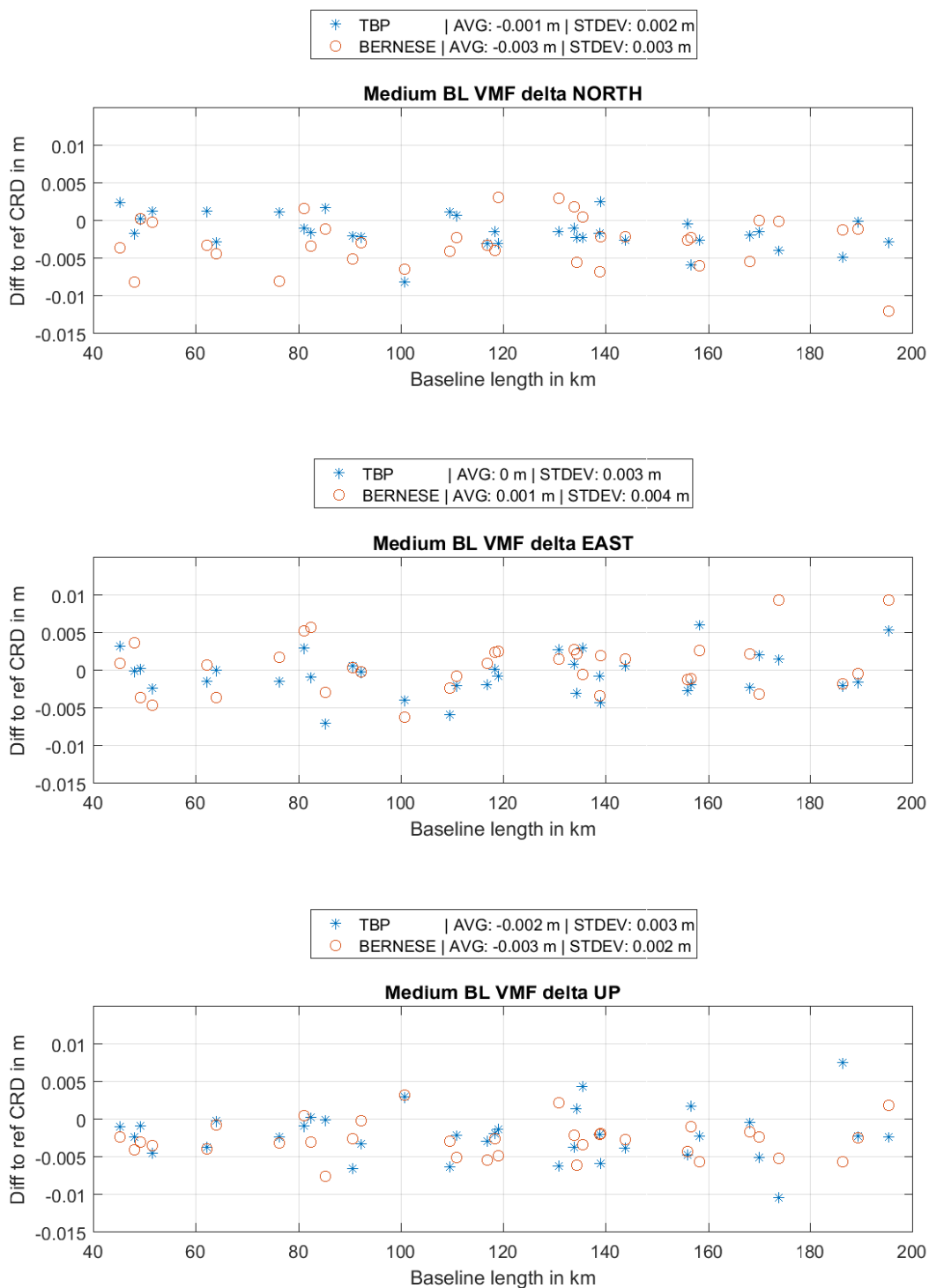


Figure 35: Delta NEU medium baselines, VMF

## 4.2.2.3 Long baselines

Figure 36 analogue shows the results for long baselines for the VMF. Again the results for long baselines are only shown to a baseline length of 6000 kilometers. The full results with the transformation parameters for dataset Africa are illustrated in figures A 14 to A 16 and table A 2 in the appendix, together with the coordinate sigmas of the 6000 km cutoff data w.r.t. the baseline length (figure A 13 in the appendix). The Bernese coordinate differences however show a change of 1 mm in the average value of the east component (0 instead of 0.001 w.r.t. to the standard processing) where the TBP results show an increase of 1 mm in the standard deviation. In the up component the average value of the Bernese results increases from 0 to 1 mm but at the same time the standard deviation decreases by 1 mm. Regarding the TBP the average value of decreases by 1 mm, the standard deviation remains unchanged. With the decrease of the mean value of the TBP in the up component it seems as both processors appear to improve the results w.r.t. GMF solutions. The increasing standard deviation of the TBP in the east component is rather contradictive. Regarding the 3D Helmert transformation parameters (table 13) the translation of the Bernese solution does not change significantly w.r.t. GMF. The values for the TBP however in Y and Z component however improve slightly. This does not follow the effects seen in Bernese perfectly but it is however an improvement. Note that also the TBP results for baselines at this length are in general a little more spread around the reference than the Bernese solution. Again regarding coordinate sigma values (figure 37, right) and resolved ambiguity percentage (figure 37, left) no changes w.r.t. the standard processing procedure is visible.

**Table 13: 3D Helmert transformation parameters for TBP and Bernese, USA-Canada, VMF**

	Bernese Parameters:	Bernese Accuracy:	TBP Parameters:	TBP Accuracy:
Translation X	-0.0011	0.0009	-0.0018	0.0012
Translation Y	-0.0003	0.0009	-0.0038	0.0012
Translation Z	0.0005	0.0009	0.0045	0.0012
Rotation w.r.t. X	0.0000	0.0000	0.0000	0.0000
Rotation w.r.t. Y	0.0000	0.0000	0.0000	0.0000
Rotation w.r.t. Z	0.0000	0.0000	0.0000	0.0000
Scale factor	1.000	0.0000	1.000	0.0000

## 4 Results and discussion

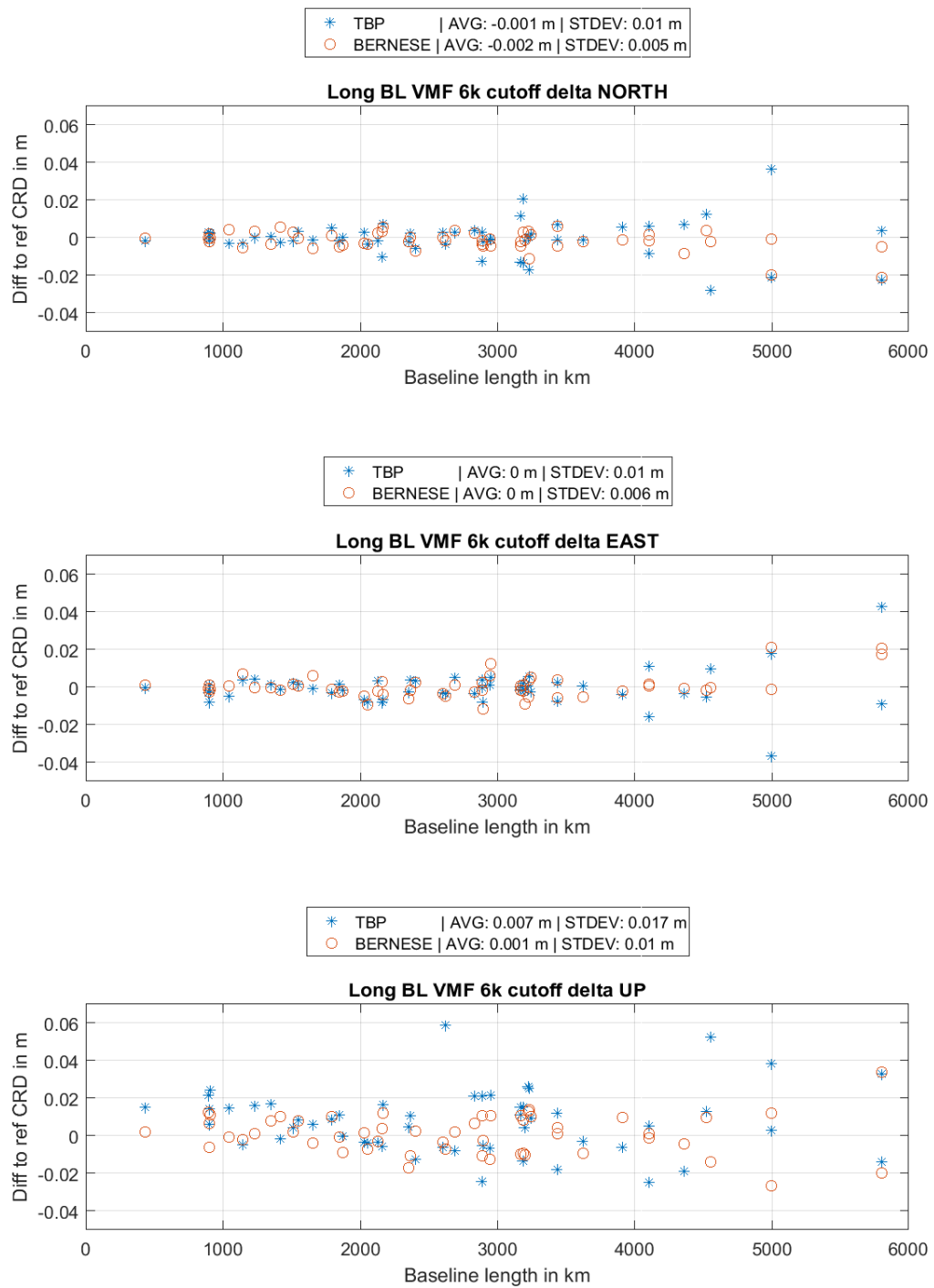
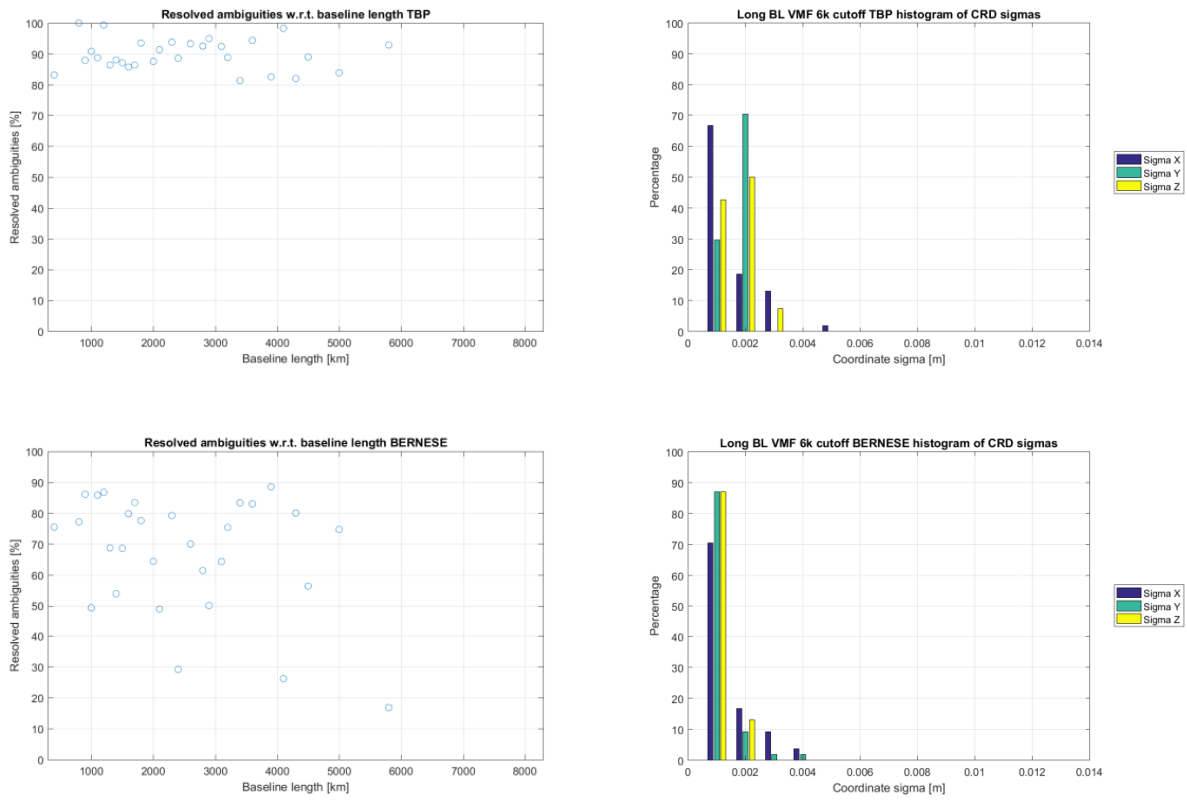


Figure 36: Delta NEU long baselines, 6000 km cutoff, VMF



**Figure 37:** Left: Percentage of resolved ambiguities for long baselines, 6000 km cutoff, VMF; Right: Histogram of coordinate sigmas for long baselines, 6000 km cutoff, VMF;

### 4.3 GPS only

In the following section the datasets are computed using only GPS. It shall reflect the influence of the additional usage of GLONASS or rather when not using GLONASS. Furthermore since GLONASS ambiguity resolution can still be an issue due to the different technology the results in this section compared to the standard procedure (regarding resolved ambiguities) will give some insight into the GLONASS ambiguity resolution performance. Comparisons regarding BEIDOU and GALILEO were discarded due to system status of both and the lack of precise orbit data.

#### 4.3.1 Short baselines

Figure 38 shows the differences between reference and estimated coordinates for short baselines computed by using GPS exclusively. With respect to the GPS/GLONASS solution Bernese shows worse results in the horizontal and up component, the mean values and standard deviations regarding the coordinate differences increase several millimeters. The TBP shows consistent

performance, the standard deviation of the coordinate differences in up even decrease 1 mm. The parameters of the 3D Helmert transformation (table 14) confirm the results. The translation for Bernese in X and Y becomes several millimeters larger whereas the in Z it approaches zero. The uncertainty of the translation is also 1 mm larger. The TBP however shows no significant changes in the transformation parameters, at best a tendency to better translation values but larger uncertainties though. The percentage of resolved ambiguities (figure 39, left) of the TBP shows no change w.r.t. the standard procedure, for Bernese however the average resolved ambiguities for the 6 km and 8 km line(s) are approximately 5 percent lower than in in the standard procedure. This corresponds to the delta plot (figure 38), where these two baseline lengths show the most significant variation of the difference to reference. It is however surprising that the Bernese results for such short baselines are affected quite significantly since the coverage of GPS is more than sufficient. Also the results of the TBP in this case show rather better convergence with the reference than the GPS/GLONASS combined. However both processors feature slightly larger coordinate sigmas (figure 39, right), but can still be considered very accurate. In this test run the TBP features more reliable products than Bernese for the GPS only case for short baselines. The coordinate sigmas w.r.t. baseline length are illustrated in figure A 17 in the appendix.

**Table 14: 3D Helmert transformation parameters for TBP and Bernese, short baselines, GPS only**

	Bernese Parameters:	Bernese Accuracy:	TBP Parameters:	TBP Accuracy:
Translation X	-0.0035	0.0030	0.0029	0.0010
Translation Y	-0.0071	0.0030	0.0006	0.0010
Translation Z	-0.0005	0.0030	0.0015	0.0010
Rotation w.r.t. X	0.0000	0.0000	-0.0000	0.0000
Rotation w.r.t. Y	0.0000	0.0000	-0.0000	0.0000
Rotation w.r.t. Z	-0.0000	0.0000	0.0000	0.0000
Scale factor	1.000	0.0000	1.000	0.0000

## 4 Results and discussion

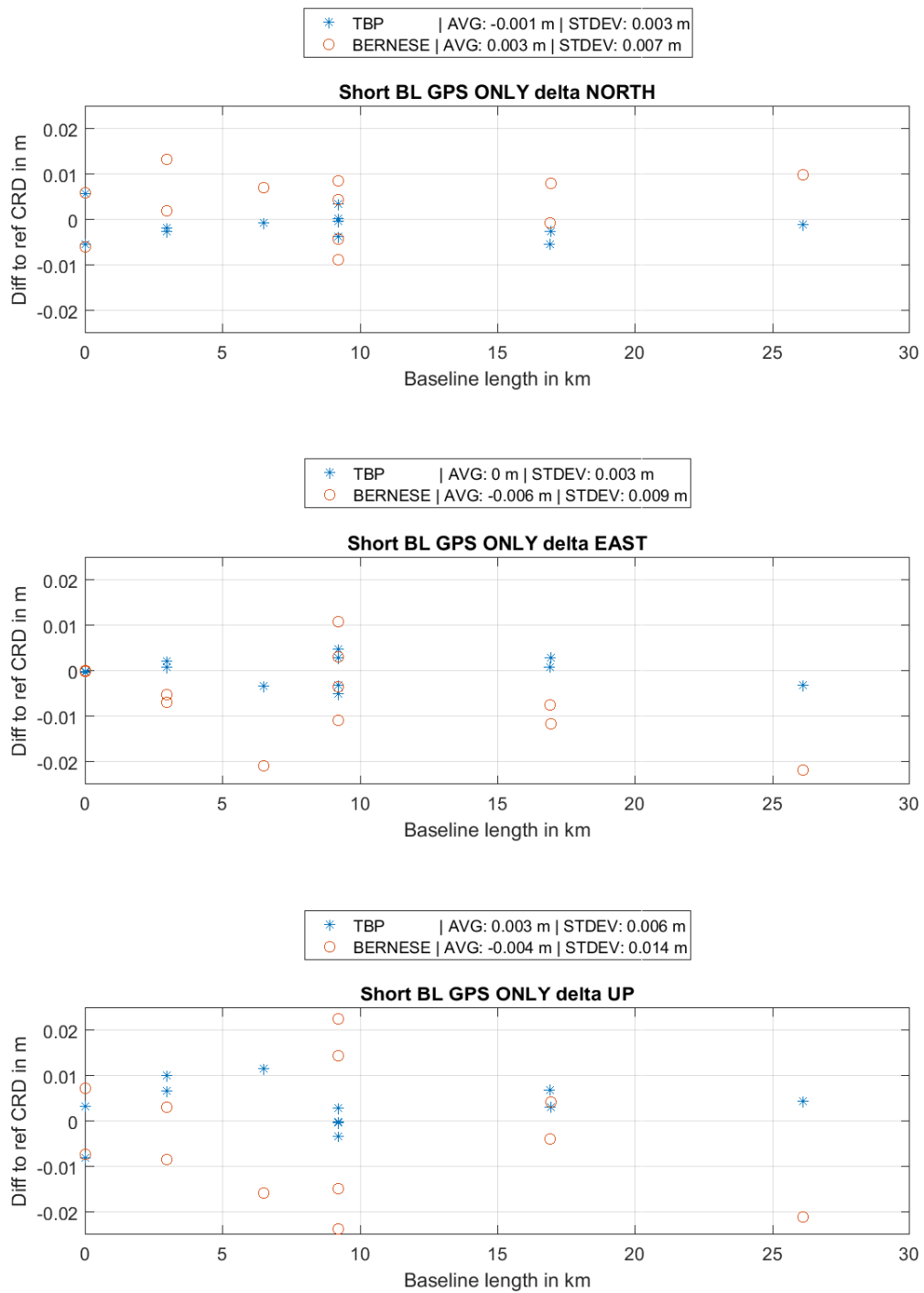
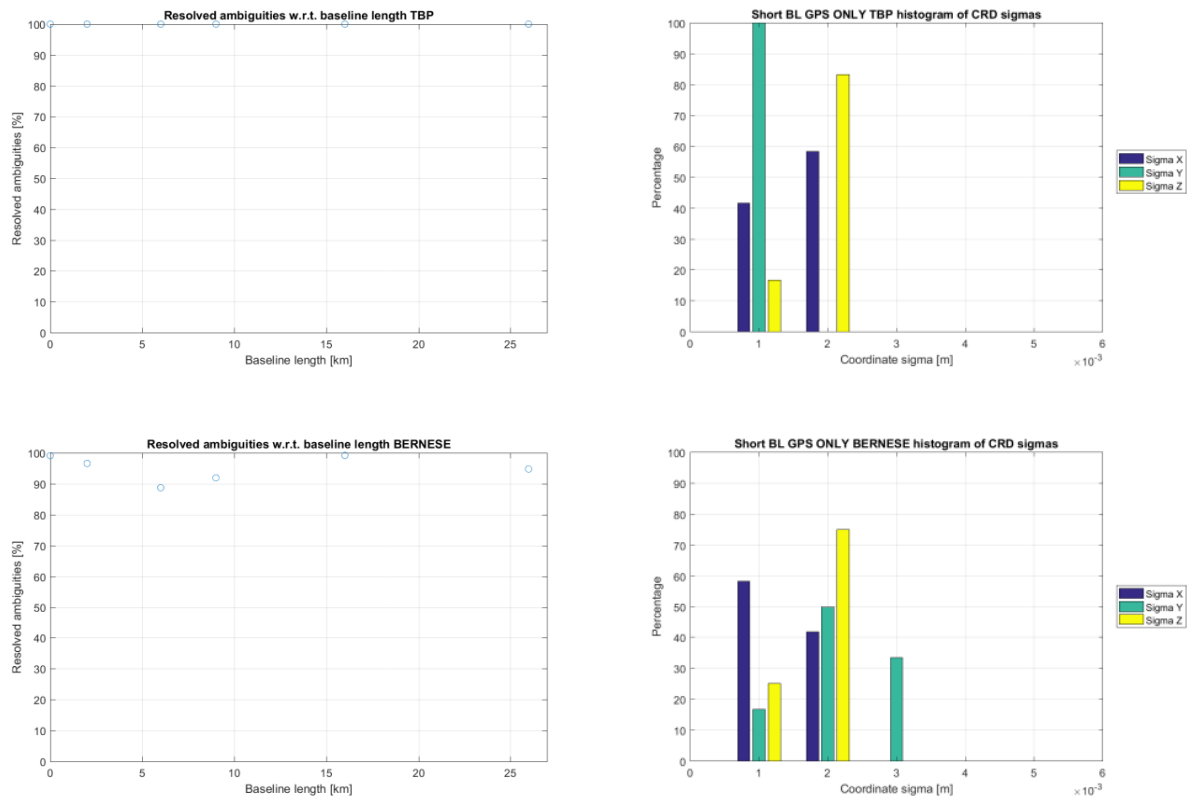


Figure 38: Delta NEU short baselines, GPS only



**Figure 39:** Left: Percentage of resolved ambiguities for short baselines, GPS only; Right: Histogram of coordinate sigmas for short baselines, GPS only;

### 4.3.2 Medium baselines

Estimated coordinates of both processors show a slight increase in the uncertainty (figure 40, right) but nothing crucial. The amount of resolved ambiguities however (figure 40, left) show a less successful resolution for both processors. Interestingly the Bernese percentage values now deviate around 65 percent (STD processing circa 80 percent). Also there appears to be a baseline length depending declination of the number of resolved ambiguities. For the first few baselines the percentage values are centered at 65 percent whereas at the end they are centered at around 60 percent with a continuous pace The TBP is mostly able to resolve about all ambiguities except for very few baselines with a worst case of about 50 percent. Figure 41 states the coordinate differences w.r.t. the reference coordinates for medium baselines computed using GPS only. The Bernese results show a similar trend to the short baselines, i.e. a slight degradation, however at a smaller magnitude. In contrast the TBP results show a slight improvement of the average value of 1 mm (with a 1 mm worse average in the north component) yet only marginal changes appear. The overall differences to the reference from Bernese though (considering the absolute magnitude of the differences) consistently manifest a larger standard deviation of about 2 mm in comparison to the TBP. The 3D Helmert parameters (table 15) regarding the translation show smaller absolute

values for all components of the TBP solution and for Bernese a smaller Z component with a slightly increased Y component (both of around 1 mm). In general, according to the delta plot (figure 41) the spectrum of differences of the TBP is narrower with fewer but larger outliers better centered around zero (compared to the GPS/GLONASS solution) whereas the Bernese results are more spread. Coordinate sigmas are plotted against baseline lengths in figure A 18 in the appendix.

**Table 15: 3D Helmert transformation parameters for TBP and Bernese, medium baselines, GPS only**

	Bernese Parameters:	Bernese Accuracy:	TBP Parameters:	TBP Accuracy:
Translation X	-0.0002	0.0007	-0.0001	0.0005
Translation Y	-0.0015	0.0007	-0.0005	0.0005
Translation Z	-0.0017	0.0007	-0.0010	0.0005
Rotation w.r.t. X	-0.0000	0.0000	0.0000	0.0000
Rotation w.r.t. Y	0.0000	0.0000	0.0000	0.0000
Rotation w.r.t. Z	0.0000	0.0000	-0.0000	0.0000
Scale factor	1.000	0.0000	1.000	0.0000

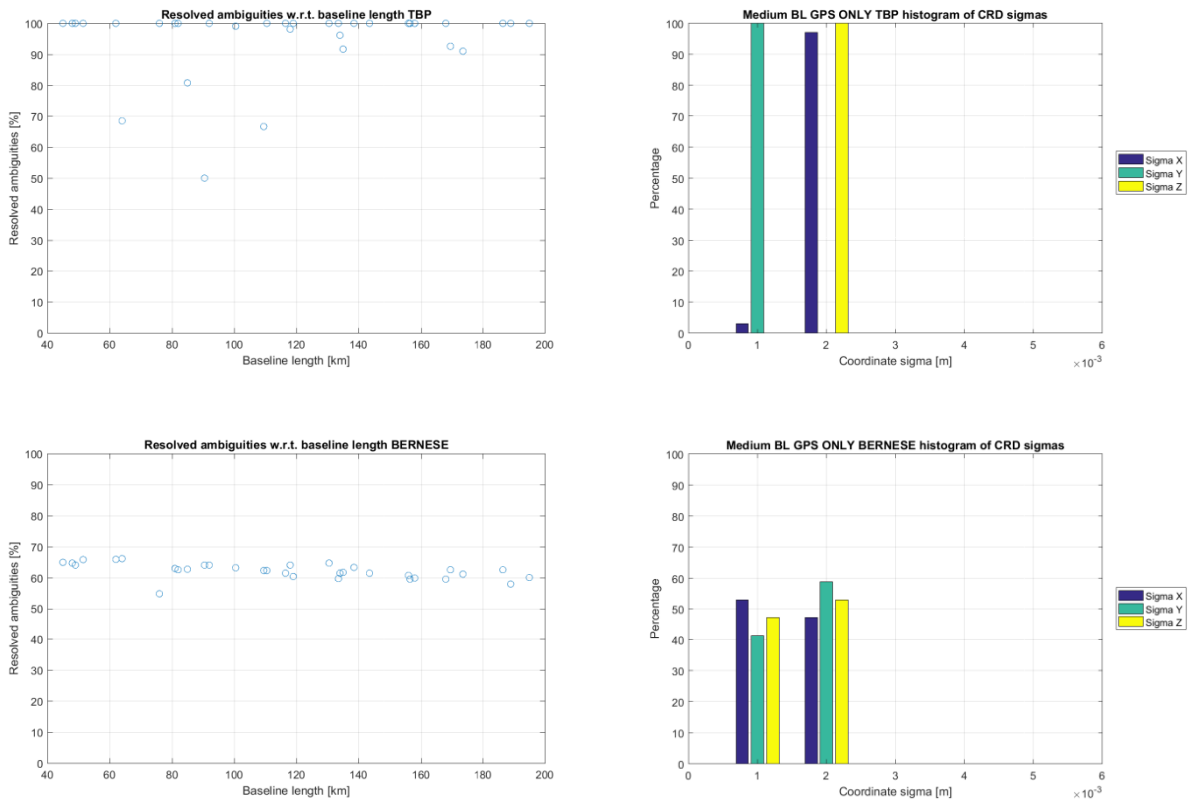


**Figure 40: Left: Percentage of resolved ambiguities for medium baselines, GPS only; Right: Histogram of coordinate sigmas for medium baselines, GPS only;**

## 4 Results and discussion

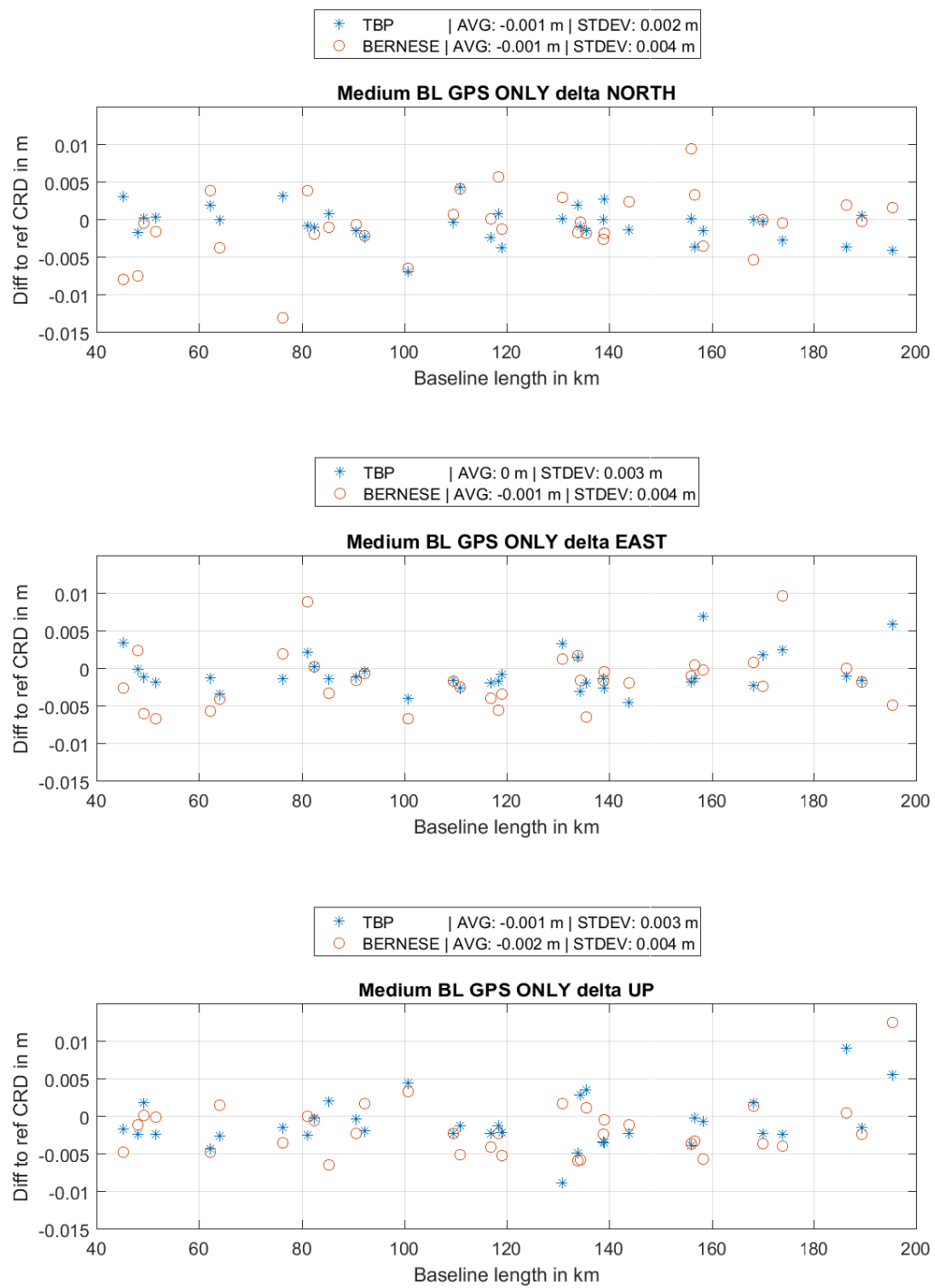


Figure 41: Delta NEU short baselines, GPS medium

### 4.3.3 Long baselines

Again the results are depicted only for baseline lengths up to 6000 km. The complete results regarding coordinate differences, sigma information and resolved ambiguities are stated in figures A 20 to A 22 together with the sigma values w.r.t. baseline length in figure A 19 in the appendix. The Helmert transformation parameters for Africa are given in table A 3 in the appendix. In figure 42 the difference between the reference and computed coordinates for long baselines using GPS only is displayed. Compared to combined (GPS/GLONASS) solution the TBP shows larger outliers with increasing baseline length whereas Bernese keeps its result coordinates fairly reliable within 4 cm w.r.t. to the reference. In fact compared to the combined solution the average and standard deviation of only the up component is off by 1 mm, the average in east improves from 1 mm to 0. Regarding the baseline lengths these changes are entirely negligible. Given the TBP results however, the average and standard deviations change significantly, mostly due to the large outliers introduced by the negligence of GLONASS. The Helmert parameters (table 16) for the dataset USA-Canada support the Bernese results, meaning slightly higher translation values. The parameters for the TBP show only differences at the tenth of a millimeter towards zero in Y and Z and increasing for X. This implies that the overall TBP solution using GPS only fits better to the reference, is however distorted due to the few large outliers. Both processors show a marginal increase in coordinate sigma values (figure 43, right). The average percentage of resolved ambiguities (figure 43, left) shows the same characteristics in distribution for both processors compared to the standard procedure but seemingly centered at another starting value. Where in the case of the TBP the percentage values were centered at around 90 they are deviating around 75 – 80. For Bernese however the resolution appears to be more successful, since the previous worst case intervals from the standard procedure featuring a resolution average below 30 to 20 percent now merely drop below 50. Also in general higher resolution rates are more consistent, with the majority lying between 95 and 70 percent compared to the former 90 to 60.

**Table 16: 3D Helmert transformation parameters for TBP and Bernese, USA-Canada, GPS only**

	Bernese Parameters:	Bernese Accuracy:	TBP Parameters:	TBP Accuracy:
Translation X	-0.0009	0.0009	-0.0023	0.0012
Translation Y	0.0019	0.0009	-0.0040	0.0012
Translation Z	-0.0014	0.0009	0.0047	0.0012
Rotation w.r.t. X	0.0000	0.0000	0.0000	0.0000
Rotation w.r.t. Y	0.0000	0.0000	0.0000	0.0000
Rotation w.r.t. Z	0.0000	0.0000	0.0000	0.0000
Scale factor	1.000	0.0000	1.000	0.0000

## 4 Results and discussion

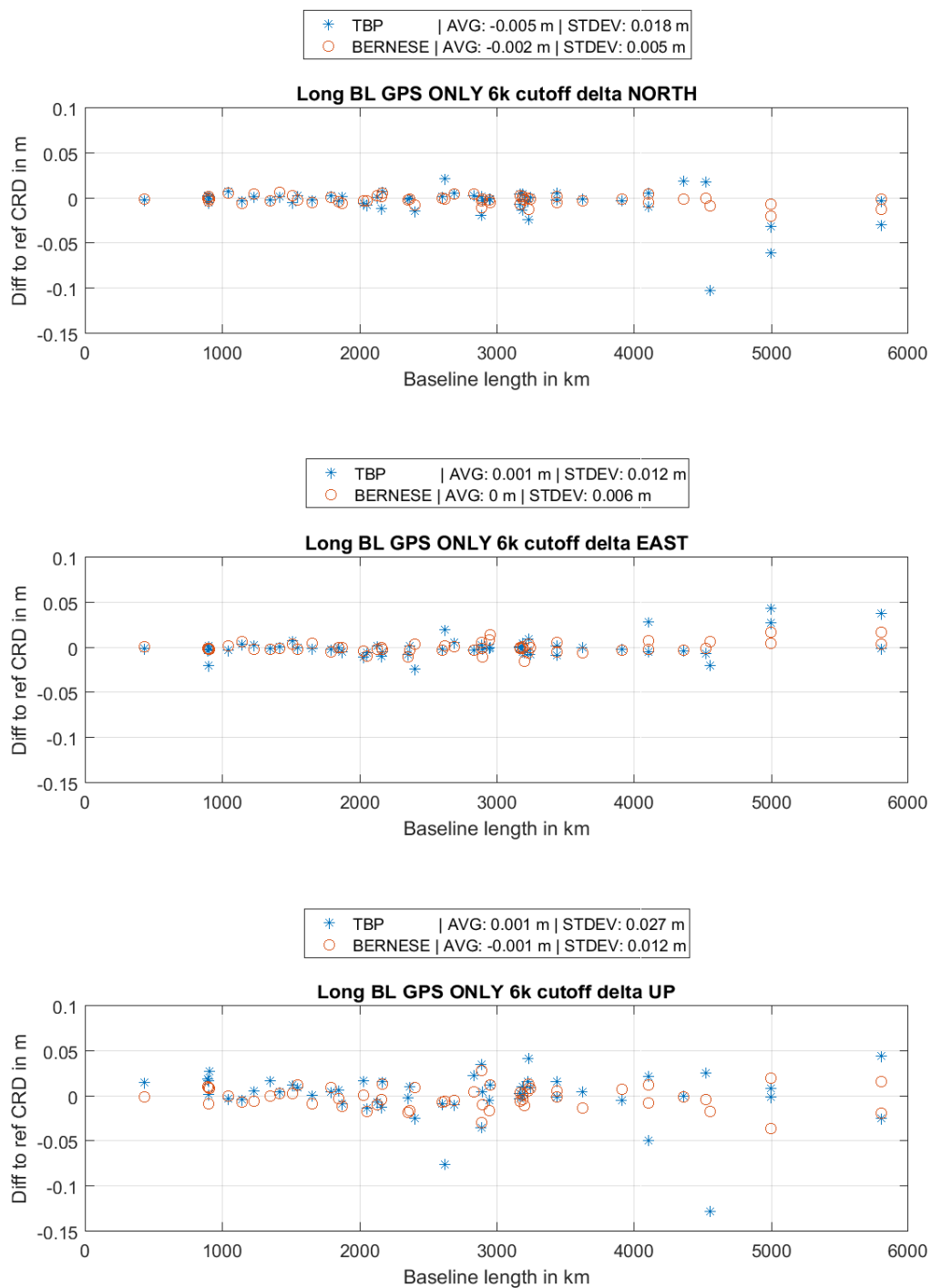
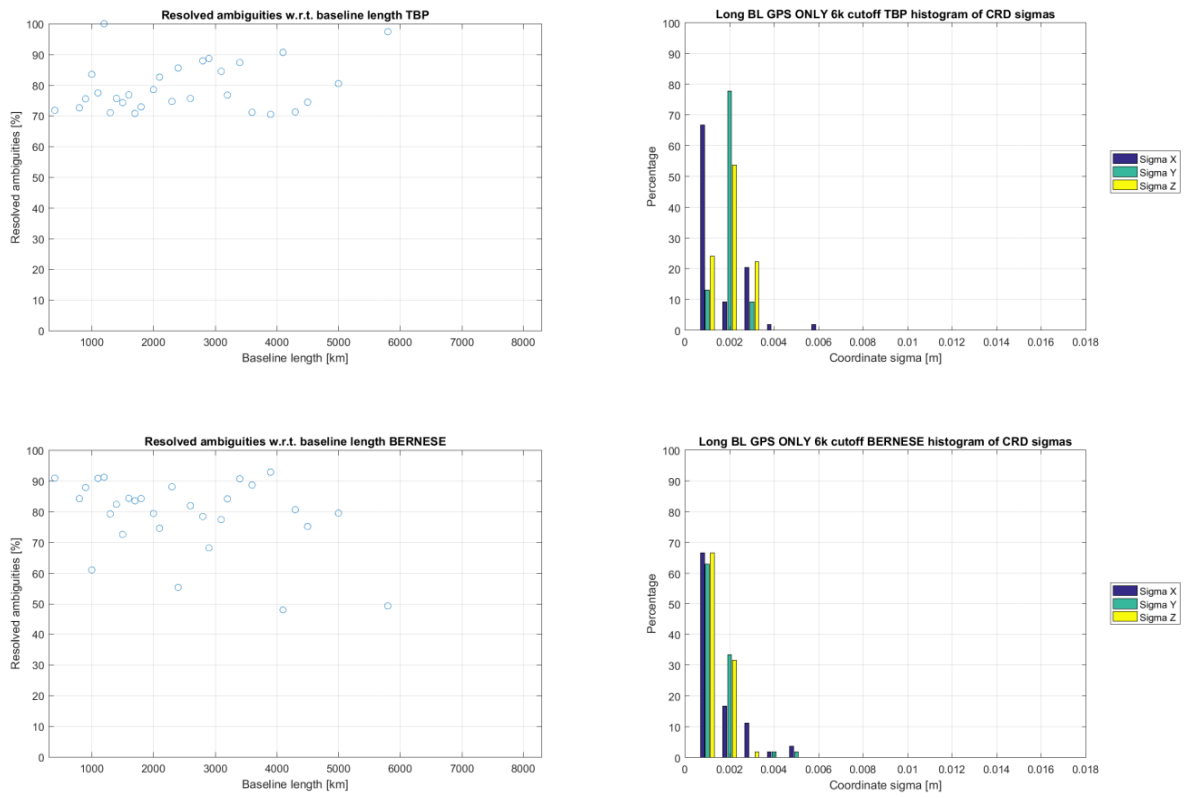


Figure 42: Delta NEU long baselines, 6000 km cutoff, GPS only

## 4 Results and discussion



**Figure 43:** Left: Percentage of resolved ambiguities for long baselines, 6000 km cutoff, GPS only; Right: Histogram of coordinate sigmas for long baselines, 6000 km cutoff, GPS only;

## 4.4 Daily Repeatability

In theory using two daily sessions of observations not far apart from each other (in this case consequent days) should yield consistently the same (or as near as makes no difference) results. For this purpose daily solutions using the standard processing procedure were acquired for DOY 312 and 314 of 2016 in addition to the existing computations for DOY 313. All displayed plot figures show the difference between 2 daily solutions regarding their difference from the reference coordinate, i.e. one figure in this section shows the difference between two delta plots of the type in the previous section for two successive daily solutions (implicit computation of the direct coordinate differences, since:  $(\text{coordsDay1} - \text{ref}) - (\text{coordsDay2} - \text{ref}) = \text{coordsDay1} - \text{coordsDay2}$ ). For a perfect match, i.e. a perfect repeatability of the coordinates (of course this would also imply the premise of perfect and consistent conditions at the GNSS sites, which is not the case) the graphics

### 4.4.1 Short Baselines

Figure 44 respective 45 shows the results for days 312 and 313 respective days 313 314 of 2016. Both processors show fairly consistent performance in the horizontal component, agreeing on the millimeter level (still one has to bear in mind that no network adjustment has been performed). The variation of the up component however exceeds an absolute value of 2 cm (worst case), mostly for the baselines between 3 and 10 km length. The fact that both tools show similar behavior throughout the consecutive days eliminates the possibility of a processing failure, or at least that the software causes these discrepancies. This rather indicates problems either with the hardware of the station or daily changing local properties regarding multipath or maybe satellite visibility. The important result however is the similar characteristics of the independently generated solutions. The TBP coordinates, especially in the horizontal show a slightly higher precision (lower standard deviation) whereas the Bernese results appear to be better centered at zero.

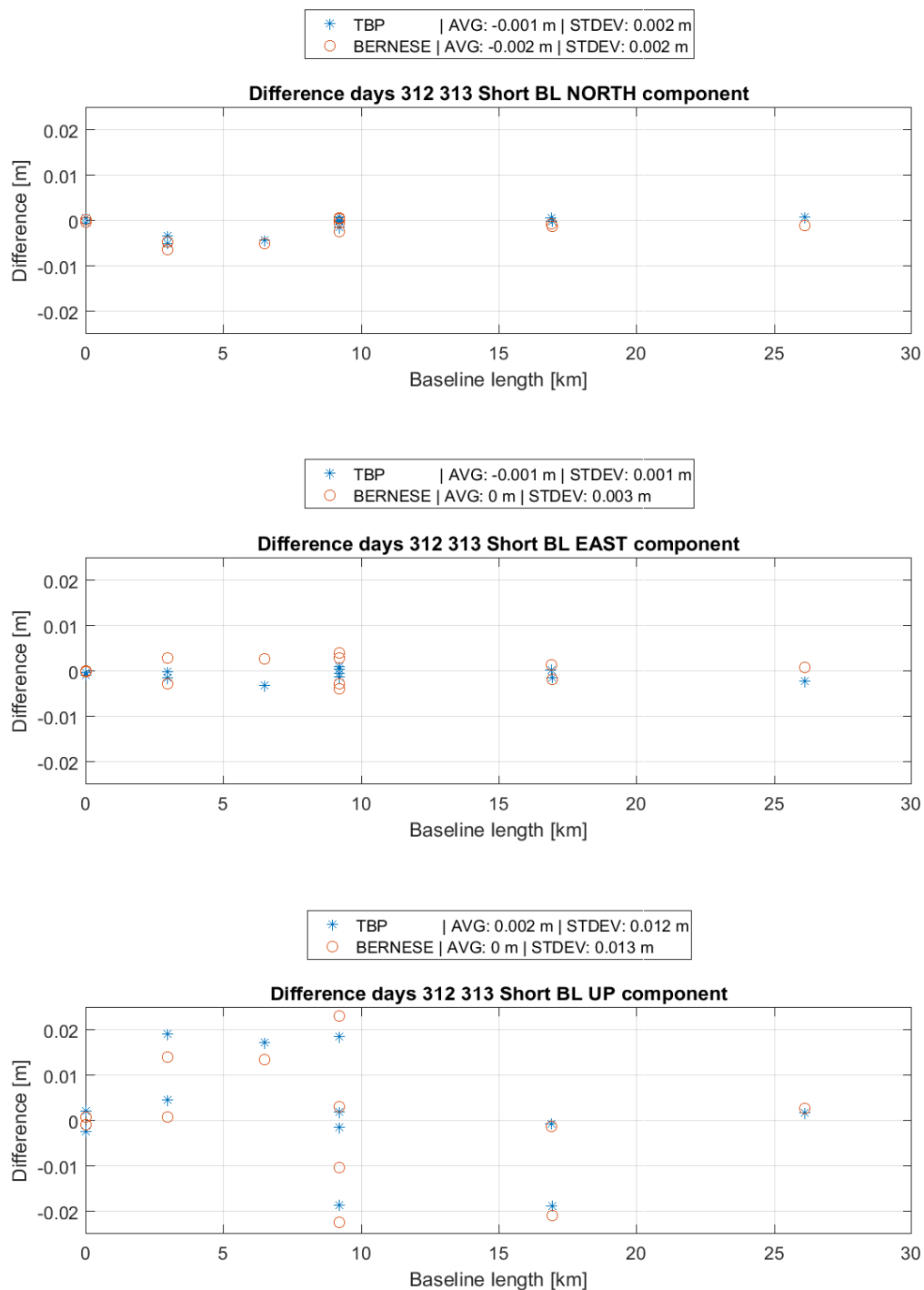


Figure 44: Difference of daily solutions DOY 312 and 313 2016, short baselines

## 4 Results and discussion

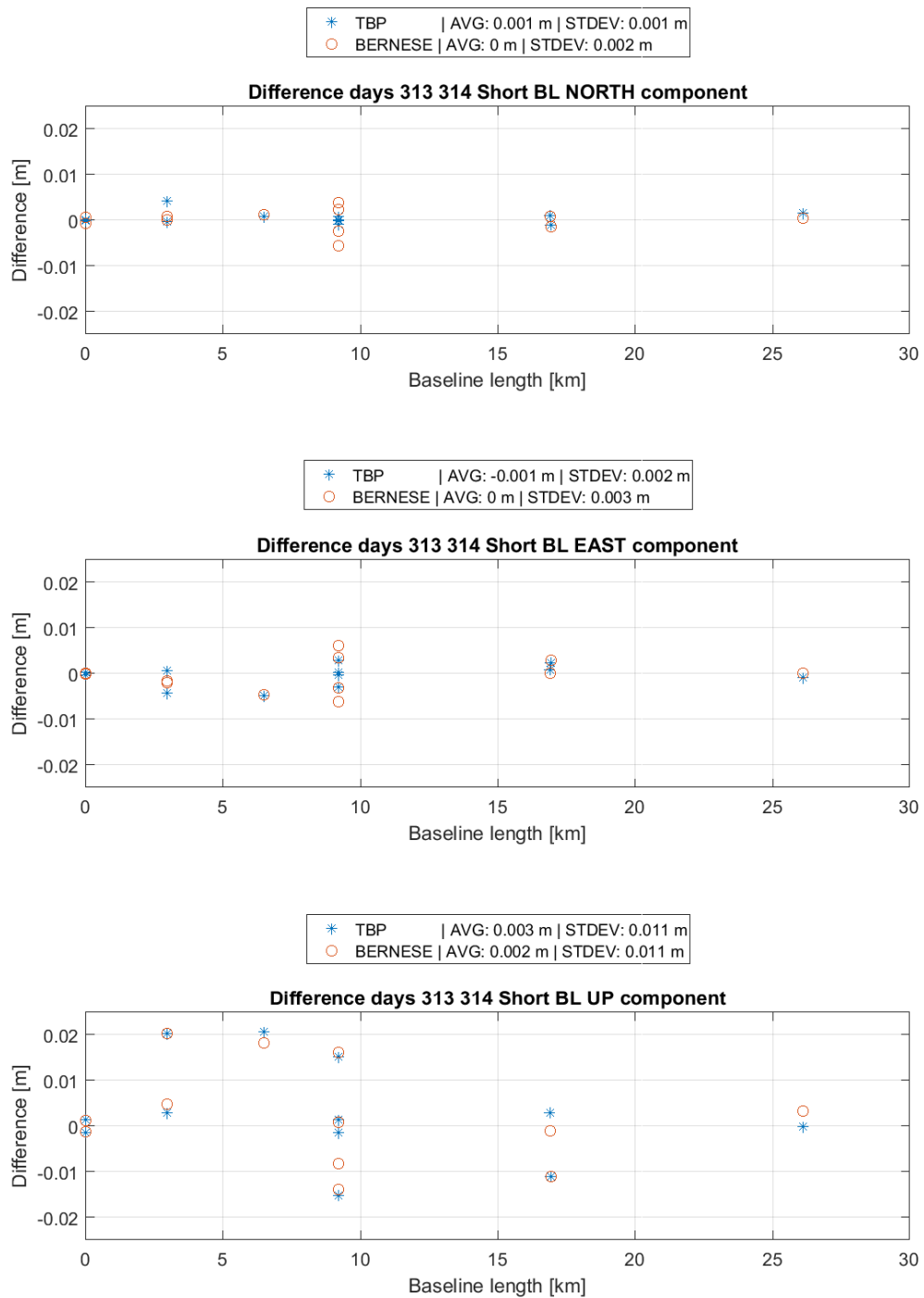


Figure 45: Difference of daily solutions DOY 313 and 314 2016, short baselines

#### 4.4.2 Medium Baselines

Figure 46 and 47 show the differences between days 312 313 and 313 314 of 2016 for medium baselines. Bernese displays up to 150 km a very promising repeatability in all components (except days 312 313 east) with up as the comparatively least stable part. In general only few large discrepancies arise but barely exceed 1 cm. The TBP however shows throughout the whole days and components (except days 312 313 east) more outliers, but also just barely exceeding 1 cm. However comparatively large outliers occur earlier than in the Bernese results, beginning at around 130 km baseline length. Overall the TBP coordinate differences show a larger uncertainty in the up component. The horizontal repeatability of both processors gives fairly even results considering all days and horizontal components, yet larger discrepancies already occur at approximately 20 to 30 kilometer shorter baselines.

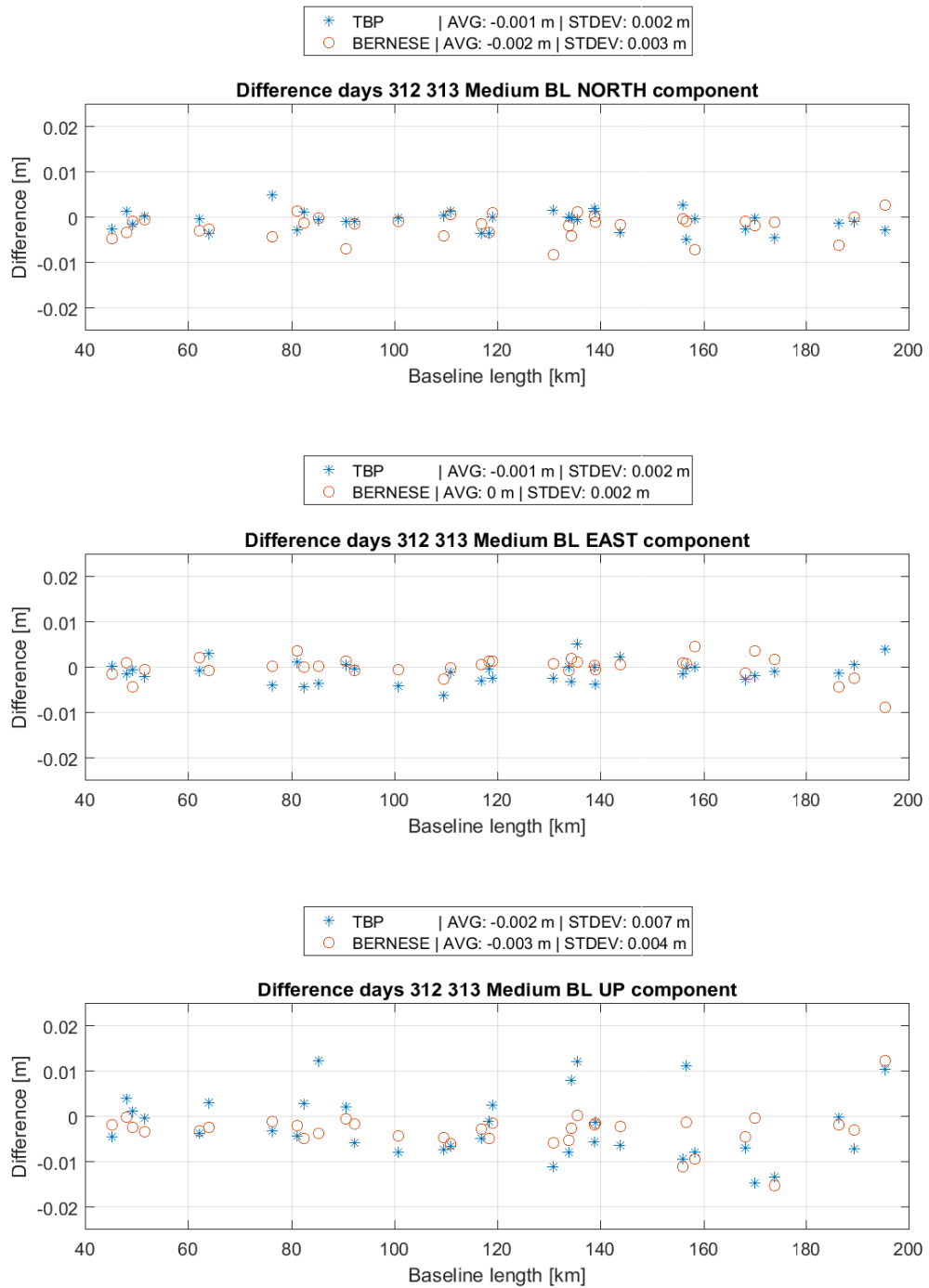


Figure 46: Difference of daily solutions DOY 312 and 313 2016, medium baselines

## 4 Results and discussion

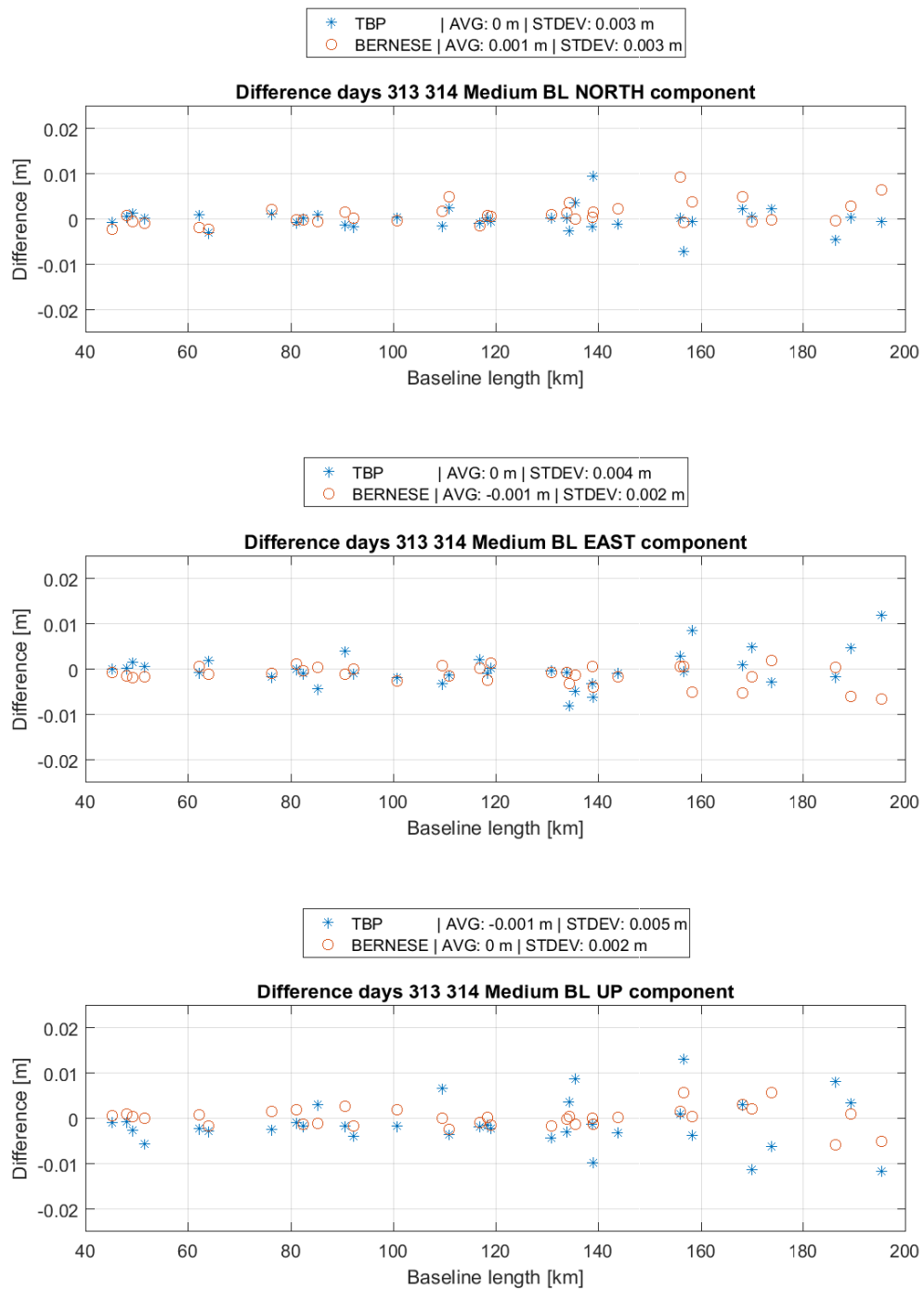


Figure 47: Difference of daily solutions DOY 313 and 314 2016, medium baselines

### 4.4.3 Long Baselines

Also for this case the maximum baseline length was set to 6000 km in order to discard extreme outliers (figures 48 and 49) regarding the TBP. The plots featuring all processed baselines are given in figures A 23 and A 24 in the appendix. The results from Bernese in this case show significantly lower uncertainty and higher precision. Large outliers do not occur at all considering the immense baseline lengths, with maximum inter day differences from Bernese not exceeding 4 cm in all components. The TBP results in general are less consistent and also contain more and larger outliers. This however may origin in the overall worse performance of the TBP for long respective very long baselines compared to Bernese. With a higher uncertainty for long baselines (compared to Bernese) the inter day precision is obviously limited, too. Considering this, the results of the TBP however can be seen as fairly repeatable within the scope of the initial accuracy of the solutions.

## 4 Results and discussion

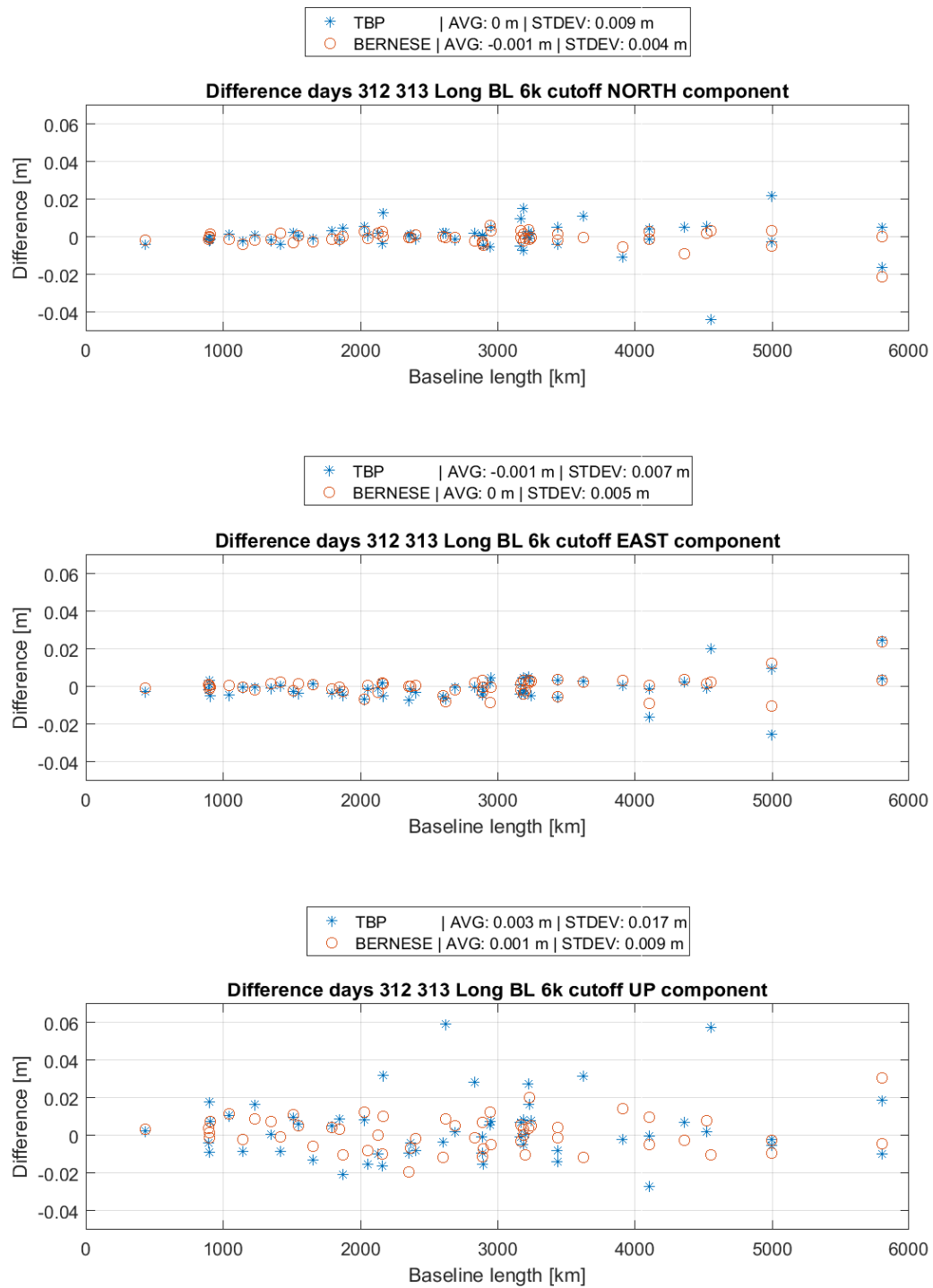


Figure 48: Difference of daily solutions DOY 312 and 313 2016, long baselines, 6000 km cutoff

## 4 Results and discussion

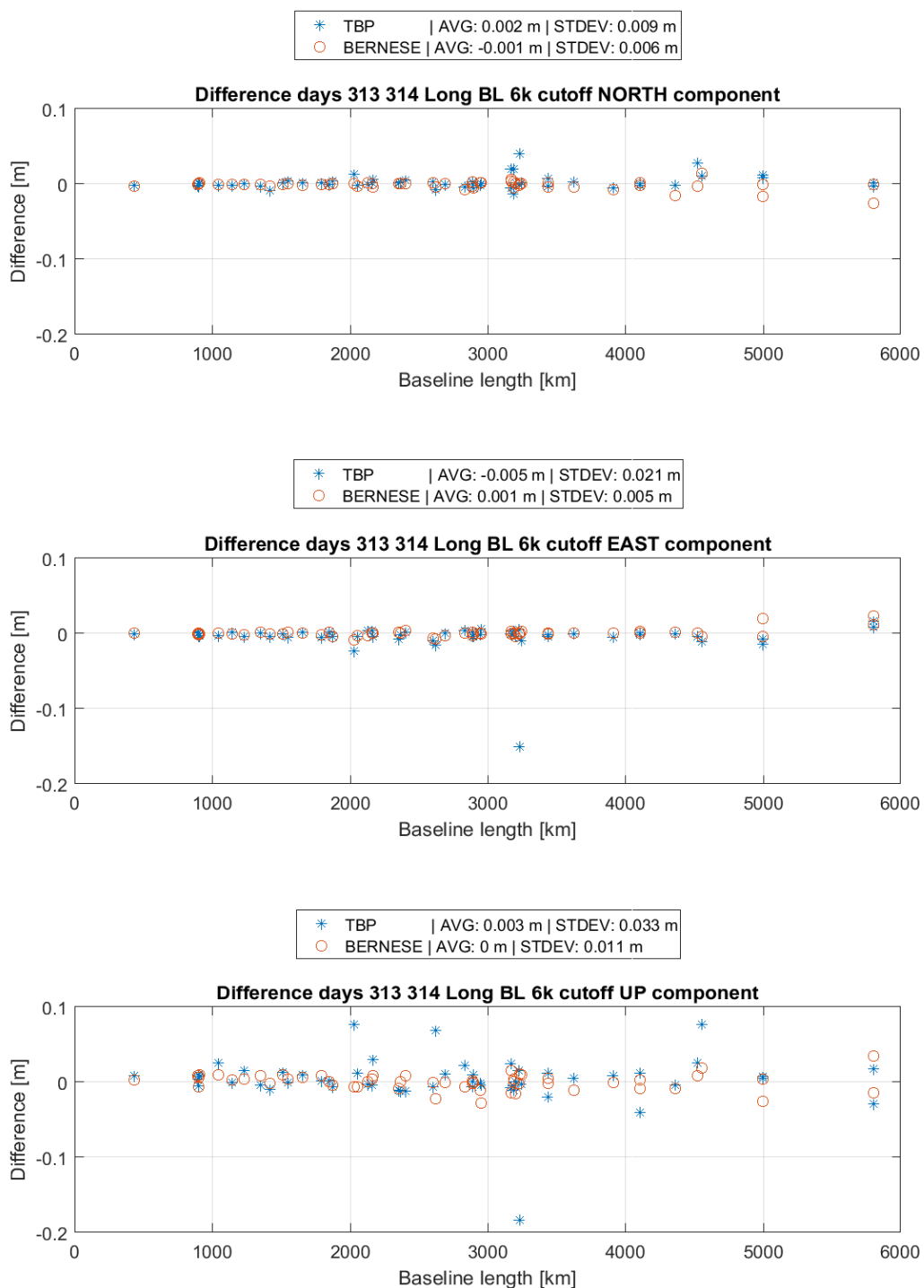


Figure 49: Difference of daily solutions DOY 313 and 314 2016, long baselines, 6000 cutoff

## 4.5 Broadcast Ephemeris

The following section reflects on quality of coordinates computed using broadcast orbits. Due to the limitations in accuracy this experiment is only done for medium and short baselines. It has to be stated that even medium baselines already exceed the range for reliable results using this ephemeris data and for guaranteed accurate results precise orbits are mandatory.

### 4.5.1 Short Baselines

Figure 50 shows the coordinate differences between reference and estimated for short BL using broadcast ephemeris. Similar characteristics compared to the case of precise orbits (standard procedure) can be recognized. Bernese shows slightly less accurate results in the north component, yielding a -2 mm offset of the average value of the differences and a 3 mm higher standard deviation, whereas the results in east do not show any changes regarding both STD and mean. The TBP differences of both horizontal components do also not show any change in the statistical parameters. In the up component interestingly, both processors show an improvement in the standard deviation of 1 mm and the mean value of the Bernese results also improves 2 mm towards zero. This is rather unexpected since the up (or in general height) component is the most vulnerable to inaccurate data of any kind. It can be argued though that this a development caused by the change of the input data and that both processors handle the ephemeris data similarly, since the trend is common between the two tools. The Helmert parameters (table 17) support the result, showing a minor trend of improvement compared to the standard procedures' translation parameters and their accuracy. The percentage of resolved ambiguities (figure 51, left) shows no significant events and the histogram of coordinate sigmas (figure 51, right) indicates a minor trend towards higher sigma values. The coordinate sigma values w.r.t. baseline length are stated in figure A 25 in the appendix.

## 4 Results and discussion

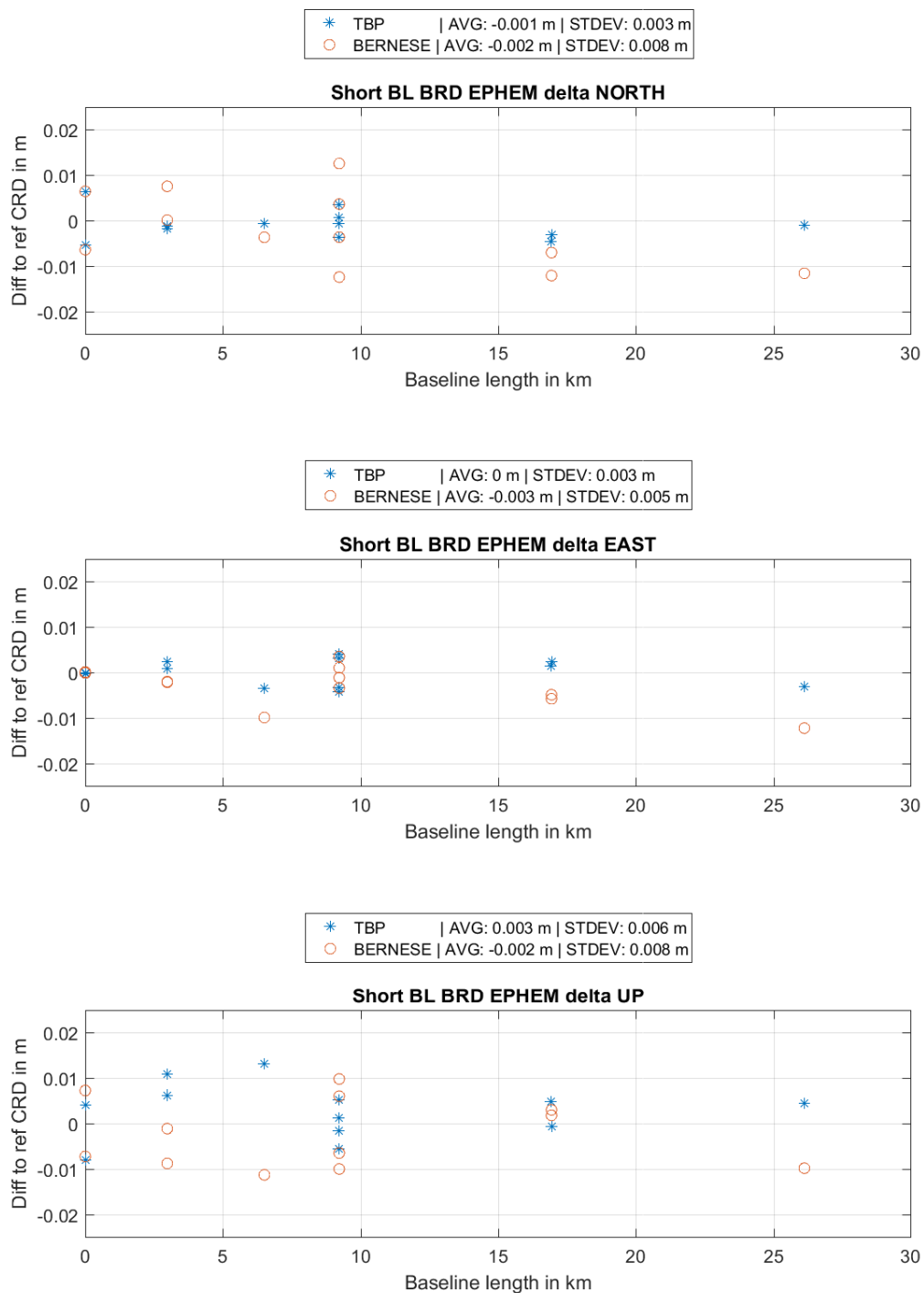
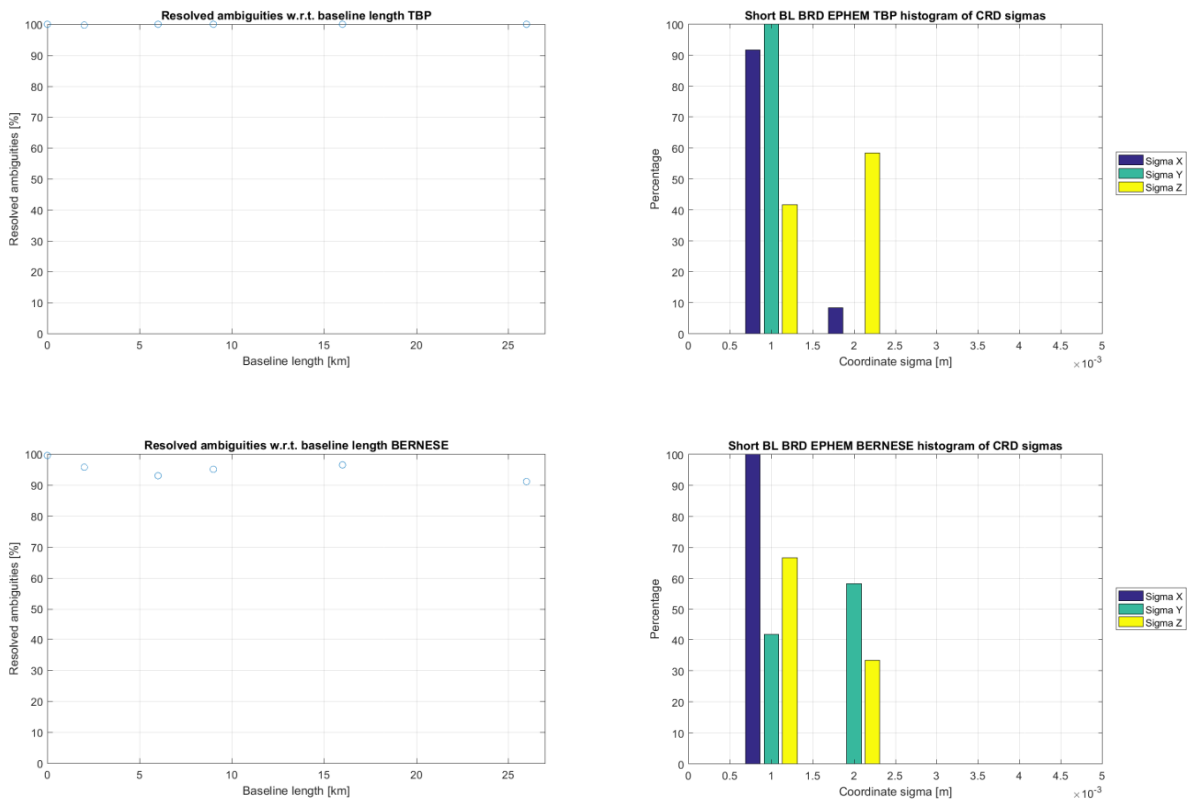


Figure 50: Delta NEU short baselines, Broadcast Ephemeris

**Table 17: 3D Helmert transformation parameters for TBP and Bernese, short baselines, Broadcast Ephemeris**

	Bernese Parameters:	Bernese Accuracy:	TBP Parameters:	TBP Accuracy:
Translation X	0.0008	0.0018	0.0026	0.0011
Translation Y	-0.0030	0.0018	0.0005	0.0011
Translation Z	-0.0032	0.0018	0.0014	0.0011
Rotation w.r.t. X	0.0000	0.0000	-0.0000	0.0000
Rotation w.r.t. Y	0.0000	0.0000	-0.0000	0.0000
Rotation w.r.t. Z	-0.0000	0.0000	0.0000	0.0000
Scale factor	1.000	0.0000	1.000	0.0000



**Figure 51: Left: Percentage of resolved ambiguities for short baselines, Broadcast Ephemeris; Right: Histogram of coordinate sigmas for short baselines, Broadcast Ephemeris;**

### 4.5.2 Medium Baselines

Figure 52 displays the differences of reference minus estimated coordinates for medium baselines using broadcast ephemeris. In this very case, the results of the TBP are remarkably accurate compared to Bernese. In contrast to the standard procedure the quality of both solution decreases, obviously, but within Bernese at a significantly higher rate. While the TBP manages to keep the discrepancies within approximately 3 cm for the largest outliers, Bernese results contradict with the reference for up to 10 cm, increasing with baseline length. By close inspection a slight increase of the deviation around zero w.r.t. baseline length can be observed in a similar manner than in the Bernese results, however with a far smaller magnitude. For Bernese the differences become larger the longer the baseline becomes (see figure 52 especially north and up component). The standard deviations of the Bernese results of each component are at the 3 to 5 cm level, compared to the maximum 4 mm of the standard procedure. For the TBP only the up component gets about 3 mm worse regarding the standard deviation. The 3D Helmert parameters compared to the standard procedure show only a minor degradation in the translation values and their accuracies (table 18). The translation regarding the Bernese results however also show only minor changes in the Y and Z translation values, however the X component is shifted by 1.1 cm, with also decreasing accuracies of the transformation parameters. The coordinate sigmas for Bernese (figure 53, right) show larger values up to 4 mm, the TBP only indicates insignificant changes (w.r.t. the standard procedure). The percentage of resolved ambiguities (figure 53, left) again only indicates a minor degradation of the TBP standard performance, regarding Bernese however the percentage value show the same linear regressive behavior but with a starting point at approximately at 75 percent resolved ambiguities instead of about 85. The coordinate sigmas w.r.t. baseline length are illustrated in figure A 26 in the appendix

## 4 Results and discussion

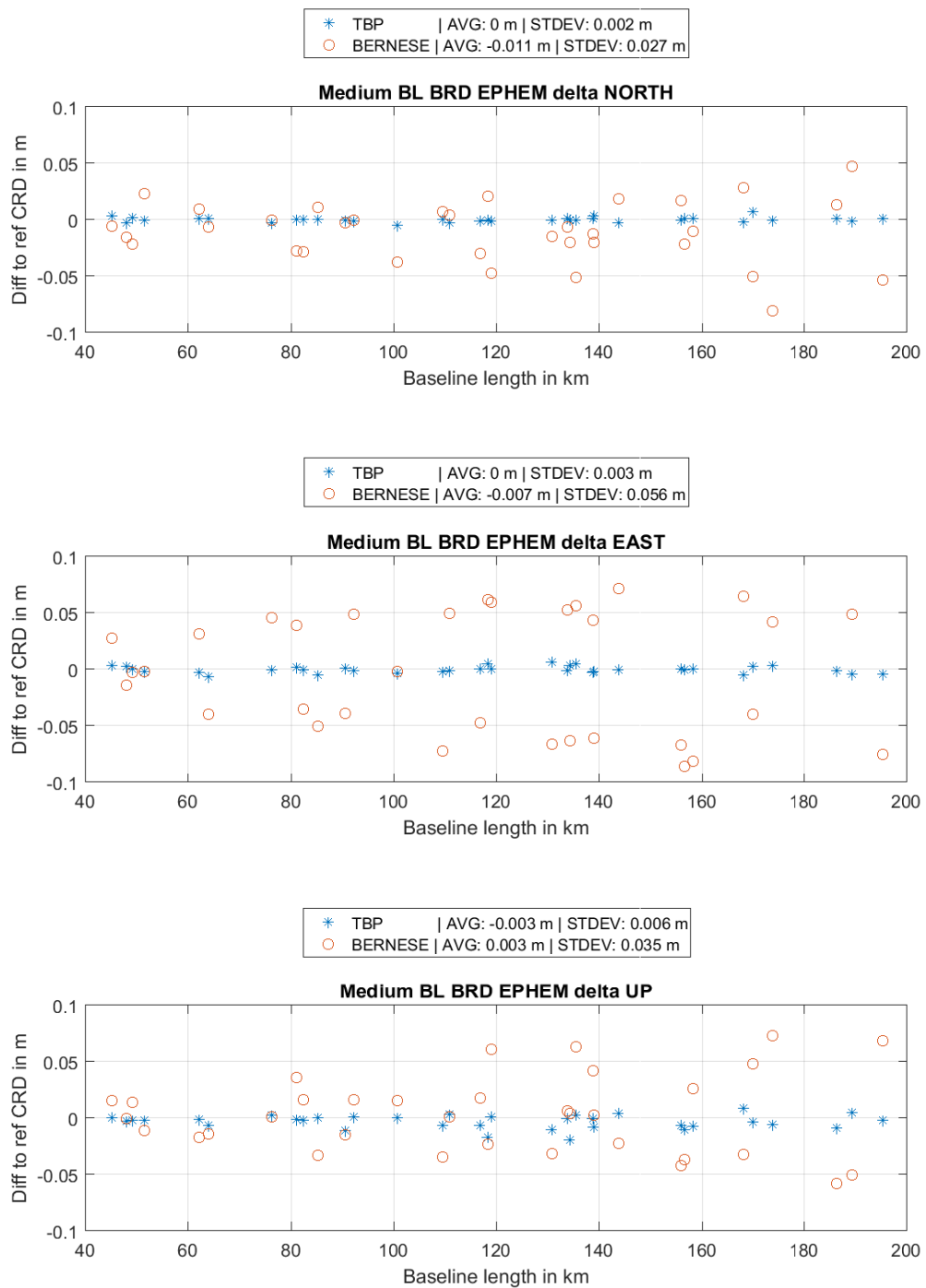
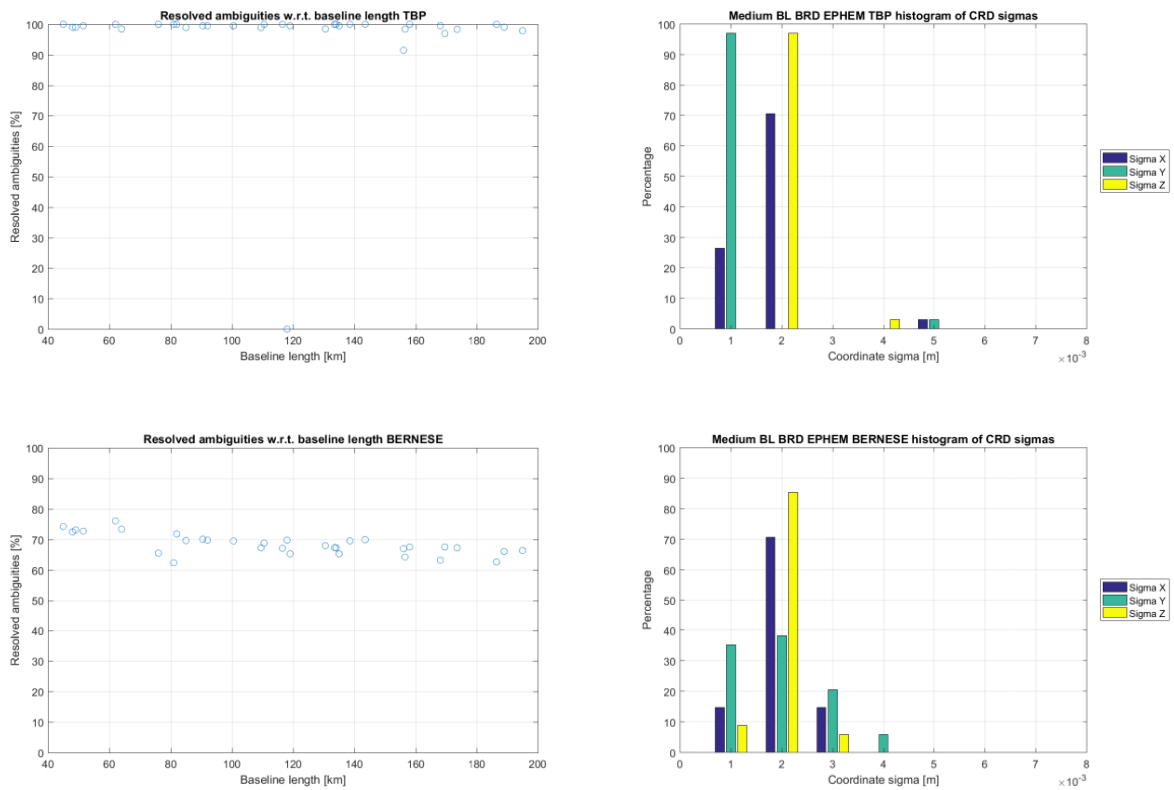


Figure 52: Delta NEU medium baselines, Broadcast Ephemeris

**Table 18: 3D Helmert transformation parameters for TBP and Bernese, medium baselines, Broadcast Ephemeris**

	Bernese Parameters:	Bernese Accuracy:	TBP Parameters:	TBP Accuracy:
Translation X	0.0111	0.0031	-0.0021	0.0006
Translation Y	-0.0038	0.0031	-0.0007	0.0006
Translation Z	-0.0047	0.0031	-0.0023	0.0006
Rotation w.r.t. X	0.0000	0.0000	0.0000	0.0000
Rotation w.r.t. Y	-0.0000	0.0000	-0.0000	0.0000
Rotation w.r.t. Z	0.0000	0.0000	-0.0000	0.0000
Scale factor	1.000	0.0000	1.000	0.0000



**Figure 53: Left: Percentage of resolved ambiguities for medium baselines, Broadcast Ephemeris; Right: Histogram of coordinate sigmas for medium baselines, Broadcast Ephemeris;**

## 4.6 Reduced occupation timespans

Finally, the very last experiment concerns the computation of reduced observation timespans for again medium and small baselines. Long and very long baselines were discarded for this purpose, since such immense networks require long observation times and when processed usually daily sessions are taken into account. For smaller and medium baselines however, especially in classic survey, shorter occupation timespans are common. Furthermore with decreasing the observation timespans significantly below the recommendations of Bernese, the behavior of both processors can be glimpsed upon when pushed beyond their limit.

Also different observation timespans regarding daytime are chosen, the first start time at 1:00 am in the night (instead of midnight to avoid the edge of the orbit arc) and 1:00 pm after noon (simply to establish a 12 hour shift between both observations, yielding one observation at total night and one during bright day) because of different ionospheric and tropospheric conditions (though due to the winter in the northern hemisphere and mid latitude the ionospheric activity is reduced in general).

### 4.6.1 Short baselines

Figure 54 depicts the differences between reference and computed coordinates for short baselines for the observation timespan 1:00 am to 2:00 am at DOY 313 2016. Compared to the full session of 1 entire day the coordinate differences increase significantly. The horizontal component is fairly untouched except for the ~26 km baseline in Bernese in the east component, where the difference jumps from approximately - 1 cm to approximately +6 cm. The up component is affected by a similar degradation in both processors of about 1 cm regarding the mean and standard deviation of the coordinate differences, yet absolute values in height differences reach up to 5 cm compared to the maximum 2 cm of the standard procedure. Except for the longest baseline in this experiment the TBP and Bernese show a similar behavior regarding the increasing coordinate differences and their direction. The parameters of the Helmert transformation (table 19) also show an increase in the translation, however in the case of the TBP not concerning the X component. The larger transformation parameters and uncertainties regarding Bernese most likely stem from the large discrepancy at the ~26 km baseline. The coordinate sigma values do not show any significant degradation (figure 55, right) yet however the ambiguity resolution percentage (figure 55, left) of Bernese increases to consistent 100 percent (again, except the ~26 km baseline. The ambiguity resolution performance for the TBP is not affected compared to the full session length. The coordinate sigma values w.r.t. baseline length, as additional information, are illustrated in figure A 27 in the appendix.

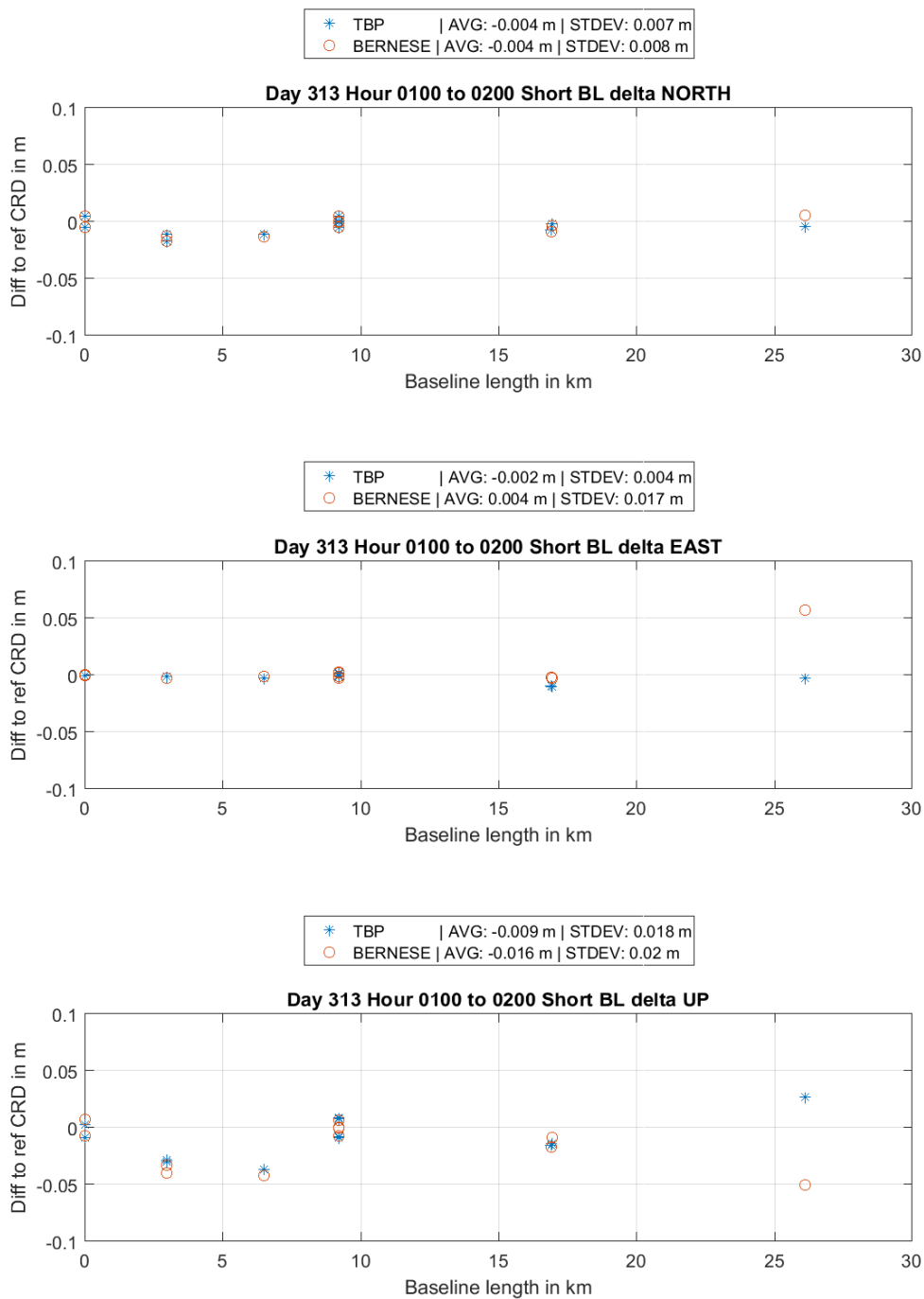
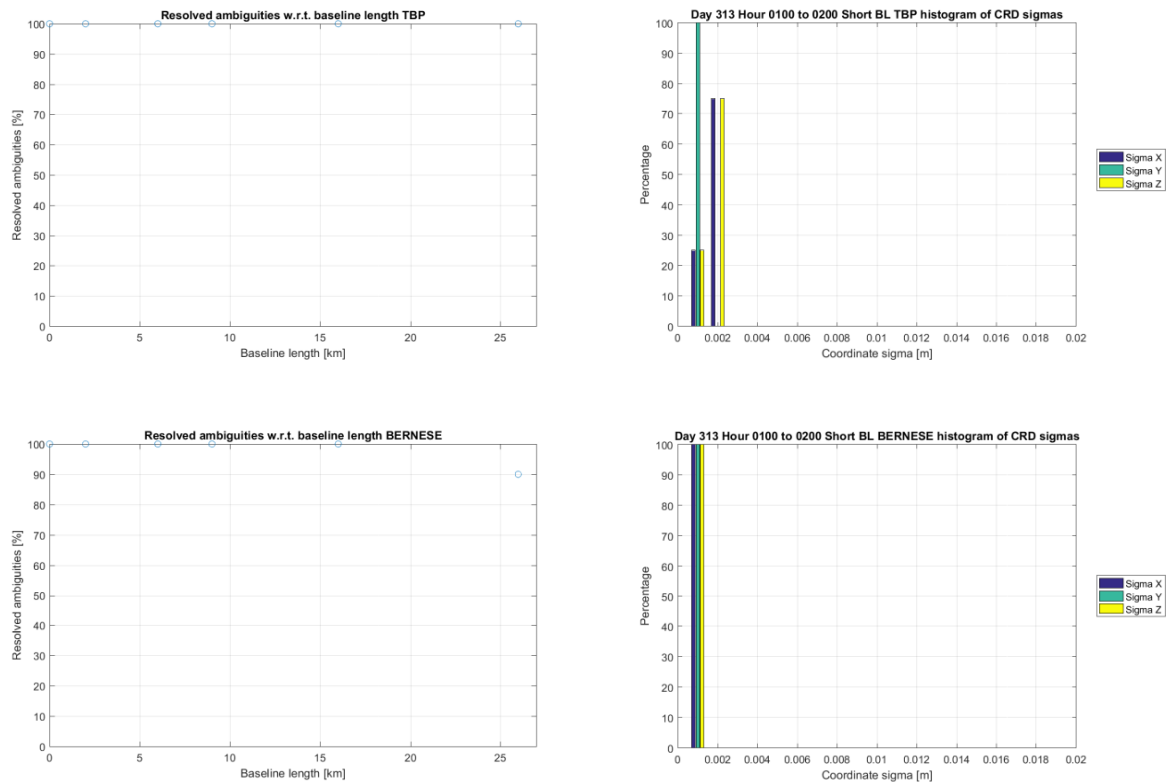


Figure 54: Delta NEU short baselines, obs. time 1:00 to 2:00, am

**Table 19: 3D Helmert transformation parameters for TBP and Bernese, short BL, obs. time 1:00 to 2:00, am**

	Bernese Parameters:	Bernese Accuracy:	TBP Parameters:	TBP Accuracy:
Translation X	-0.0083	0.0036	-0.0020	0.0028
Translation Y	0.0022	0.0036	-0.0026	0.0028
Translation Z	-0.0145	0.0036	-0.0093	0.0028
Rotation w.r.t. X	0.0000	0.0000	0.0000	0.0000
Rotation w.r.t. Y	0.0000	0.0000	0.0000	0.0000
Rotation w.r.t. Z	-0.0000	0.0000	-0.0000	0.0000
Scale factor	1.000	0.0000	1.000	0.0000



**Figure 55: Left: Percentage of resolved ambiguities for short baselines, obs. time 1:00 to 2:00, am; Right: Histogram of coordinate sigmas for short baselines, obs. time 1:00 to 2:00, am;**

For the occupation time from 1:00 pm to 2:00 pm the ambiguity resolution percentages (figure 56, left) show all ambiguities were resolved, for the first time also for Bernese. The coordinate sigma histogram (figure 56, right) indicates no changes w.r.t. to the previous processing. The corresponding results for the coordinate differences for the occupation time from 1:00 pm to 2:00 pm are illustrated in figure 57. The ~26 km baseline was computed correct this time in Bernese, i.e. no large outlier occurs. With the Bernese results improving, the TBP results depreciate with respect to mean value and standard deviation at the mm level. However the main improvement in the statistical sizes for Bernese stem from the elimination of the large outlier. The results are now in a similar order of quality, yet the TBP appears to be more accurate in north whereas Bernese shows in this case marginally superior results in the east and up component. The translation

parameters of the Helmert transformation (table 20) also suggest improvement regarding the Bernese solution, though the Y component remains untouched. The TBP translation indicates a minor trend to worse results in X and Y and the overall accuracy, however a small improvement in the Z coordinate. The coordinate sigmas w.r.t. baseline length are depicted in figure A 28 in the appendix.

**Table 20: 3D Helmert transformation parameters for TBP and Bernese, short BL, obs. time 1:00 to 2:00, pm**

	Bernese Parameters:	Bernese Accuracy:	TBP Parameters:	TBP Accuracy:
Translation X	-0.0030	0.0025	-0.0004	0.0031
Translation Y	-0.0022	0.0025	-0.0031	0.0031
Translation Z	-0.0122	0.0025	-0.0072	0.0031
Rotation w.r.t. X	0.0000	0.0000	0.0000	0.0000
Rotation w.r.t. Y	0.0000	0.0000	0.0000	0.0000
Rotation w.r.t. Z	-0.0000	0.0000	-0.0000	0.0000
Scale factor	1.000	0.0000	1.000	0.0000

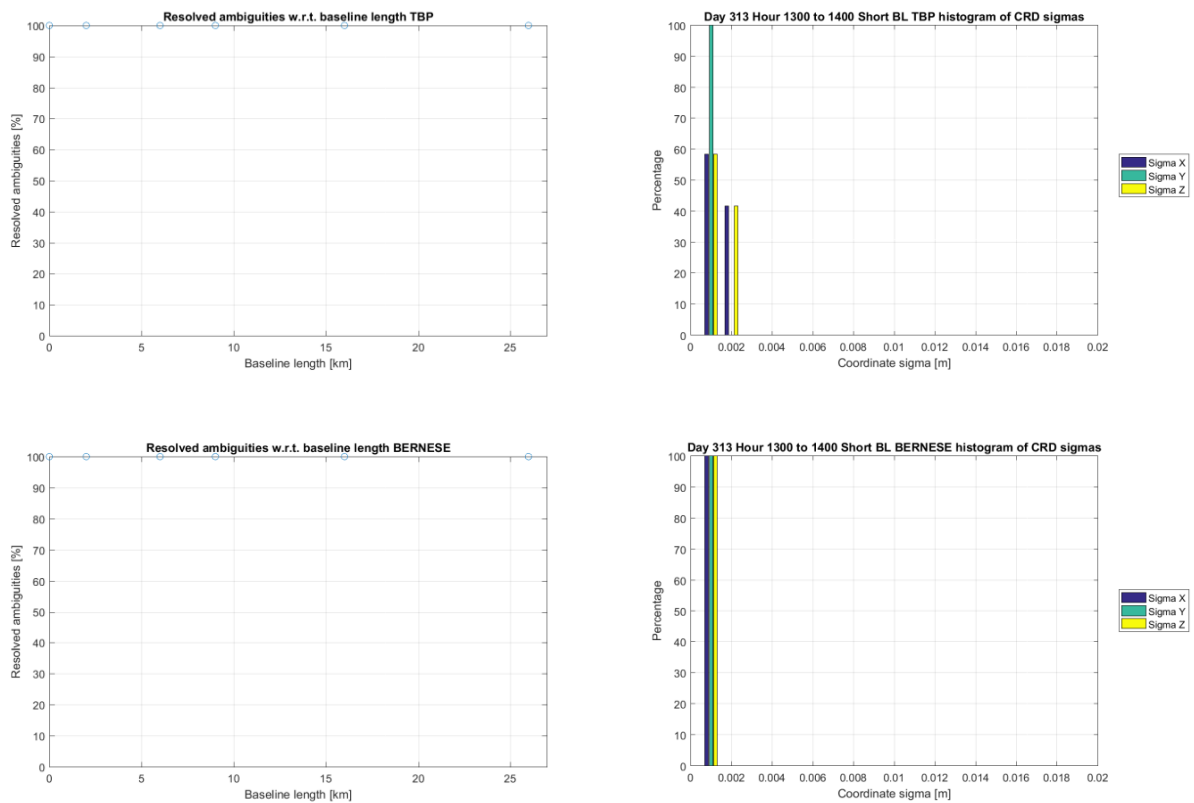


**Figure 56: Left: Percentage of resolved ambiguities for short baselines, obs. time 1:00 to 2:00, pm; Right: Histogram of coordinate sigmas for short baselines, obs. time 1:00 to 2:00, pm;**

## 4 Results and discussion

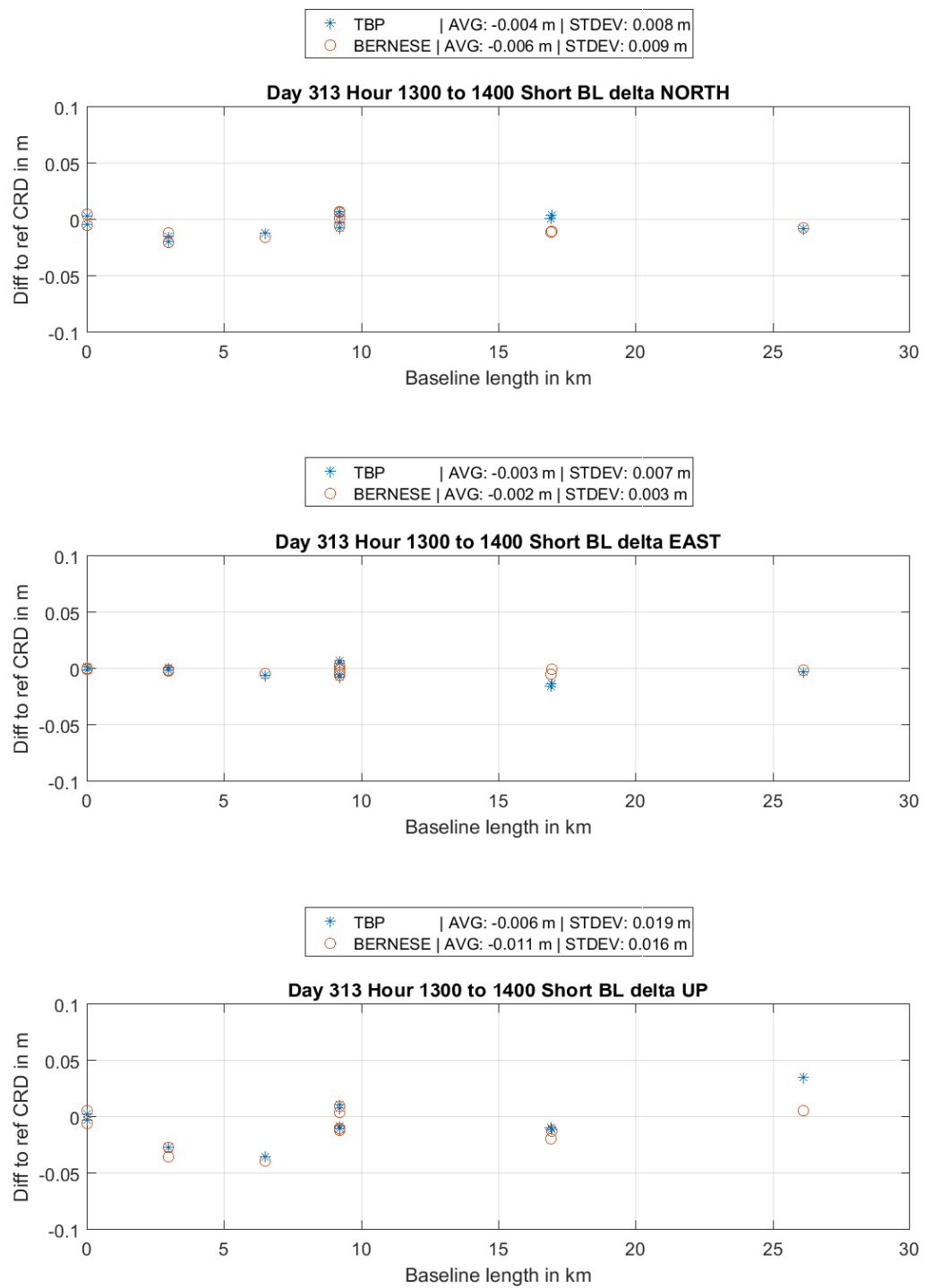


Figure 57: Delta NEU short baselines, obs. time 1:00 to 2:00, pm

The following two tests now reflect on the use of only 10 minutes of observation data. Figure 58 shows the coordinate differences of the computed positions according to the reference for the observation timespan between 1:00 am and 1:10 am on DOY 313 2016. Again, as in the corresponding 1 hour dataset Bernese produces a significant difference for the ~ 26 km baseline even double the absolute value of before in the up component. The east component in general though appears to fit better. Yet both processors show a continuing degradation of the results with reduced occupation time span according to the coordinate difference average and standard deviation, as also supported by the Helmert transformation parameters (table 21). The TBP due to the relatively proper estimation of the ~ 26 km baseline yields more stable results, although the number of resolved ambiguities of this very baseline (figure 59, left) for the first time does not reach 100 percent. In the case of Bernese the ambiguity resolution performance coincides with the corresponding 1 hour session. The coordinate sigmas (figure 59, right) for the TBP show no surprises and for Bernese only one baseline shows elevated sigma values, the ~ 26 km line (as confirmed by figure A 29 in the appendix, displaying the coordinate sigmas w.r.t. baseline length).

**Table 21: 3D Helmert transformation parameters for TBP and Bernese, short BL, obs. time 1:00 to 1:10, am**

	Bernese Parameters:	Bernese Accuracy:	TBP Parameters:	TBP Accuracy:
Translation X	-0.0111	0.0058	-0.0073	0.0018
Translation Y	-0.0054	0.0058	-0.0038	0.0018
Translation Z	-0.0144	0.0058	-0.0131	0.0018
Rotation w.r.t. X	0.0000	0.0000	0.0000	0.0000
Rotation w.r.t. Y	0.0000	0.0000	0.0000	0.0000
Rotation w.r.t. Z	-0.0000	0.0000	-0.0000	0.0000
Scale factor	1.000	0.0000	1.000	0.0000

## 4 Results and discussion

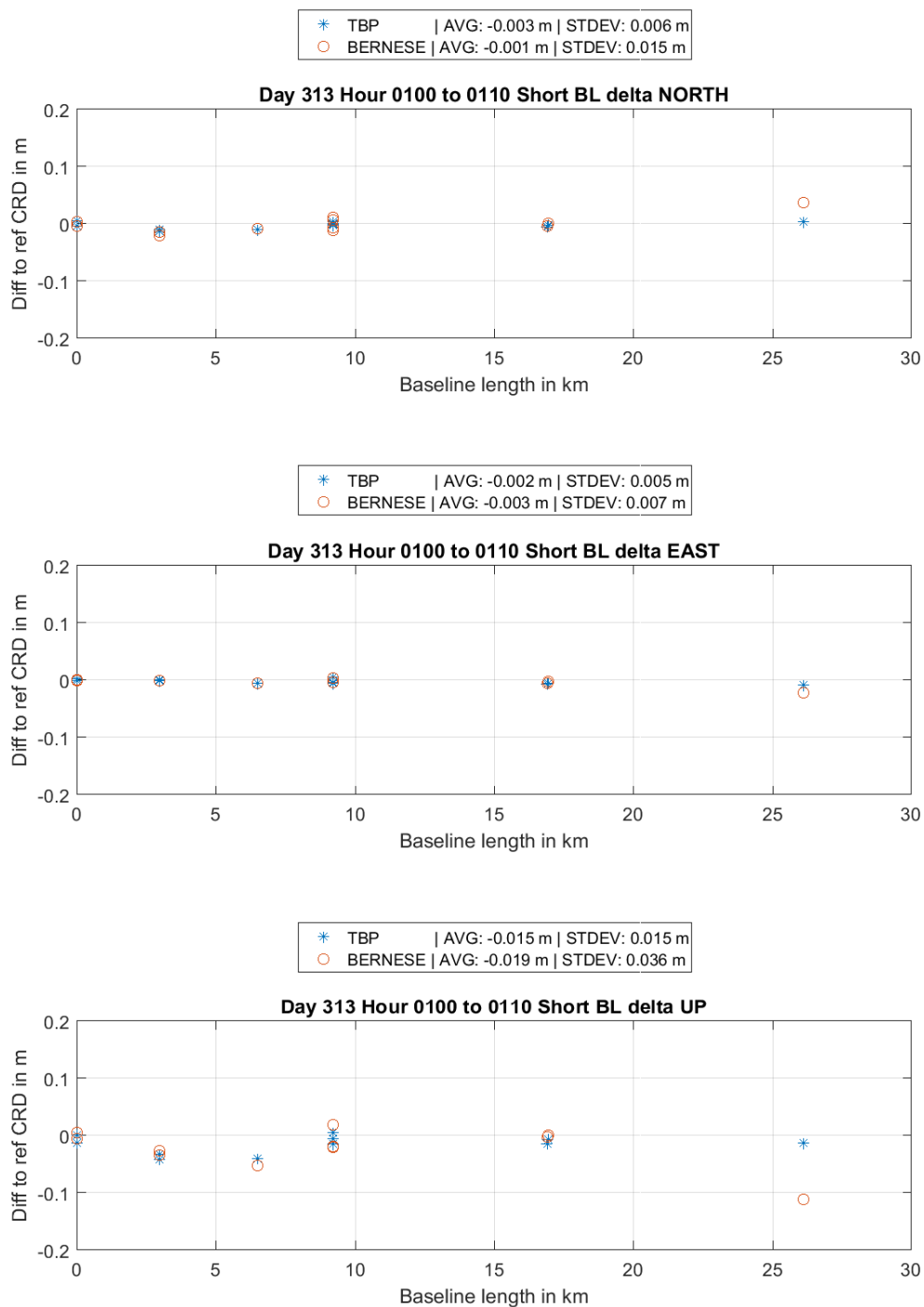


**Figure 58: Delta NEU short baselines, obs. time 1:00 to 1:10, am**

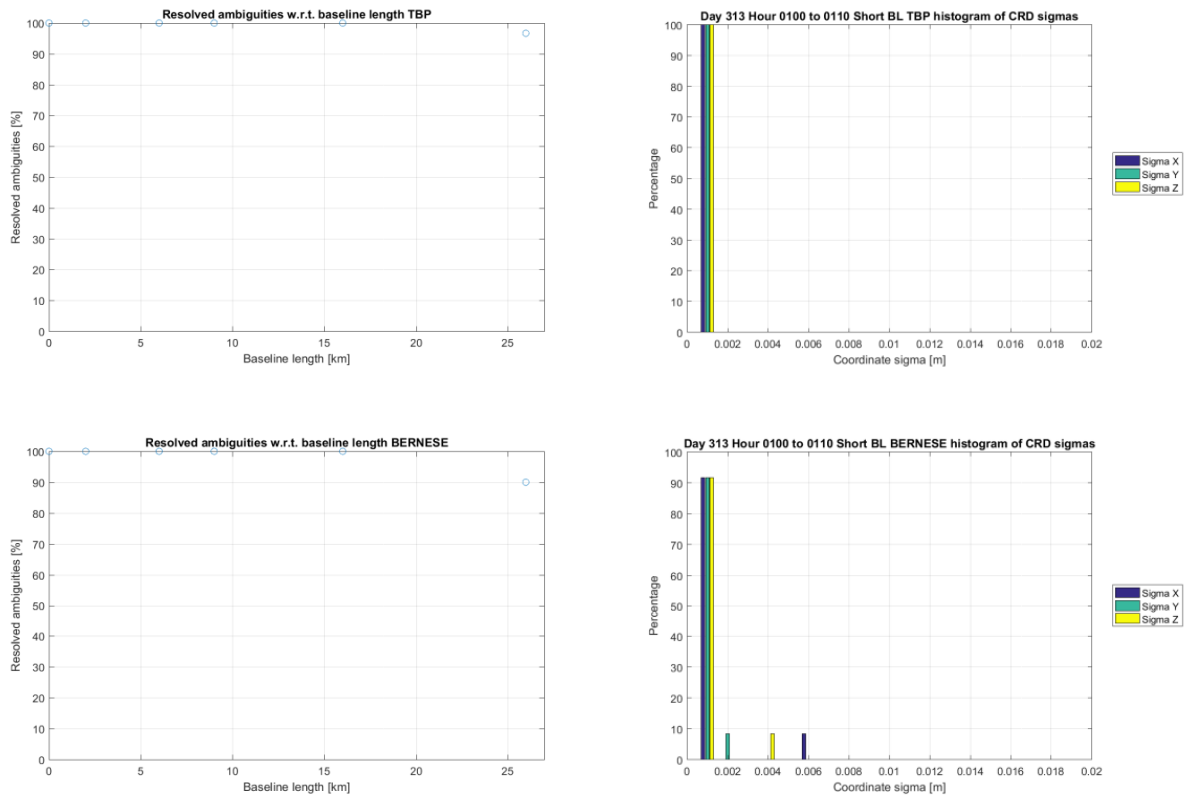


**Figure 59:** Left: Percentage of resolved ambiguities for short baselines, obs. time 1:00 to 1:10, am; Right: Histogram of coordinate sigmas for short baselines, obs. time 1:00 to 1:10, am;

The last experiment for short baselines is the evaluation of the occupation timespan 1:00 pm to 1:10 pm DOY 313 2016. In this very scenario Bernese again is not able to compute a reasonable solution for the ~ 26 km baseline and the up component exhibits significantly larger differences of the computed coordinates w.r.t. the reference (figure 60). The parameters of the Helmert transformation (table 22) however show smaller values for the translation in X and Z with a higher uncertainty in all components compared to the corresponding 1 hour session. However this may not be mistaken with an improved result. The 3D Helmert transformation merely reflects a possible translation, rotation and scale factor affecting all coordinates the same way. This however may not be the case even if the results are of rather poor quality, only systematic offsets are unraveled. The coordinate sigma values (figure 61, right) however do not show significant changes w.r.t. the corresponding 1 hour session. The ambiguity resolution percentage (figure 61, left) for the TBP as in the previous 10 minute session fixes all ambiguities except for the ~ 26 km baseline (ratio drops to about 90 percent), whereas Bernese shows reduced resolution rates for all baselines, especially the overall problematic longest one of this dataset. The coordinate sigmas w.r.t. baseline length are displayed in figure A 30 in the appendix.

## 4 Results and discussion

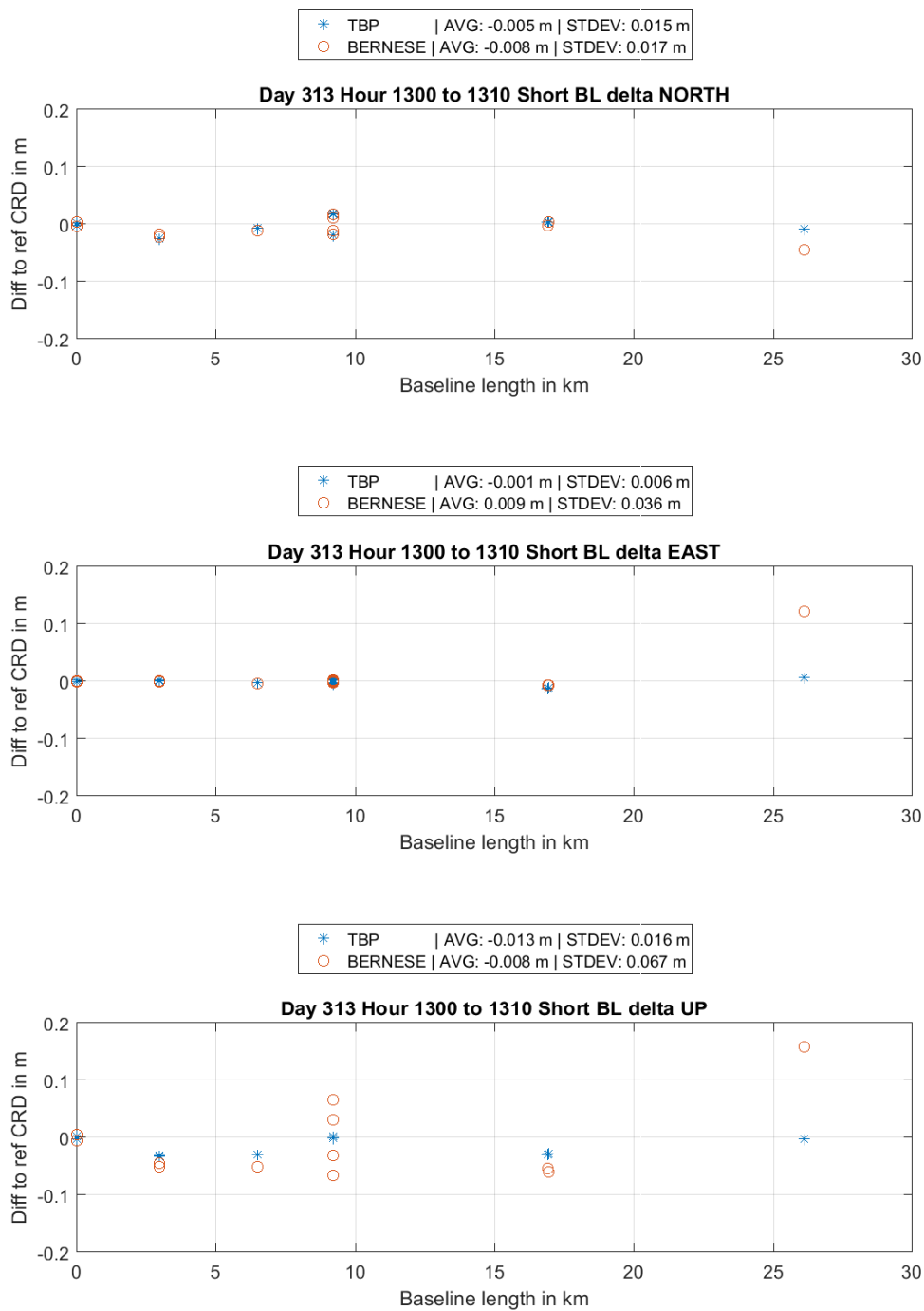


Figure 60: Delta NEU short baselines, obs. time 1:00 to 1:10, pm

Table 22: 3D Helmert transformation parameters for TBP and Bernese, short BL, obs. time 1:00 to 1:10, pm

	Bernese Parameters:	Bernese Accuracy:	TBP Parameters:	TBP Accuracy:
Translation X	-0.0016	0.0133	-0.0046	0.0029
Translation Y	0.0086	0.0133	-0.0022	0.0029
Translation Z	-0.0116	0.0133	-0.0127	0.0029
Rotation w.r.t. X	0.0000	0.0000	0.0000	0.0000
Rotation w.r.t. Y	0.0000	0.0000	0.0000	0.0000
Rotation w.r.t. Z	-0.0000	0.0000	-0.0000	0.0000
Scale factor	1.000	0.0000	1.000	0.0000

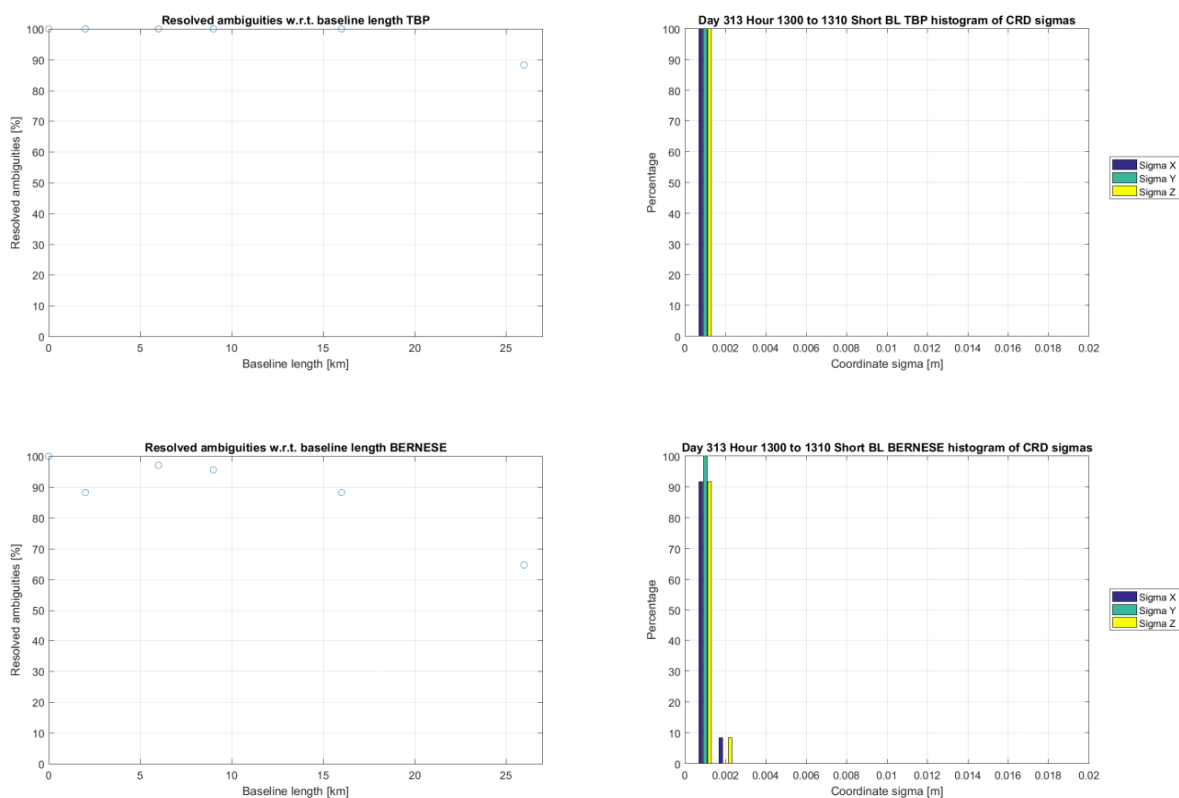


Figure 61: Left: Percentage of resolved ambiguities for short baselines, obs. time 1:00 to 1:10, pm; Right: Histogram of coordinate sigmas for short baselines, obs. time 1:00 to 1:10, pm;

### 4.6.2 Medium baselines

The first results regard the observation timespan between 1:00 am and 3:00 am DOY 313 2016. Figure 62 shows the coordinate differences between reference and computed. Both processors show a shift towards negative differences in the horizontal components of a few millimeters, however the Bernese results show a significantly higher standard deviation in the coordinate differences. In the north component this effect is more significantly present for Bernese than for the TBP. The up component however features an interesting effect. The discrepancies between both processors' solutions and the reference increase, but with an opposite sign. The TBP shows a tendency to estimate the height persistently too high (positive coordinate difference in up = space between the estimated coordinate and the reference coordinate with direction starting from the estimated coordinate) and Bernese too low, with also a higher standard deviation. The results from both also show an increased translation in the Helmert transformation (table 23), indicating a systematic effect. The coordinate sigma values (figure 63, right) do not show any surprises w.r.t. the standard procedure, the ambiguity resolution on the other hand performs significantly worse for Bernese (figure 63, left). Where the TBP manages to still fix most of the ambiguity parameters (only few baseline intervals below 90 percent) the percentages for Bernese drop from a center of around 80 to 50 percent. The effect however of the reduced occupation can be exhibited in the results of both processors. Additional information regarding the coordinate sigma values w.r.t. to baseline length is illustrated in figure A 31 in the appendix.

**Table 23: 3D Helmert transformation parameters for TBP and Bernese, medium BL, obs. time 1:00 to 3:00, am**

	Bernese Parameters:	Bernese Accuracy:	TBP Parameters:	TBP Accuracy:
Translation X	0.0087	0.0019	-0.0033	0.0008
Translation Y	-0.0027	0.0019	-0.0033	0.0008
Translation Z	-0.0015	0.0019	-0.0033	0.0008
Rotation w.r.t. X	0.0000	0.0000	0.0000	0.0000
Rotation w.r.t. Y	-0.0000	0.0000	0.0000	0.0000
Rotation w.r.t. Z	0.0000	0.0000	-0.0000	0.0000
Scale factor	1.000	0.0000	1.000	0.0000

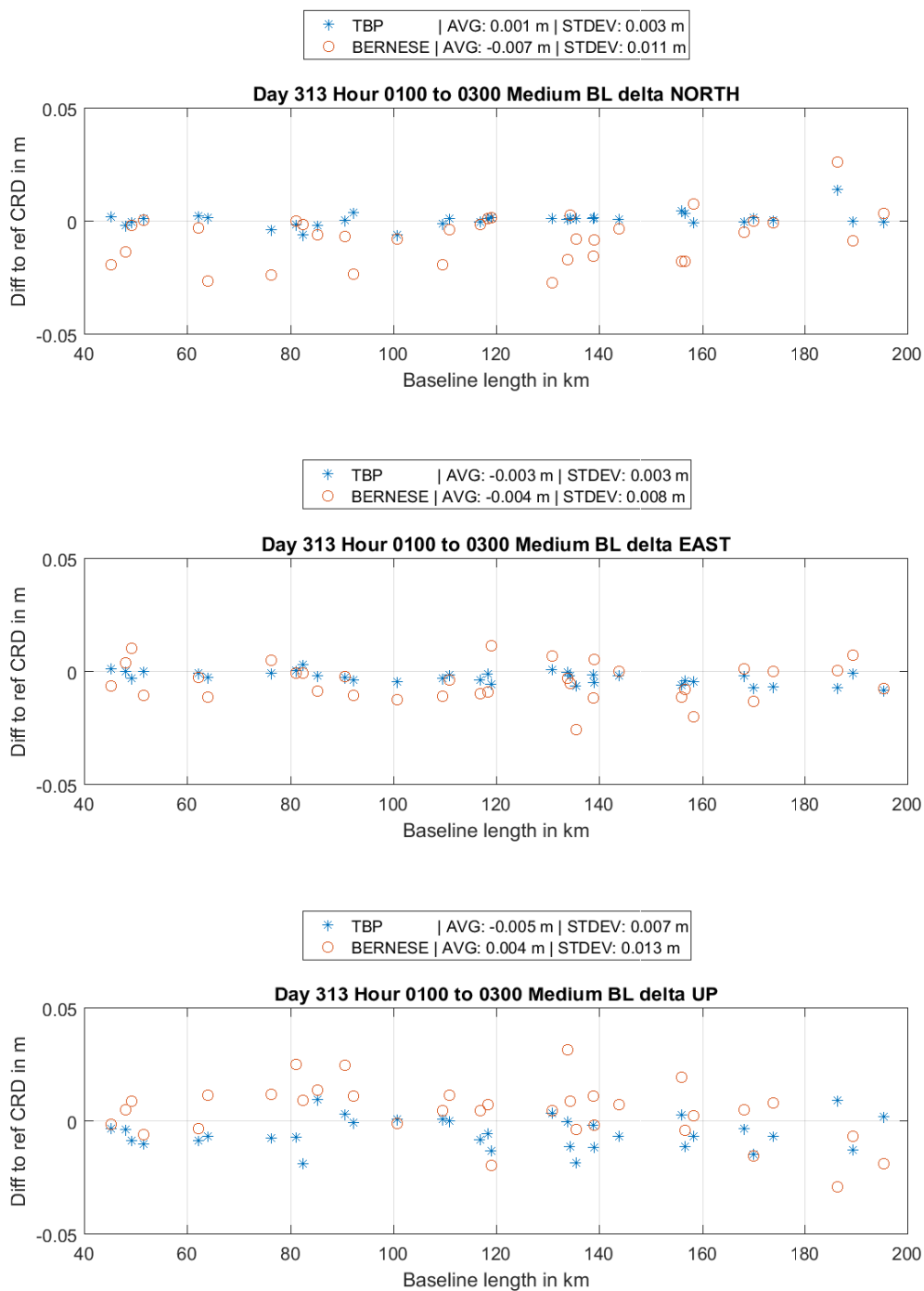
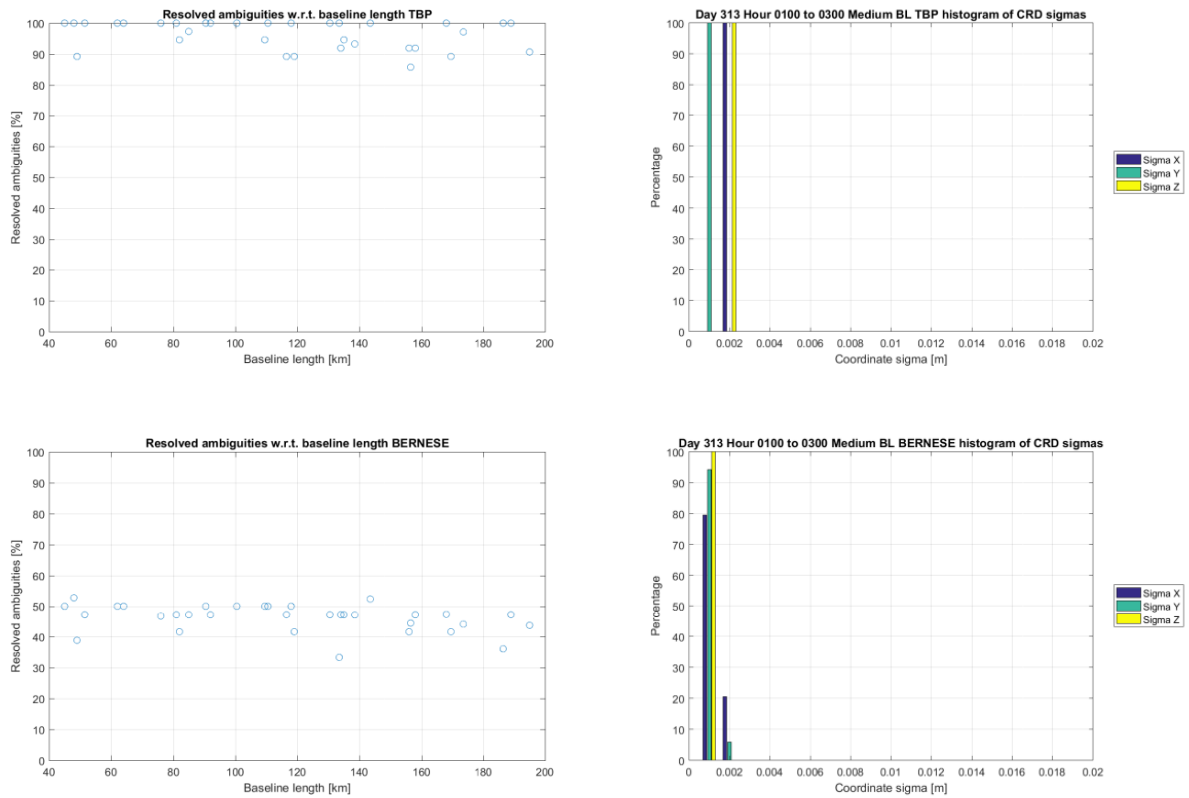


Figure 62: Delta NEU medium baselines, obs. time 1:00 to 3:00, am



**Figure 63:** Left: Percentage of resolved ambiguities for medium baselines, obs. time 1:00 to 3:00, am; Right: Histogram of coordinate sigmas for medium baselines, obs. time 1:00 to 3:00, am;

Figure 64 illustrates the coordinate deltas for the same observation interval length but starting at 1:00 pm to 3:00 pm. With respect to the previous reduced occupation computations the results regarding Bernese show a similar distribution in the north component, a negative tendency. The differences in the east component are better centered at zero with the mean value shifted from  $-4$  mm to  $+2$  mm in compared to the previous run. The up component in the foregoing example established a positive trend in the differences but this time is shifted nearly completely below zero (height estimated too high). The differences however for Bernese are distributed more narrowly around their respective mean value than before. In contrast the TBP shows improvement in the results regarding the mean value of the coordinate differences with unchanged standard deviations. Also in the up component the previous negative trend is compensated slightly. In general both processors agree better for this observation interval than the one before, mostly due to the split discrepancies in the height. Compared to the previous Helmert parameters the translation of this dataset (table 24) shows similar values for Bernese but with X and Z interchanged and the translation in X being negative. Since for mid Europe, Germany in this case these two components have the highest impact on north and up. The standard procedure however did produce very accurate results for both processors close to the reference coordinates. Yet it

seems that the TBP is able to maintain a certain level of precision independent of shorter occupation timespans. For Bernese the daily solution appears, regarding the high variations in the up component, as a mean of quite deviating epoch solutions. Of course this is not entirely true due to the least squares adjustment, this is just mentioned as in intuitive interpretation. The coordinate sigmas (figure 65, right) do not show any changes w.r.t. the previous example, the ambiguity resolution (figure 65, left) although shows a minor improvement for the TBP (no resolution percentage below ~92 percent) and a strong improvement for Bernese (same linear regressive characteristics as before but with a starting value around 70 instead of 50 percent). The coordinate sigma values w.r.t. to baseline length are illustrated in figure A 32 in the appendix.

**Table 24: 3D Helmert transformation parameters for TBP and Bernese, medium BL, obs. time 1:00 to 3:00, pm**

	Bernese Parameters:	Bernese Accuracy:	TBP Parameters:	TBP Accuracy:
Translation X	-0.0016	0.0015	-0.0019	0.0007
Translation Y	0.0013	0.0015	-0.0002	0.0007
Translation Z	-0.0097	0.0015	-0.0028	0.0007
Rotation w.r.t. X	0.0000	0.0000	0.0000	0.0000
Rotation w.r.t. Y	-0.0000	0.0000	-0.0000	0.0000
Rotation w.r.t. Z	-0.0000	0.0000	0.0000	0.0000
Scale factor	1.000	0.0000	1.000	0.0000

## 4 Results and discussion

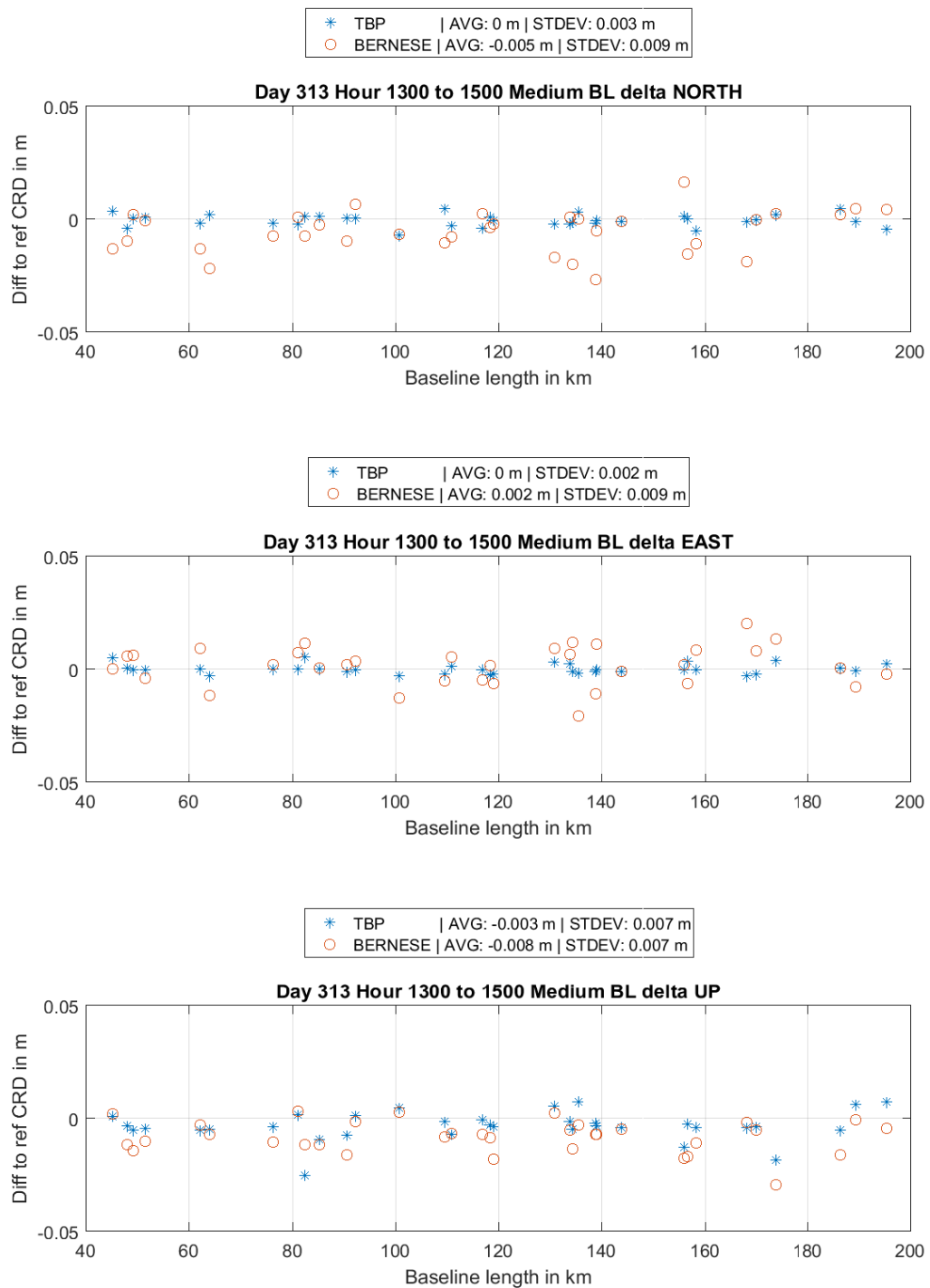
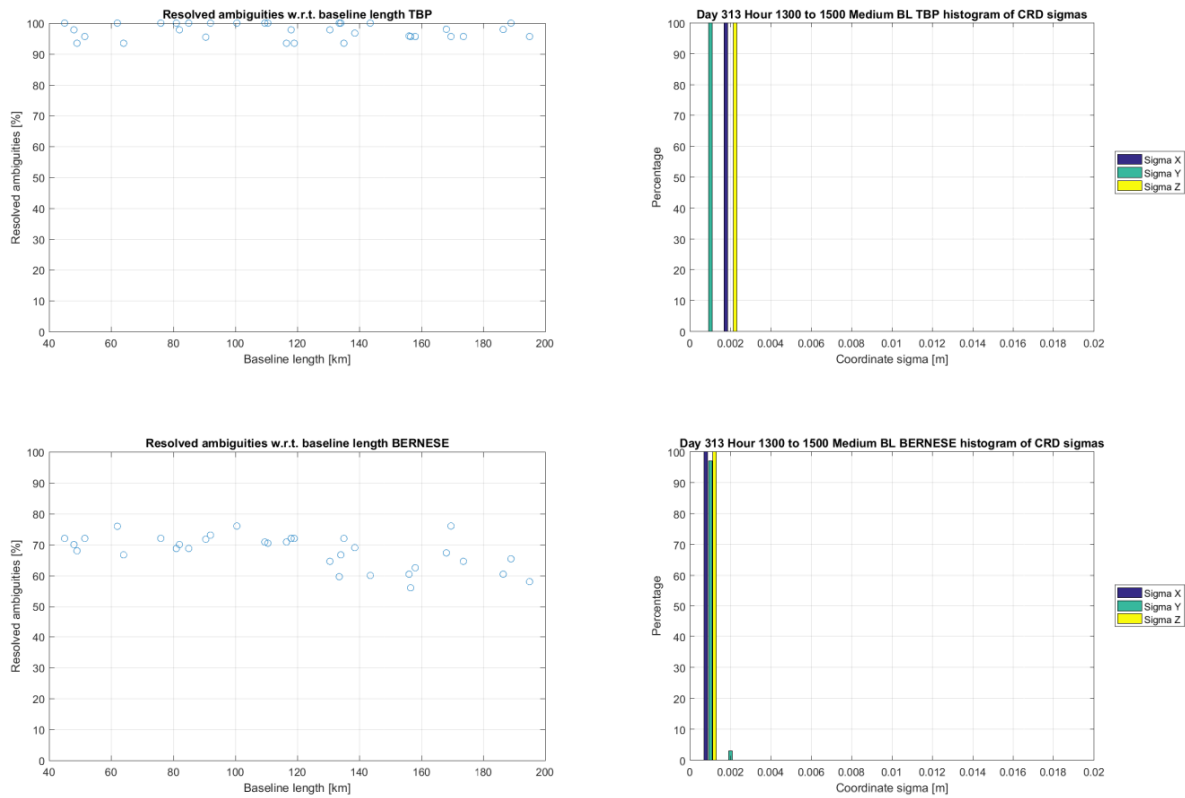


Figure 64: Delta NEU medium baselines, obs. time 1:00 to 3:00, pm



**Figure 65** Left: Percentage of resolved ambiguities for medium baselines, obs. time 1:00 to 3:00, pm; Right: Histogram of coordinate sigmas for medium baselines, obs. time 1:00 to 3:00, pm;

The two final experiments now evaluate the performance of both processors when deliberately disregarding the minimum occupation time for medium baselines. Figure 66 depicts the coordinate differences between reference and computed for the occupation interval 1:00 am to 1:30 am DOY 313 2016. Both processors show only a minor continuation of the trends established for the corresponding 2 hour session regarding the horizontal component with Bernese introducing few comparatively larger outliers in east. In up however the previous trend reinforces, nearly completely splitting the discrepancies between the TBP and Bernese in solely negative respective positive values (obvious shift in the Helmert transformation parameters, table 25). Also the standard deviation for both processors' differences in up is increased by approximately a factor 2. Also both seem to be affected by a linear regressive effect, a negative trend with increasing baseline length. The differences regarding Bernese in height however range up to 10 cm in absolute value, up to 5 cm for the TBP. This trend however is only visible in the nightly session. The reduction of the occupation yields significantly less simultaneously observed satellites for each baseline and depending on the time window very bad geometrical conditions (i.e. low elevation for most of the commonly observed SVs) are possible. Additionally the ionosphere may have a higher impact on the measurements, if ionospheric activity differs significantly from the model at the

particular time window but would be compensated regarding a daily solution. Anyway, the coordinate sigmas (figure 67, right) for the TBP would not indicate a degradation of the result, for Bernese however the reduced quality is visible. Also the ambiguity resolution (figure 67, left) of both processors shows difficulties. The TBP appears to have problems especially solving for the shorter baselines (with larger outliers in the range up to 100 km), whereas Bernese shows a similar performance characteristics w.r.t. the corresponding 2 hour session but with overall lower percentages. This very dataset is a prime showcase for how both processors deal with badly conditioned observations as well as performance outside of the recommended “comfort zone”. Coordinate accuracies regarding the baseline length for this scenario are illustrated in figure A 33 in the appendix.

**Table 25: 3D Helmert transformation parameters for TBP and Bernese, medium BL, obs. time 1:00 to 1:30, am**

	Bernese Parameters:	Bernese Accuracy:	TBP Parameters:	TBP Accuracy:
Translation X	0.0336	0.0037	-0.0101	0.0010
Translation Y	0.0036	0.0037	-0.0052	0.0010
Translation Z	0.0252	0.0037	-0.0119	0.0010
Rotation w.r.t. X	-0.0000	0.0000	-0.0000	0.0000
Rotation w.r.t. Y	0.0000	0.0000	0.0000	0.0000
Rotation w.r.t. Z	0.0000	0.0000	0.0000	0.0000
Scale factor	1.000	0.0000	1.000	0.0000

## 4 Results and discussion

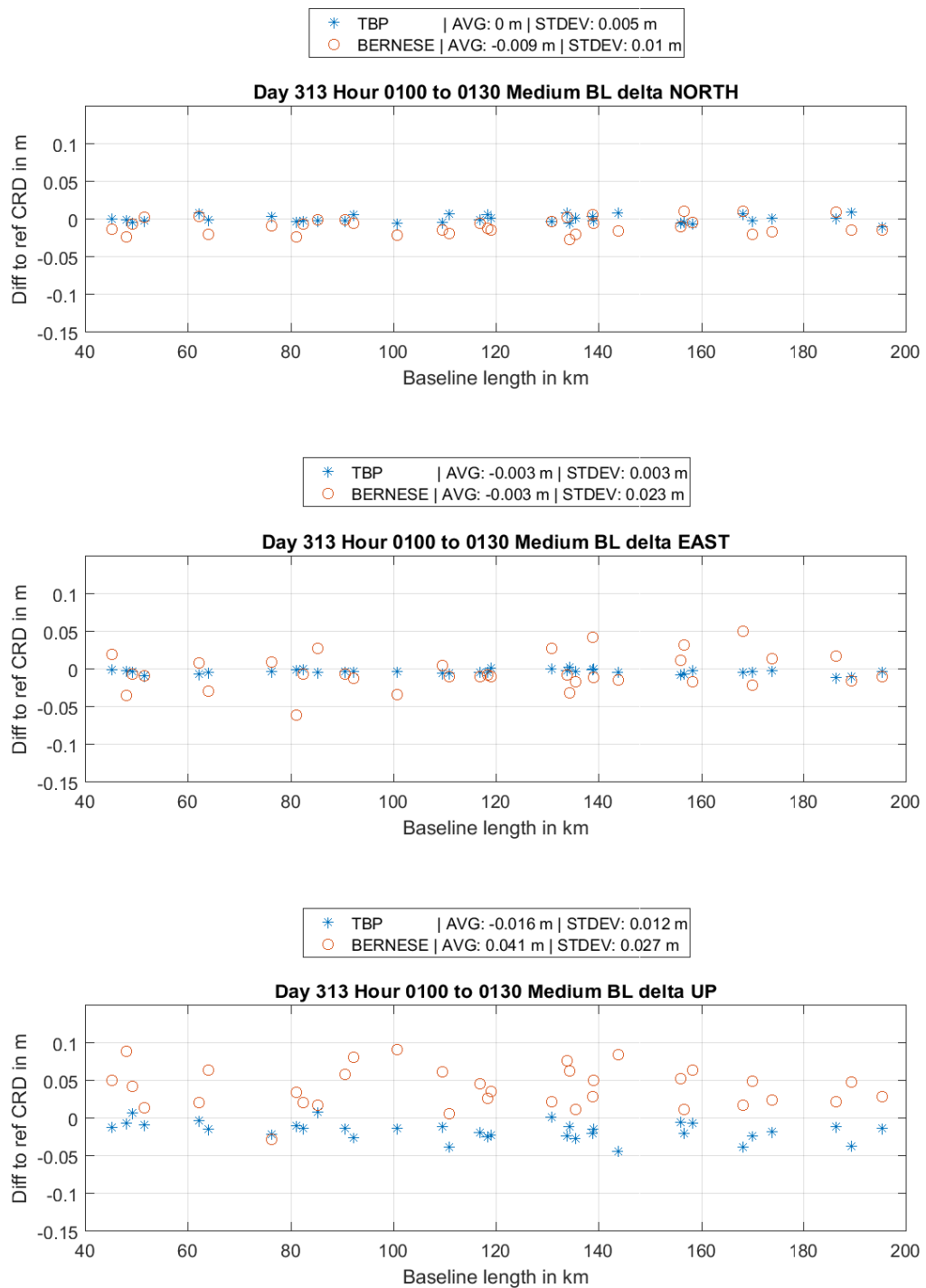
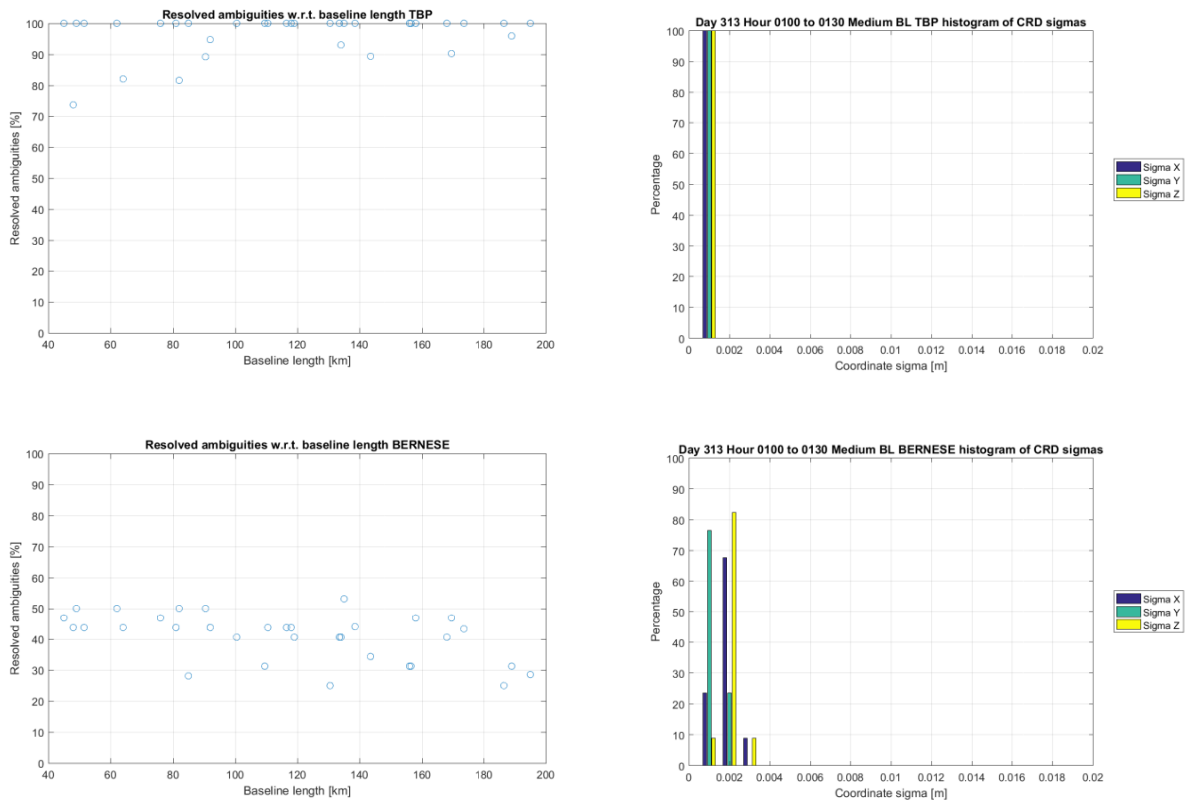


Figure 66: Delta NEU medium baselines, obs. time 1:00 to 1:30, am



**Figure 67:** Left: Percentage of resolved ambiguities for medium baselines, obs. time 1:00 to 1:30, am; Right: Histogram of coordinate sigmas for medium baselines, obs. time 1:00 to 1:30, am;

For the final experiment, the observation timespan from 1:00 pm to 1:30 pm, the coordinate sigma histogram (figure 68, right) suggests a successful processing of the TBP (of course the actual 1 mm of each coordinate is very optimistic) and for Bernese it corresponds to the depreciation w.r.t. the 2 hour session. The ambiguity resolution (figure 68, left) of Bernese also shows a slightly worse performance, again especially at longer baselines, for the TBP actually more ambiguities were resolved than before (relatively speaking, since the absolute number of ambiguities very likely has decreased due to less simultaneously observed satellites and fewer observations in total). Figure 69 depicts the differences in north east up between reference and estimated for the session 1:00 pm to 1:30 pm. The results show similar characteristics as in the corresponding 2 hour session. The standard deviation for all components and both processors increase in absolute value for about a factor of 2, except for the height computed by Bernese with a factor of about 5. The overall height estimation did not fail the standard deviation value is simply biased by few large outliers. In general the TBP again renders relatively stable results where Bernese, especially as the baseline lengths increase, introduces larger outliers (in all components at different degrees of magnitude). Up to 130 kilometers both software analysis tools yield results with a fairly even quality with some exceptions in Bernese. Within the Helmert transformation (table 26) the translation shows a

significant shift of the Bernese results regarding the Y component. This however again might be due larger differences starting at baseline length 130 km, since the accuracy of the Bernese translation values is at nearly 5 mm. The TBP indicates no significant systematic shift, merely an increased uncertainty of the results. Overall the TBP delivers more reliable results when introducing severely limiting observation windows. Also a reasonable accuracy is maintained even way below the recommended observation timespans by Bernese. The coordinate sigmas w.r.t. the baseline length is depicted in figure 34 in the appendix.

**Table 26: 3D Helmert transformation parameters for TBP and Bernese, medium BL, obs. time 1:00 to 1:30, pm**

	Bernese Parameters:	Bernese Accuracy:	TBP Parameters:	TBP Accuracy:
Translation X	-0.0036	0.0047	0.0059	0.0010
Translation Y	-0.0124	0.0047	0.0013	0.0010
Translation Z	-0.0078	0.0047	0.0039	0.0010
Rotation w.r.t. X	-0.0000	0.0000	0.0000	0.0000
Rotation w.r.t. Y	0.0000	0.0000	0.0000	0.0000
Rotation w.r.t. Z	0.0000	0.0000	-0.0000	0.0000
Scale factor	1.000	0.0000	1.000	0.0000

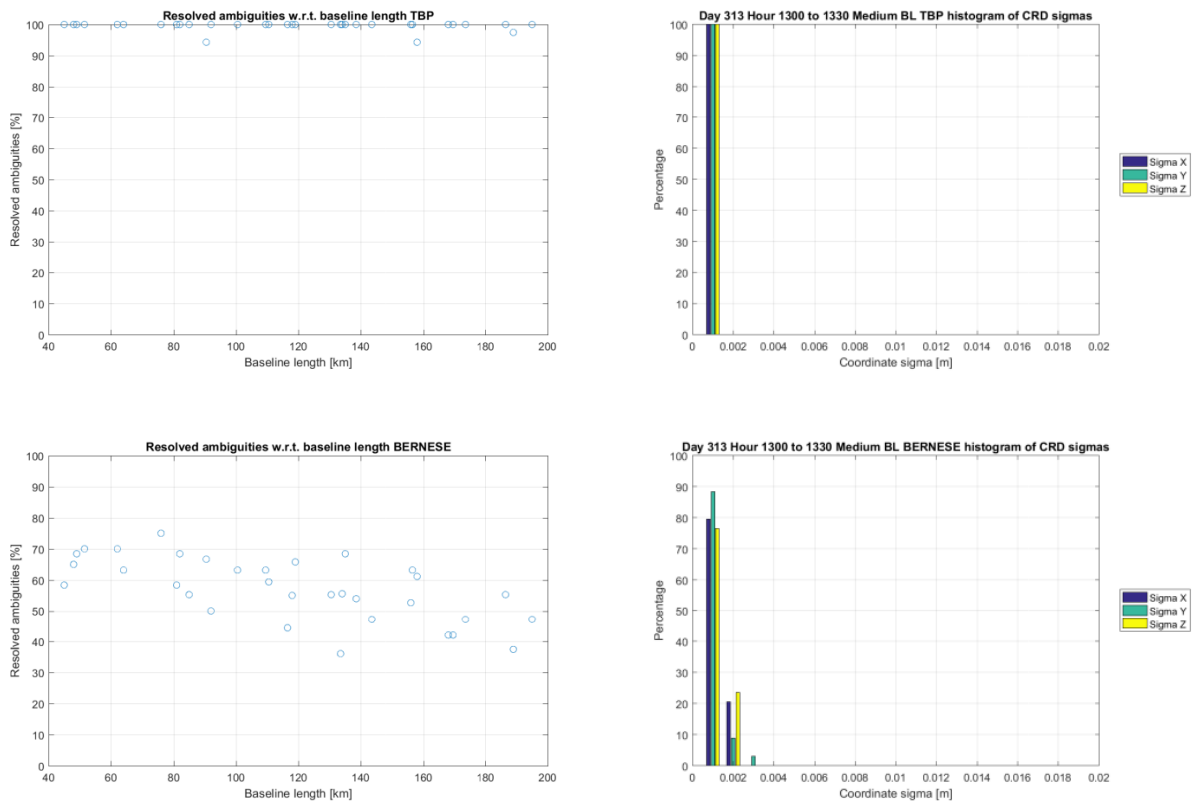


**Figure 68:** Left: Percentage of resolved ambiguities for medium baselines, obs. time 1:00 to 1:30, pm; Right: Histogram of coordinate sigmas for medium baselines, obs. time 1:00 to 1:30, pm;

## 4 Results and discussion

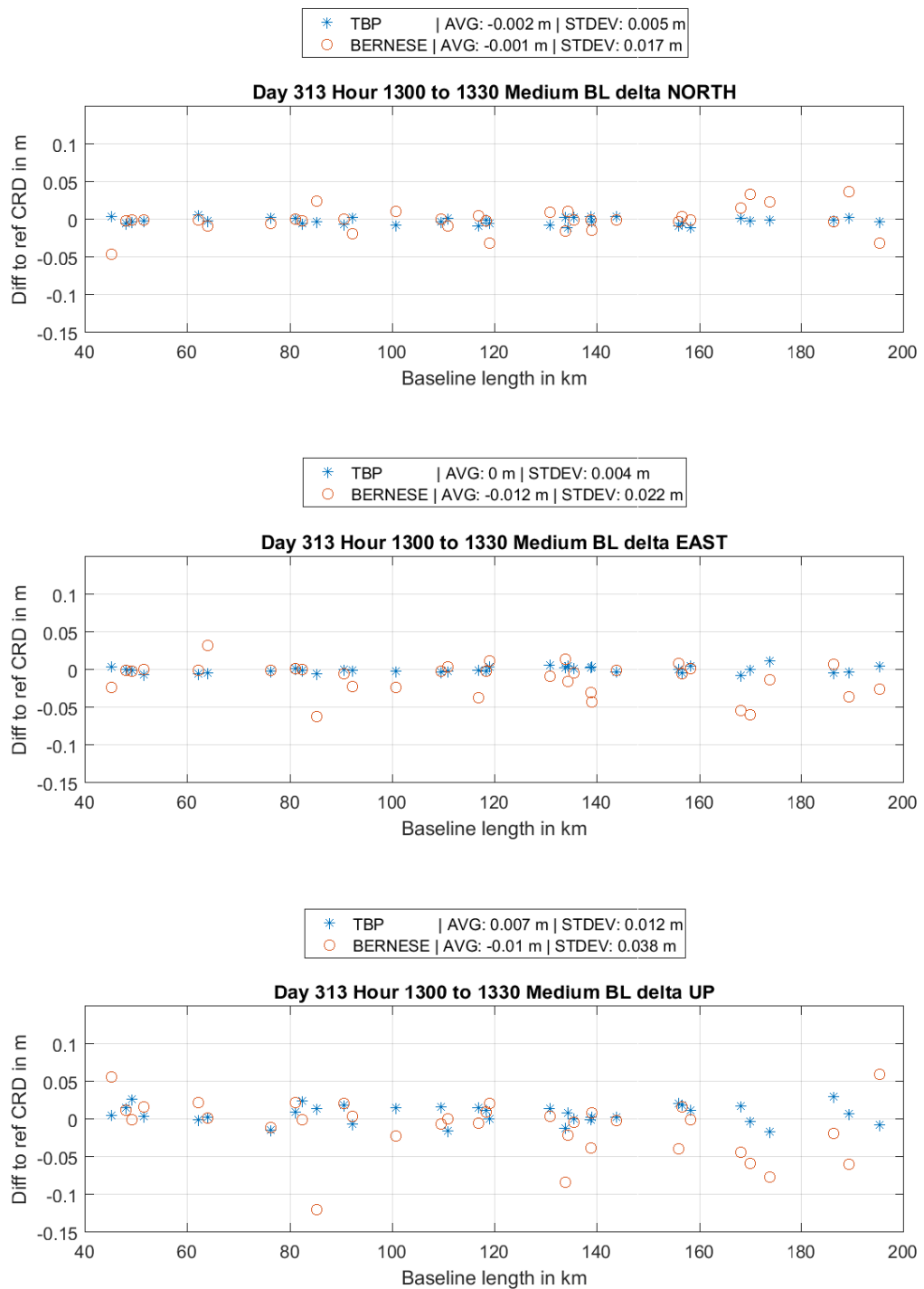


Figure 69: Delta NEU medium baselines, obs. time 1:00 to 1:30, pm

## 4.7 Processing conclusion

In conclusion both processors show similar capabilities regarding accuracy w.r.t. the established standard procedure, however the TBP shows slightly better performance regarding small and medium baselines. Bernese on the other hand outperforms the TBP for long baselines and significantly for very long baselines. The TBP tends to estimate heights slightly too low with respect to reference coordinates and Bernese slightly too high. Results from both processors agree on the millimeter level for medium to small baselines and on the centimeter level for long baselines.

The choice of the troposphere correction regarding GMF, VMF and NMF shows only minor differences in the results w.r.t. each other as it should be. Also similar effects on the results are observed for both processors when switching the models. In conclusion the models seem to be applied in a similar manner causing similar effects on the results.

Processing GPS only instead of a GPS/GLONASS combined solution produces marginally less accurate results in Bernese in all baseline intervals. The TBP solutions for short and medium baselines are widely equal to the GPS/GLONASS solution, anyway long baselines show larger outliers and the results become unreliable.

Both processors show the ability to reproduce results on consecutive days, however Bernese for medium and long baselines Bernese is more reliable than the TBP, however for short BL the TBP showed better performance. Similar patterns regarding the discrepancies between daily solutions can be observed in the results of both software suites.

Using broadcast ephemeris instead of precise orbits is possible in both analysis suites yet not recommended. Short baselines are evaluated with a fairly equal quality in both software solutions, however for medium baselines the TBP outperforms Bernese significantly, but also with a significant degradation in accuracy.

Processing data with reduced occupation timespans for short baselines performs similar to the standard procedure in the TBP as well as Bernese as long as thresholds for length and minimum occupation time are respected. For medium baselines Bernese already showed weaknesses when requesting computations at the minimum time window. In general the TBP is able to produce reasonable results for shorter observation timespans than Bernese.

Due to the nature of the sigma dependent algorithm (preferring to leave ambiguities as float instead of fixing them to a wrong value) and the Lambda strategy (trying to fix all ambiguities and verify the parameters) the TBP produces generally a higher resolution rate. For a brief overview, the average ambiguity resolution percentage per baseline length is displayed in figure 70 (bin width 10 km), TBP on the left and Bernese on the right. Note that even for low ambiguity resolution rates at long baselines the Bernese results are still outstanding. Figure 71 shows a histogram

illustrating the cumulative number of baselines for a given ambiguity resolution percentage (Note that the blue columns reach to the ground behind the red columns instead of starting upon them). The red columns represent the TBP, the blue ones Bernese. For about half of all baselines Bernese solves at least 75 percent of all initial ambiguities where the TBP solves 100 percent.

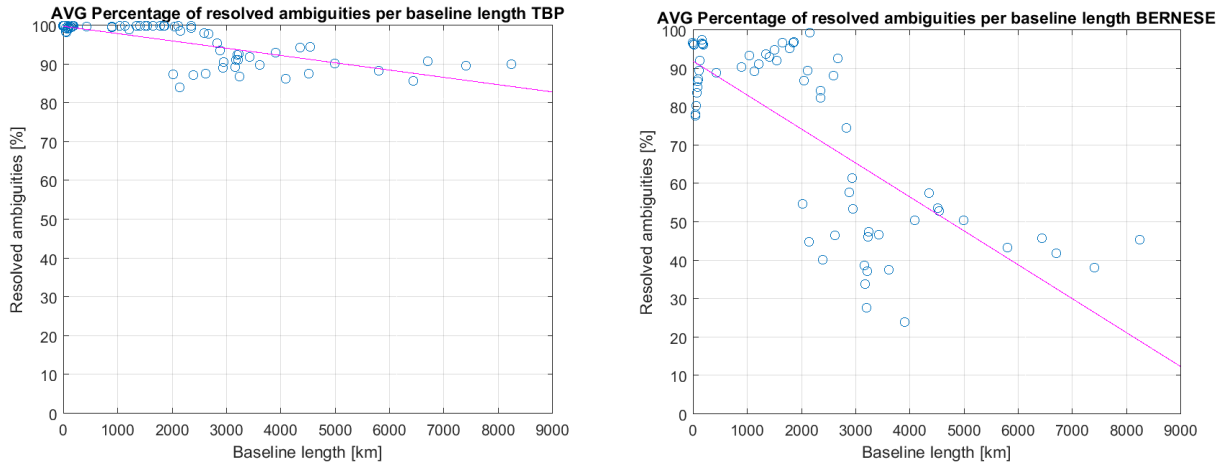


**Figure 70:** Left: TBP average percentage of resolved ambiguities per baseline length bin width 10 km); Right: Bernese avg percentage of resolved ambiguities per baseline length (bin width 10 km);

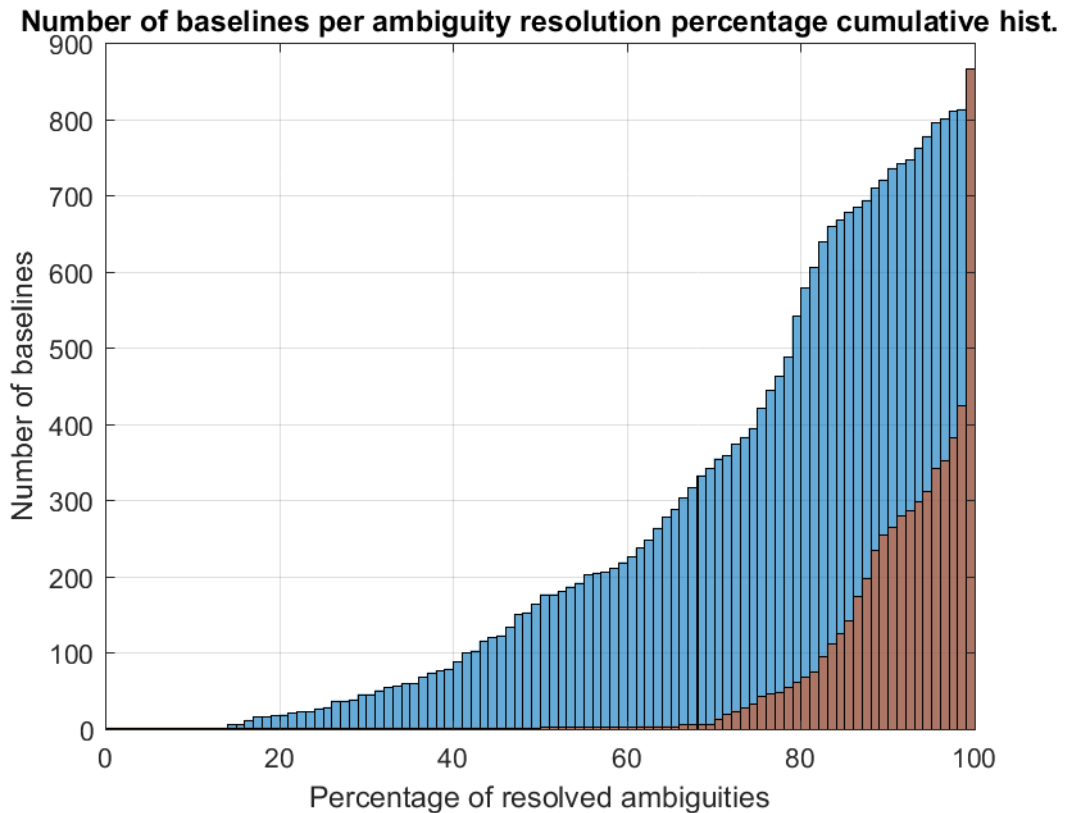


**Figure 71:** Amount of baselines per ambi. Res. Perc. per processor, bin width 1 percent, TBP: red, Bernese: blue

## 4.8 Soft factors

Finally, some factors shall be stated regarding additional capabilities and design factors. There are two use cases which have to be treated here, on the one hand the classic commercial user e.g. a surveyor evaluating a measurement campaign and on the other hand a scientist, for example evaluating the impact of certain events in the observations on the results.

### 4.8.1 Processing possibilities

This topic yields the largest division into commercial and scientific use cases. In Bernese the user is able to perform scientific analyses for a huge amount of GNSS and geophysics related subjects, also processing of SLR data is possible. Computing station velocities due to continental drift, estimating tropospheric parameters using different models for any application, estimating global ionosphere maps and precisely estimate orbits tailored to the very needs of processing are just a few of the capabilities. Additional functionalities (e.g. to compare orbits) are built in which allow not just generating but also immediately evaluating results. These functionalities, as powerful as they might be, have however only limited applications in the commercial environment. Another aspect also appealing to the scientific community is the ability to change the Fortran scripts the programs are written on, i.e. the very foundation of Bernese. It enables the user to implement own ideas and methods.

The Trimble Business Center offers a wide range of survey and construction related functionalities apart from pure GNSS data computation, like classic tachymetric, photogrammetric and laser scanning point cloud data evaluation. It furthermore offers GIS and CAD features for creating plans of e.g. construction projects. For the classic survey company it is a well-equipped suite to work with, but for the scientific user these features are simply of no interest. Also a problem for scientific use is the limited output regarding intermediate results, such as from preprocessing or residual screening, for example.

### 4.8.2 Graphical User Interface

In chapter 3 the user interface of both software solutions were already introduced, for Bernese rather shortly. For this reason figure 72 depicts a typical settings window in Bernese (GPSEST panel 3.1, in this very case). Overall the design is kept simple, concentrating on the important parts: the actual data processing settings. Every program is called via a drop down menu and its belonging settings may be stated in consecutive pages. The design of TBC (figures 4, 5 and 8 to 11) is the pure contrary. It is colorful, with programs started by unique icons in toolbars. Its' design

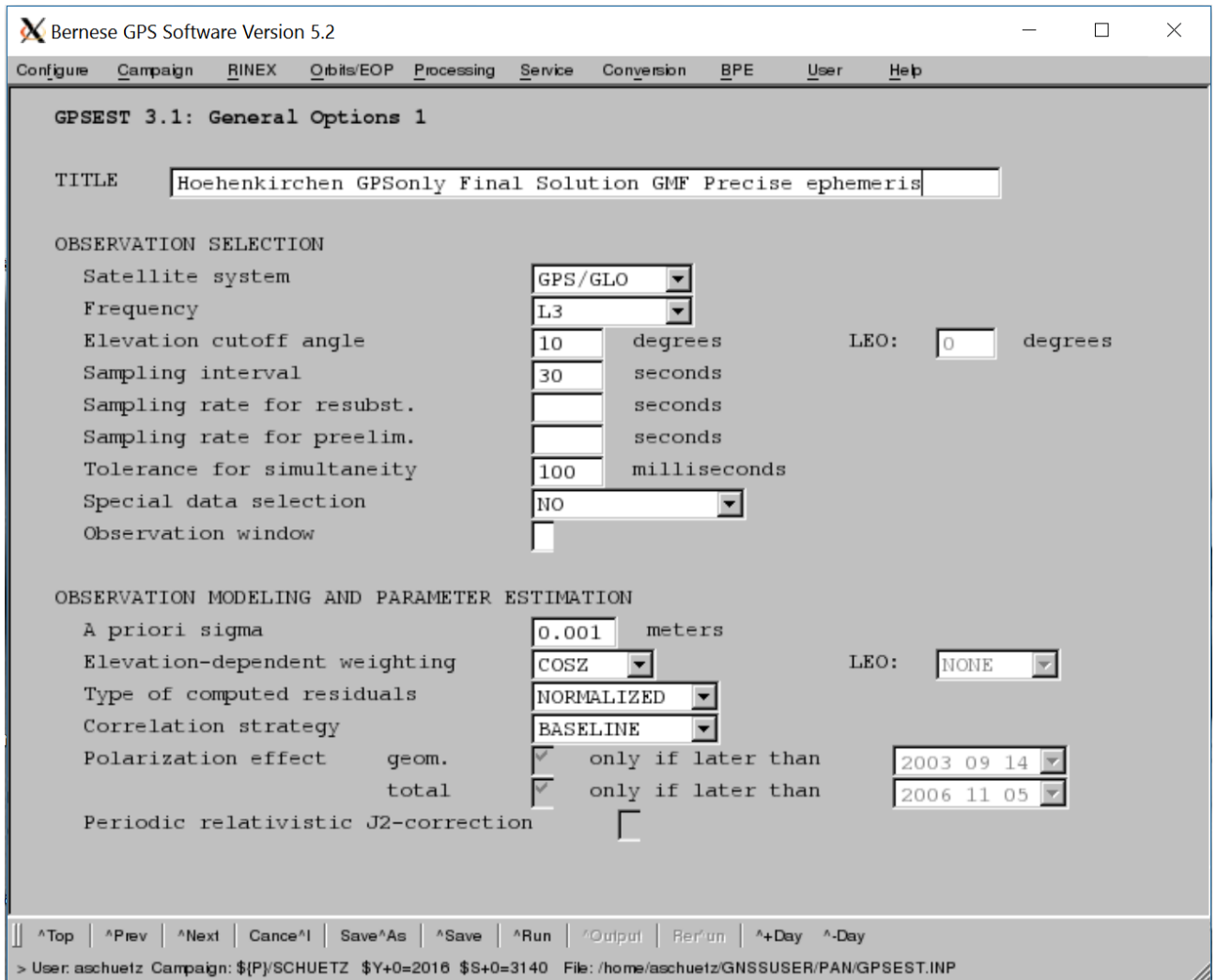


Figure 72: Bernese GPSEST settings panel 3.1

is modern and comparable to other classic Microsoft Windows based software suites. The settings for specific programs are stated in separate windows, where the user only can choose between predefined settings, in order to ensure valid parameters submitted to the programs. But, from an ergonomic point of view, the toolbar is overloaded. Icons are too small and there are lots of functionalities which can be called by a shortcut. This reduces the general clear view for the user, because there are simply too much functionalities displayed at once to be used in an efficient manner. A nice part however is the graphic representation of the station or point network in a coordinate grid, where information about stations or baselines can be acquired by clicking on the objects. This gives a good impression of the data processed and allows to quickly determine problematic sites or network arrangements.

### 4.8.3 User friendliness

The last point concerns the user friendliness of both suites. For the successful usage of Bernese a profound knowledge of GNSS postprocessing as well as basic scripting language knowledge is necessary. The structure of the settings and the program flow may be confusing to somebody who is not used to data evaluation or processing. Another aspect is the more or less complete freedom in the settings. Settings may be chosen for each processing step completely individual, however may also be contradictive to one another. This is a small drawback from the modular design. TBC on the other hand shows to be conceptual. It is kept more general regarding the setting and also certain selection criteria (i.e. sampling rate) only need to be set at one place and are valid throughout the whole project. In fact, the whole process described in section 3.2.3.1 needs manual setup. Using the tutorial script of the official 1 week training course and the email support a PC experienced user might be able to produce first results in several days for one network. With TBC a solution with similar accuracy can be produced in several minutes just by drag and drop and clicking one button in several minutes (using the adaptive mode, of course). Also, for example, the TBC has a built in precise orbit file downloader. The Bernese manual suggests, in case of automatizing this process, to write a script within the personal environment of the user to perform this task. Now for somebody with a programming or engineering background this might not be a problem, but for an inexperienced user this might be. This also shows the most important factors for both tools: For Bernese it is accuracy and freedom of the user, for TBC it is accuracy and convenience for the user. And even in the scientific mode, all adjustable parameters for the estimation can be set in one window. It might not be as much as in Bernese, but regarding baseline postprocessing the most important aspects are covered.

When moving away from the GUI or single project based processing, TBC is no longer viable. Bernese on the other hand can be set up and ran without the GUI, enabling vast datasets and scheduled processing (i.e. a cronjob) done on servers. TBC is simply not designed for this.

Again, depending on the use case both tools bring different advantages and disadvantages for the user to the table. Where the commercial user might be lost in the depth of Bernese, a scientific user might feel too constrained by the possibilities offered by TBC.

## 5 Outlook

Given the fact that Bernese is now established for decades as one of the most accurate and famous GNSS processing software, the TBP inside TBC shows very promising performance as well as the will to move away from a pure convenience based data processing (of course, in addition to highest accuracy requirements) and offer the customer a choice between convenience and introducing personal experience/preferences. It might also encourage current users to familiarize deeper with the matter at hand, not just to press the “Processing” button. As for performance and eventual shortcomings, be advised that this is only the very first release of a Trimble baseline processor inside TBC with so called “scientific settings” that can be set by the user. The module of course will further be maintained, updated and improved as well as possible new features will be introduced. With its final release it will also support CMRX data, Trimble’s own atmospheric correction data service.

The very last statement is obviously not just true for the TBP. Bernese did not maintain its high standard by being left in a corner. It is undergoing constant change and development with a high amount of resources. An example can be given by the implementation of the LAMBDA ambiguity resolution strategy in the next version of Bernese, as promoted in the Bernese user manual. Also the persistent adaptation to the expanding number of GNSSs and SBASs is in progress.

As far as potential products are concerned, the future might bring a command line version of the TBP and GNSS related processing from Trimble. With increasing bandwidth and the broad availability of high speed internet maybe the future also lies in web based services, such as RTX PP, the online service for PPP from Trimble.

Anyway, even though GNSS, especially GPS, and its data postprocessing have been around for nearly 40 years now the applications and use for research are still increasing. With its constant change, improvement and additional features and capabilities the software manufacturers also compete to adapt and improve, not just between each other but also regarding their own solutions.

## References

Arora BS, Morgan J, Ord SM, Tingay SJ, Hurley-Walker N, Bell M, Bernardi G, Bhat R, Briggs F, Callingham JR, Deshpande AA, Dwarakanath KS, Ewall-Wice A, Feng L, For BQ, Hancock P, Hazelton BJ, Hindson L, Jacobs D, Johnston-Hollitt M, Kapińska AD, Kudryavtseva N, Lenc E, McKinley B, Mitchell D, Oberoi D, Offringa AR, Pindor B, Procopio P, Riding J, Staveley-Smith L, Wayth RB, Wu C, Zheng Q, Bowman JD, Cappallo RJ, Corey BE, Emrich D, Goeke R, Greenhill LJ, Kaplan DL, Kasper JC, Kratzenberg E, Lonsdale CJ, Lynch MJ, McWhirter SR, Morales MF, Morgan E, Prabu T, Rogers AEE, Roshi A, Udaya Shankar N, Srivani KS, Subrahmanyam R, Waterson M, Webster RL, Whitney AR, Williams A, Williams CL (2015): Ionospheric modelling using GPS to calibrate the MWA. 1: Comparison of first order ionospheric effects between GPS models and MWA observations. *Publications of the Astronomical Society of Australia*: vol. 32, doi: 10.1017/pasa.2015.29

Boehm J, Niell A, Tregoning P, Schuh H (2006): Global Mapping Function (GMF): A new empirical mapping function based on numerical weather model data. *Geophysical Research Letters*: vol. 33 issue 7, doi: 10.1029/2005GL025546

Boehm J, Schuh H (2004): Vienna mapping functions in VLBI analyses. *Geophysical Research Letters*: vol. 31 Issue 1, doi: 10.1029/2003GL018984

Boehm J, Werl B, Schuh H (2006): Troposphere mapping functions for GPS and very long baseline interferometry from European Centre for Medium-Range Weather Forecasts operational analysis data. *Journal of Geophysical Research*: vol. 111 Issue B2, doi: 10.1029/2005JB003629

Chen G, Herring TA (1997): Effects of atmospheric azimuthal asymmetry on the analysis of space geodetic data, *Journal of Geophysical Research*: vol. 102 Issue B9, pp. 20489-20502, doi: 10.1029/97JB01739

Dach R, Fridez P (2016), Bernese GNSS Software Version 5.2 Tutorial, official tutorial, Astronomical Institute University of Bern, <http://www.bernese.unibe.ch/docs/TUTORIAL.pdf> (01.05.2017)

Dach R, Lutz S, Walser P, Fridez P (Eds) (2015): Bernese GNSS Software Version 5.2 User Manual. Bern: Astronomical Institute, University of Bern, Bern Open Publishing. –ISBN 978-3-906813-05-9

Davis JL, Herring TA, Shapiro II, Rogers AEE, Elgered G (1985): Geodesy by radio interferometry: Effects of atmospheric modeling errors on estimates of baseline length. *Radio Science*, vol. 20 Issue 6, pp. 1593-1607

De Jonge P, Tiberius C (1996): The LAMBDA method for integer ambiguity estimation: implementation aspects, Publications of the Delft Geodetic Computing Centre, LGR series No. 12

Hofmann-Wellenhof B, Lichtenegger H, Collins J (2001): *Global Positioning System Theory and Practice*. 5<sup>th</sup> rev. edition, Wien: Springer

Klobuchar JA (1987): Ionospheric Time-Delay Algorithm for Single-Frequency GPS Users. *IEEE Transactions on Aerospace and Electronic Systems*: vol. 23 Issue 3, pp. 325-331, doi: 10.1109/TAES.1987.310829

Leick A (1995): *GPS Satellite Surveying*. 2<sup>nd</sup> rev. edition, New York: Wiley

Marini JW (1972): Correction of Satellite Tracking Data for an Arbitrary Tropospheric Profile, *Radio Science*, vol. 7 Issue 2, pp. 223-231, doi: 10.1029/RS007i002p00223

Niell AE (1996): Global mapping functions for the atmosphere delay at radio wavelengths, *Journal of Geophysical Research*, vol. 101 Issue B2, pp. 3227-3246, doi: 10.1029/95JB03048

Saastamoinen J (1973): Contributions to the theory of atmospheric refraction, part II, *Bull. Geod.*, vol. 107, pp. 13-34

Teunissen PJG (1995): The least squares ambiguity decorrelation adjustment: a method for fast GPS integer ambiguity estimation. *Journal of geodesy*: 70(1-2), pp. 65-82

# Attehements

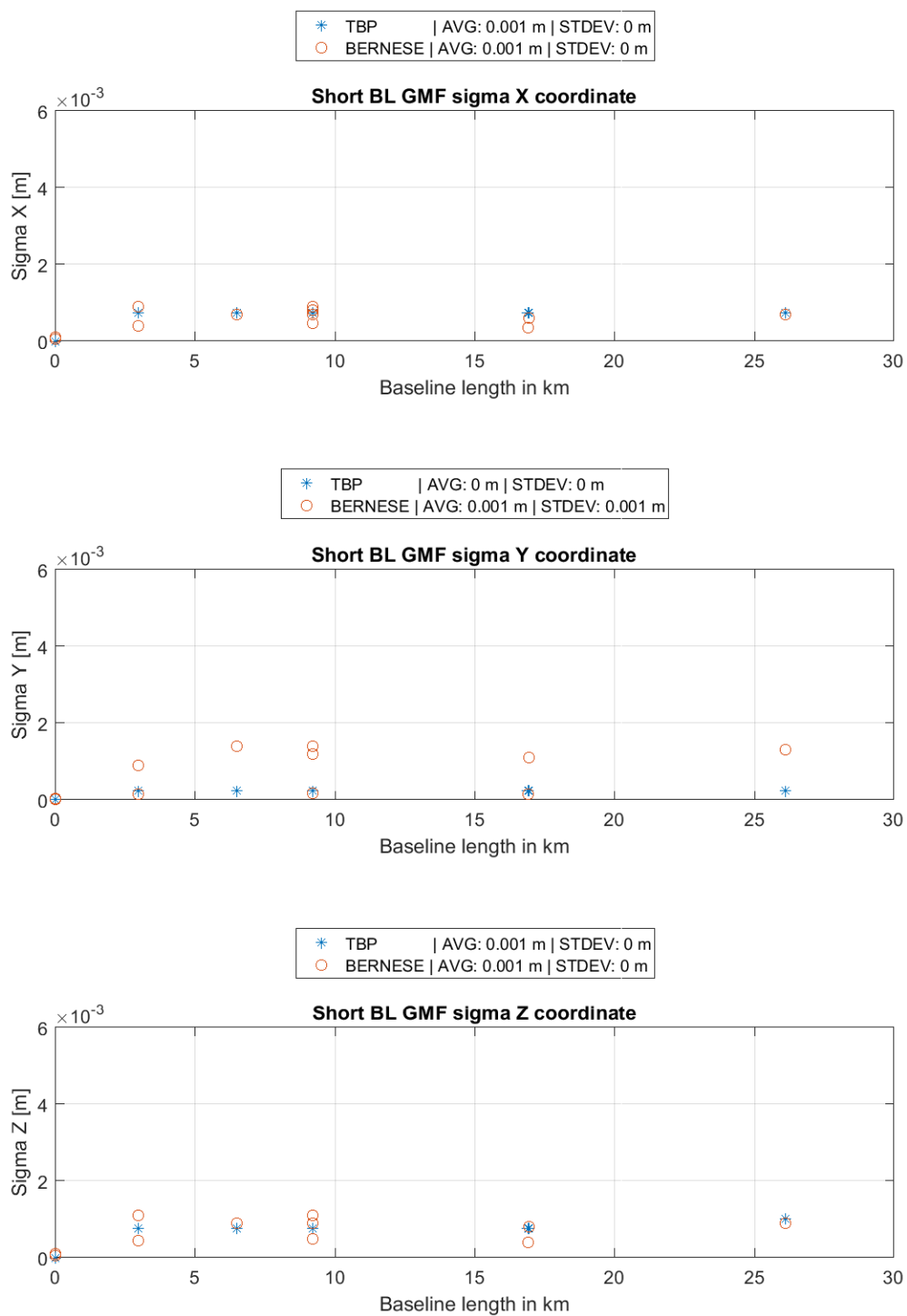


Figure A 1: Coordinate sigma w.r.t. to baseline length, short BL, standard processing procedure

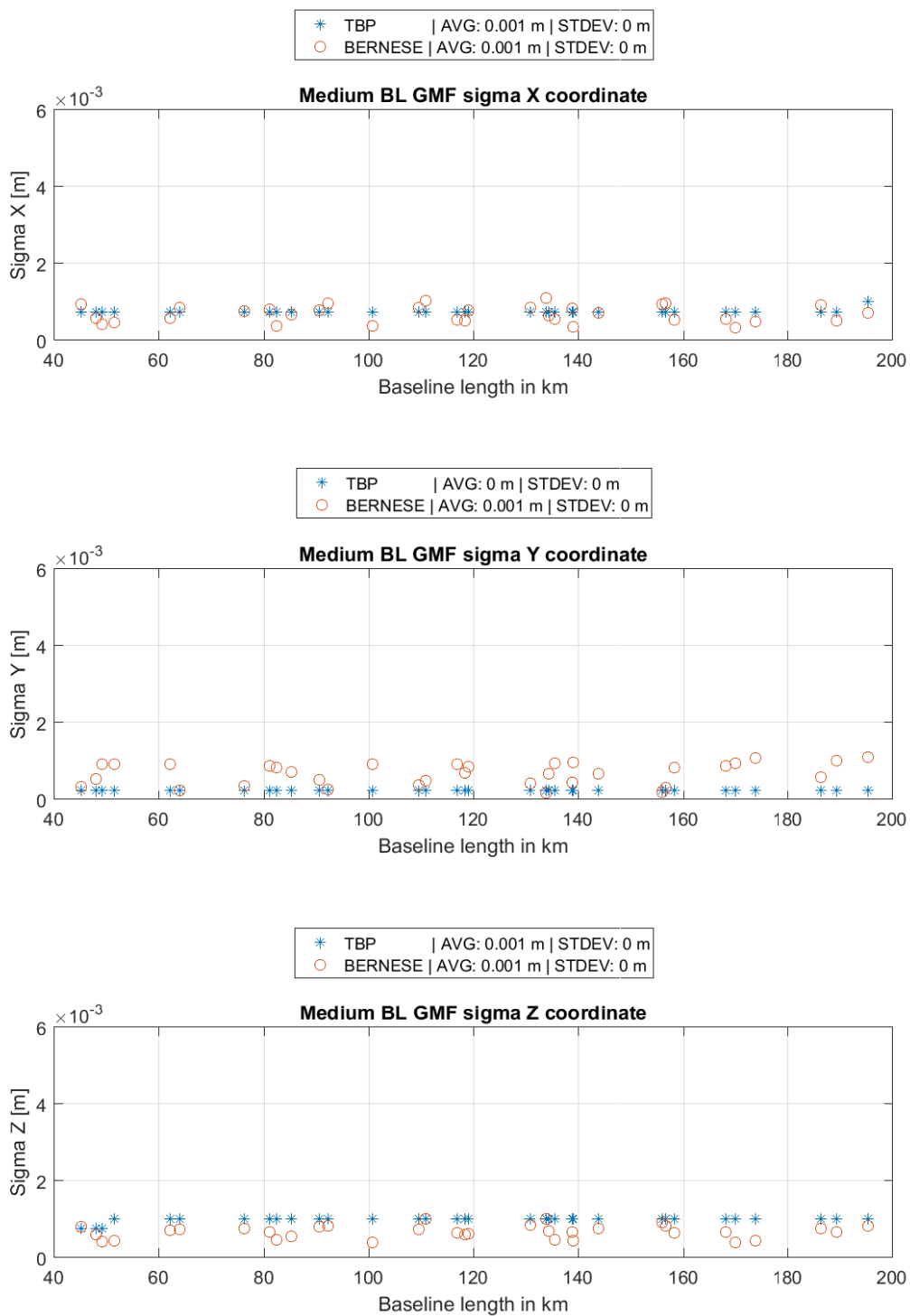


Figure A 2: Coordinate sigma w.r.t. to baseline length, medium BL, standard processing procedure

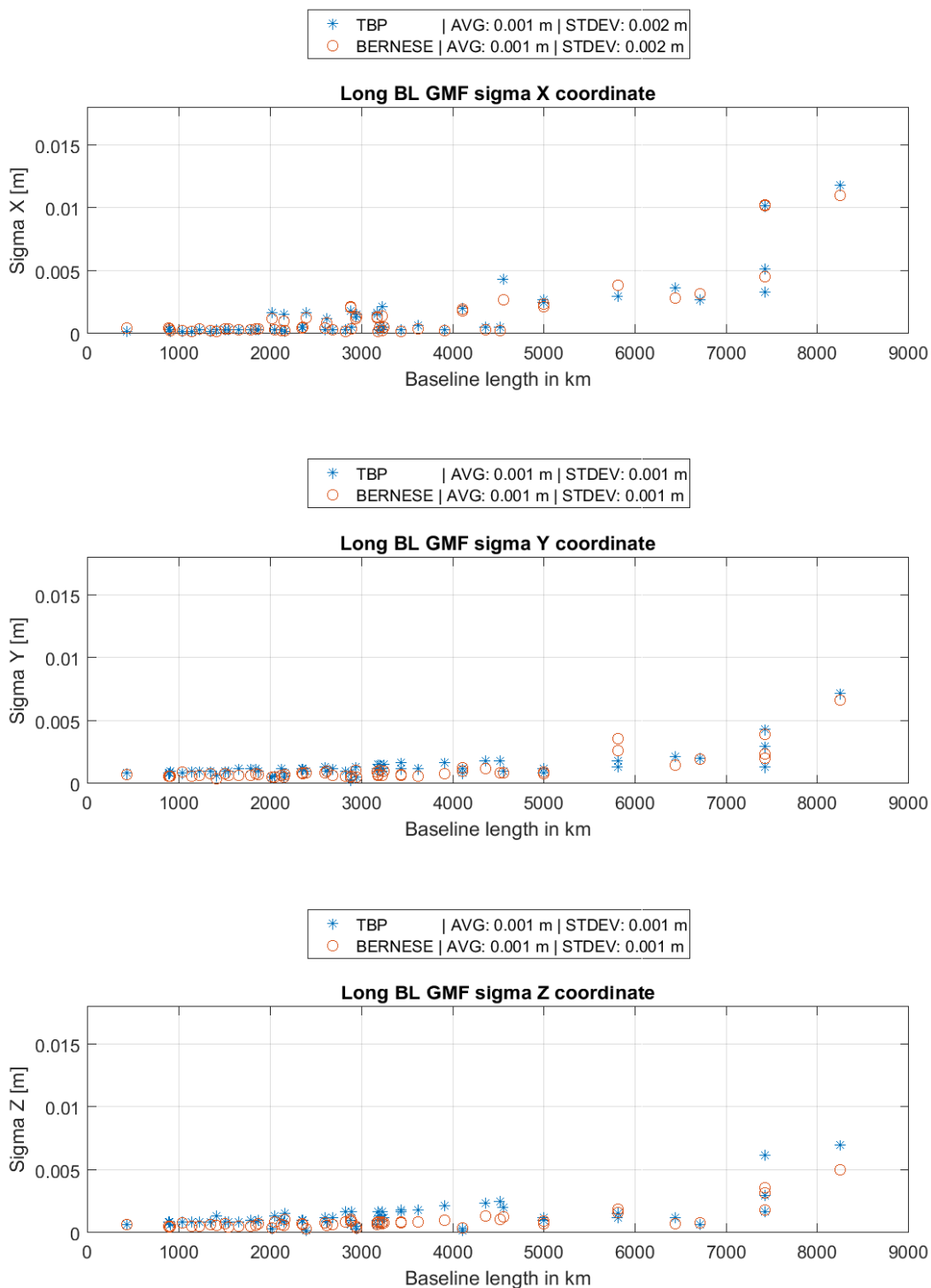


Figure A 3: Coordinate sigma w.r.t. to baseline length, long BL, standard processing procedure

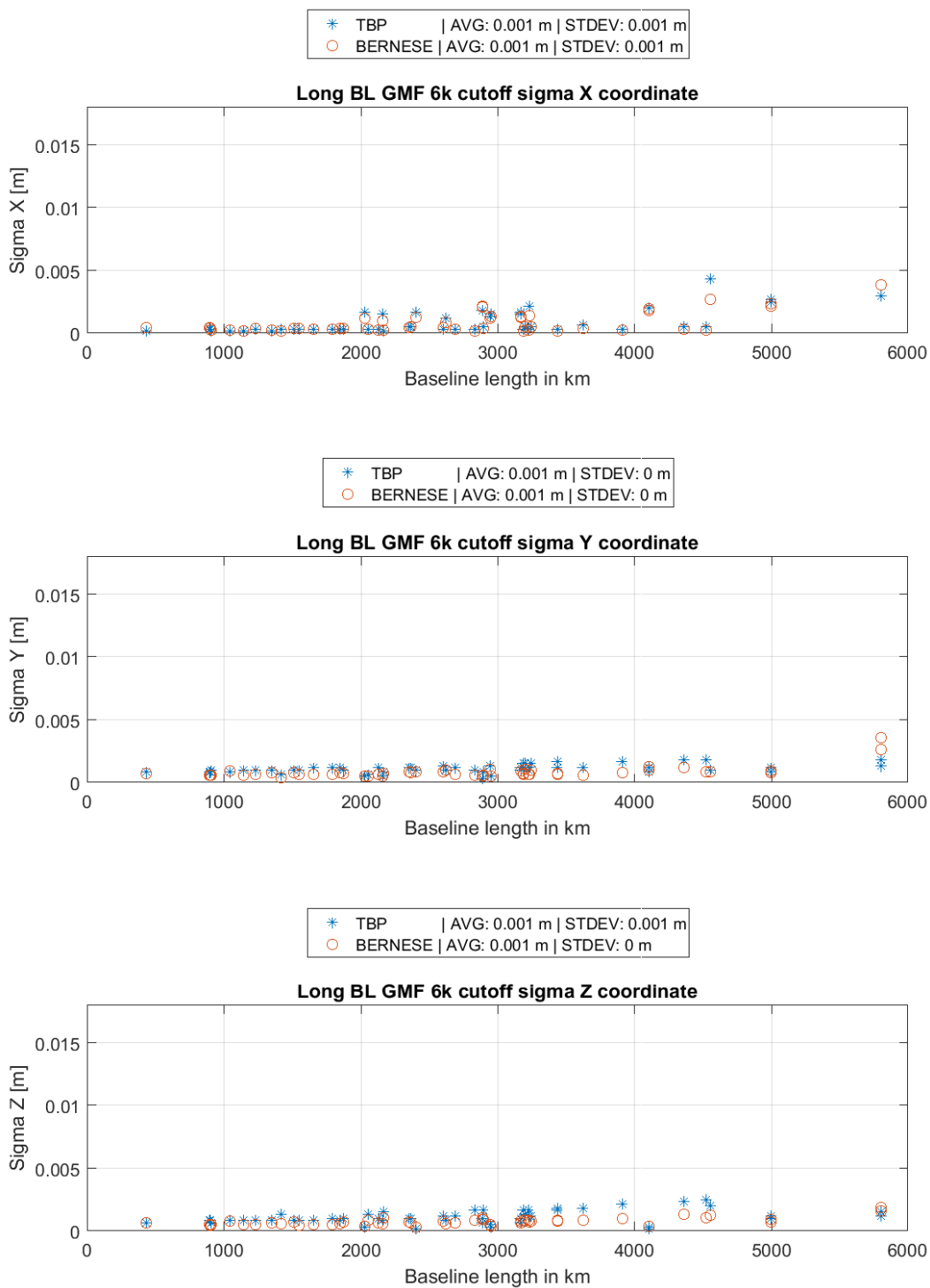


Figure A 4: Coordinate sigma w.r.t. to baseline length, long BL, 6000 km cutoff, standard processing procedure

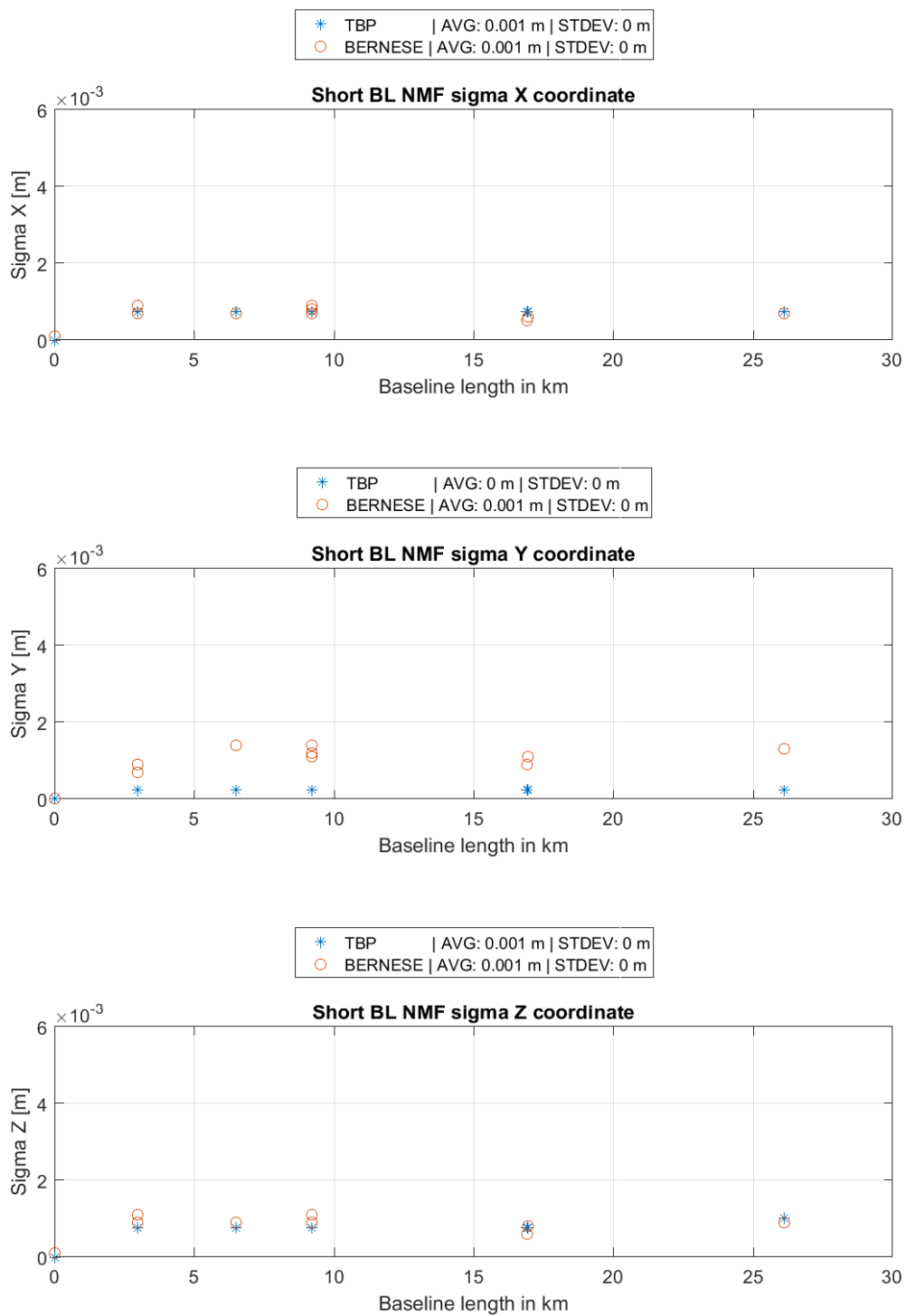


Figure A 5: Coordinate sigma w.r.t. to baseline length, short BL, NMF

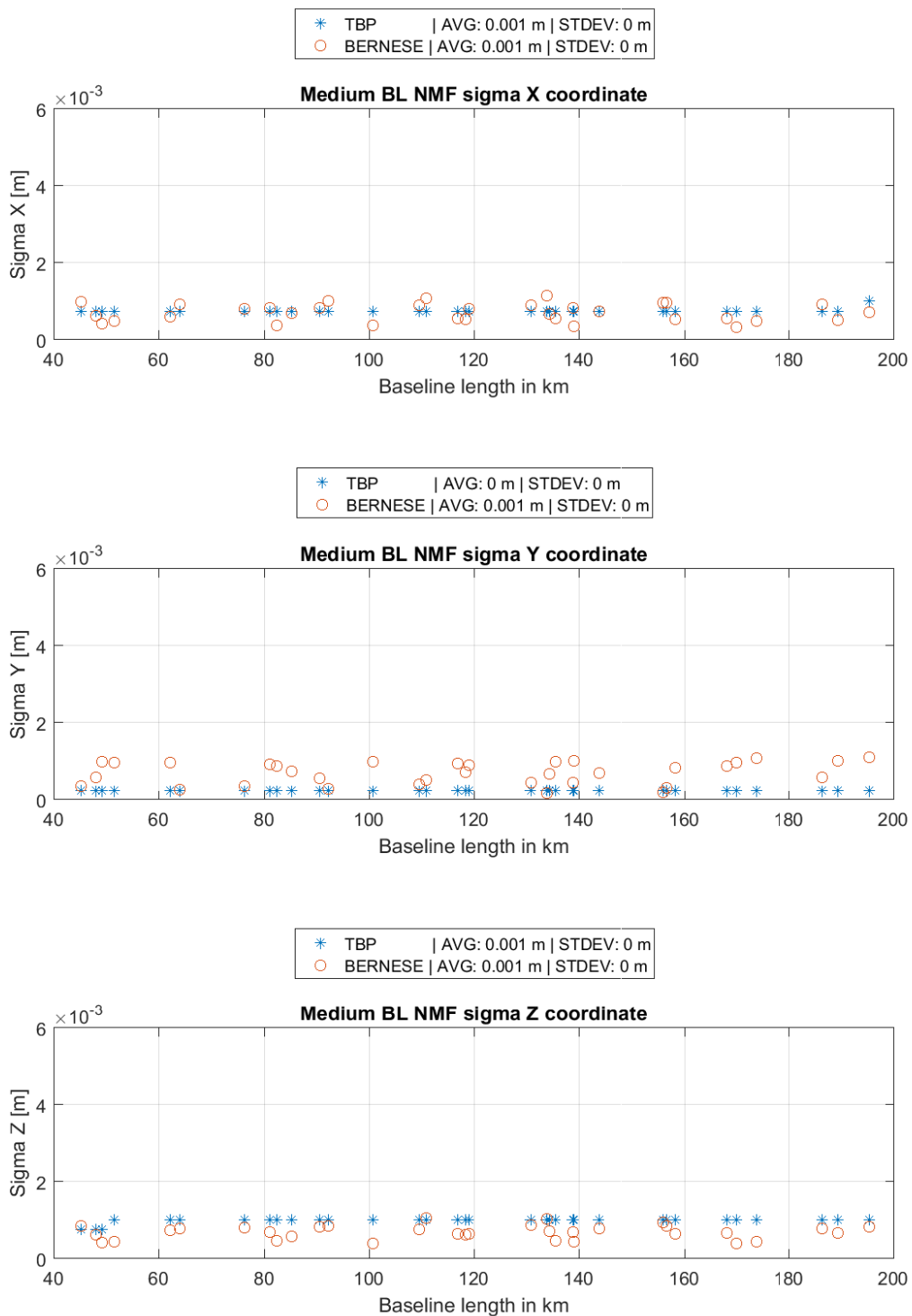


Figure A 6: Coordinate sigma w.r.t. to baseline length, medium BL, NMF

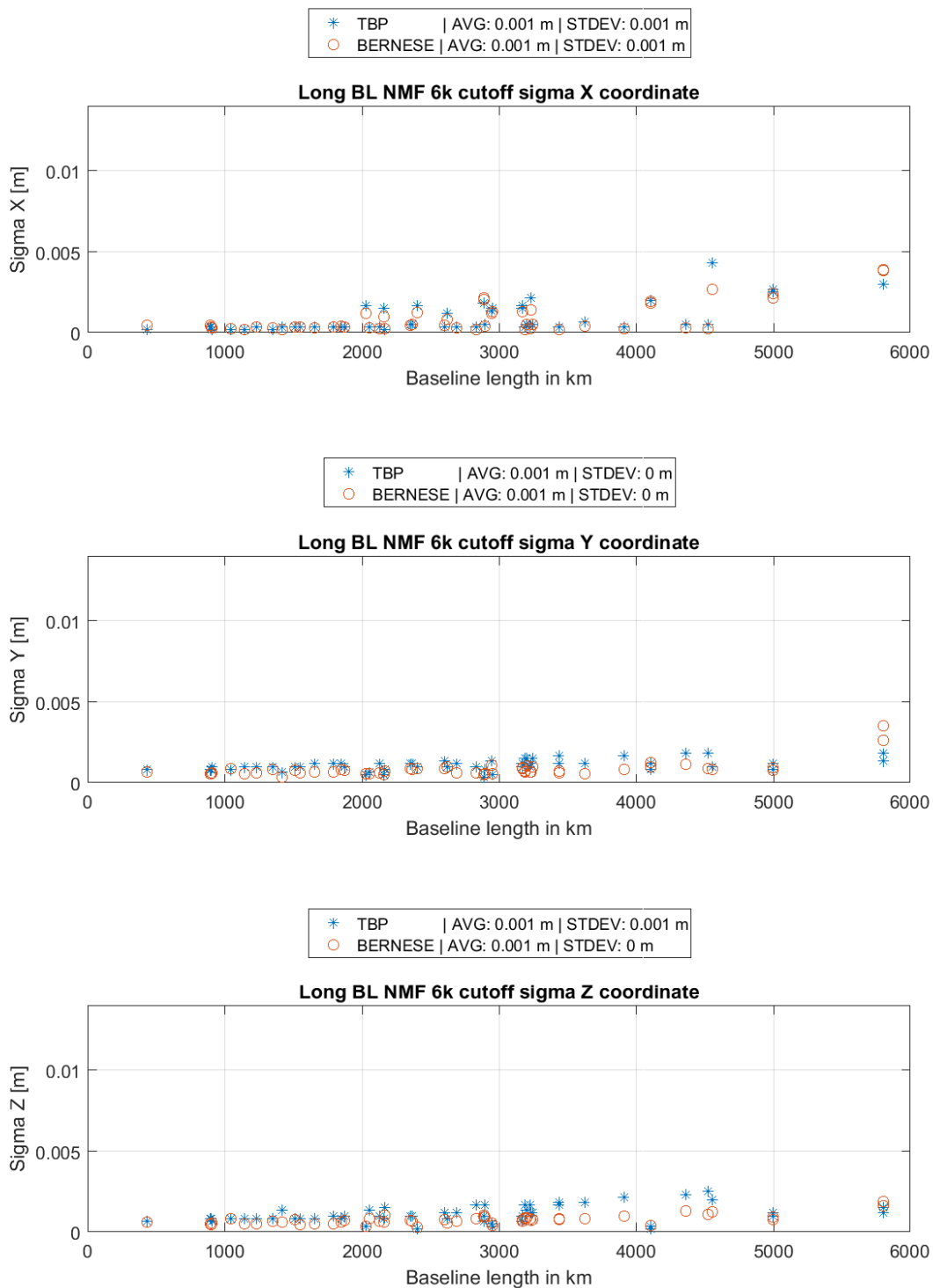


Figure A 7: Coordinate sigma w.r.t. to baseline length, long BL, 6000 km cutoff, NMF

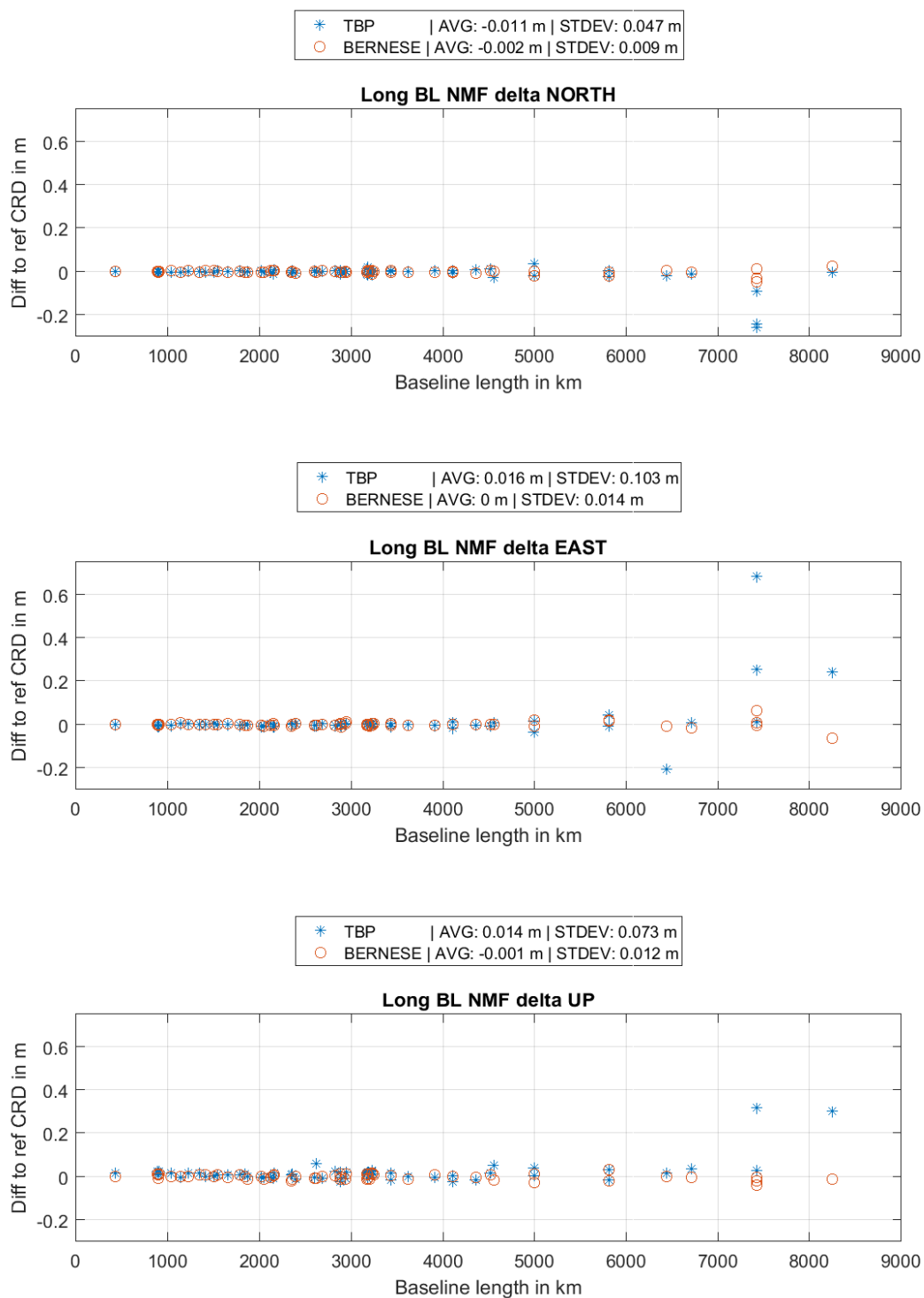
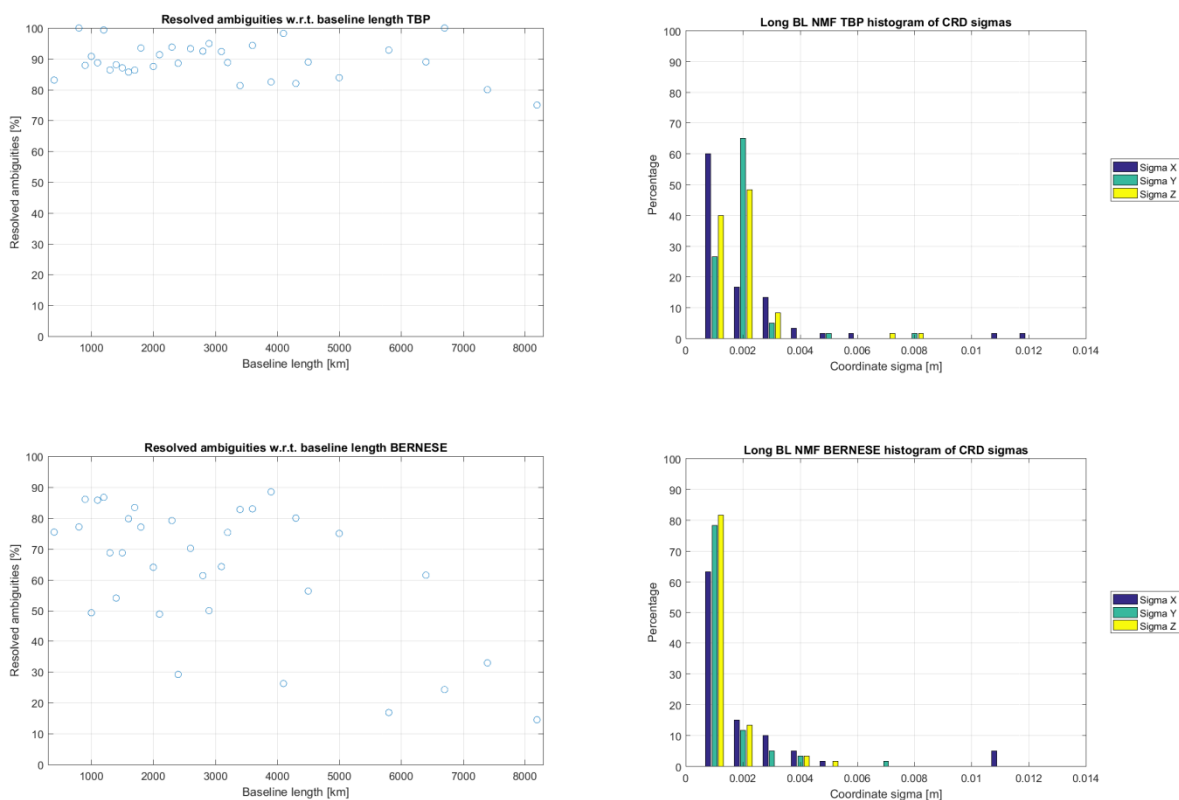


Figure A 8: Delta NEU, long baselines, NMF

**Table A 1: 3D Helmert transformation parameters for TBP and Bernese, Africa, NMF**

	Bernese Parameters:	Bernese Accuracy:	TBP Parameters:	TBP Accuracy:
Translation X	0.0033	0.0032	0.0270	0.0242
Translation Y	0.0002	0.0032	0.0395	0.0242
Translation Z	-0.0023	0.0032	-0.0178	0.0242
Rotation w.r.t. X	0.0000	0.0000	0.0000	0.0000
Rotation w.r.t. Y	-0.0000	0.0000	-0.0000	0.0000
Rotation w.r.t. Z	0.0000	0.0000	0.0000	0.0000
Scale factor	1.000	0.0000	1.000	0.0000



**Figure A 9: Left: Percentage of resolved ambiguities for long baselines, NMF; Right: Histogram of coordinate sigmas for long baselines, NMF;**

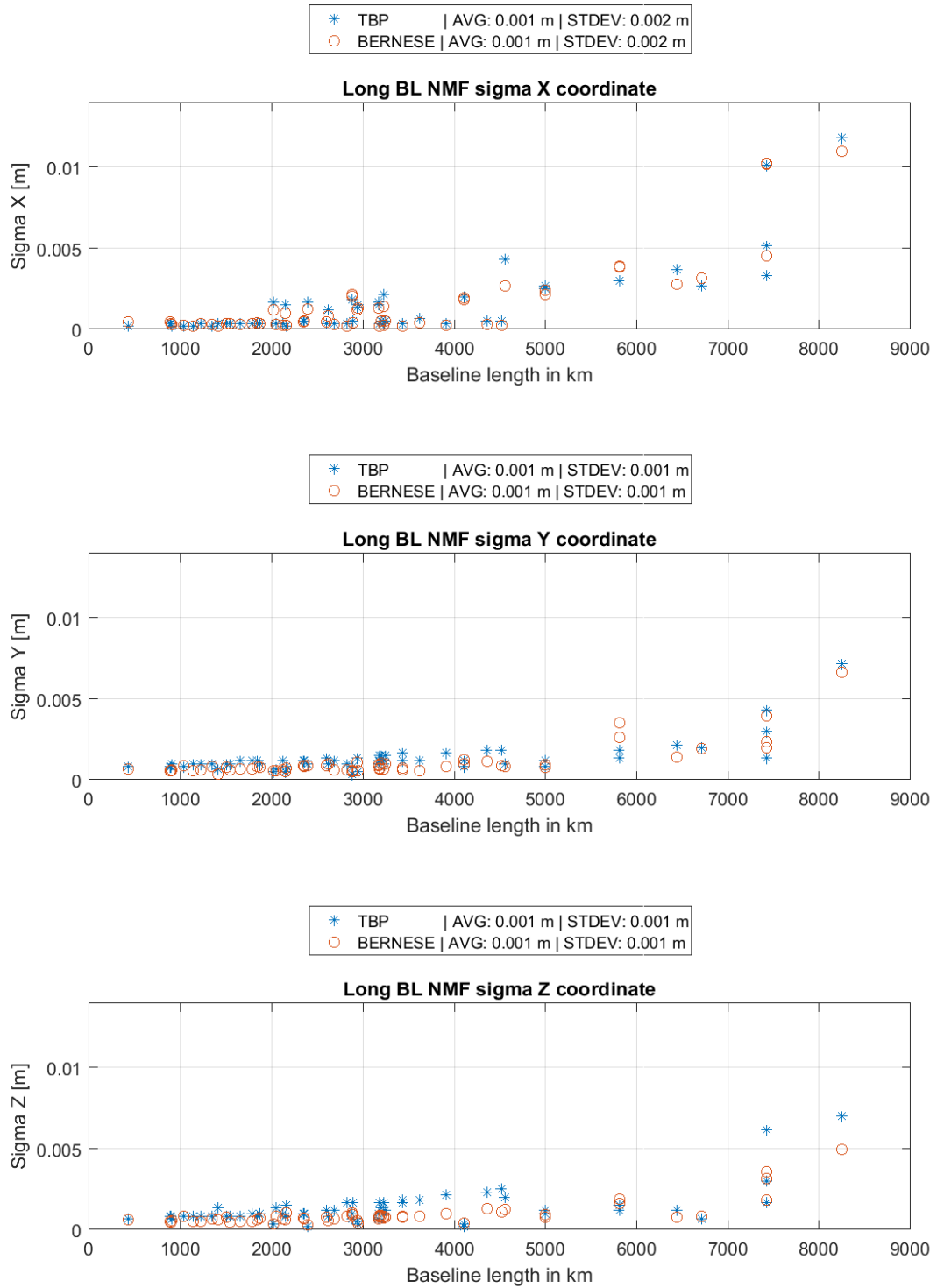


Figure A 10: Coordinate sigma w.r.t. to baseline length, long BL, NMF

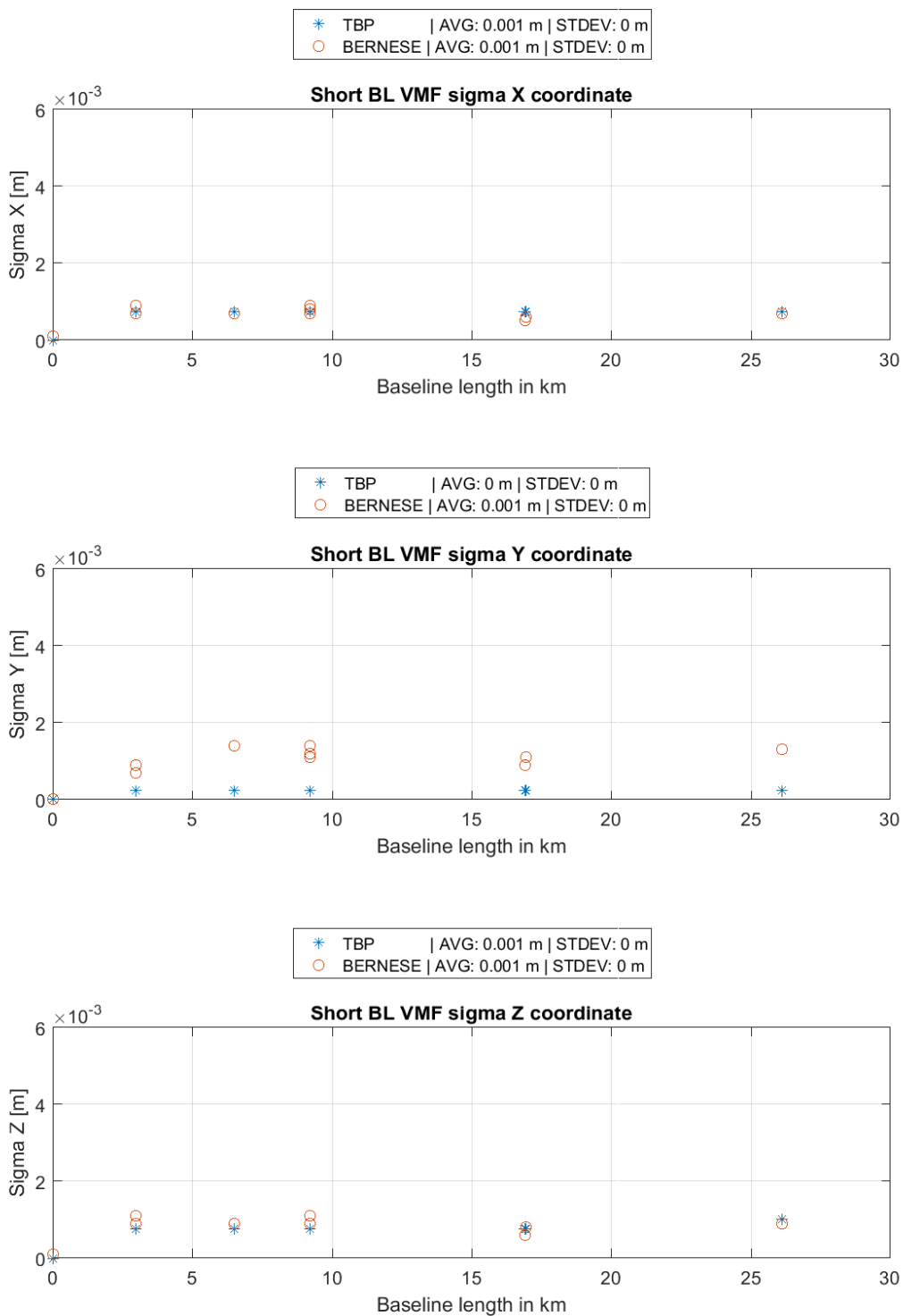


Figure A 11: Coordinate sigma w.r.t. to baseline length, short BL, VMF

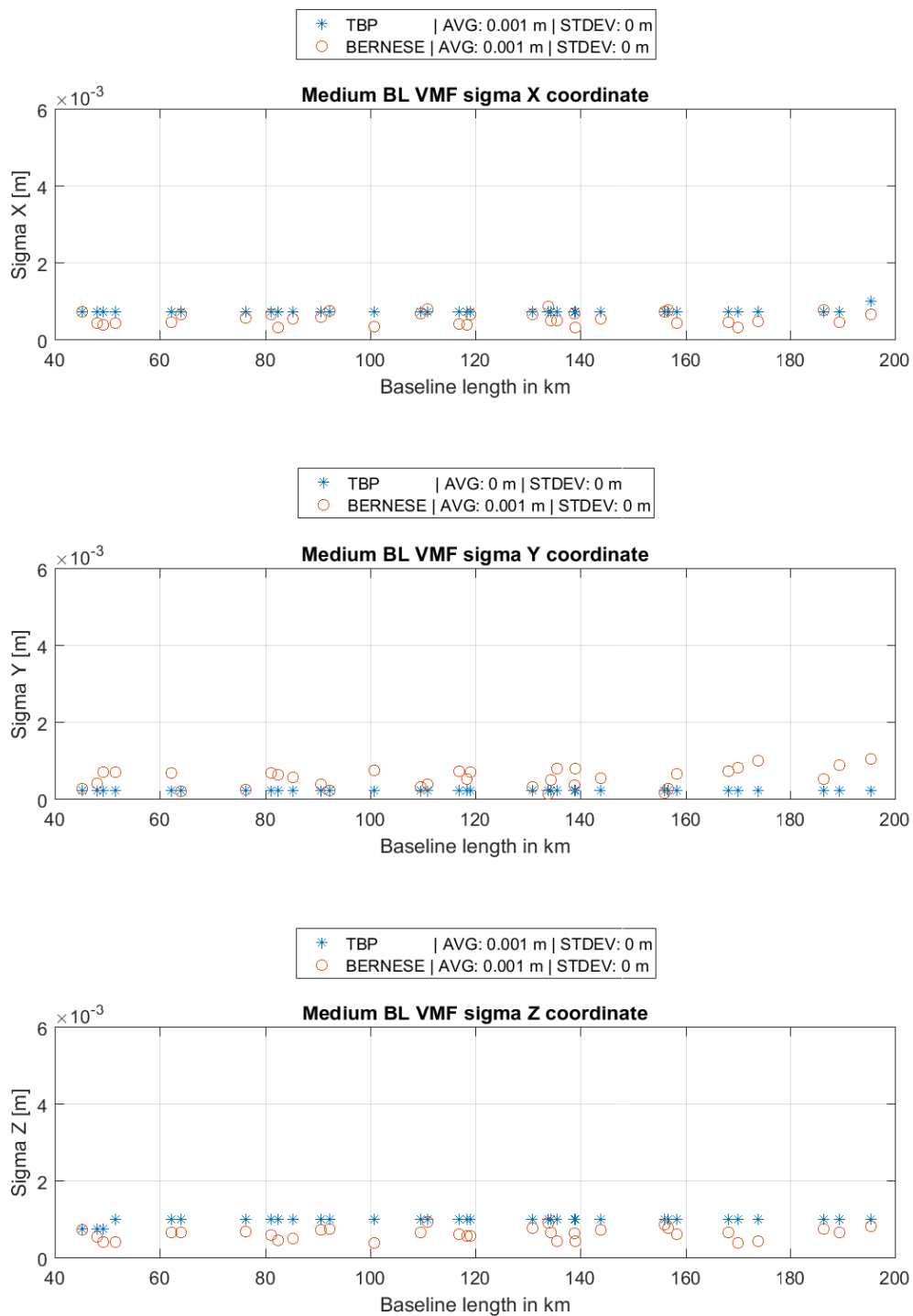


Figure A 12: Coordinate sigma w.r.t. to baseline length, medium BL, VMF

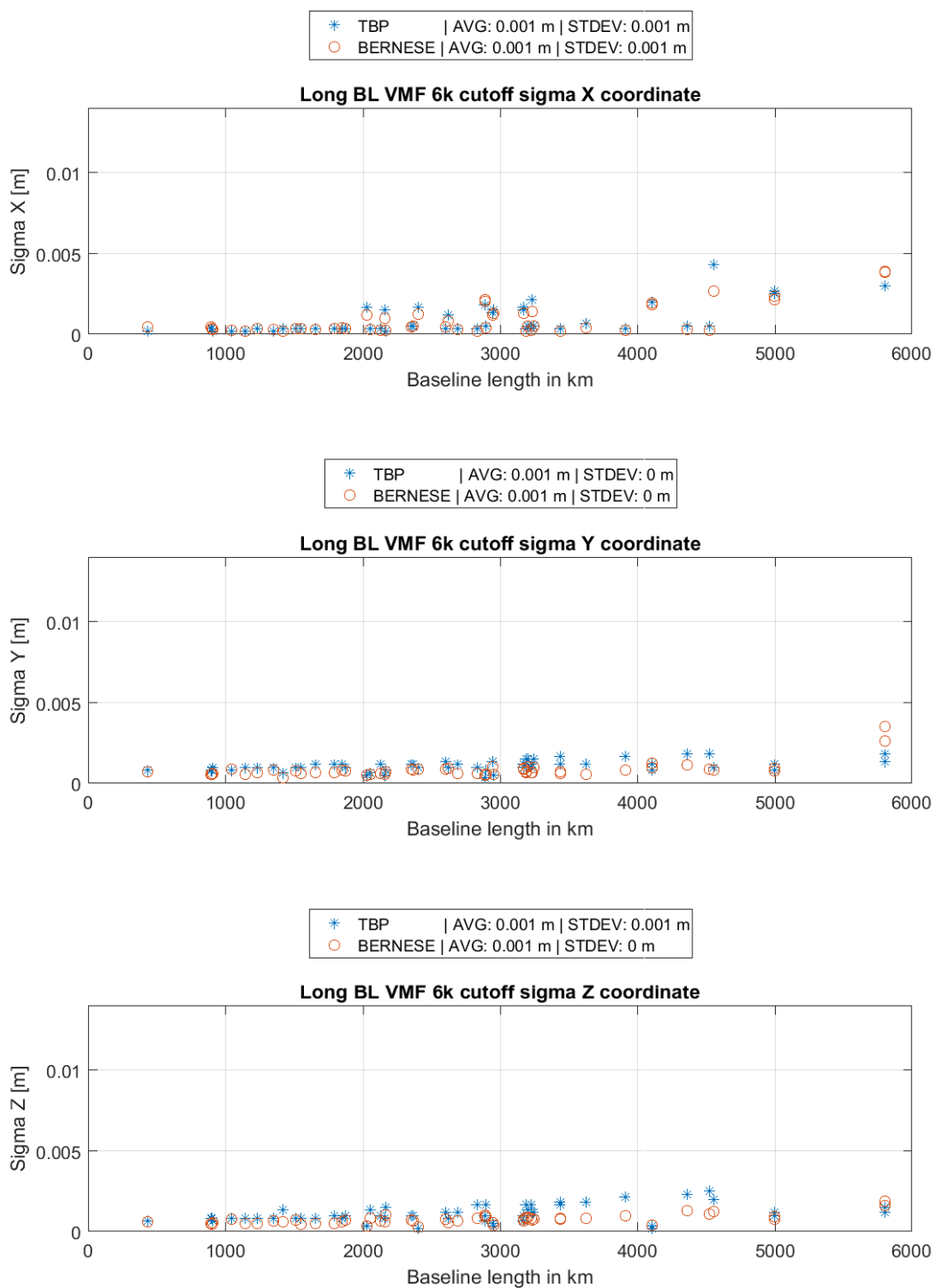


Figure A 13: Coordinate sigma w.r.t. to baseline length, long BL, 6000 km cutoff, VMF

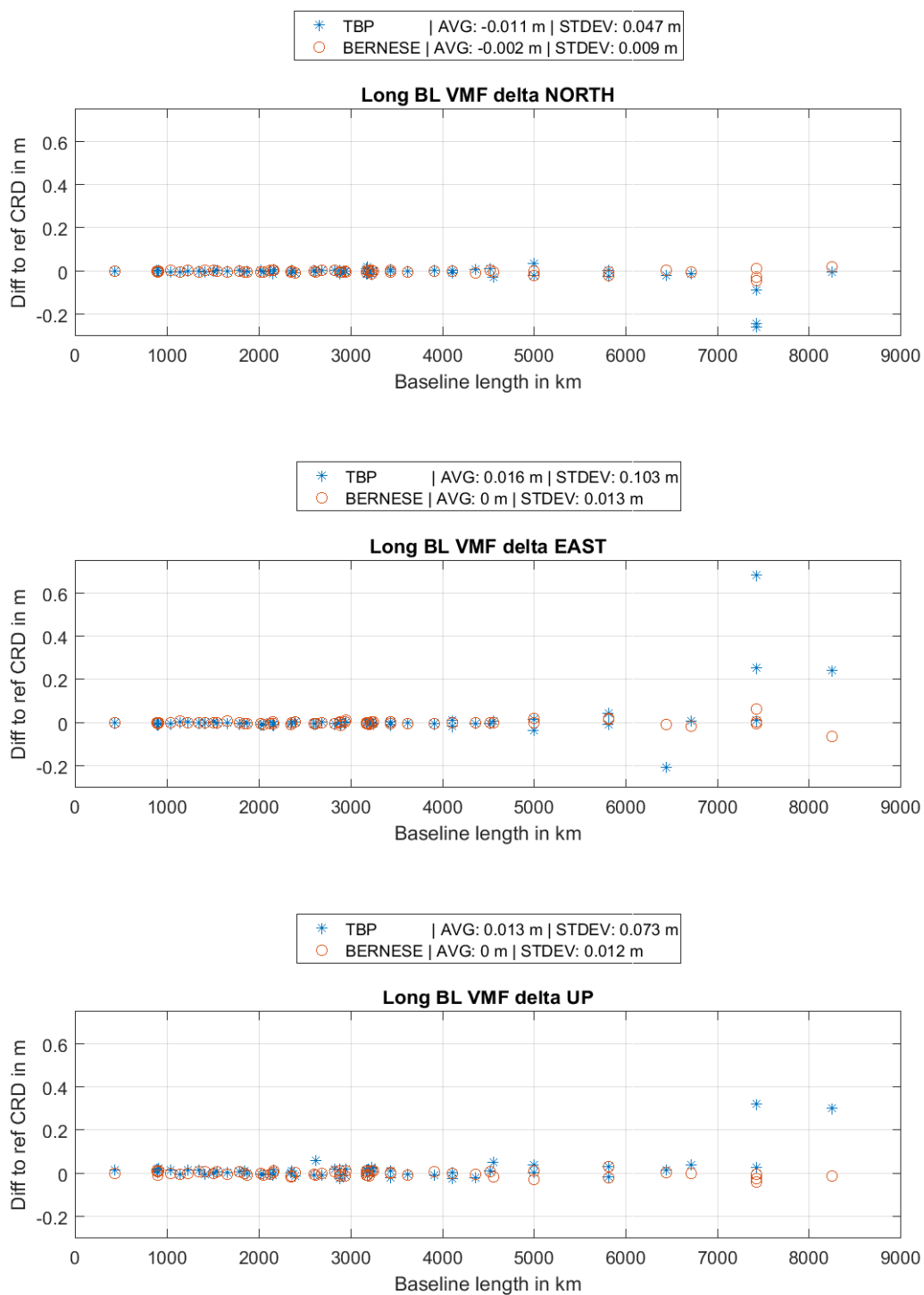
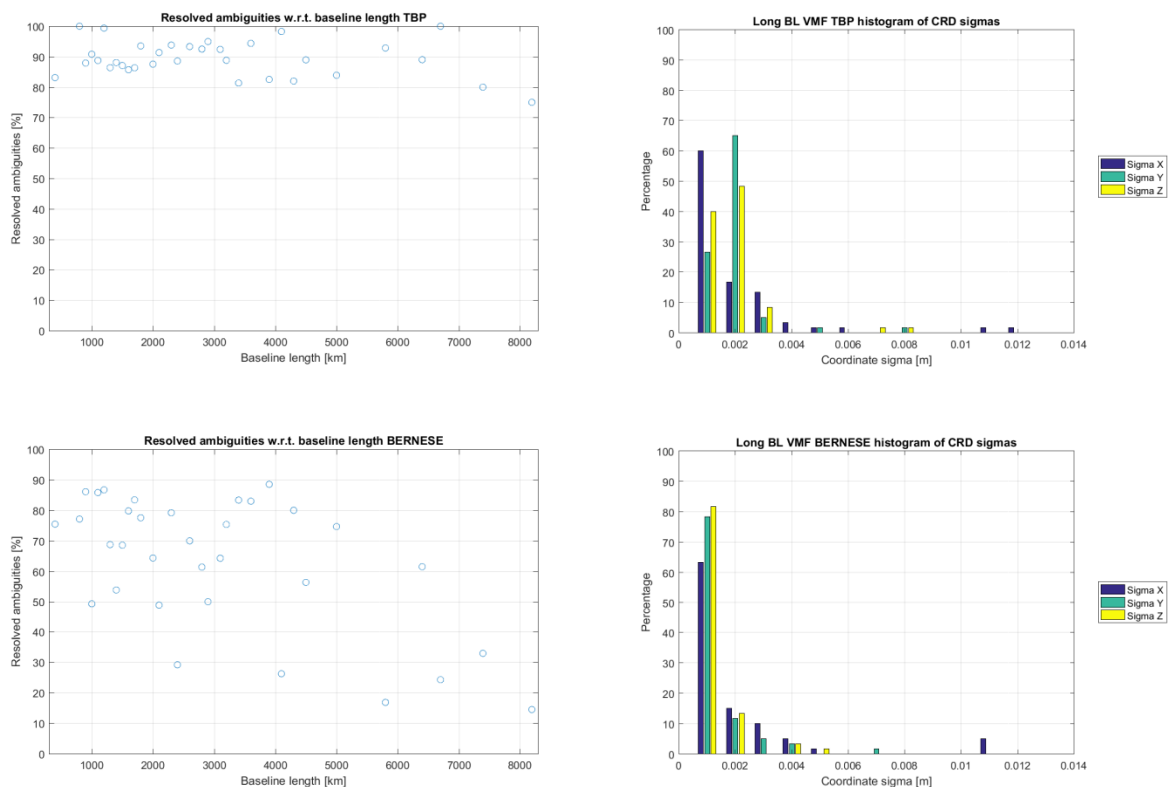


Figure A 14: Delta NEU, long baselines, VMF

**Table A 2: 3D Helmert transformation parameters for TBP and Bernese, Africa, VMF**

	Bernese Parameters:	Bernese Accuracy:	TBP Parameters:	TBP Accuracy:
Translation X	0.0030	0.0031	0.0273	0.0242
Translation Y	0.0002	0.0031	0.0395	0.0242
Translation Z	-0.0023	0.0031	-0.0175	0.0242
Rotation w.r.t. X	0.0000	0.0000	0.0000	0.0000
Rotation w.r.t. Y	-0.0000	0.0000	-0.0000	0.0000
Rotation w.r.t. Z	-0.0000	0.0000	0.0000	0.0000
Scale factor	1.000	0.0000	1.000	0.0000



**Figure A 15: Left: Percentage of resolved ambiguities for long baselines, VMF; Right: Histogram of coordinate sigmas for long baselines, VMF;**

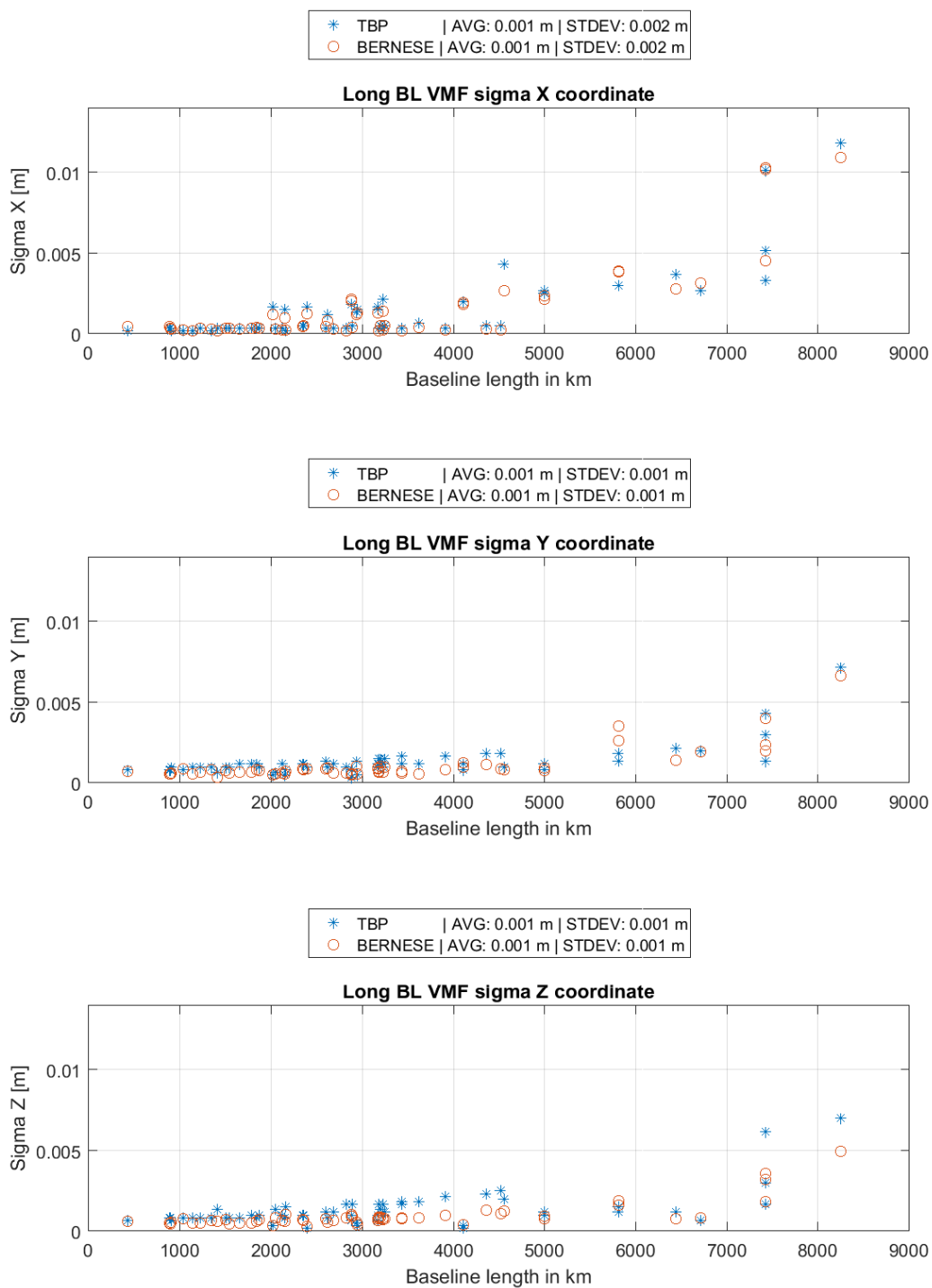


Figure A 16: Coordinate sigma w.r.t. to baseline length, long BL, VMF

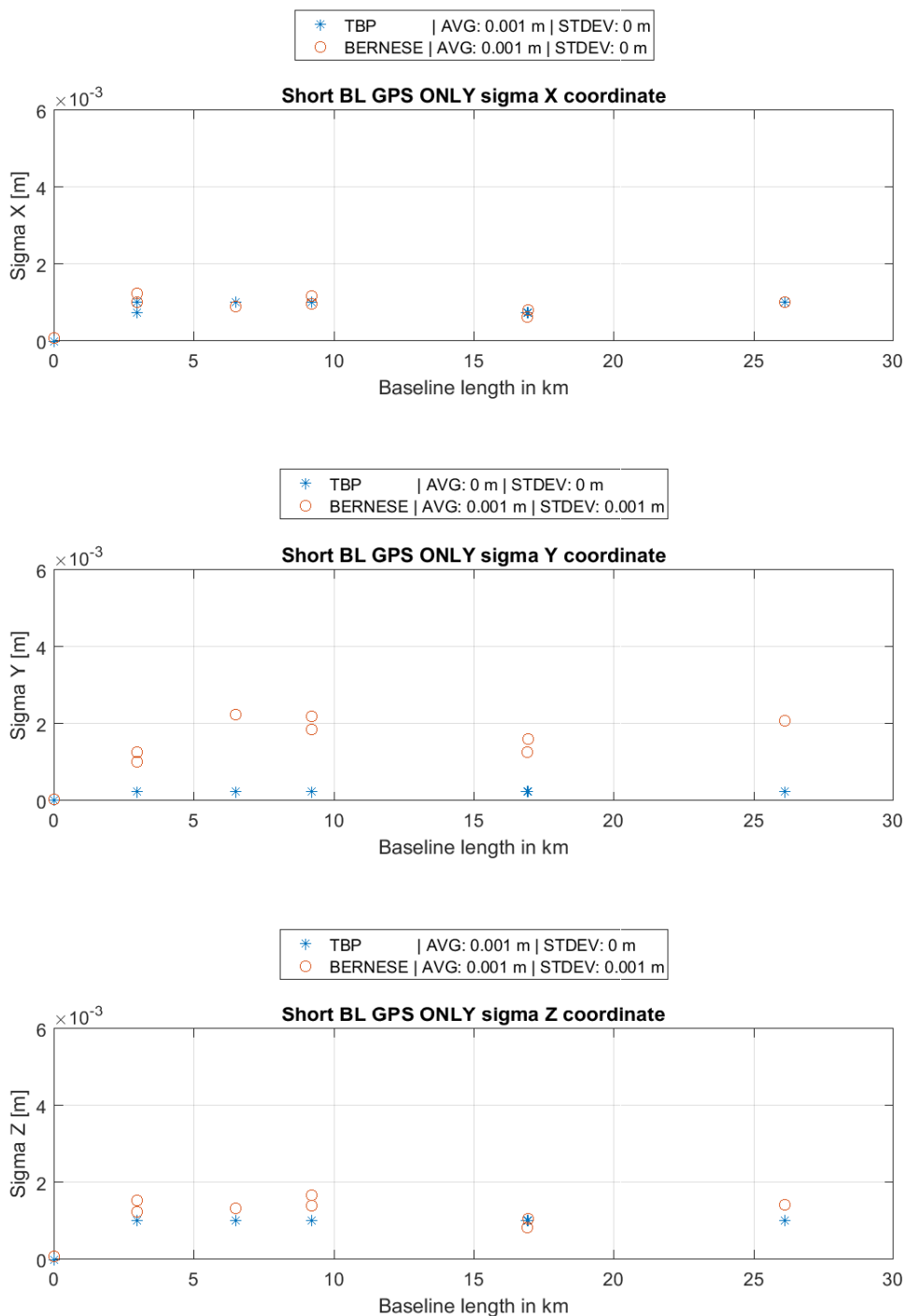


Figure A 17: Coordinate sigma w.r.t. to baseline length, short BL, GPS only

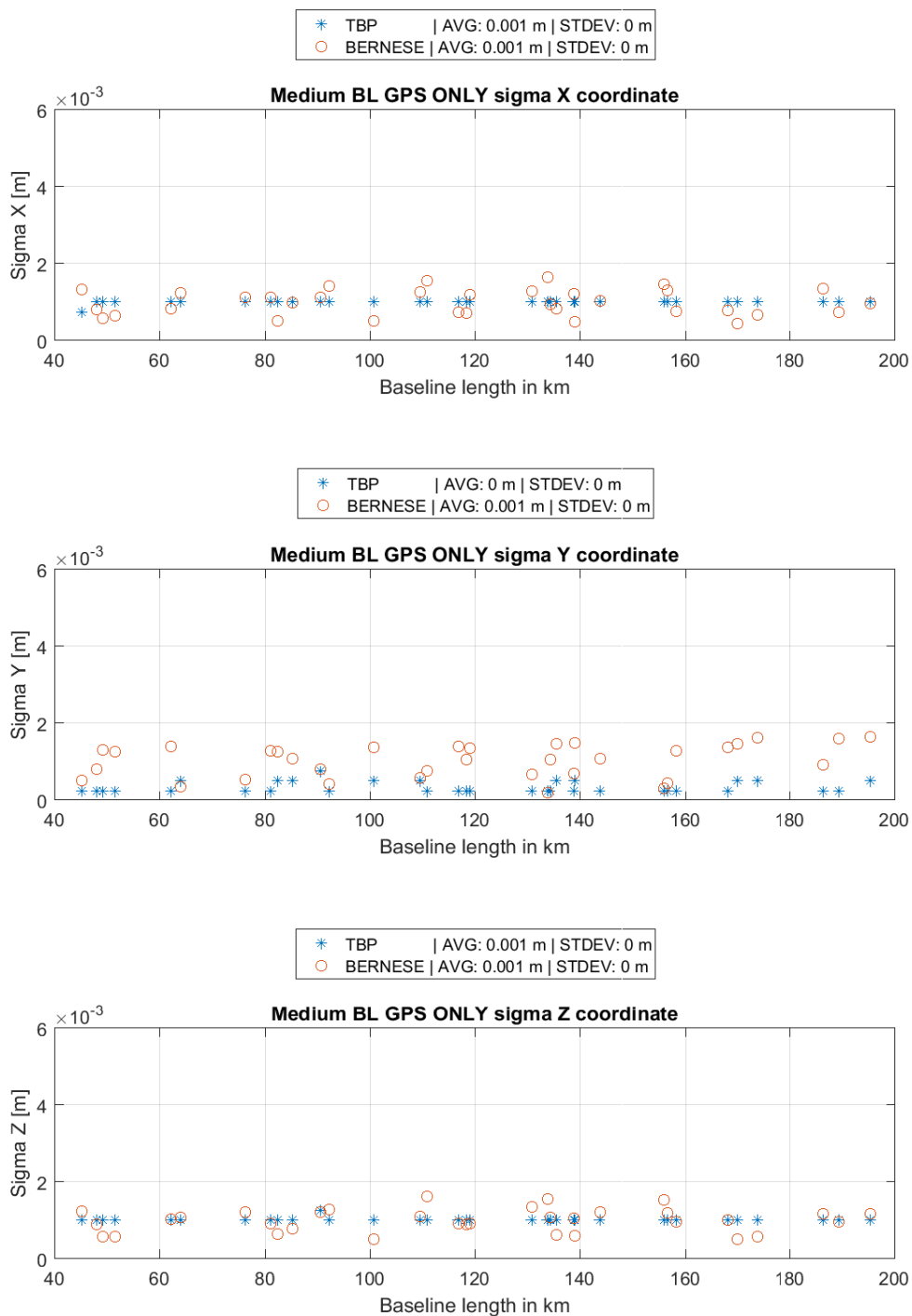


Figure A 18: Coordinate sigma w.r.t. to baseline length, medium BL, GPS only

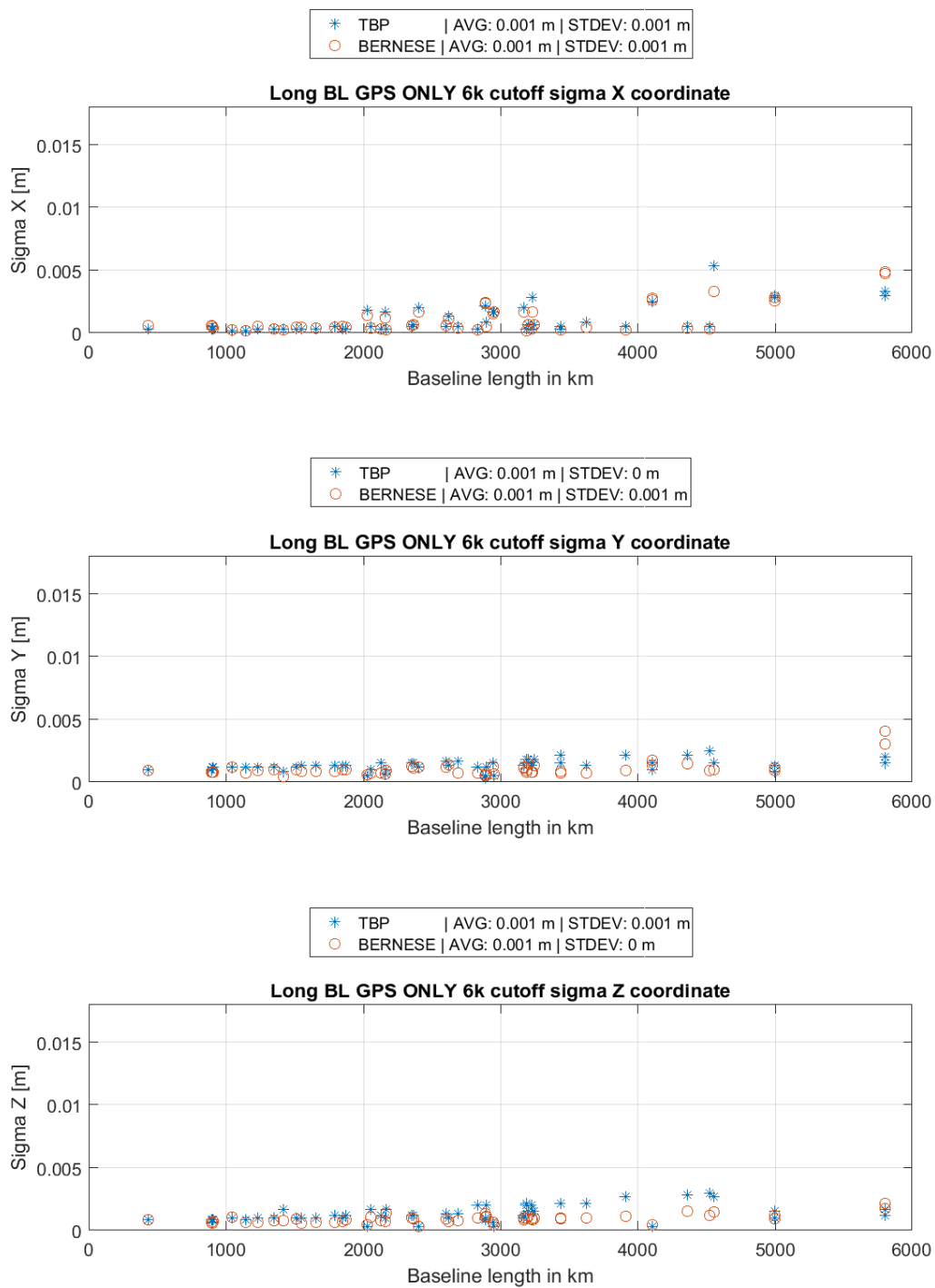


Figure A 19: Coordinate sigma w.r.t. to baseline length, long BL, 6000 km cutoff, GPS only

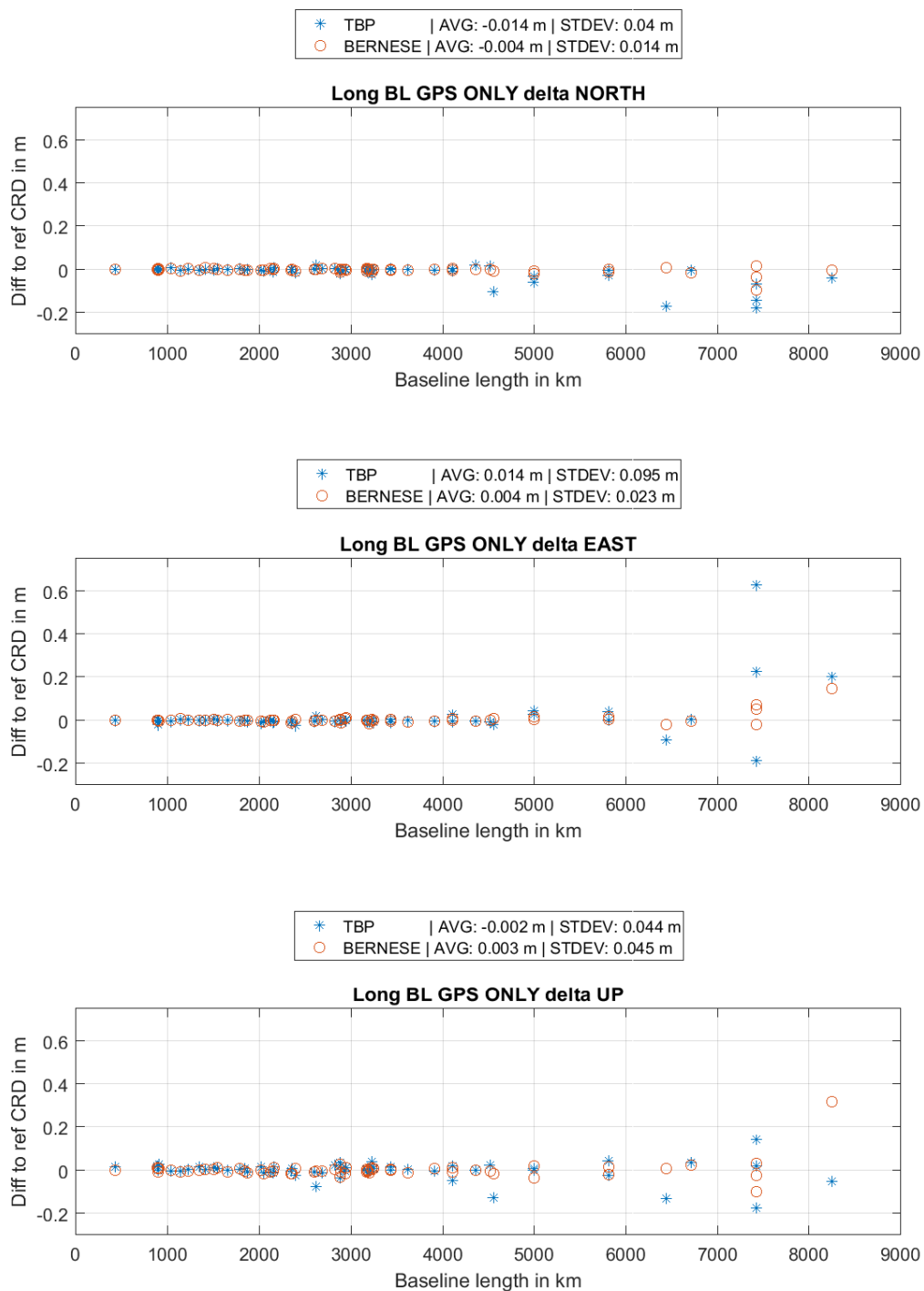
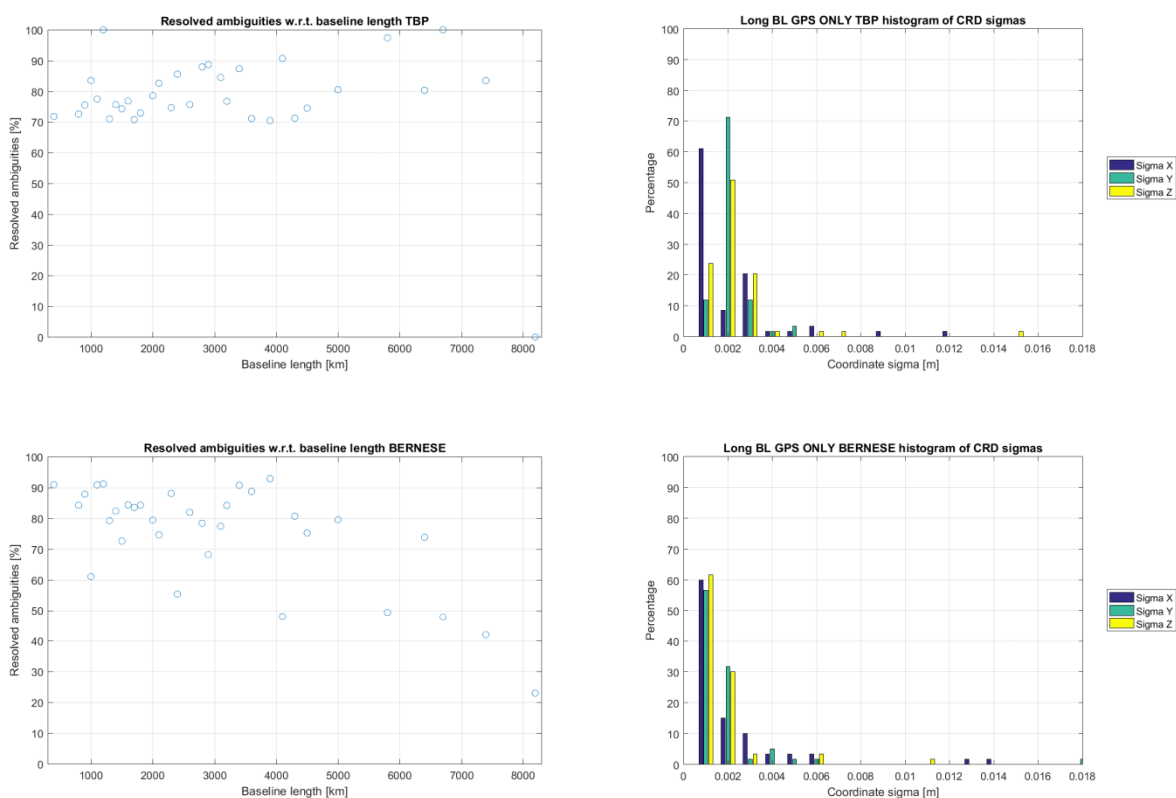


Figure A 20: Delta NEU, long baselines, GPS only

**Table A 3: 3D Helmert transformation parameters for TBP and Bernese, Africa, GPS only**

	Bernese Parameters:	Bernese Accuracy:	TBP Parameters:	TBP Accuracy:
Translation X	0.0052	0.0097	-0.0019	0.0192
Translation Y	0.0155	0.0097	0.0113	0.0192
Translation Z	-0.0088	0.0097	-0.0209	0.0192
Rotation w.r.t. X	0.0000	0.0000	0.0000	0.0000
Rotation w.r.t. Y	-0.0000	0.0000	-0.0000	0.0000
Rotation w.r.t. Z	0.0000	0.0000	-0.0000	0.0000
Scale factor	1.000	0.0000	1.000	0.0000



**Figure A 21: Left: Percentage of resolved ambiguities for long baselines, GPS only; Right: Histogram of coordinate sigmas for long baselines, GPS only;**

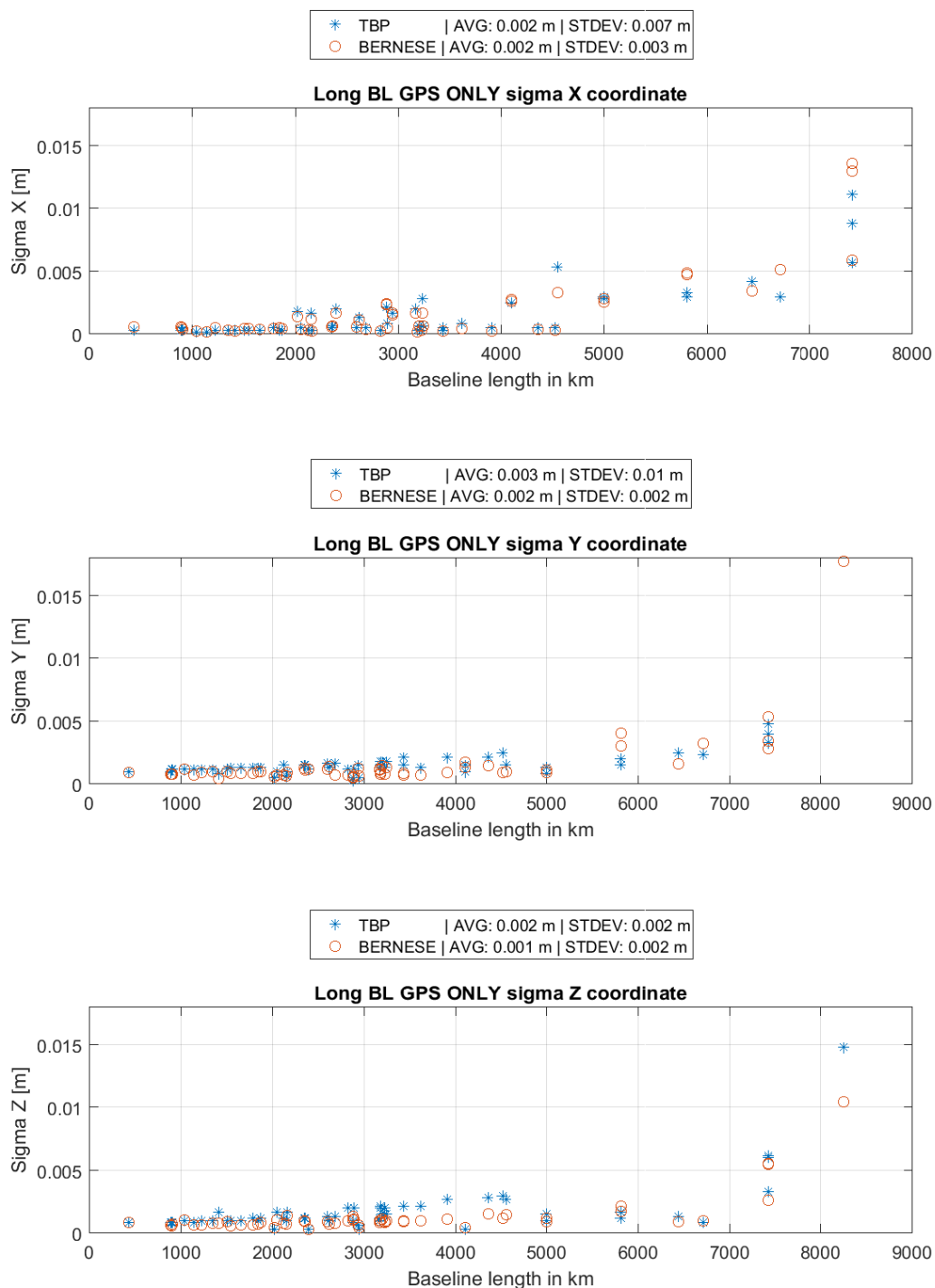


Figure A 22: Coordinate sigma w.r.t. to baseline length, long BL, GPS only

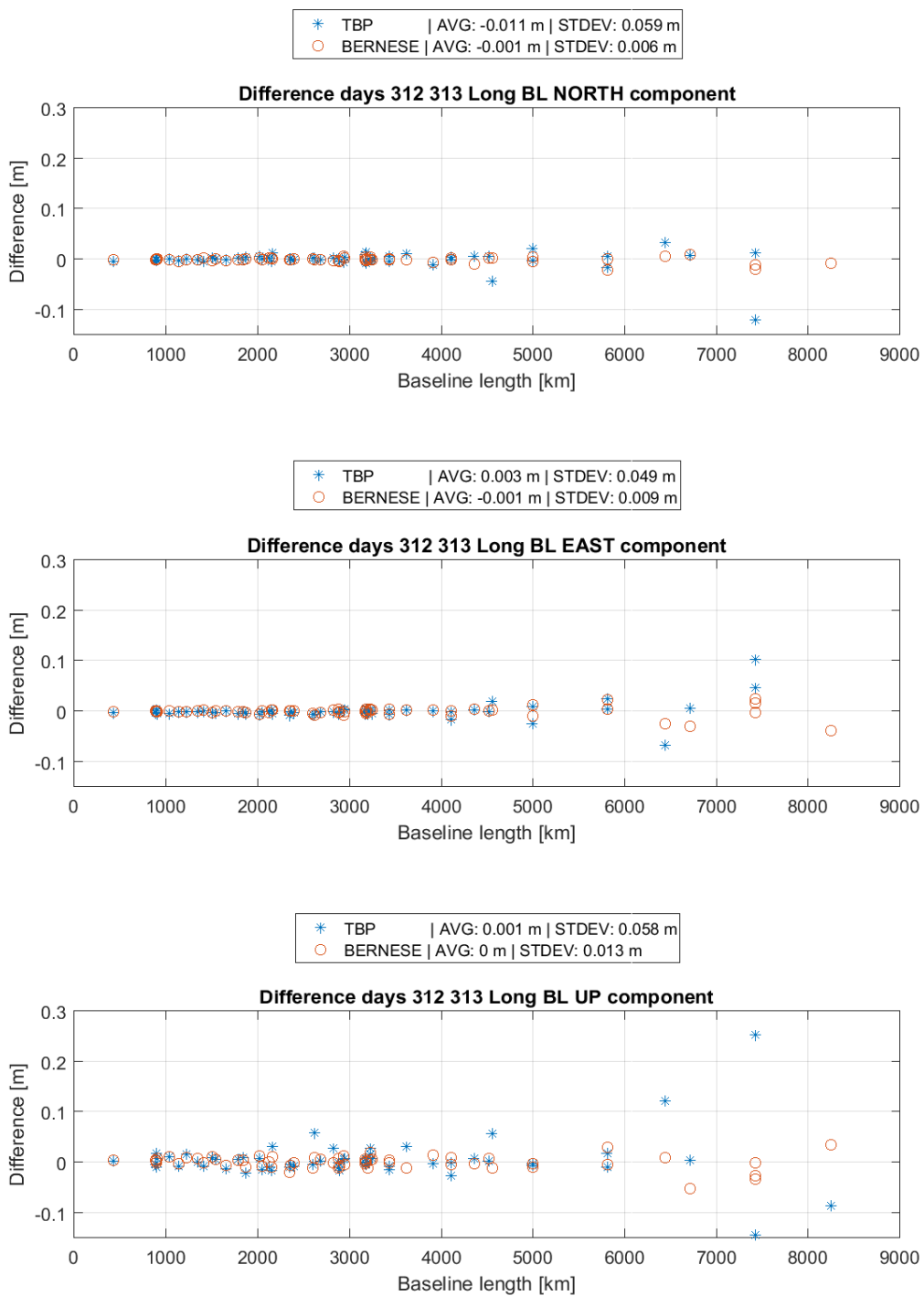


Figure A 23: Difference of daily solutions DOY 312 and 313 2016, long baselines

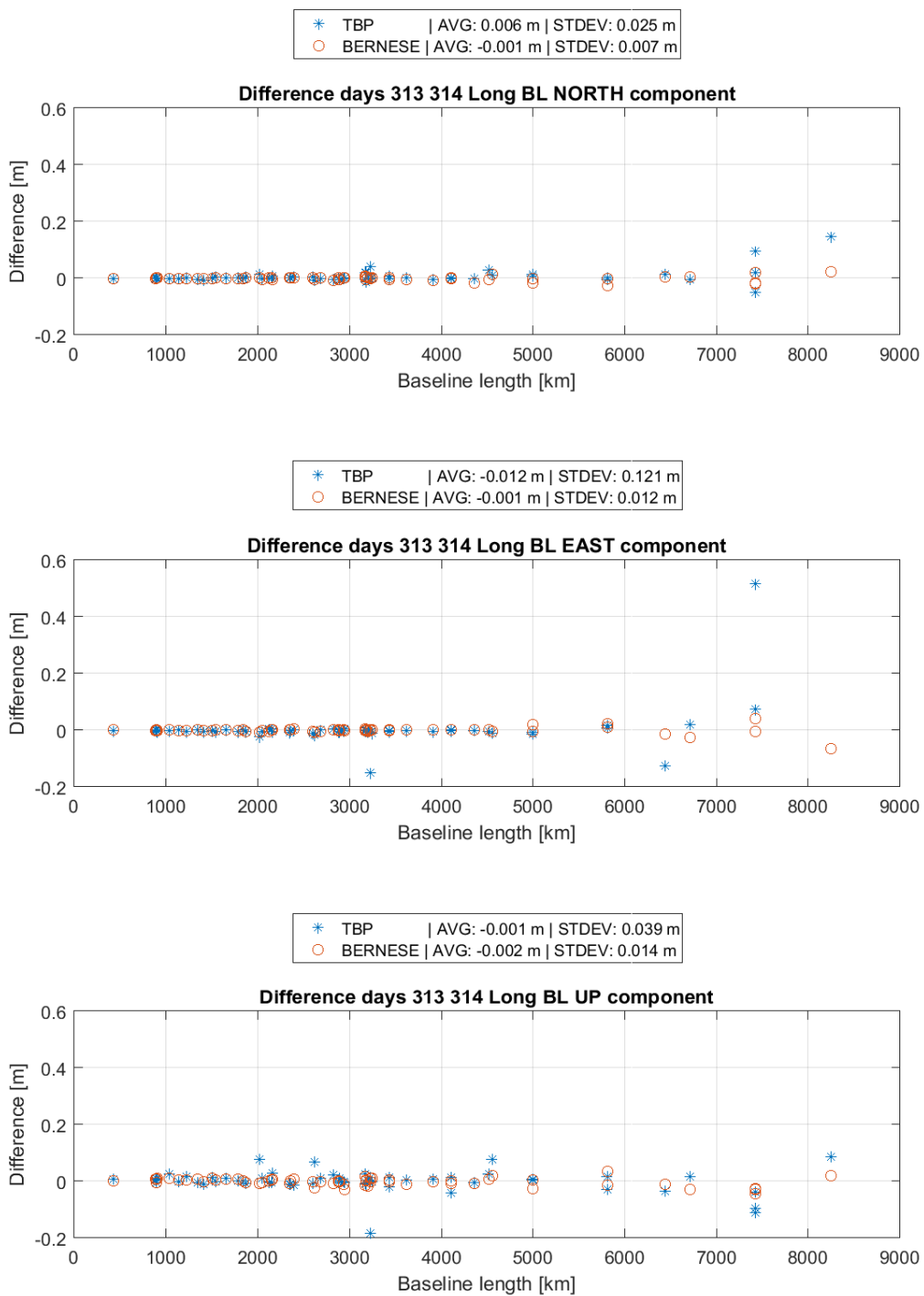


Figure A 24: Difference of daily solutions DOY 313 and 314 2016, long baselines,

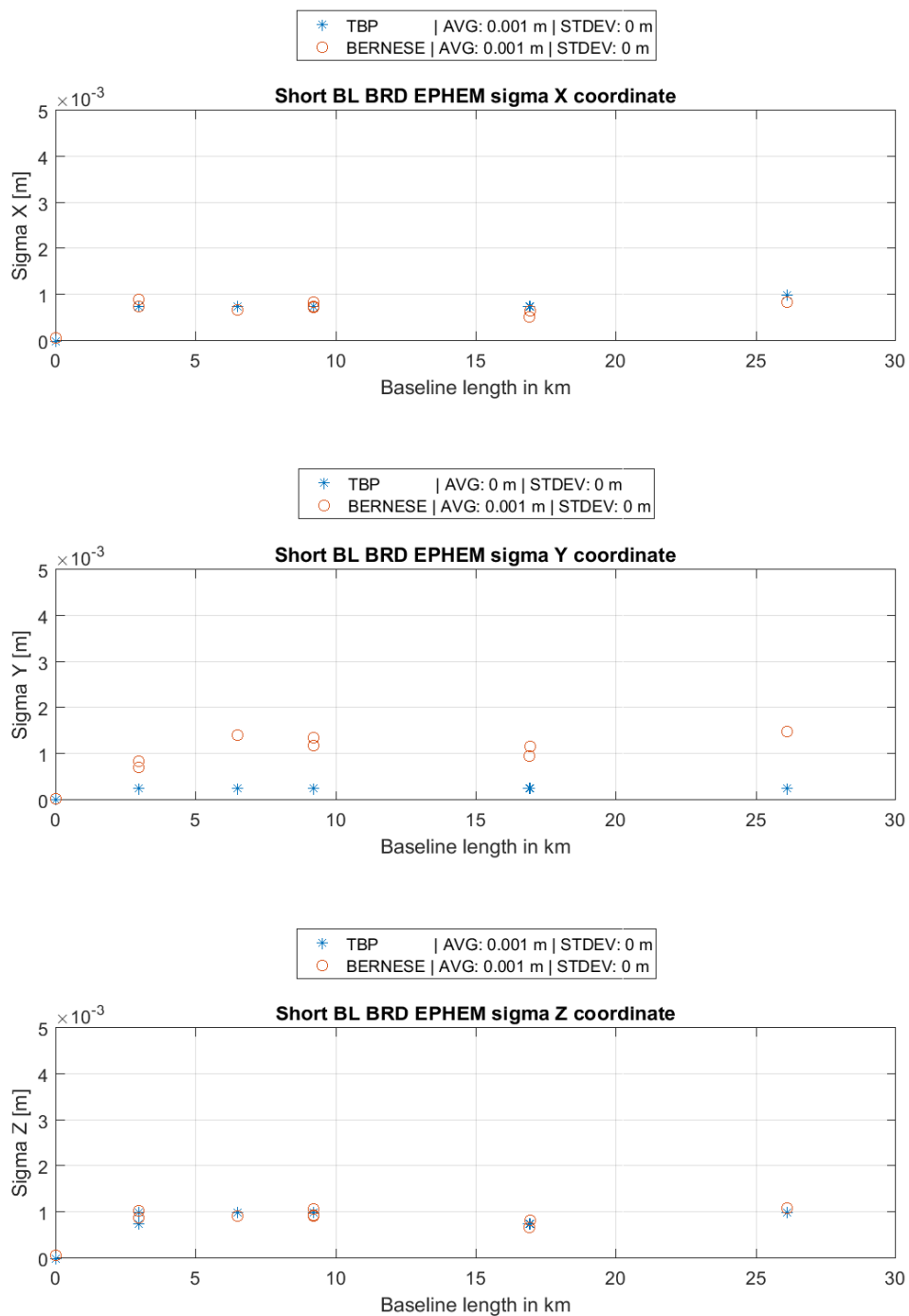


Figure A 25: Coordinate sigma w.r.t. to baseline length, short BL, Broadcast Ephemeris

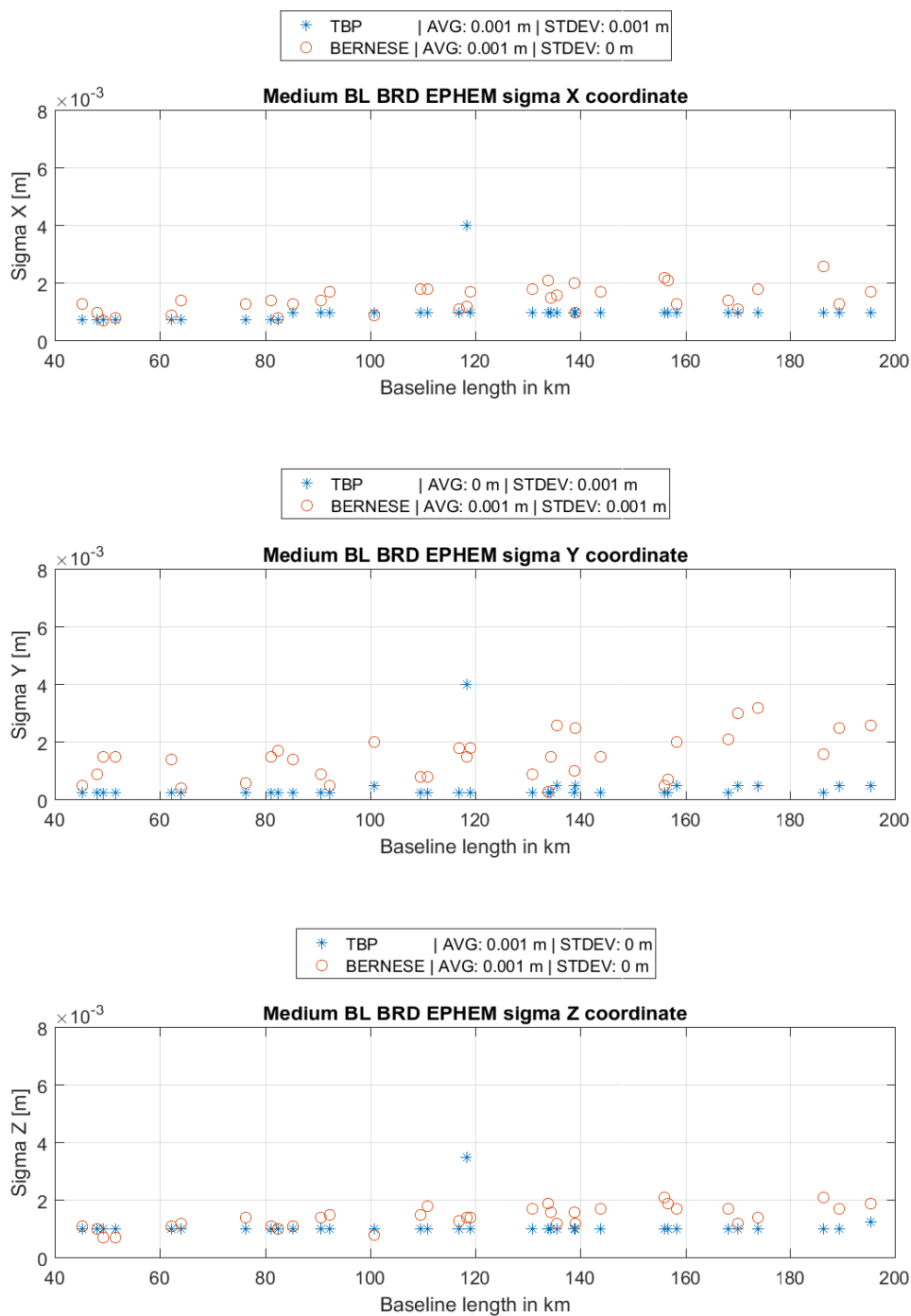


Figure A 26: Coordinate sigma w.r.t. to baseline length, medium BL, Broadcast Ephemeris

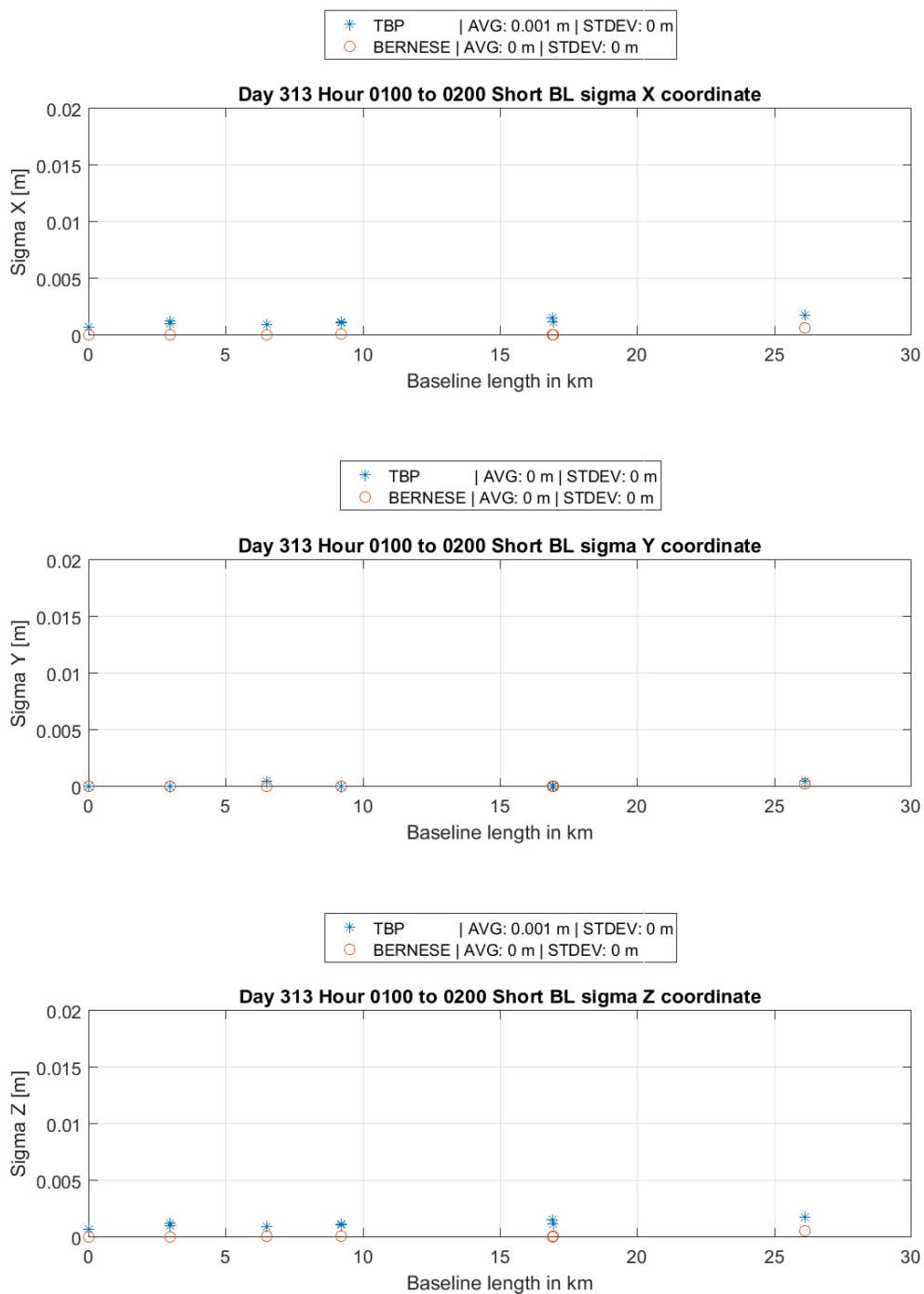


Figure A 27: Coordinate sigma w.r.t. to baseline length, short BL, obs. time 1:00 to 2:00, am

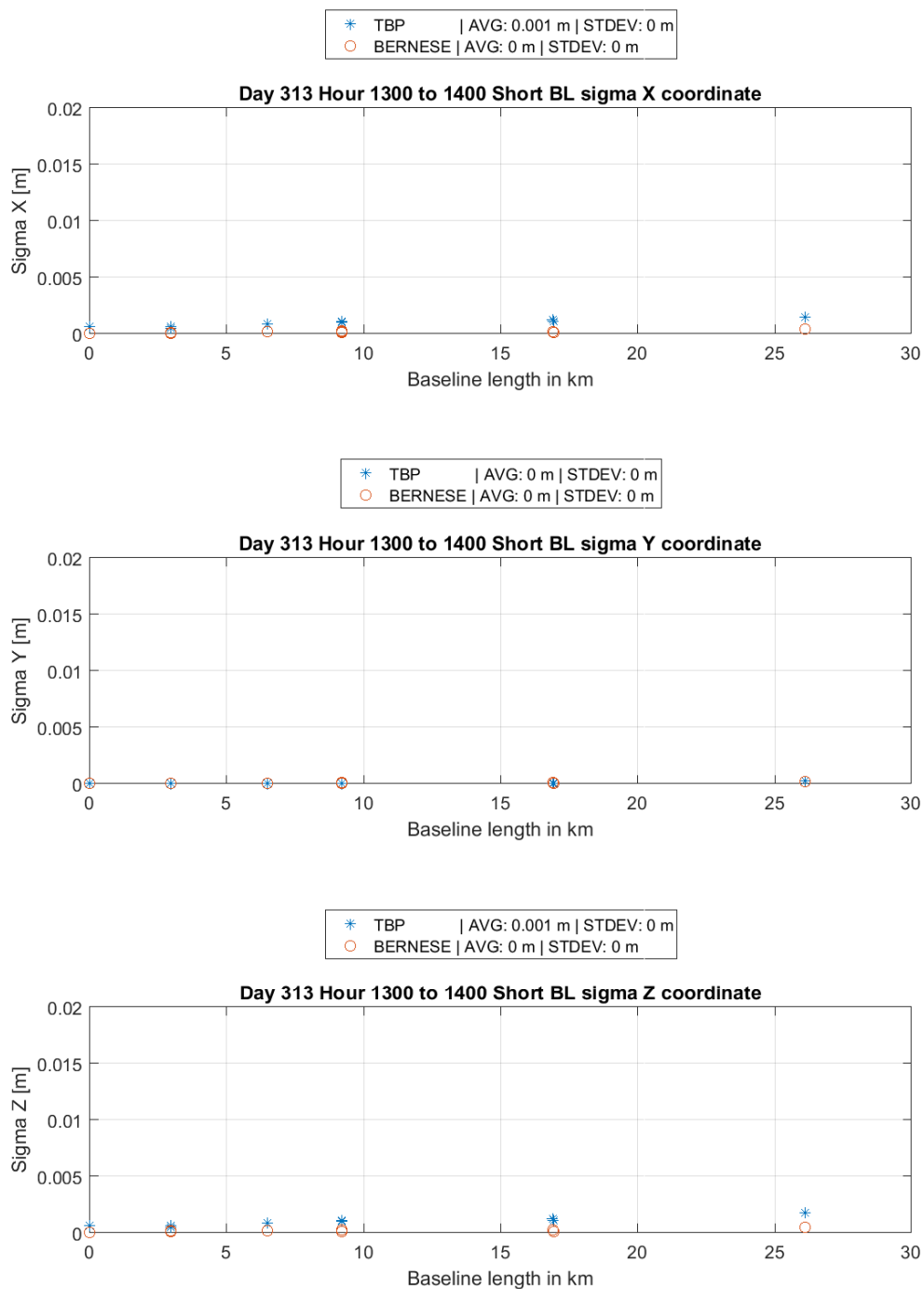


Figure A 28: Coordinate sigma w.r.t. to baseline length, short BL, obs. time 1:00 to 2:00, pm

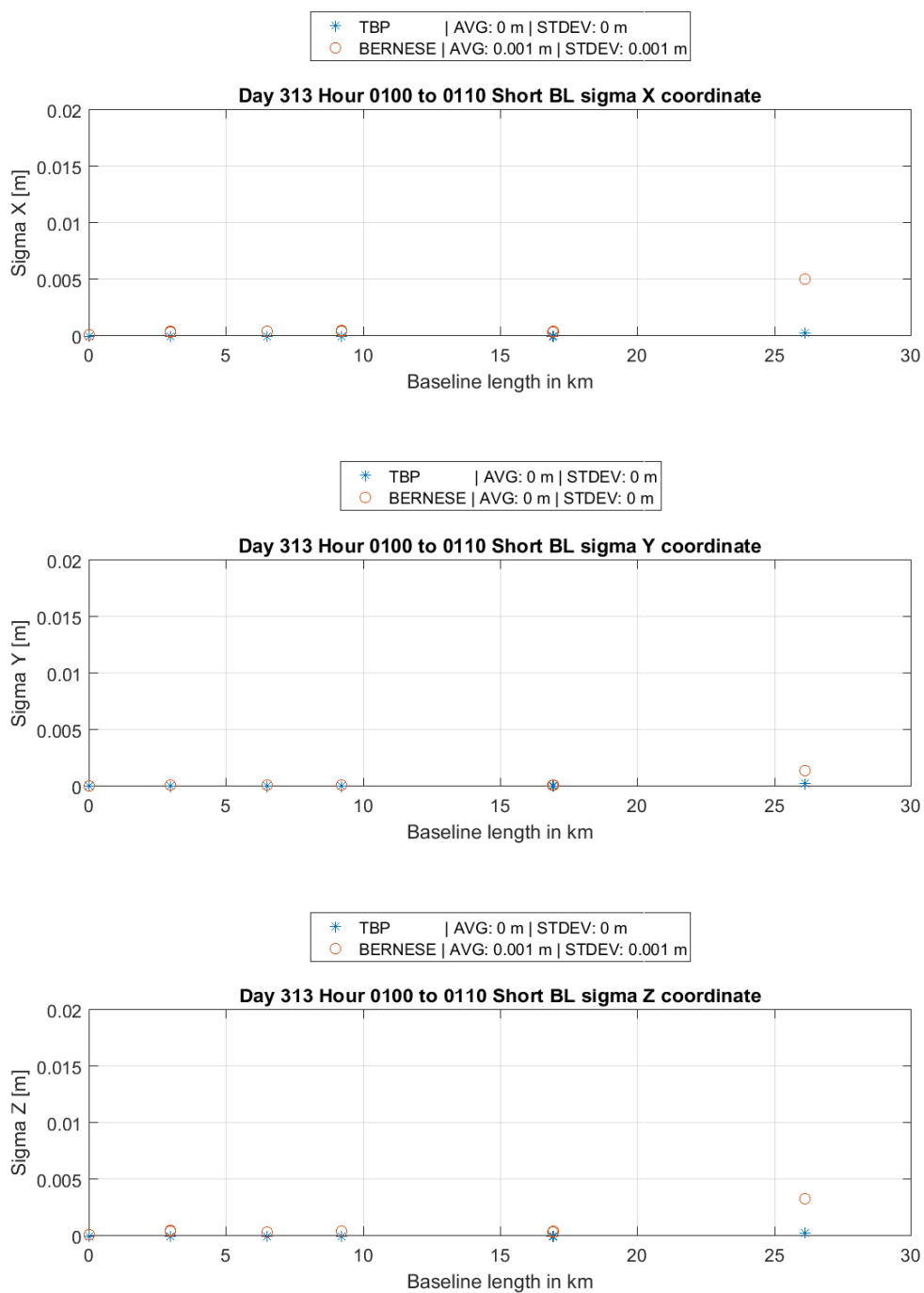


Figure A 29: Coordinate sigma w.r.t. to baseline length, short BL, obs. time 1:00 to 1:10, am

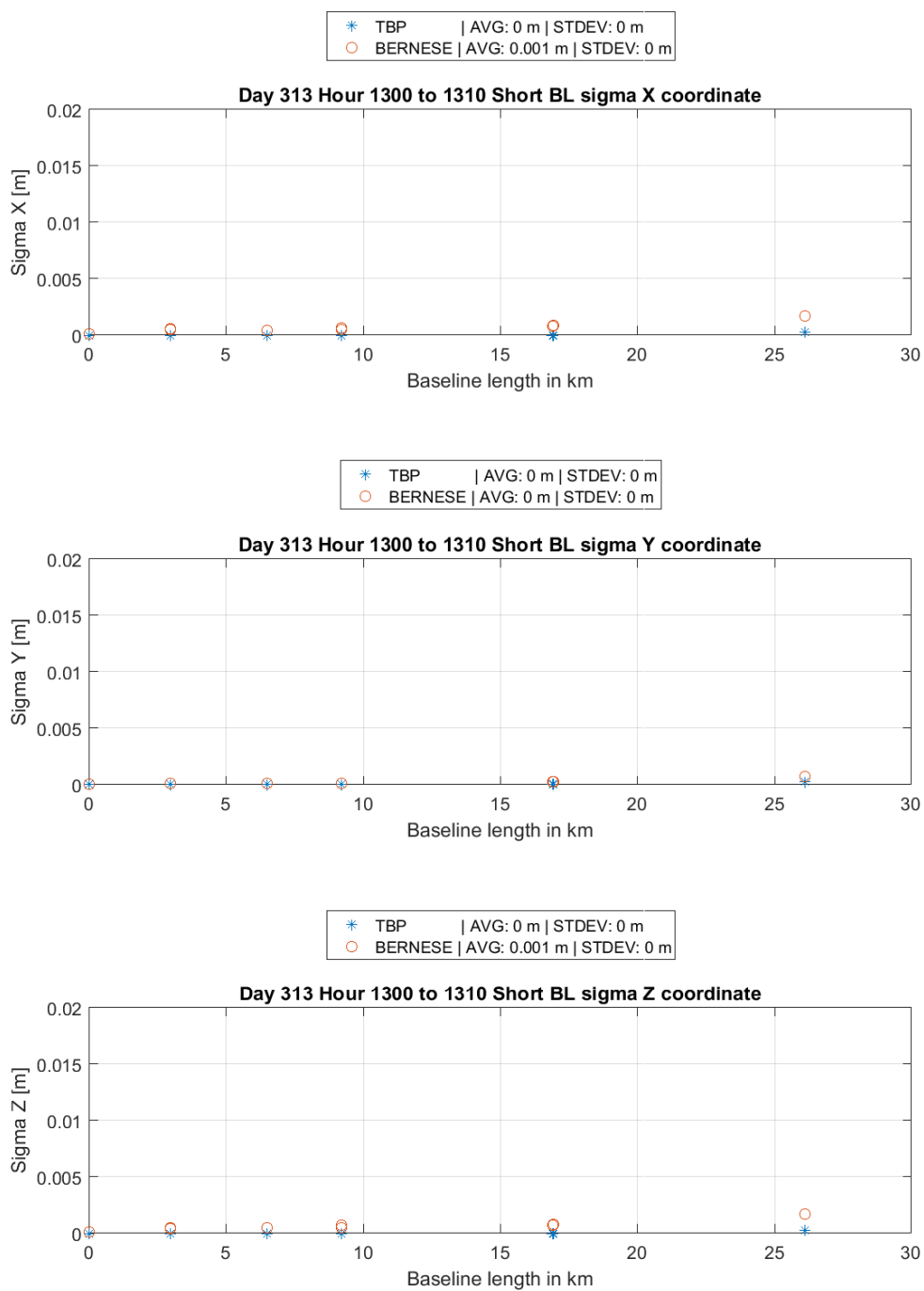


Figure A 30: Coordinate sigma w.r.t. to baseline length, short BL, obs. time 1:00 to 1:10, pm

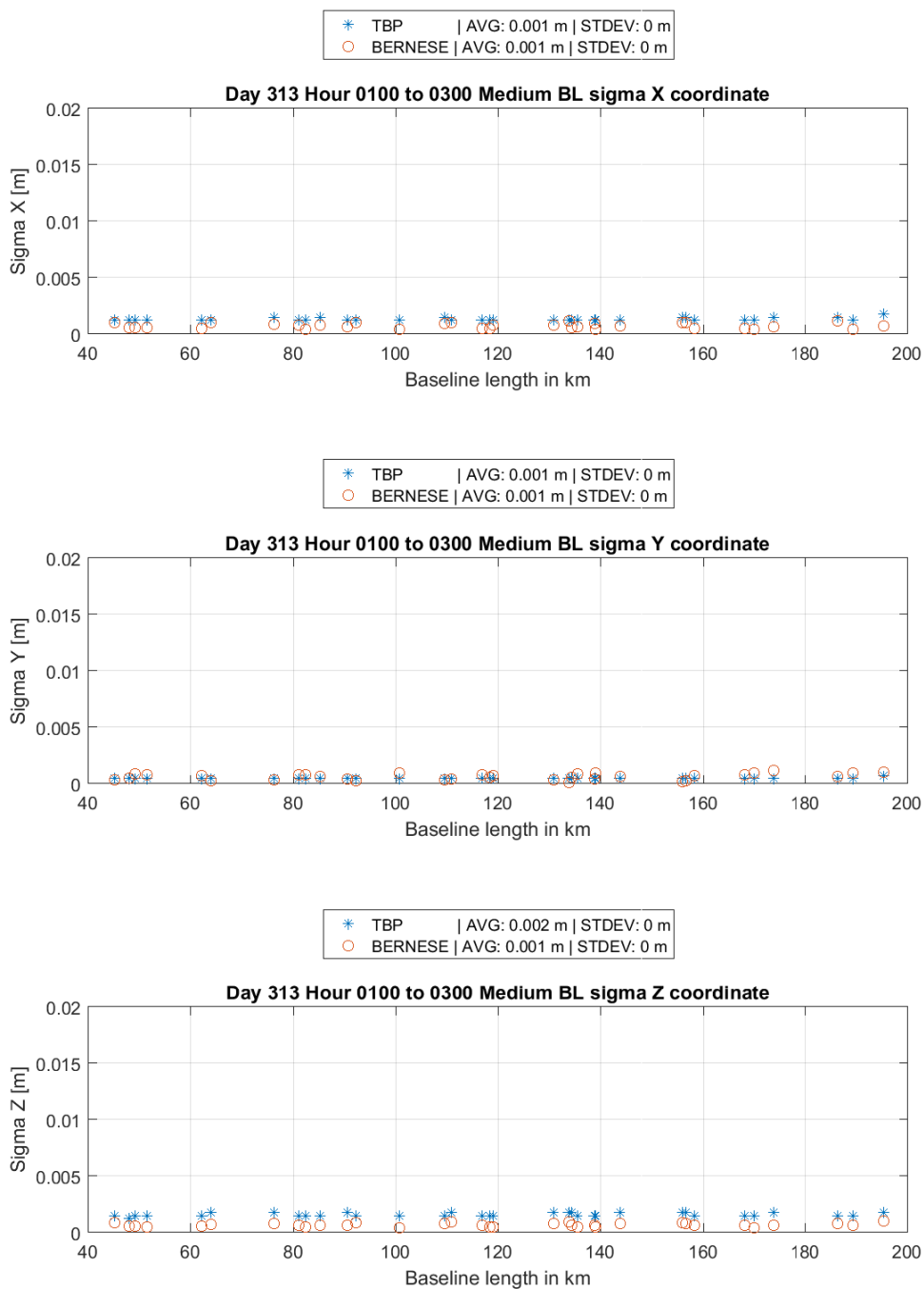


Figure A 31: Coordinate sigma w.r.t. to baseline length, medium BL, obs. time 1:00 to 3:00, am

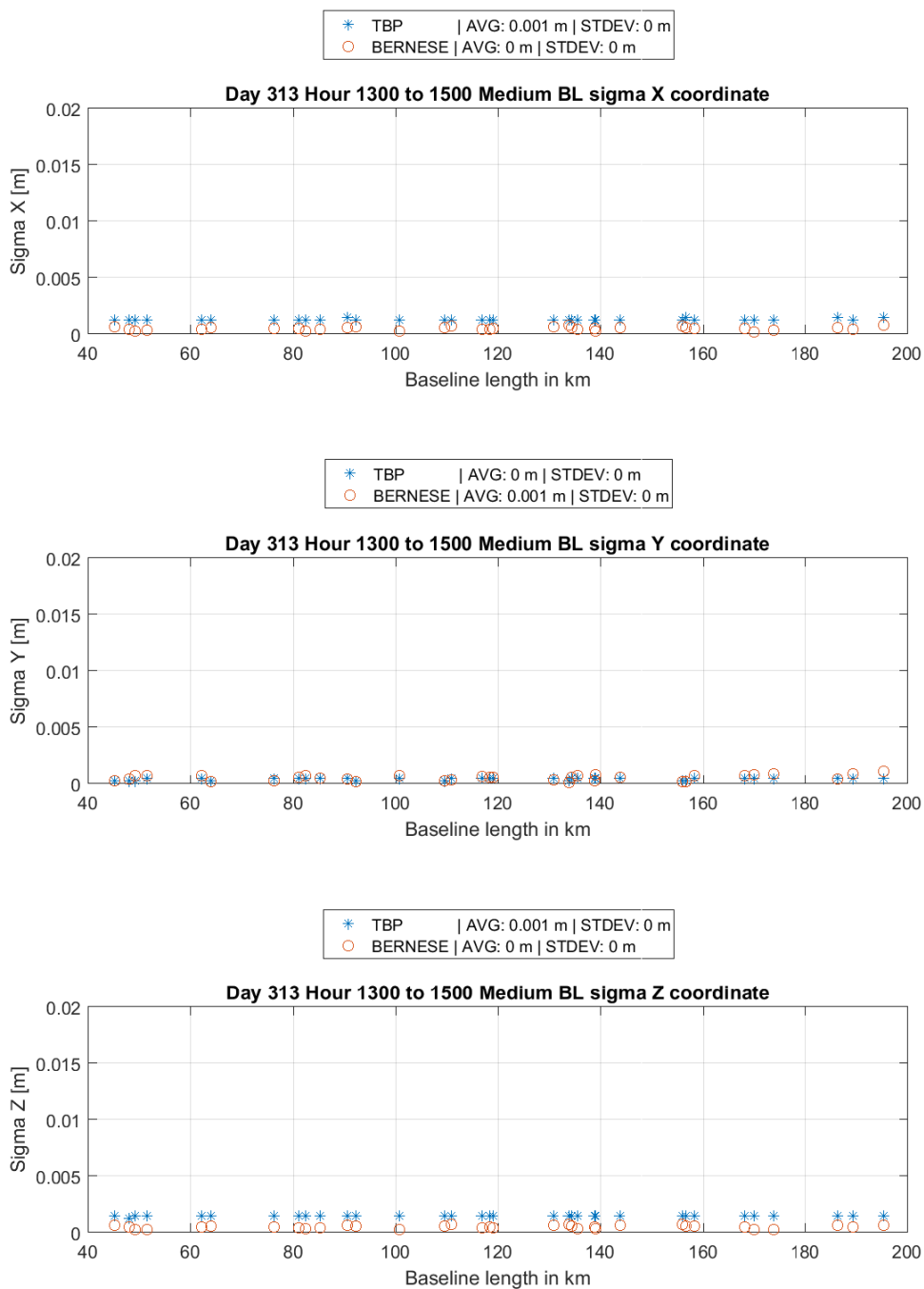


Figure A 32: Coordinate sigma w.r.t. to baseline length, medium BL, obs. time 1:00 to 3:00, pm

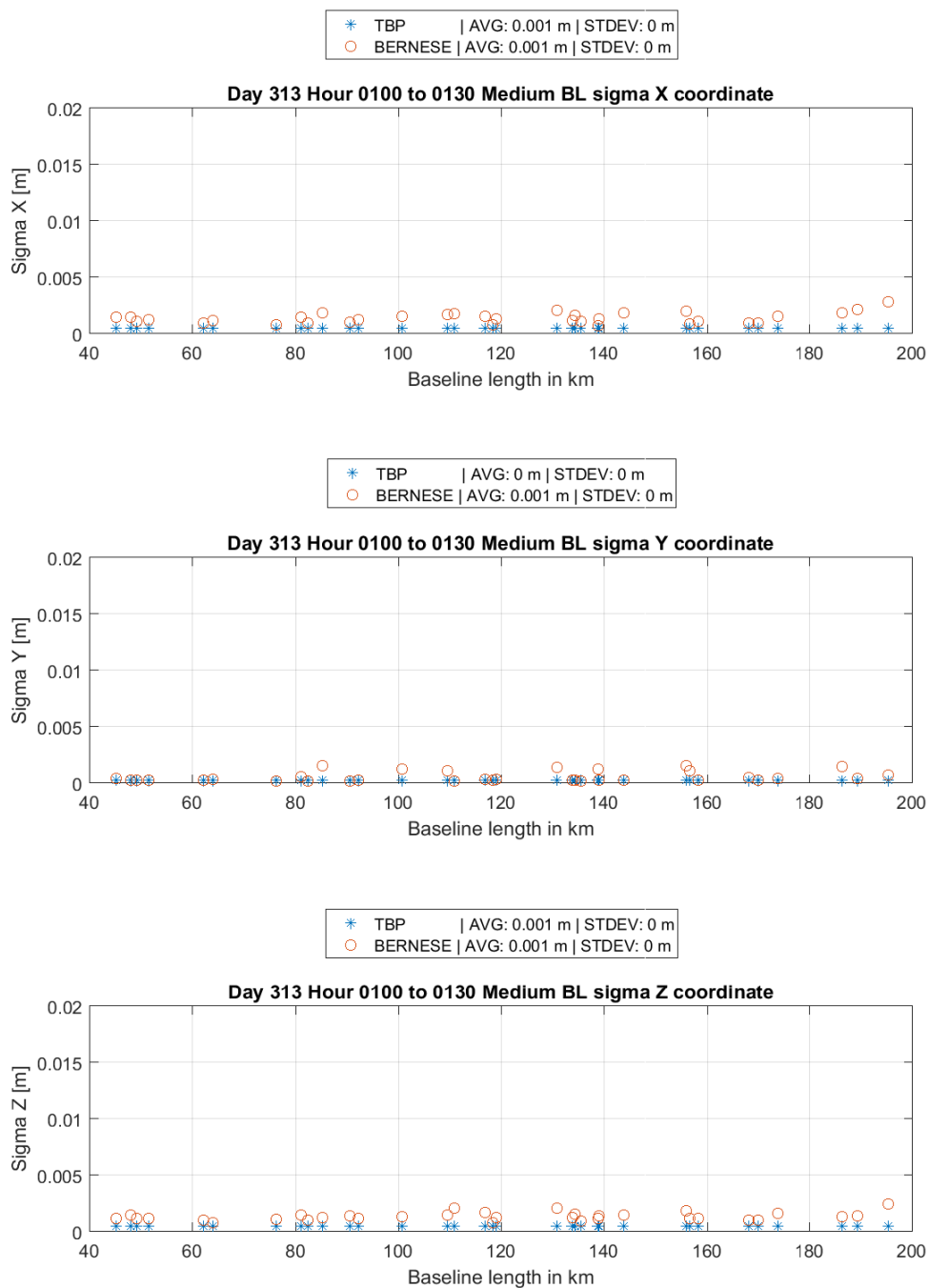


Figure A 33: Coordinate sigma w.r.t. to baseline length, medium BL, obs. time 1:00 to 1:30, am

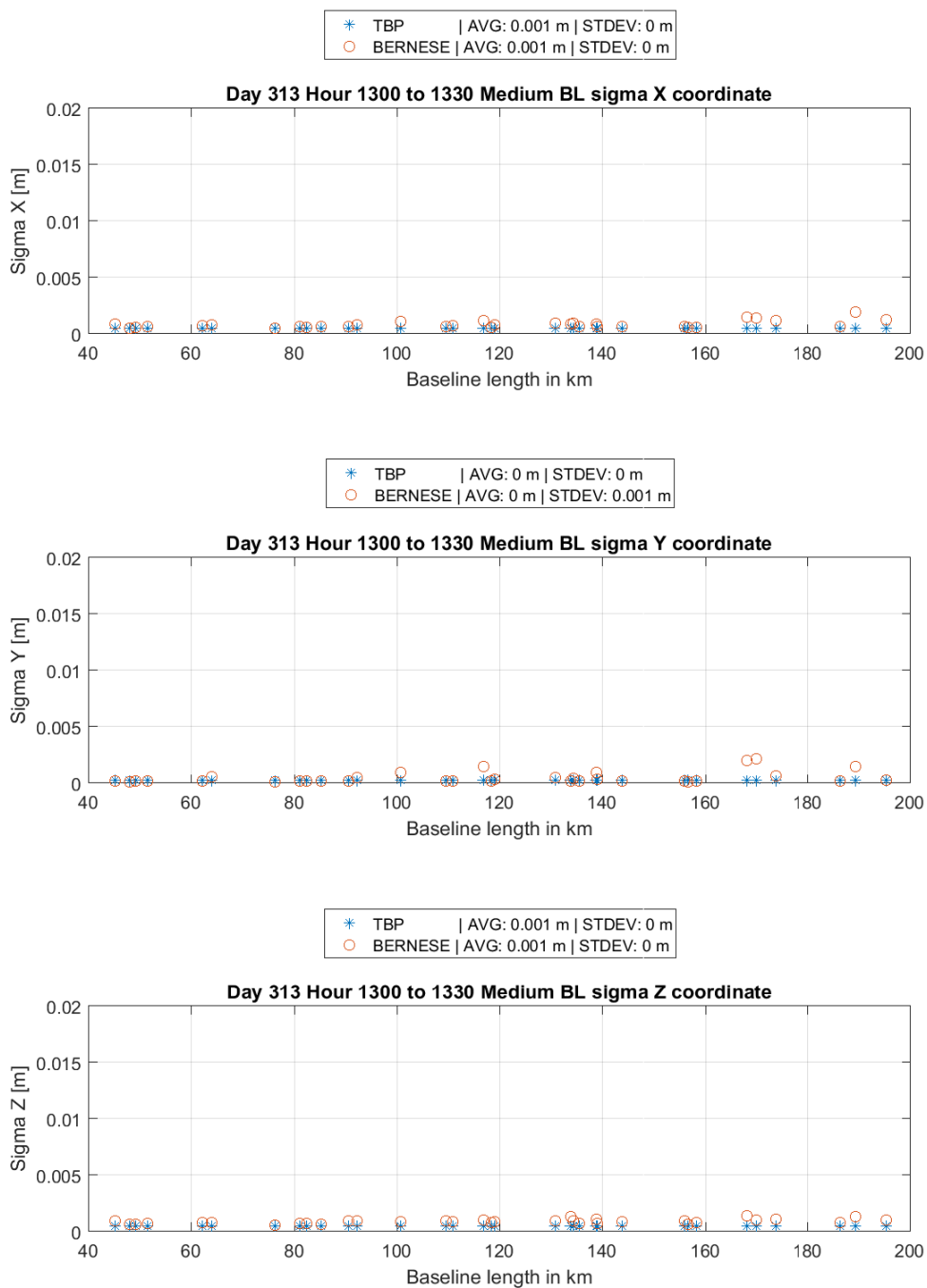


Figure A 34: Coordinate sigma w.r.t. to baseline length, medium BL, obs. time 1:00 to 1:30, pm

List of files on CD-ROM by folder:

Atmospheric correction data:

- VMF grid files downloaded from <http://ggosatm.hg.tuwien.ac.at/DELAY/>, files from 2016 11 07 hour 18 until 2016 11 09 hour 06 with 1 file each six hours
- COD3120.ION, COD3130.ION, COD3140.ION ionosphere correction from CODE, downloaded at <ftp://ftp.unibe.ch/aiub/>

CRD, STA, ABB:

- ABBREV.ABB abbreviation table
- A priori/reference coordinates for all datasets; AFRICA.CRD, Hoehenkir.CRD, SAPOS.CRD, USACAN.CRD
- Station information files for all datasets: Africa.STA, HOEHEN.STA, SAPOS.STA, USACAN.STA

Extended Bernese Result Files: Bernese output files from several additional programs in the processing procedure.

MatlabEvalToolbox:

- filePrepScripts: Helper functions to format data or rename files for Bernese conformity
- GeodeticToolbox: Toolbox containing geodetic functionalities by Peter Wasmeier, TUM
- Matlab scripts for evaluation; Note that the program will most probably not execute properly since the Trimble owned scripts had to be extracted.

Orbits, EOP, clocks:

- ALL.DCB: DCBs file generated from CODE's monthly P1-P2 and P1-C1 mean files for November 2016
- C04\_2016.ERP: Earth rotation parameters downloaded at <ftp://ftp.unibe.ch/aiub/>, at the BSWUSER52 directory
- Standard Orbits and clocks for GPS and GLONASS generated from IGS and IGL files, downloaded at <ftp.igs.org/pub/>, namely GPGL3120.STD, GPGL3130.STD, GPGL3140.STD, GPGL3120.CLK, GPGL3130.CLK, GPGL3140.CLK
- Broadcast orbits and clocks generated from all available navigation data for DOY 3130, named GGBR.CLK and GGBR.STD

Results (as processed in Matlab): Folder structure supported by the Matlab evaluation toolbox with all necessary result data containing:

- Bernese Results (GPSEST.OUT files, GPSXTR.SUM files, .CRD coordinate files.
- Pots, folder to save plots and Helmert transformation parameter files.
- REFERENCE, containing Bernese .CRD files with the reference coordinates
- TBPResults, containing the log files from the TBP command line application

Scripts and PCFs: Bernese process control files with the relevant subscripts called:

- AmbiRes.PCF: Performs the Melbourne-Wübbena linear combination/ambiguity resolution using the sigma strategy
- L1AndL2Res.PCF: Performs a direct L1&L2 ambiguity resolution using the sigma strategy
- L1L2WideLane.PCF: Selects baselines depending on length and performs either a L1&L2 or a L5L3 ambiguity resolution
- L5L3Resolution: Performs a L5L3 ambiguity resolution using the sigma strategy

Graphics: Additional figures and tables used in this thesis.

ExampleBaselineReport.pdf: Example report generated automatically by TBC (there is no special Bernese report attached since the official reports/output programs were used for the data evaluation)

ThesisSchuetz03625585.pdf, electronic version of this document.